

AD-A121 268

PROCESS PARAMETERS FOR BANDING 155-MM M483A1
PROJECTILES IN HIGH-CAPACITY. (U) CHAMBERLAIN MFG CORP
WATERLOO IA RESEARCH AND DEVELOPMENT DIV.

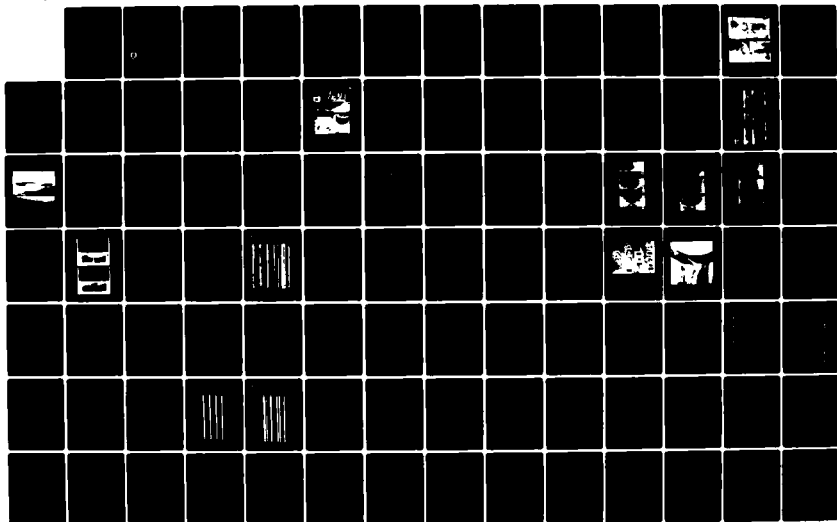
1/3

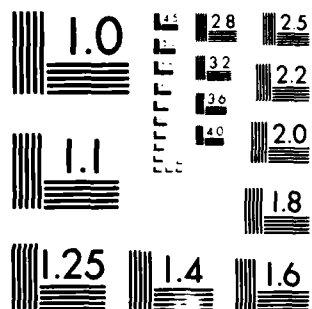
UNCLASSIFIED

J A YTTERHUS SEP 82 C8184-PR-072

F/G 19/1

NL





MICROCOPY RESOLUTION TEST CHART
NATIONAL BUREAU OF STANDARDS-1963-A

AD A121268

1

AD E400 855

CONTRACTOR REPORT ARLCD-CR-82028

PROCESS PARAMETERS FOR BANDING 155-mm M483A1 PROJECTILES IN
HIGH-CAPACITY INERTIA WELDING MACHINE

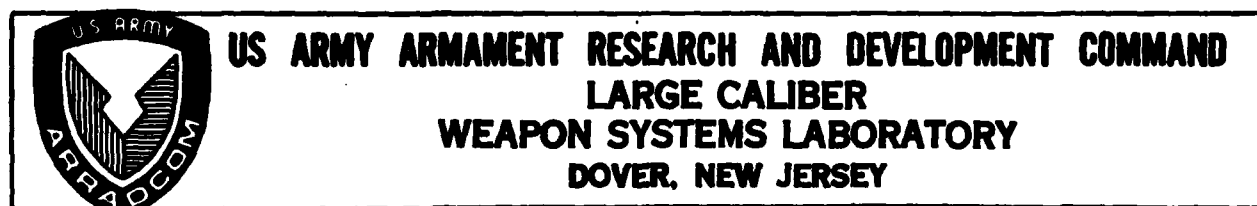
J. Arthur Ytterhus
Chamberlain Manufacturing Corporation
Research and Development Division
550 Esther Street
Waterloo, Iowa 50704

William Sharpe
Project Engineer
ARRADCOM

DTIC
ELECTE
NOV 3 1982
S D

B

September 1982



APPROVED FOR PUBLIC RELEASE; DISTRIBUTION UNLIMITED.

DTIC FILE COPY

82 10 12 06 2

"Original contains color
plates: All DTIC reproductions
will be in black and
white"

The views, opinions and/or findings contained in this report are those of the author(s) and should not be construed as an official Department of the Army position, policy, or decision, unless so designated by other documentation.

The citation in this report of the names of commercial firms or commercially-available products does not constitute official endorsement by or approval of the U.S. Government.

Destroy this report when no longer needed. Do not return to the originator.

UNCLASSIFIED

SECURITY CLASSIFICATION OF THIS PAGE (When Data Entered)

REPORT DOCUMENTATION PAGE		READ INSTRUCTIONS BEFORE COMPLETING FORM
1. REPORT NUMBER Contractor Report ARLCD-CR-82028	2. GOVT ACCESSION NO. AD A121 268	3. RECIPIENT'S CATALOG NUMBER
4. TITLE (and Subtitle) PROCESS PARAMETERS FOR BANDING 155-mm, M483A1 PROJECTILES IN HIGH-CAPACITY INERTIA WELDING MACHINE	5. TYPE OF REPORT & PERIOD COVERED FINAL FEB. 1979 - JAN. 1982	
7. AUTHOR(s) J. Arthur Ytterhus	6. PERFORMING ORG. REPORT NUMBER C8184-PR-072	
9. PERFORMING ORGANIZATION NAME AND ADDRESS CHAMBERLAIN MANUFACTURING CORPORATION Research and Development Division 550 Esther Street, P.O. Box 2545 Waterloo, IA 50704	8. CONTRACT OR GRANT NUMBER(s) DAAK10-79-C-0093	
11. CONTROLLING OFFICE NAME AND ADDRESS ARRADCOM, TSD STINFO Div. (DRDAR-TSS) Dover, NJ 07801	10. PROGRAM ELEMENT, PROJECT, TASK AREA & WORK UNIT NUMBERS MMT-5784153	
14. MONITORING AGENCY NAME & ADDRESS (if different from Controlling Office) ARRADCOM, LCWSL Munitions System Div. (DRDAR-LCU-M) Dover, NJ 07801	12. REPORT DATE September 1982	
	13. NUMBER OF PAGES	
	15. SECURITY CLASS. (of this report) Unclassified	
	16. DECLASSIFICATION/DOWNGRADING SCHEDULE	
18. DISTRIBUTION STATEMENT (of this Report) APPROVED FOR PUBLIC RELEASE; Distribution Unlimited		
17. DISTRIBUTION STATEMENT (of the abstract entered in Block 20, if different from Report)		
19. SUPPLEMENTARY NOTES This project was accomplished as part of the U.S. Army's Manufacturing Methods and Technology Program. The primary objective of this program is to develop, on a timely basis, manufacturing processes, techniques, and equipment for use in production of Army materiel.		
20. KEY WORDS (Continue on reverse side if necessary and identify by block number) MMT: Shear Tests Martensite Inertia Weld Tear Tests Nondestructive Tests M483 Projectile Peel Tests Ultrasonic Scanning Destructive Testing Acid Etching Dye Penetrant Bend Tests Heat Treatment Light microscopy		
21. ABSTRACT (Continue on reverse side if necessary and identify by block number) Chamberlain defined production process parameters for inertia welding rotating bands to 155-mm M483A1 Projectiles on the high-capacity inertia welder at the Company's New Bedford Division. To reduce disbond at the weld interface, oxidation and impurity levels must be minimized. Acid etching, chemical degreasing and detergent washing were acceptable cleaning methods. Long exposure times were found deleterious to weld quality. (OVER)		

DD FORM 1473 EDITION OF 1 NOV 66 IS OBSOLETE

UNCLASSIFIED

SECURITY CLASSIFICATION OF THIS PAGE (When Data Entered)

UNCLASSIFIED

SECURITY CLASSIFICATION OF THIS PAGE(When Data Entered)

Nondestructive ultrasonic testing of inertia welds was verified by correlating data from ultrasonic scans on the linear transducer array at AMMRC and the single-transducer scanner at Chamberlain. Comparing these data to data from destructive shear and bend tests verified that ultrasonic scanning is an accurate and reliable inspection method of inertia welds.

61 each M483A1 Projectiles with inertia welded rotating bands were heat treated using a relatively fast oil quench. Ultrasonic scanning indicated that projectiles with poorly bonded rotating bands will show a greater degree of disbond after heat treatment; projectiles with well-bonded bands are not adversely affected by heat treatment. It is possible that intimate contact between the steel and copper band would indicate a good bond. However, experimental work performed at AMMRC and at Chamberlain could not demonstrate this effect.

The band and band seat geometry were studied to determine the reasons for poor bonding along the forward edge of the inertia welded rotating band. Since this forward-edge disbond was due to nonuniform pressure on the band during inertia welding, modifying the band seat dimensions to maintain uniform collet pressure will minimize this problem.

Inertia welding rotating bands using various lubricants and coatings was studied to determine the effects on tooling and weld quality. In the limited testing performed, lubricants extended machine deceleration time, reduced the tooling load (hypothetically extending tooling life), and did not adversely affect weld strength.

An intensive metallurgical examination of the rotating band-projectile body interface was conducted by analyzing microstructure, microhardness, and electron microprobe data. These data show that the heat generated by inertia welding forms a martensite layer under the band-band seat interface and recrystallizes the band and band-set material.

20 each abrasion-cleaned and heat-treated M483A1 Projectiles with inertia welded rotating bands were fired in a series of acceptance tests. These projectiles represented a wide range of weld quality, with disbond usually more severe at the leading and trailing edges of the rotating band than at the center of the band. The projectiles were fired to determine any correlation between rotating band damage and deviation from the projectile's desired impact point. Researchers identified no such correlation. In some instances in which ultrasonic scanning showed disbond at the band's edges, there was a loss of band material in these areas due to firing or impact.

A quasi-production run of 261 each M483A1 Projectiles with inertia welded rotating bands was performed at New Bedford using the high-capacity inertia welder. Machine parameters for the inertia welded were: $WK^2 = 1477 \text{ lb.-ft.}^2$; flywheel spin rate = 1740 rpm; and ram pressure = 3600 psi. The dynamic performance of these projectiles was equal to that of 40 control projectiles with overlay welded bands.

UNCLASSIFIED

SECURITY CLASSIFICATION OF THIS PAGE(When Data Entered)

TABLE OF CONTENTS

<u>Section</u>	<u>Page No.</u>
1. INTRODUCTION	1
2. BAND AND BAND SEAT CLEANING	4
2.1 Introduction	4
2.2 Preparation and Cleaning Methods	4
2.3 Component Storage Conditions	9
2.4 Cleaning Procedures	9
2.5 Summary	10
3. INSPECTION FOR QUALITY OF INERTIA WELD BOND	11
3.1 Introduction	11
3.2 Ultrasonic Scanning	11
3.3 Microstructure and Hardness Near Weld	18
3.4 Interface Studies	26
3.5 Scanning Electron Microscopy (SEM)	29
3.6 Ultrasonic Scan Verification by Band Etching and Peeling	30
3.7 Ultrasonic Scan Verification by Torch Heating	34
3.8 Rotating Band Tear Tests	35
3.9 Shear Testing	37
3.10 Bend Testing	43
4. HEAT TREATMENT OF PROJECTILES WITH INERTIA WELDED ROTATING BANDS	47
4.1 Order of Processes	47
4.2 Investigation of Disbond Attributable to Heat Treatment	47
4.3 "Fast" Oil Quench Tolerance	52
4.4 Use of Water Base Quench	53
4.5 Related Stress Study	56
4.6 Conclusions	57
5. VARIATION OF BAND AND BAND SEAT GEOMETRY	58
5.1 Band Seat Parameters	58
5.2 Rotating Collet Geometry	58
5.3 Band and Band Seat Dimensional Variants	60
6. EFFECT OF BAND SEAT COATINGS AND BAND SEAT RAMP ANGLES ON WELDS	65
6.1 Hydraulic Fluid Lubrication	65
6.2 Resin-Based Solder Flux	69
6.3 Additional Observations	70
6.4 Investigation of Various Lubrications	72
6.5 Modified Band Seat Configuration	75

TABLE OF CONTENTS, CONTINUED

<u>SECTION</u>	<u>Page No.</u>
7. INERTIA WELDER ACCEPTANCE TEST FIRING	78
7.1 Test Warhead Preparation	78
7.2 Test Results	78
8. QUASI-PRODUCTION RUN AND TEST FIRING	81
8.1 Quasi-Production Run	81
8.2 Test Firing	83
8.3 Inertia Weld Tooling	85
9. CONCLUSIONS	88
10. RECOMMENDATIONS	91
DISTRIBUTION LIST	92

Accession For	
NTIS GRA&I	<input checked="" type="checkbox"/>
DTIC TAB	<input type="checkbox"/>
Unannounced	<input type="checkbox"/>
Justification	
By	
Distribution/	
Availability Codes	
Avail and/or	
Special	
A	



CHAMBERLAIN MANUFACTURING CORPORATION

1. INTRODUCTION

1.1 Preface

ARRADCOM Contract DAAK10-79-C-0093, an MM&T effort, was awarded to Chamberlain in February 1979 to establish process and production parameters for the high-capacity inertia welding machine installed at Chamberlain's New Bedford Division in February 1980.

1.2 Contract Summary

Chamberlain defined production process parameters for inertia welding rotating bands to 155-mm, M483A1 Projectile bodies on the high-capacity inertia welder located at the Company's New Bedford Division. New welding parameters were established for this inertia welder because it operates on a higher capacity than does Research and Development's and will be used to inertia weld rotating bands on a production basis. Research and Development's machine has been used in several previous contractual efforts related to the development of the inertia welding process, and was also used extensively for this contract prior to the purchase and setup of New Bedford's machine.

To help prevent areas of disbond at the weld interface, program researchers studied cleaning and storing procedures to minimize oxidation and impurity levels on the rotating band and projectile band seat. Either acid etching the bands or machining them without using a lubricant proved to be acceptable band cleaning methods. A detergent wash and hot water rinse, followed by immersion in chemical degreaser, were the accepted steps in cleaning bodies. Various exposure conditions and times were examined; long storage times were found to be deleterious to weld quality.

Nondestructive ultrasonic testing of inertia welds was verified by correlating data from two sources: 1) ultrasonic scanning on the linear transducer array at the Army Materials and Mechanics Research Command

CHAMBERLAIN MANUFACTURING CORPORATION

(AMMRC); and 2) ultrasonic scanning on the single-transducer scanner at Chamberlain R&D. These data, which were compared to data from destructive shear and bend tests, verified that ultrasonic scanning is an accurate and reliable inspection method of inertia welds.

A total of 61 each M483Al Projectiles with inertia welded rotating bands was heat treated using a relatively fast oil quench. Ultrasonic scanning indicated that projectiles with poorly-bonded rotating bands will show a greater degree of disbond after heat treatment, and that projectiles with well-bonded bands are not adversely affected by heat treatment. It is theoretically possible that intimate contact between the steel and the copper band may be indicated as a good bond by ultrasonic scanning. However, experimental work performed at AMMRC and Chamberlain could not demonstrate this effect. As a correlated project, a mathematical model was developed to examine the stresses in the M483Al Projectile during the quench phase of heat treatment. The stresses in the steel were calculated by using finite element analysis. The mathematical analysis is supported by the following observed behavior: 1) increasing frequency of cracking with increasing quench severity for projectiles with welded overlay bands; and 2) absence of cracking with severe quenches in projectiles with inertia welded bands.

Project personnel studied the band and band seat geometry to determine reasons for poor bonding along the forward edge of the inertia welded rotating band. Since this forward-edge disbond was due to nonuniform pressure on the band during inertia welding, modifying the band seat taper and maintaining uniform collet pressure will minimize this problem.

Inertia welding rotating bands using various lubricants and coatings was studied to determine the effects on tooling and weld quality. In the limited testing performed, lubricants extended machine deceleration time, reduced the tooling load (hypothetically extending tooling life), and did not adversely affect weld strength.

CHAMBERLAIN MANUFACTURING CORPORATION

Company personnel conducted an intensive metallurgical examination of the rotating band-projectile body interface by analyzing microstructure, microhardness and electron microprobe data. These data show that the heat generated by inertia welding forms a martensite layer under the band-band seat interface and recrystallizes the band material.

20 abrasion-cleaned and heat-treated M483Al Projectiles with inertia welded rotating bands were fired in a series of acceptance tests. These projectiles represented a wide range of weld quality. Disbond was much more severe at the leading and trailing edges than at the center of the band. The projectiles were fired to determine any correlation between rotating band damage and deviations from the projectile's desired target impact point. Researchers identified no such correlation. In some areas where the ultrasonic scan indicated disbond at the edge of the rotating band, there was a loss of band material. This loss is believed to be due to firing or impact.

A quasi-production run of 261 each M483Al Projectiles with inertia welded rotating bands was performed at New Bedford using the high-capacity inertia welder. Machine parameters for the inertia welder were: $WK^2 = 1477 \text{ lb-ft}^2$; flywheel spin rate = 1740 rpm; and ram pressure = 3600 psi. The dynamic performance of these projectiles was equal to that of 40 control projectiles with welded overlay bands.

CHAMBERLAIN MANUFACTURING CORPORATION

2. BAND AND BAND SEAT CLEANING

2.1 Introduction

In traditional inertia welding, in which the parts to be welded are brought together by an axial thrust, surface contaminants are driven out of the weld area by a "washing action" at the weld interface. Because of this cleaning action during welding, little needs to be done to prepare the surfaces being welded. In inertia welding of rotating bands to projectiles, the axial thrust of the welder is converted to a radial motion and the nature of the weld is such that there is little self-cleaning action. Most of the contaminants on the surfaces being welded are expected to be trapped in the weld.

Surface contaminants can be materials used in machining operations, coatings applied after machining, inert material deposited during storage (dust, oil film etc.), or reactants formed during storage (e.g., metal oxides). Some tests were performed to study the importance of these contaminants in inertia welding. The welding in this series of tests was done on the Materials Technology, Inc. Model 250B inertial welder located at Chamberlain's Research and Development Division and shown in Photo No. 10734. Machine parameters for all welds were: $WK^2 = 425 \text{ lb-ft}^2$ (where: W = rotating group weight, in pounds; and K = radius of gyration, in feet), rotational speed = 2200 revolutions per minute (rpm); and hydraulic pressure = 3800 pounds per square inch (psi).

2.2 Preparation and Cleaning Methods

In the first group of eight welds, the band seats were all machined dry (i.e., no coolants or lubricants were used), immediately coated with a rust inhibitor for protection and wiped clean with reagent grade acetone immediately before welding. Four different methods were used for preparation of the eight rotating bands (the four tests were duplicated) as shown in Table 1.

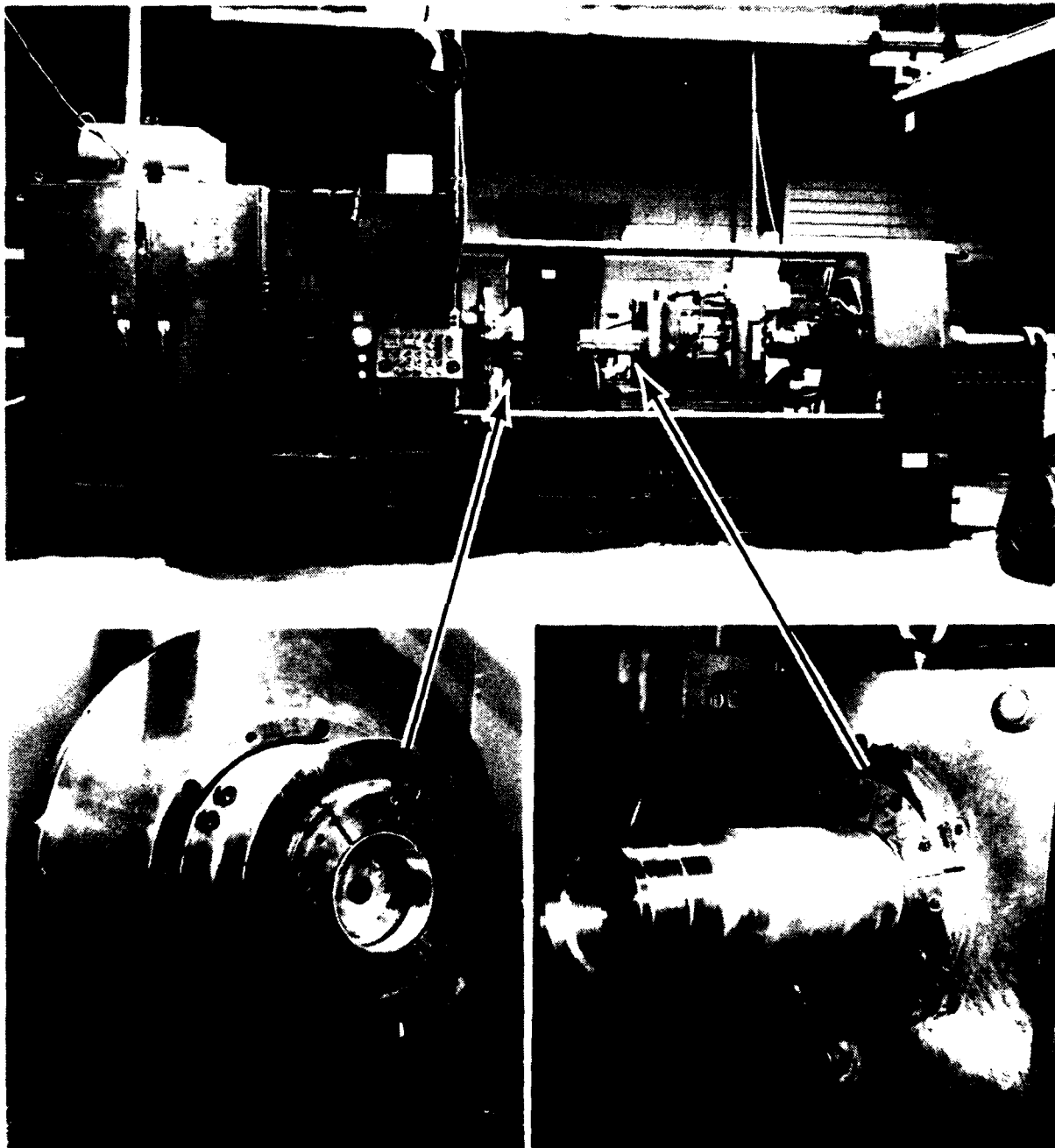


PHOTO NO. 10734

TOP: MODEL 250B INERTIA-WELDING MACHINE.

LEFT: CLOSEUP OF HEADSTOCK SHOWING FLYWHEEL AND 6-JAW COLLET CONTAINING ROTATING BAND.

RIGHT: CLOSEUP OF TAILSTOCK SHOWING 155MM, M483A1 PROJECTILE BODY IN 6-JAW COLLET.

CHAMBERLAIN MANUFACTURING CORPORATION

TABLE 1. COMPARISON OF ROTATING BAND PREPARATION METHODS

Weld Number	Bonded Area		Band Preparation and Cleaning ¹
		Average	
1.1.A 1.1.B	93.35 95.18	94.27	Machine dry. Acetone wipe. ²
1.2.A 1.2.B	92.24 90.67	91.46	Machine dry. Acid etch ³ . Acetone wipe. ²
1.3.A 1.3.B	92.17 95.80	93.99	Machine with lube. ⁴ Acetone wipe. ²
1.4.A 1.4.B	88.45 87.87	88.16	Machine with lube. ⁴ Acid etch. ³ Acetone wipe. ²
¹ All bands stored in polyethylene bags after washing. Removed shortly before welding. ² Band wiped with reagent grade acetone (using clean cheesecloth) immediately before welding. ³ Acid solution: 40% HND ₃ (reagent grade), 60% H ₂ O (deionized). ⁴ Johnson's J-Wax used as lubricant.			

The eight bodies and bands were machined on the same day and the welding was done the following morning. These welds were inspected by ultrasonic scan and were found to contain some disbond due to the incorrect angle of the collet pads during welding (ultrasonic scanning methods and equipment will be described in detail in Section 3.2). Since all welds in this series were made using the same tooling, disbond from that source should be constant. Additional disbond was attributed to surface contaminations.

The data in Table 1 show that there is not a large difference in the bonded area for the four conditions. Considering the average percentage of bonded area, dry machining the bands is marginally better than machining with a lubricant. The acid etch degraded the weld somewhat when machined dry but degraded the weld to a greater extent when machined using a lubricant. Of

CHAMBERLAIN MANUFACTURING CORPORATION

the conditions considered, Chamberlain has concluded that dry machining the bands and wiping them with acetone before welding will yield the best welds.

2.3 Component Storage Conditions

A set of 10 welds (five conditions in duplicate) was made to determine the effect of storage of machined bodies on weld quality. The 10 band seats were dry machined. Six of the bodies were coated immediately with Rust Veto® (a rust preventive coating manufactured by E.F. Houghton and Co.). The other four bodies were left in the dry, as-machined condition.

The 10 bodies were stored in the shop area away from operating machines. After various exposure times (see Table 2), bands were inertia welded to the bodies. The band seats on the four bodies stored dry were not wiped before welding.

The bands used for these 10 welds were dry machined 1 to 2 days before welding, stored in polyethylene bags, removed and wiped with acetone immediately before welding. All 10 band seats looked clean and were as bright as newly machined steel when they were ready for welding. An additional weld was made on a body that was dry machined and stored with no protective coating in a roofed, outdoor environment for 4 to 5 months. The band seat had a very light rust layer over much of its area; the rust was not wiped off prior to welding. Results of the 11 welds are shown in Table 2.

Another set of 10 welds (five conditions in duplicate) was made to determine what effect storage of machined rotating bands has on weld quality. The 10 bands were dry machined. Six of the bands were placed in polyethylene bags immediately after machining. The other four were left exposed in the dry, as-machined condition.

CHAMBERLAIN MANUFACTURING CORPORATION

The 10 bands were stored with the previously-described bodies in the shop area. After various exposure times, the bands were inertia welded to freshly machined bodies. The band seats of these bodies, which were machined a maximum of 1 day before welding, were coated with Rust Veto® after machining and wiped clean with acetone immediately before welding. The bands were not wiped or cleaned in any way before welding. Results of these welds are shown in Table 2. Bagging the rotating bands was an ineffective method of preventing contamination.

TABLE 2. EFFECT OF COMPONENT STORAGE TIME
(AFTER CLEANING) ON INERTIA WELD QUALITY

Component Exposed	Storage Condition	Exposure time (days)	% of Bonded Area	Average
Body	Rust Veto	32	98.22	97.33
		32	96.44	
		68	99.00	97.79
		68	96.58	
		79	90.64	
	Air	79	98.39	94.52
		32	93.88	93.30
		32	92.72	
		69	94.63	95.94
		69	97.24	
		120-150	52.00	52.00
Rotating Band	Bagged	29	82.50	76.83
		29	71.15	
		66	86.19	92.92
		66	99.64	
		79	83.42	
	Air	79	83.01	83.22
		29	84.96	90.51
		29	96.05	
		68	99.29	93.53
		68	87.76	

CHAMBERLAIN MANUFACTURING CORPORATION

The data are fairly scattered, but it is generally observed that exposure to air for a given time is more deleterious to bands than to bodies. Bodies stored for up to 69 days with no protection and up to 79 days with a rust preventive coating showed no significant decrease in weld quality when welded to freshly made bands. However, a body exposed for approximately 135 days and having light rust on the band seat surface made a very poor weld. For welds made with stored bands there was a variation in degree of bonding that did not correlate with the length of storage time or protection. In general, these welds were of significantly poorer quality than those made with freshly machined bodies and bands. The average bonded area for welds with stored bands was 87.4 percent, compared to 94.3 percent for welds made with freshly machined components. (These values are for welds made under the best conditions shown in Table 1.)

2.4 Cleaning Procedures

For initial trials at Chamberlain's New Bedford Division, rotating bands were not machined or chemically cleaned, but simply wiped with a solvent. Weld quality was very poor. Improvements were made during the program and prior to the welding of 261 rounds in the quasi-production run. In accordance with these improvements, the following procedures were established: 1) bodies were cleaned in the standard production cleaning line using a detergent and hot water rinse; 2) immediately before loading into the inertia welder, the aft end of each body (including the band seat area) was immersed in a commercial degreaser solution; 3) the bodies were removed from the solution, wiped dry, and mounted in the welder; and 4) rotating bands were cleaned by immersion for about 10 minutes in a 95-percent phosphoric acid/ 5-percent nitric acid solution, then water rinsed and dried by wiping.

New Bedford personnel observed that rotating bands began to show visible tarnish about 10 to 15 minutes after cleaning, and that weld quality

CHAMBERLAIN MANUFACTURING CORPORATION

decreased when a tarnished band was used. For the quasi-production run, if delays resulted in a band becoming tarnished, the band was either cleaned with steel wool or put back into the acid solution. Machined rotating bands remained bright for a minimum of 3 days, and only very slight darkening was noted even after 29 days exposure to air. This difference in behavior between the machined and acid-etched bands can be attributed to the more chemically active surface created by acid etching.

2.5 Summary

In summary, component cleanliness has been shown to be essential to good quality welds, although cleanliness requirements are more stringent for rotating bands than for bodies. Bands may be cleaned either by machining the bands without lubricant or by acid etching. When acid etching is used, the active surface will begin to tarnish in 10 to 15 minutes, so it is essential that the welding is done immediately after cleaning. If the band is machined, it can be stored for at least 1 day before welding. Bodies can be stored for longer times (up to 2 months) after machining, but they must be stored in a sufficiently dry environment so that rusting does not occur.

CHAMBERLAIN MANUFACTURING CORPORATION

3. INSPECTION FOR QUALITY OF INERTIA WELD BOND

3.1 Introduction

A rapid and reliable method for inspecting inertia welded rotating bands is necessary to make inertia welding a viable production process. Inspection by ultrasonic scanning has been used in earlier contract work and has been the primary inspection method used in work associated with this contract.

A number of auxiliary tests have been performed on welded bands in an attempt to verify ultrasonic scan information and to better understand the welding process. Ultrasonic scanning results and the results of auxiliary tests will be described in subsequent sections of this report.

3.2 Ultrasonic Scanning

3.2.1 Equipment

The ultrasonic scanning equipment used throughout the contract period consisted of a Tektran Immerscope II, a Tektran Immersion Tank, and a 5-megahertz transducer with an in-water focal length of 2-1/2 inches (shown in Photo No. 10732). The immersion tank and its associated scan recorder were designed so that the shell being inspected and the recording drum rotated synchronously about their axes while the transducer and writing tip were translated synchronously parallel to the axes. The writing tip then described a fine pitch screw pattern on the electrostatic dry recording paper. Scans were taken from either the inside or outside of the shell, whichever was more convenient. Tests showed that the same result was obtained for either method. Transducer standoff was adjusted so that the transducer was focused on the weld interface as much as possible. This maximized the sensitivity in locating small areas of disbond.



PHOTO NO. 10732

ULTRASONIC SCANNING EQUIPMENT - - INSET: PROBE AT BOTTOM AND CHART
RECORDER AT TOP.

CHAMBERLAIN MANUFACTURING CORPORATION

3.2.2 Transducer Alignment with Shell Wall

Before parts with standard machined flaws were available, the transducer was aligned by adjusting its position until the signals reflected from the shell wall were maximized, indicating that the ultrasonic beam was perpendicular to the shell wall. The transducer was positioned so that its beam struck on the shell wall just forward of the rotating band. The signal amplification was set by adjusting the gain until the first-order reflected peak from the back wall of the shell was at full scale (10 cm) on the oscilloscope display. The 10-cm oscilloscope display was defined as a 100-percent reflection.

3.2.3 Flaw Level Settings

The reflection from a good quality inertia weld was found to be 5 to 8 percent. The flaw level was typically set at 20 percent; any reflections from the welded interface above 20 percent were indicated on the recording paper as flaws, or regions of disbond. Tests showed that the flaw level setting (over a relatively wide range) had little or no effect on the ultrasonic scan obtained for a given weld. The reason for this could be seen by slowing the rotation of the shell during scanning and observing the reflection from the weld interface on the oscilloscope screen. In going from a bonded to disbonded region, the reflection typically changed suddenly from a 5- to 10-percent reading to a 50- to 100-percent reading. Therefore, flaw level settings between approximately 10 percent and 50 percent gave the same recording.

3.2.4 Comparison with AMMRC Results

Approximately 60 projectiles with inertia welded rotating bands were ultrasonically scanned at Chamberlain using the ultrasonic equipment described above. These were shipped to the Army Materials and Mechanics Research Command (AMMRC) to be scanned on their equipment, which was a

CHAMBERLAIN MANUFACTURING CORPORATION

multiple-head transducer that is capable of recording the entire width of the rotating band in one rotation. Total scanning time for AMMRC's unit is about 10 seconds, compared to 3 to 5 minutes for scans made with a single transducer. Despite the equipment differences, Chamberlain and AMMRC scanning results were in excellent agreement.

There is a possibility that ultrasonic scanning could indicate a good bond where a disbond actually exists. Theory indicates that, for the conditions of this work, any air gap greater than 10^{-7} mm should be indicated by ultrasonic scanning as a disbond. However, this estimate is for atomically smooth and perfectly clean surfaces. With a layer of foreign material in the gap having a higher impedance than air, a significantly larger gap could cause sufficient reflection to indicate a good bond.

While this possibility of erroneous ultrasonic scanning does exist, it was not evident in any of the projectiles whose ultrasonic scan indication was verified by destructive testing, as described in Sections 3.6 through 3.10

3.2.5 Weld Quality Rating

The percentage of band seat area that is welded (as indicated by ultrasonic scanning) is used throughout this report as one measure of weld quality. It should be recognized that the distribution of disbanded areas is also an important parameter, but is difficult to quantify. In general, it is expected that one large disbond area is a more severe condition than several small, widely-separated disbond areas. Also, disbonds at the edges of the band are a more severe condition than disbonds toward the center of the band.

3.2.6 Standard Flaws for Production Inspection

For production inspection, an ultrasonic standard (i.e., a part similar to the inspected hardware that has known, "standard" flaws) is necessary for

CHAMBERLAIN MANUFACTURING CORPORATION

use in aligning and verifying the sensitivity of the ultrasonic inspection equipment. Such a standard was made under contract DAAA25-76-C-0345 by: 1) scanning the portion of a shell containing an inertia welded rotating band into quarter sections; 2) drilling flat-bottomed holes ranging from 0.025 to 0.080 inch in diameter through the steel to the steel/rotating band interface; and 3) welding the quarter sections back together to form a ring. When the standard is ultrasonically scanned, sound waves, directed from the outside of the projectile, pass through the rotating band and reflect from the flat-bottomed holes, which simulate areas of disbond. In Contracts -0345 and -0093, reflections were detected for all hole sizes down to the 0.025-inch diameter, indicating that actual disbond areas of this size should be detectable. The total intensities reflected should have varied monotonically with hole size, but this variation was not observed. Apparently, the bottoms of the holes were not uniformly flat and smooth (possibly due to corrosion from long use in water), or were not perpendicular to the radii of the projectile. New ultrasonic standards were fabricated, with careful attention paid to the orientation and flatness of the hole bottom and to the avoidance of corrosion during use. Since it was not yet established whether production parts would be scanned from the inside or outside, standards were prepared for both methods. To select parts from which standards were to be made, a group of 20 projectiles known to have nearly defect-free inertia welded bands was carefully inspected. Two parts with the lowest weld interface reflection were chosen.

A series of nine holes, ranging from 0.120 to 0.020 inch in diameter, was drilled in each part by electrical discharge machining (EDM). To calibrate for scanning from inside the shell, one of the standards was drilled from the outside. For outside scanning, the other standard was drilled from the inside. This was possible with EDM by using an electrode with a 90-degree bend for drilling. By frequent removal and redressing of the electrode, holes with very flat and smooth bottoms were drilled. After drilling, the holes were cleaned by injecting alcohol into them with a hypodermic needle.

CHAMBERLAIN MANUFACTURING CORPORATION

This was repeated several times to remove any oil and moisture from the holes. The parts were then held for several hours at approximately 180°F to evaporate all liquid. A commercial rust inhibitor, Houghton's Rust Veto®, was injected into each hole while the hole was still warm, and the holes were covered with a rubberized water-sealing tape. Drawings of the standards are shown in Figures 1 and 2.

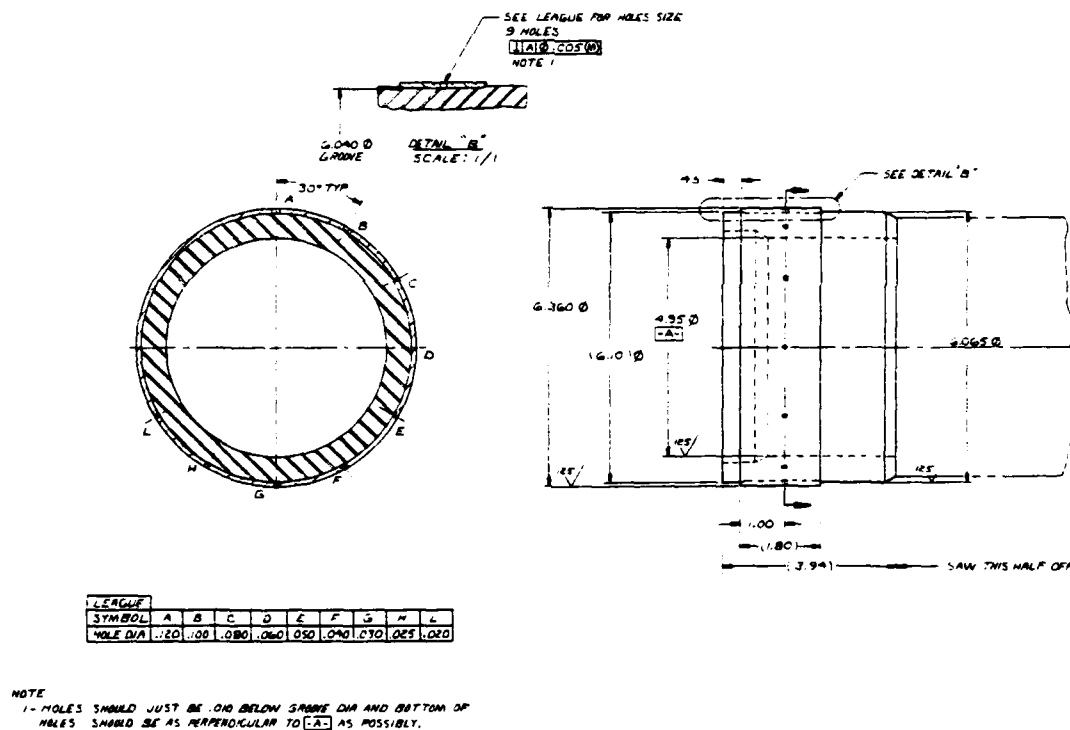


FIGURE 1. ULTRASONIC TEST STANDARD FOR
SCANNING FROM INSIDE (DRAWING NO. J8184-1D)

With the signal gain set as described in Section 3.2.2, the 0.040-inch diameter holes in both shells with standard flaws were clearly visible, and

CHAMBERLAIN MANUFACTURING CORPORATION

the 0.030- inch diameter holes were faintly visible. By increasing the gain, it was possible to see all the holes down to 0.020 inch in diameter. The relative size of the indication of the holes on the scan tracer varied correctly with the actual size of the holes. However, the indicated hole sizes on the tracer were two to three times larger than the actual hole sizes. This is at least in part attributable to the fact that a sound beam from a circular transducer striking a cylindrical surface will not focus precisely at the weld interface. Thus, flaw indications will be somewhat larger than the actual flaws. With amplification set at the value required to clearly show the 0.020-inch diameter hole, the background noise became so high that random flaw indications were generated. The smallest flaw size detectable by the Chamberlain equipment is approximately 0.030 inch in diameter. Up to this point in Contract -0093, the gain settings that were used apparently permitted seeing flaw sizes down to 0.040 inch in diameter.

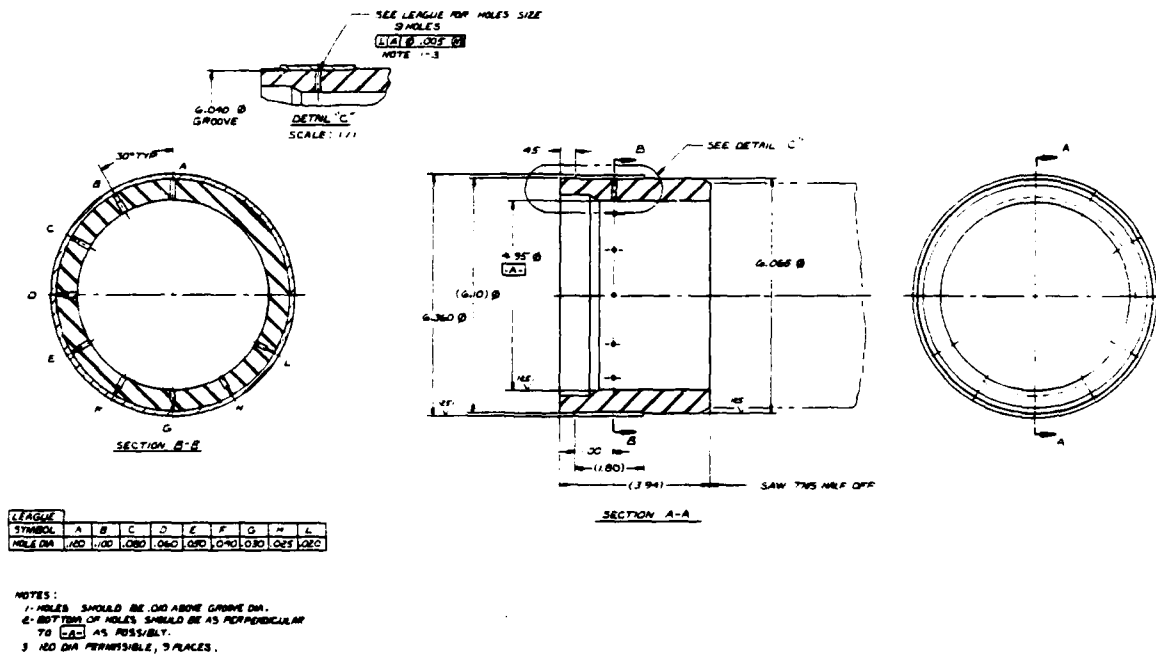


FIGURE 2. ULTRASONIC TEST STANDARD FOR
SCANNING FROM OUTSIDE (DRAWING NO. J8184-2D)

3.3 Microstructure and Hardness Near Weld

3.3.1 Effect of Increased Temperature

In the inertia welding process, a large amount of energy is converted to heat in a very short time. The elevated temperatures reached at and near the weld interface are expected to cause some microstructural and hardness changes. Chamberlain researchers wished to identify any correlation between these changes and weld quality (as shown by ultrasonic scan).

3.3.1.1 Martensite Formation

An important microstructural change is the formation of martensite in steel near the weld interface. The temperature reached at the interface is believed to be near the melting point of the steel. Some of this heat is conducted away through the steel, forming a steep temperature gradient away from the weld interface. When the weld is completed, heat generation ceases, and the heat in material close to the interface is rapidly conducted into the relatively cool steel, away from the interface. This rapid cooling constitutes a quench for the steel, so that material which has exceeded the critical temperature for the conditions (probably about 1500°F) will be converted to the martensitic phase. The thickness of this martensite should be a function of: 1) the total amount of energy generated at the weld interface; and 2) the rate at which this energy is generated.

A selected set of specimens was prepared for measuring the thickness of the martensite layer. Ultrasonic scans of the inertia welds are shown in Photograph No. 11567, as is the location of cross-sections cut from these welds. The thickness of the martensite layers as a function of position along the rotating band is shown in Figure 3. The two samples from Weld 2B were taken from regions of good weld and revealed a martensite thickness that varied smoothly from about 0.015 to 0.017 inch for both samples. For

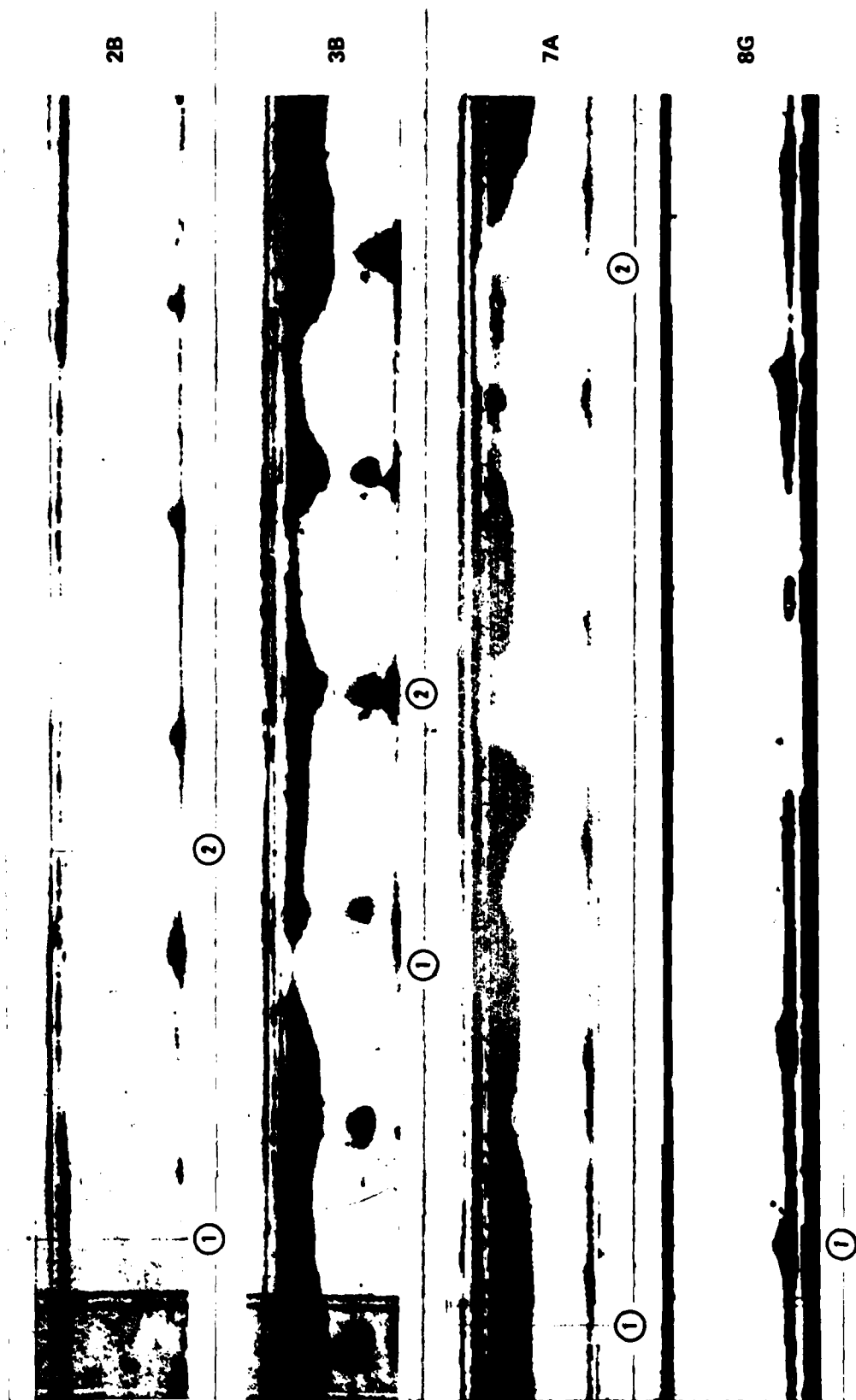


PHOTO NO. 11567

ULTRASONIC C-SCAN OF WELDS FOR MARTENSITE THICKNESS MEASUREMENTS

CHAMBERLAIN MANUFACTURING CORPORATION

Weld 3B, Sample No. 1 was from a region of good weld and Sample No. 2 was from a region which was almost completely disbonded. The martensite thickness did not vary smoothly along the interface, but the curves, as seen in Figure 3, are very similar. This result indicates that the martensite thickness is not a good indicator of weld quality.

For Weld G8, the rotating band was machined so that it tapered fore to aft. The pressure applied during welding was greatest at the leading edge and decreased toward the aft of the band. Photograph No. C3958 shows this section after it was etched to show the martensite layer. The measured thickness of martensite is reasonably consistent with this condition, indicating that, at lower pressures, less heat was generated and less martensite formed. The ultrasonic scan showed disbond only for the aft 0.1 to 0.2 inch, which indicates that a good weld was obtained with only enough heat to generate a martensite layer 0.004 to 0.008 inch thick. Considering that Weld 3B at Section No. 2 had disbond with a martensite thickness of about 0.020 inch, it is evident that heat input alone is not sufficient to ensure a good weld.

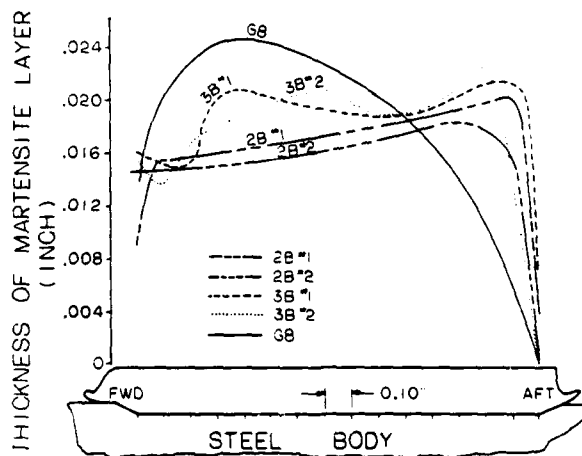


FIGURE 3. MARTENSITE THICKNESS UNDER ROTATING BAND
FOR SEVERAL INERTIA WELDS



PHOTO NO C-3958

CROSS SECTION OF INERTIA WELD G8 SHOWING MARTENSITE UNDER BAND

3.3.1.2 Recrystallization

The heat generated during welding is expected to affect the grain size of the copper bands by recrystallization and grain growth mechanisms. Measurements on samples of the starting band material showed the grain size (average grain diameter) to be about 0.025 inch. The grain size distribution in the bands after welding is shown in Figure 4.

The refinement of the grain size near the weld interface is interpreted as being recrystallization caused by heating above a critical temperature. Because of the very short times involved, the recrystallized grains have no opportunity to grow. The 0.0025-inch grain size regions have not become hot enough to recrystallize, so they retain their original size.

Welds 2B1 and 2B2, both good welds, show a uniform layer (0.045 to 0.050 inch thick) of recrystallized material adjacent to the weld interface. The section at Position 1 of Weld 3B was shown by ultrasonic scan to be bonded across the full band width. However, most of Weld 3B had disbond about 0.5 inch wide along the leading edge. Section 1 was taken at a location where there was full band width bonding for a short distance along the circumference. The microstructure of the band (see Figure 4) shows a uniform layer (0.045-0.050 inch thick) of recrystallized material from the aft end of the band to a point 0.4 to 0.5 inch from the forward end. At this point, the thickness of the recrystallized material begins to decrease at the forward end of the band. This indicates a diminished heat input near the leading edge of the band compared to the aft two-thirds of the band. Apparently, there was reduced pressure during welding along the leading edge and the heat was insufficient to cause a weld around most of the circumference. The heat input was, for some reason, slightly higher at Section 1 and welding occurred.

The section at Location 2 of Weld 3B (Figure 4) shows a similar effect. Here, bonding occurred for a short distance near the center of the band, and a corresponding layer of recrystallized material is seen in this

CHAMBERLAIN MANUFACTURING CORPORATION

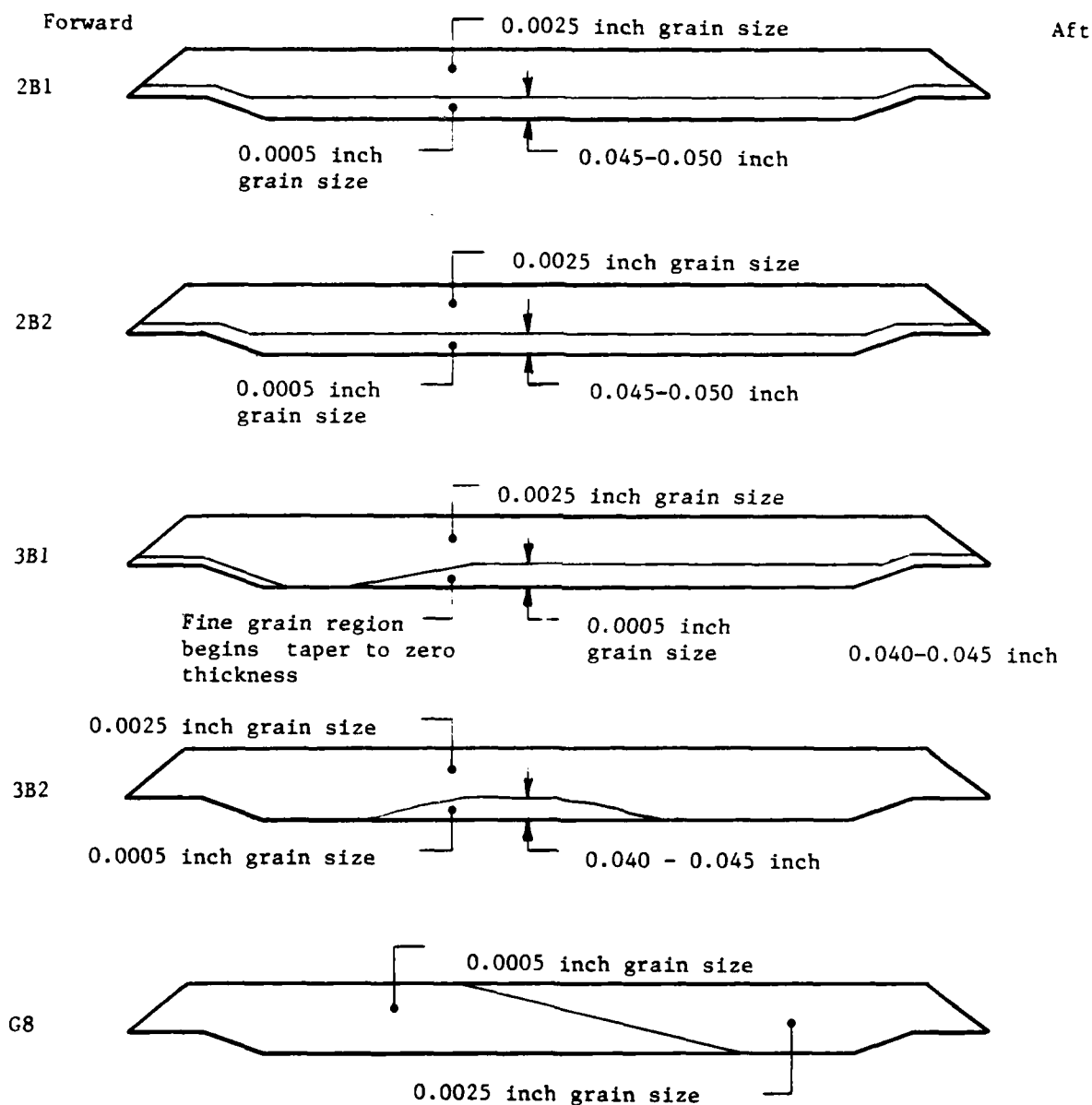


FIGURE 4. GRAIN SIZE DISTRIBUTION IN COPPER
ROTATING BANDS AFTER INERTIA WELDING

CHAMBERLAIN MANUFACTURING CORPORATION

region. Weld G8, in which the band was tapered fore to aft to create a steep pressure gradient during welding, shows extreme microstructural effects. The forward portion of this section, in which weld pressure was large, is recrystallized completely through the band thickness. Moving toward the aft section of the band, the weld pressure decreased and the thickness of recrystallized material decreased, reaching zero shortly beyond the mid-point of the band.

The thickness variation of the recrystallized portion of the bands correlated well with indications of bond and disbond by ultrasonic scan. Further, the ultrasonic scan (for a selected acceptance-gate level) shows only bond or disbond. The thickness of the recrystallized layer of band material is more sensitive and will show variations in pressure during welding.

The foregoing analysis of microstructure was based on structures analyzed immediately after welding. The manufacturing method used in this program required quench and temper heat treatment after welding. After this heat treatment, the steel microstructure was uniform; there was no apparent difference between the region connected to martensite during welding and the surrounding material. The material in the rotating band also became uniform, with grain diameters of 0.025 to 0.040 inch.

3.3.2 Hardness Measurements

Hardness of the steel after inertia welding was measured using the Vickers scale with a 200-gram load. The indentations were of such a size that readings could be spaced at 0.002-inch intervals. Measurements were made in the steel over the range 0.002 to 0.032 inch from the weld interface. Two bonded regions and two unbonded regions from Welds 3B and 7A, all with a martensite layer thickness of about 0.018 to 0.020 inch, were measured. The data were all within the relatively narrow band shown in Figure 5. Note that the hardness is at its minimum just beyond the martensite layer, and then rises a small but discernible amount. This is interpreted as

CHAMBERLAIN MANUFACTURING CORPORATION

indicating subcritical annealing of the forged structure just beyond the martensite.

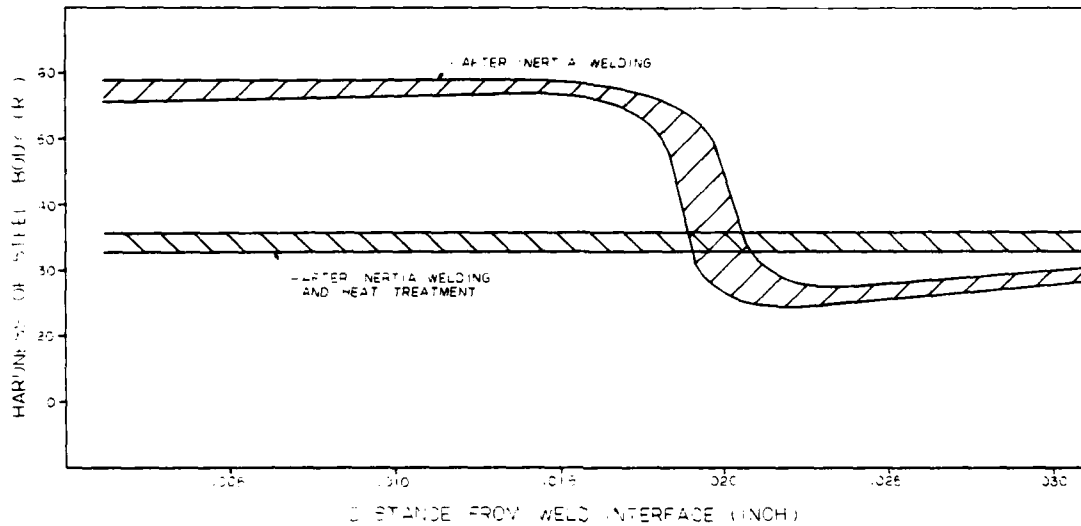


FIGURE 5. HARDNESS IN STEEL BODY UNDER ROTATING BAND

Hardness measurements using the Rockwell 15-T superficial scale were made on several rotating bands in the as-welded condition. These were made near regions of bond and disbond in the band. No significant difference in hardness existed between bonded and disbanded regions. Weld G8 yielded several measurements in the fine-grained and coarse-grained material. No difference in hardness was found. The average value for six sets of measurements was:

$$71.2 R_{15-T} \approx 33 R_B \approx 76 R_F$$

Hardness measurements were made in the steel body and the rotating band after heat treatment. All the hardness values for four sets of data in the

CHAMBERLAIN MANUFACTURING CORPORATION

steel fit within the band shown in Figure 5. It is seen that the hardness is level to within 0.002 inch of the weld interface at a value of $38 \pm 1.5 R_C$. Measurements in the rotating band material of samples from several heat treated shells gave an average value of:

$$54.5 R_{15-T} \approx 50 R_F$$

There was significant softening in the band material due to heat treatment.

3.4 Interface Studies

3.4.1 Light Microscopy

Chamberlain conducted tests in an attempt to correlate the appearance of a bond line, as viewed by a light microscope, with ultrasonic scan results. A total of seven cross sections was taken from three previously-scanned projectiles. These projectiles had all been heat treated by oil quench and temper. The sections were ground flat, polished and examined in a metallurgical microscope with normal-incident light. The results are shown in Figure 6. The quality ratings given in the figure (good, medium, bad) for light microscopy observations are somewhat subjective. No regions at the weld interface could positively be called disbonds. In four of the samples, regions shown by ultrasonic scanning to be disbonded showed no evidence of disbonding through the microscope.

Conversely, in two of the samples, portions of the interface that appeared to be disbonded in the microscope were shown by ultrasonic scanning to be bonded. Therefore, it is concluded that light microscopy is not a suitable method for determining whether or not bonding has occurred.

3.4.2 Liquid Penetrant

The liquid penetrant Zyglo® was applied to the samples from heat-treated projectiles shown in Figure 6 to indicate areas of disbond. Only one

CHAMBERLAIN MANUFACTURING CORPORATION

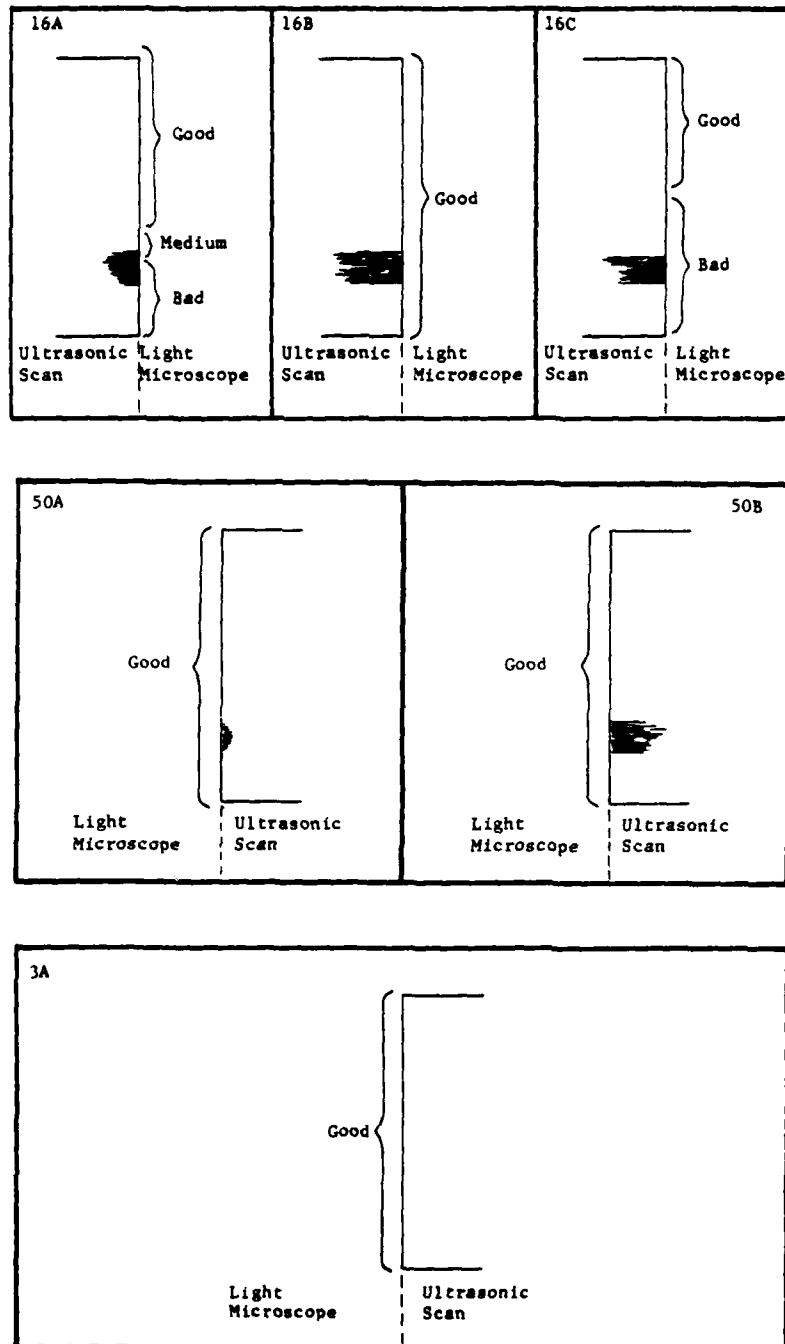


FIGURE 6. COMPARISON BETWEEN ULTRASONIC SCANNING INDICATION AND MICROSCOPIC INDICATION

CHAMBERLAIN MANUFACTURING CORPORATION

sample, 16C, indicated disbond in a location that was in agreement with the disbond area indicated by the ultrasonic scan. On two other samples, 16B and 50B, the Zyglo® gave a faint indication of disbond in areas where the ultrasonic scan showed good bonding. In Samples 3A, 16A and 50A, Zyglo® gave no indication of disbond, which should have been the case in Sample 3A, although discrepancies in correlation among the other samples detract from this particular "no show" correlation.

A sample was cut from a poorly bonded 105-mm projectile whose band was inertia welded in a previous study (Contract DAAK10-78-C-0426). Ultrasonic scanning indicated poor bonding along most of the sectioned band seat. Penetrant testing with Zyglo® gave positive indications at only two spots along the indicated disbond. When the bond was subsequently torn from the band seat with pliers, blackened areas on the band seat were revealed in the two small areas that gave positive indications with Zyglo®. These indicate regions where there was no contact between the band and band seat and where the band seat was oxidized during the inertia welding operation. The use of Zyglo® in another previous study (Contract DAAA25-76-C-0345) resulted in good correlation with ultrasonic scans, although samples used in that contract contained far poorer welds than the samples in question here.

Chamberlain researchers have concluded that the dye penetrant Zyglo® is a less sensitive indicator of disbond than is ultrasonic scanning.

3.4.3 Interface Inspection of Ballistically Tested Projectiles

Three ballistically tested M483A1 Projectiles with bands inertia welded after heat treatment were inspected for cracks in the band seat. The projectiles were of interest because the inertia welding resulted in a brittle layer of martensite forming directly under the band. There was no loss of band material due to firing or impact and ultrasonic scanning revealed no disbonding. The bands were machined to a 0.010 to 0.020-inch

CHAMBERLAIN MANUFACTURING CORPORATION

thickness and the last portion was chemically removed with an acid mixture, which did not attack the steel band seat. Zyglo® testing gave several indications about 0.1 inch long and parallel to the projectile axis. Sections cut through these indications showed that they were not cracks, but were shallow cavities left when elongated, nonmetallic impurities (normal in this grade of steel) were removed by the acid used to remove the band material. A tentative (due to small sample size) conclusion is that the brittle layer that is formed in the band seat during inertia welding will not fracture during gun firing and subsequent ground impact.

3.5 Scanning Election Microscopy (SEM)

Samples for scanning electron microscopy (SEM) were obtained from an M483A1 Projectile with a conventional overlay welded band, designated OW, and two M483A1 Projectiles with inertia welded rotating bands, designated 3A and 3B. The three projectiles were given a standard heat treatment prior to sample removal. Ultrasonic scanning showed no disbond in the 3A and 3B welds. Cross-sectional samples of the three projectiles' band/band seat interfaces were examined at a consultant's laboratory by electron microprobe and by SEM. Scanning electron micrographs of the samples are shown in Photograph Nos. 11602, 11603 and 11604. Two observations from a comparison of these microphotographs are:

- There is a definite alloying region 0.0003 to 0.0005 inch wide at the interface of the welded overlay band; no corresponding interface is apparent in the inertia welded samples.
- There is a significant amount of porosity at the interface of the welded overlay band; none is evident in the inertia welded bands.

Microprobe analyses of the apparent alloying region at the interface of the welded overlay band indicated that the alloy was 78 percent copper and 11 percent iron near the band edge, and 48 percent copper and 50 percent iron

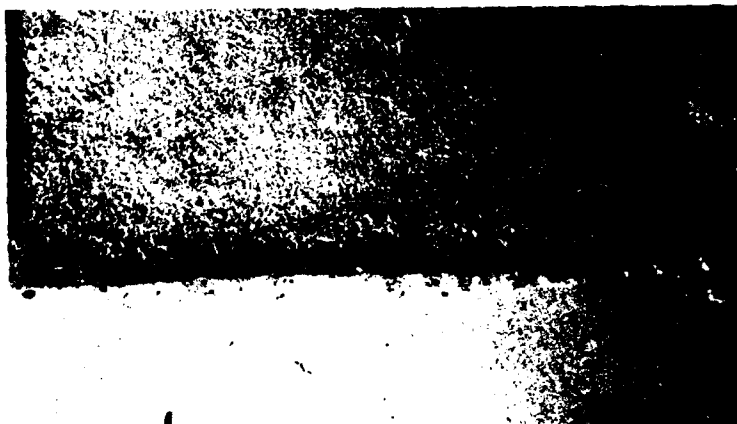
near the steel band seat edge. This indicates a continuously varying composition across the alloying region, which would be expected from the phase diagram that shows limited solid solubility and no compounds. There was significant diffusion of copper into steel for a distance of 0.0024 inch from the interface, and of iron into copper for 0.0014 inch from the interface. These are rather short distances for a fusion weld, primarily because of the rapid cooling of the weld region by the internal water spray used during welding.

In inertia welding, as compared to overlay welding, the heating and cooling rates are higher and the time at elevated temperatures is shorter. Consequently, no alloying zones can be seen at magnifications below 1000X. There was significant diffusion of copper into steel for 0.00004 to 0.00030 inch from the interface, and of iron into copper for 0.001 to 0.002 inch from the interface.

Comparison of the diffusion results shows that diffusion of copper into steel in overlay welding was at least 10 times greater than in inertia welding. This indicates that, in overlay welding, the steel becomes hotter and/or remains at elevated temperatures longer than in inertia welding. Diffusion of iron into copper is nearly the same for the two processes, indicating that the time/temperature histories of the rotating band, in the vicinity of the interface, are comparable.

3.6 Ultrasonic Scan Verification by Band Etching and Peeling

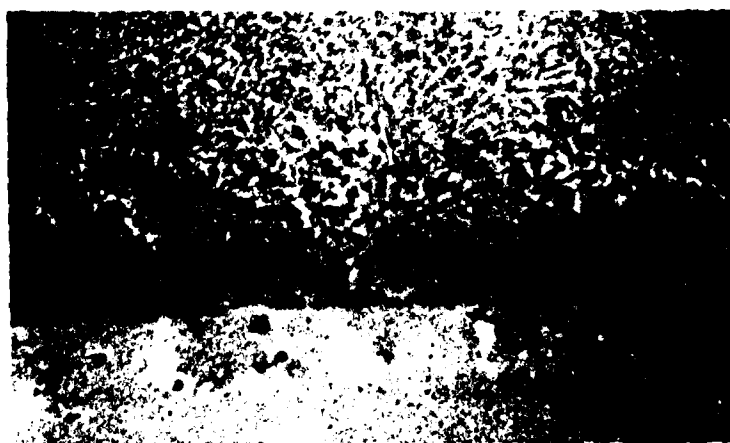
In previous work on inertia welding (Contract -0345) ultrasonic indications of disbonded areas were verified by machining the band to within a few-thousandths of an inch of the interface and then peeling away the band in the disbonded areas. Attempts to duplicate this in the present contract were only partially successful. Since the band seats were not machined relative to a good surface on the projectile body, it was not possible to obtain thin and uniform band layers by machining. Ten heat-treated projectiles with inertia welded bands, each with some degree



300X



500X



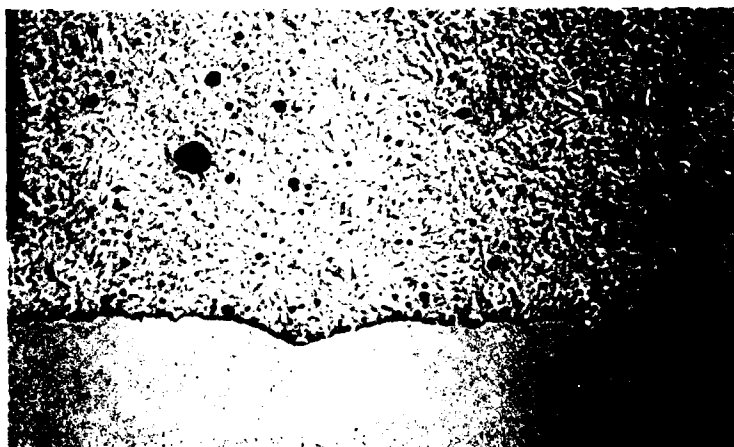
1000X

PHOTO NO. 11602

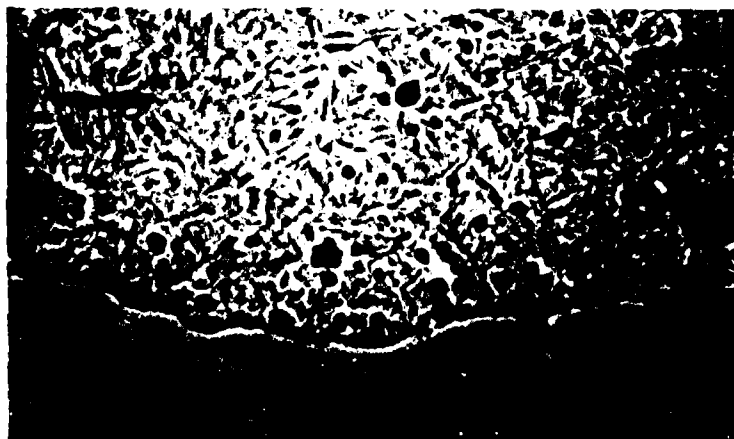
SCANNING ELECTRON MICROGRAPH OF BAND/BAND SEAT INTERFACE FOR OVERLAY WELDING.



300X



500X



1000X

PHOTO NO. 11603

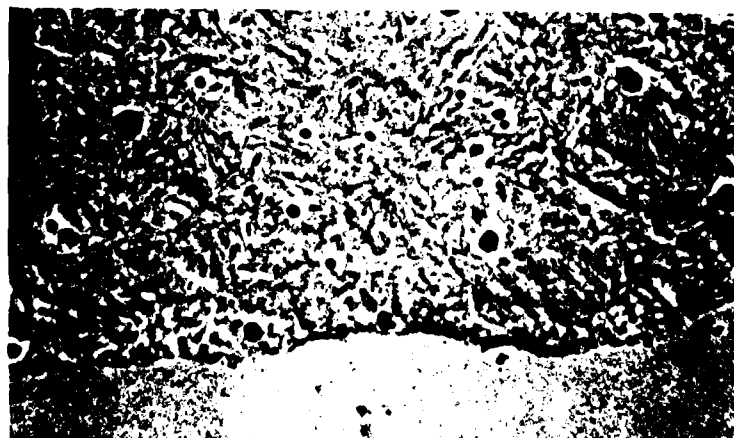
SCANNING ELECTRON MICROGRAPH OF BAND/BAND SEAT INTERFACE FOR INERTIA WELDING.



300X



500X



1000X

PHOTO NO. 11604

SCANNING ELECTRON MICROGRAPH OF BAND/BAND SEAT INTERFACE FOR INERTIA WELDING.

CHAMBERLAIN MANUFACTURING CORPORATION

of disbond indicated by ultrasonic scan, were machined until the cutting tool went through the band and into the steel band seat at one location around the circumference. In four of these parts, disbond was detected in the region where the band was very thin. Since the band was easily peeled away in those regions indicated by ultrasonic scan to be disbanded, Chamberlain researchers concluded that the test did verify the ultrasonic scan results.

A more satisfactory test would require that the band seat be machined by holding the projectile on a machined surface so that the band could later be machined to a uniform thickness.

To overcome the difficulty described in the previous paragraph, several bands were machined to within an estimated 0.040 inch of the band seat and the band was further removed by chemical etching. It was found to be very difficult to stop the etching action when the band was thin enough for peeling. Usually, the band etched away completely. There was no visible difference in the band seat at bonded versus disbanded areas, and the tests were deemed inconclusive.

3.7 Ultrasonic Scan Verification by Torch Heating

Ultrasonic scan verification tests were conducted using the response of unbonded areas to oxyacetylene torch flame and to oxyacetylene torch flame with a reduced oxygen flow followed by a flame with a normal oxygen flow. For both types of tests, an inertia welded band on a heat-treated projectile showing considerable disbond on ultrasonic scans was machined to a thickness ranging from 0 to 0.020 inch, a variation caused by projectile eccentricity relative to the lathe axis.

Oxyacetylene torch flame was applied to the band. Shallow bubbles, (i.e., raised areas), appeared within seconds as areas of the band over regions of disbond expanded. Areas of the band over well-bonded regions did not

CHAMBERLAIN MANUFACTURING CORPORATION

bubble. It was concluded that the lack of bonding allowed thermal expansion to cause bubbles in response to applied oxyacetylene torch flame.

An oxyacetylene torch flame with a reduced oxygen flow was applied to a second band on a heat-treated projectile. The reducing flame caused a uniform black layer of carbon to form on the band. The oxygen flow of the flame was increased to a normal level, causing the carbon on unbonded areas to become oxidized. These unbonded regions appeared as bright surfaces and were surrounded by carbon-blackened, well-bonded areas. It was concluded that heat was conducted rapidly from the band to the body in well-bonded regions; therefore, carbon on the band surface did not get hot enough to oxidize. Heat was conducted from band to body poorly, if at all, in unbonded regions; therefore, band temperature increased rapidly, and the carbon was oxidized away.

Disbond locations on ultrasonic scans of the welds were compared to bubbles on the first weld, and bright regions on the second weld. The correlation was excellent. The bubbled regions on one of the bands were removed by peeling. These regions came off relatively easily, but at the boundaries of the bubbles, the band material tore. Photograph No. C3838 shows two angles of the band after tearing off all loose material and the corresponding ultrasonic scan. The correlation between the scan and the disbanded areas is seen to be quite good.

3.8 Rotating Band Tear Tests

Attempts were made to compare the peel strength of welded overlay bands with the peel strength of inertia welded bands. All projectiles were heat treated prior to testing. The procedure was to machine the band to a thickness of about 0.030 inch and to make a cut parallel to the projectile axis through the band. A lip of band material was generated by chiselling under the band. This lip was clamped in the jaws of a tensile machine and pulled in an attempt to peel away the band. With welded overlay bands and with well-bonded inertia welded bands, the lip always tore away before any

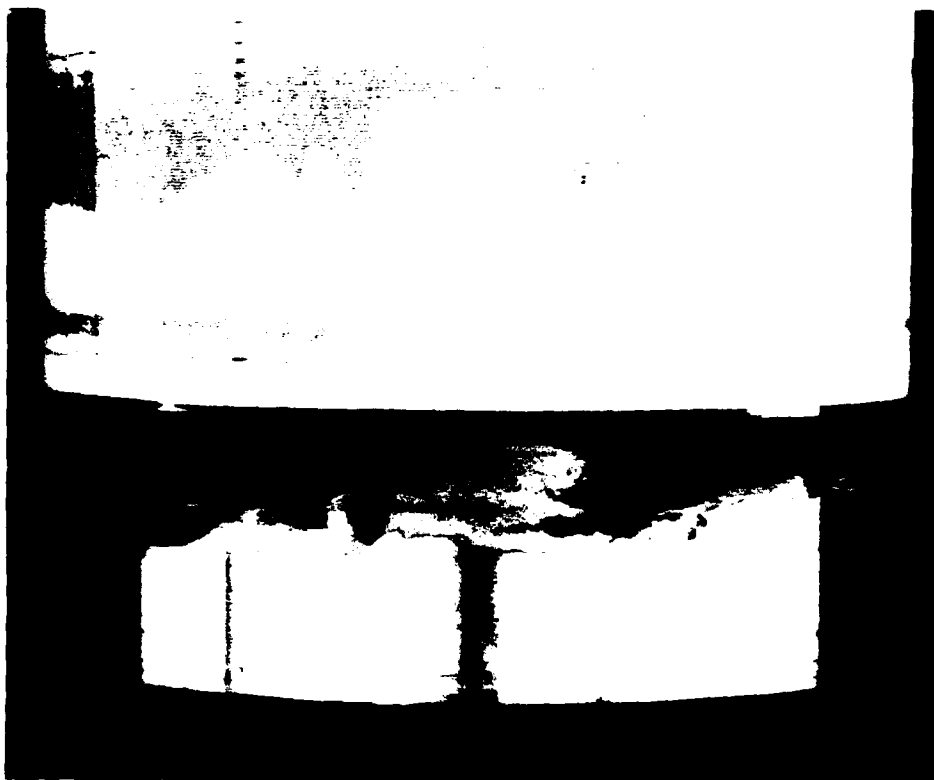
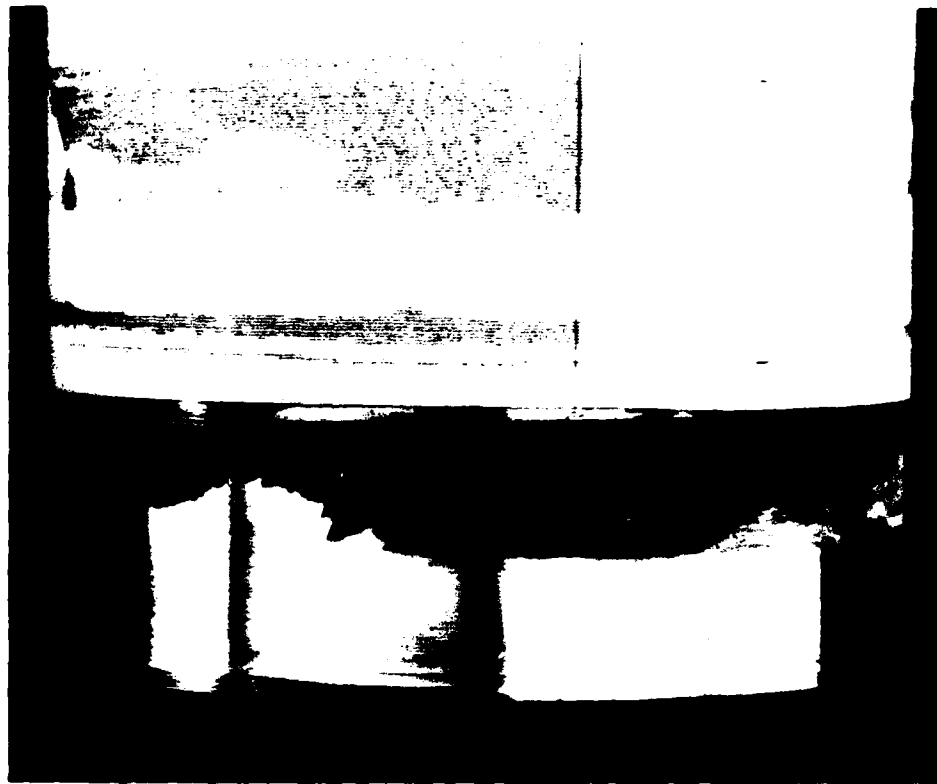


PHOTO NO C-3838

BAND WITH LOOSE MATERIAL REMOVED AND CORRESPONDING ULTRASONIC SCAN

CHAMBERLAIN MANUFACTURING CORPORATION

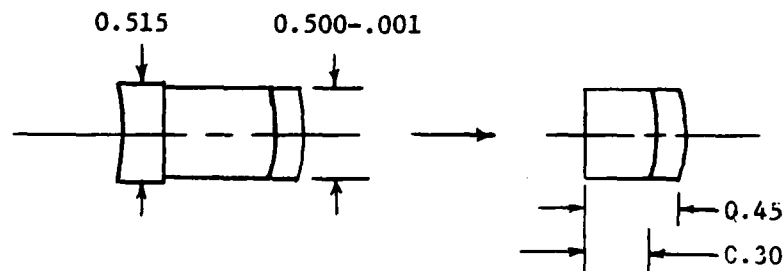
peeling occurred. The same procedure was applied to an inertia welded band which was shown by ultrasonic scan to be disbonded over half of its length. The lip of band material again tore in the region of good bonding; but along the disbonded region, the band peeled away with little resistance. This is further verification of the ability of ultrasonic scanning to distinguish bonded and unbonded areas.

The maximum load applied in testing the fully welded parts was 1500 pounds, which would give a lower limit of 1500 pounds per 1.6 inches, which is equivalent to the 940 pounds-per-inch adhesive strength of the weld bond.

3.9 Shear Testing

3.9.1 Shear Test Samples

A shear test fixture was designed and built to measure the shear strength of inertia welded bonds and to further verify ultrasonic testing as a means of determining disbonded areas. The following procedure was developed for making and testing shear test samples: 1) a 1/2-inch diameter area is selected and a line parallel to the projectile axis is scribed through the center of this circle; 2) an 11/16-inch hole saw, with the centering drill removed, is used to cut a plug, which is a 0.515-inch diameter cylinder, perpendicular to the rotating band surface; and 3) this plug is turned to 0.500-.001 inch diameter and cut to a shorter length as shown in the following sketch:



CHAMBERLAIN MANUFACTURING CORPORATION

The axis of the projectile is perpendicular to the plane of the paper in the preceding sketch, as is the direction of shearing. The line scribed on the sample prior to cutting it from the projectile is then used to accurately align the sample in the shear test fixture so that the direction of shear is parallel to this scribed line. The shearing heads are curved to match the curvature of the projectile band seat, so careful alignment is necessary to ensure that the shearing head maintains a small but constant distance from the weld interface.

3.9.2 First Series of Shear Tests

Six heat treated projectiles with inertia welded rotating bands were selected for a series of shear tests. Ultrasonic scans of these bands, taken after sample removal, are shown in Photograph No. 11228. There was no evidence of disbonding at the circumference of the holes cut to remove shear test samples, indicating that the samples: 1) are representative of the condition shown by scans; and 2) are not degraded by the sample removal method. It had been observed during work on another project that sawing must be done with great care. If sawing is too aggressive, or if the hole saw is not sharp, the sawing action can cause significant disbond and shear test results will be affected.

The results of the shear tests are presented in Table 3. Three samples from Projectile 5A (1, 4 and 7) were sheared through the rotating band material 0.04 inch away from the weld interface. The average shear stress value and standard deviation is 29.8 ± 0.4 kpsi (shown as "ksi" in Table 3); this is in reasonably good agreement with the tabulated values of 28 kpsi for the shear strength of the rotating band material (90 percent copper, 10 percent zinc) and leads to confidence in the validity of the shear test method.

5A

7A

9A

S.F.3

999

1-4-B

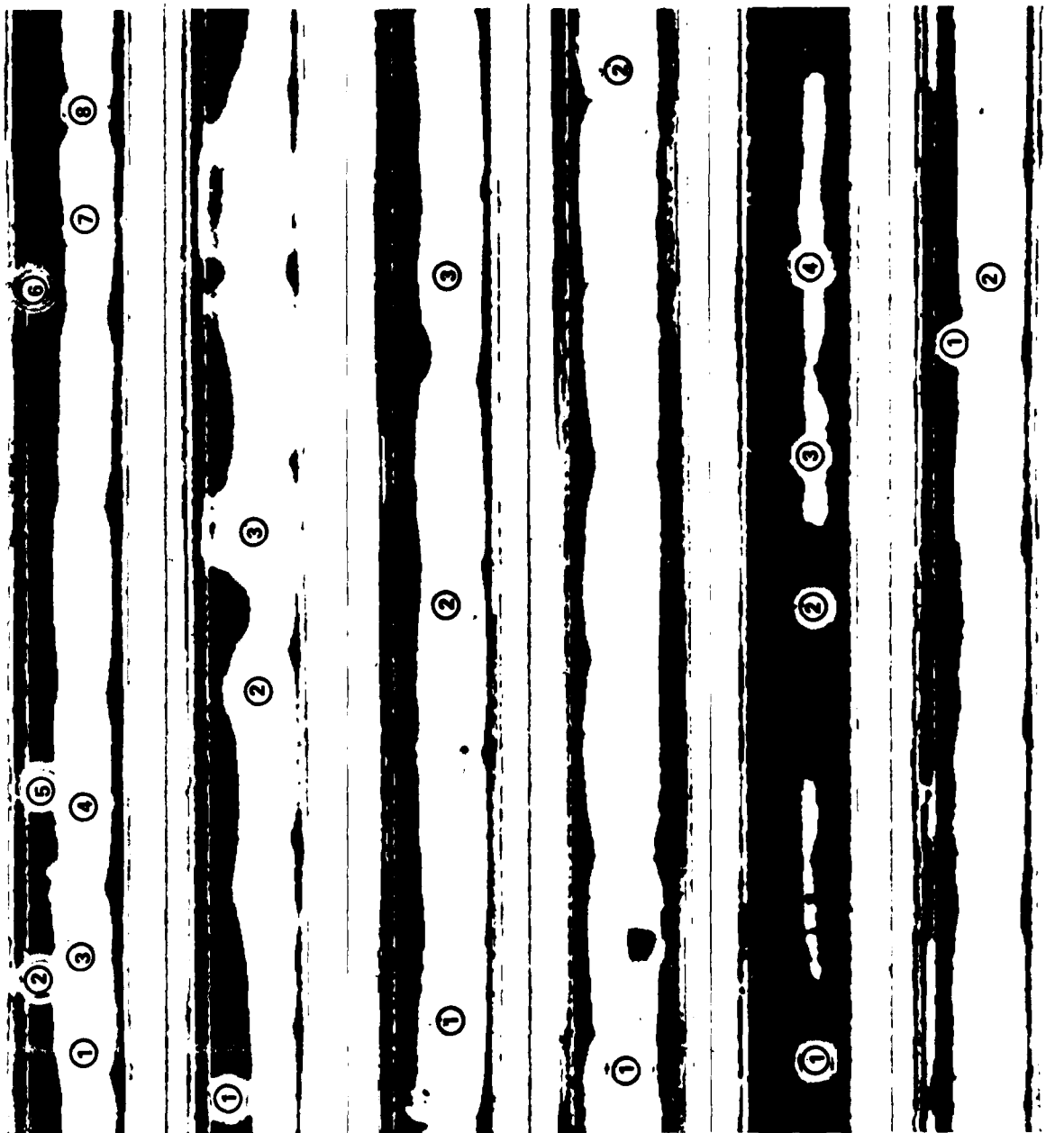


PHOTO NO. 11228

ULTRASONIC SCANS OF INERTIA WELDED M483 ROTATING BANDS AFTER
REMOVAL OF SHEAR TEST SAMPLES.

CHAMBERLAIN MANUFACTURING CORPORATION

TABLE 3. SHEAR TEST RESULTS

PROJECTILE	SAMPLE	MAXIMUM SHEAR STRESS (ksi)	COMMENTS
5A	1	29.5 ¹	Average shear stress of rotating band material (samples 1, 4 and 7) = 29.4±0.4 ksi Average (interface) = 34.6±2.1 ksi
	2	0 ³	
	3	33.2 ²	
	4	29.8 ²	
	5	0 ³	
	6	0 ³	
	7	30.2 ²	
	8	36.1	
7A	1	0 ³	Average (interface) = 36.0±0.4 ksi
	2	35.7	
	3	36.2	
9A	1	32.7	Average (interface) = 34.3±1.4 ksi
	2	34.7	
	3	35.4	
SF3	1	30.4	Average (interface) = 32.4±2.9 ksi
	2	34.5	
999	1	0 ³	Average (interface) = 29.0±4.4 ksi
	2	0 ³	
	3	25.9	
	4	32.1	
I-4-B	1	24.3	Half of sample from disbanded area.
	2	34.6	

NOTES:

¹Maximum shear stress= maximum load/original cross-sectional area.

²Shear through rotating band material, 0.04 inch away from interface.

³Samples came apart at interface during machining.

Six samples, taken from areas that ultrasonic scanning indicated to be totally unbonded, broke apart during the trepanning operation; these are listed in Table 3 as having zero shear strength.

All samples tested for interfacial shear strength were sheared in the rotating band material within 0.001 to 0.003 inch of the interface and are believed to closely represent the shear strength of the interface. Samples 5A (3 and 8), 7A (2 and 3), 9A (1, 2 and 3), and I-4-B (2) were taken from areas that ultrasonic scanning indicated to be well bonded and, further, were from bodies and bands with relatively clean surfaces. The average shear strength of these samples was 34.8±1.3 kpsi, significantly higher than the shear strength of the rotating band material. Projectile SF3 was coated with a soft solder flux before welding, and the average shear

CHAMBERLAIN MANUFACTURING CORPORATION

strength of 32.4 ± 2.9 kpsi for the two samples tested is not definitive in establishing whether or not the solder flux gave any advantage.

The average shear strength of the two samples from bonded areas of Projectile 999, 29.0 ± 4.4 kpsi, was comparable to the values from welds with clean interfaces, but the overall poor quality of the weld indicates that light rust on the band seat is detrimental to weld quality. Sample 1 from Projectile 1-4-B was taken from an area that ultrasonic scanning indicated to be approximately half bonded; the shear strength of 24.3 kpsi is significantly lower than the values obtained from samples indicated by ultrasonic scanning to be well bonded.

3.9.3 Second Series of Shear Tests

A second series of shear tests was performed and the results are presented in Table 4. For these tests, inertia welded band shear test samples were taken from areas shown to be well bonded by ultrasonic scanning. Scans of the inertia weld made with clean interfacing surfaces and the inertia weld made with Sunvis 931[®] hydraulic fluid at the interface showed 100-percent bonding. The scan of the weld made with silicone spray at the interface showed several large areas of disbond; samples were taken from between these areas. The welded overlay band was not scanned.

Shear strength data are similar for the overlay weld, the inertia weld made with clean interfacing surfaces, and the inertia weld made with Sunvis 931[®] hydraulic fluid at the interface. The inertia weld made with silicone spray at the interface was significantly weaker than the first three welds.

CHAMBERLAIN MANUFACTURING CORPORATION

TABLE 4. SHEAR STRENGTH OF BODY/BAND INTERFACE

WELD PROCEDURE	NUMBER OF TESTS	AVERAGE SHEAR STRESS ± STANDARD DEVIATION (kpsi)
Overlay	2	33.5 + 0.8
Inertia, interface clean	5	33.5 ± 0.7
Inertia, Sunvis 931 at interface	5	33.4 ± 1.0
Inertia, silicone spray at interface	2	30.7 ± 0.9

Metallographic examination of interface cross-sections showed a continuous interface for clean and for Sunvis 931® welds. However, the silicone weld had a large number of discontinuities approximately 0.0005 inch long. These discontinuities were apparently too small to be detected by ultrasonic scanning, but they may have reduced shear strength.

3.9.4 Conclusions

Data from both series of tests are combined in Figure 7. For 13 tests of inertia welded band interfaces with clean surfaces, the average shear stress is 34.3 ± 1.3 kpsi. The band material, with a shear strength of 29.8 ± 0.4 kpsi, is significantly weaker than the weld interfaces.

Other conclusions from the shear testing results are: 1) inertia weld interfaces are at least as strong as welded overlay interfaces; and 2) shear testing offers quantitative support of ultrasonic scanning as a valid nondestructive weld quality test.

CHAMBERLAIN MANUFACTURING CORPORATION

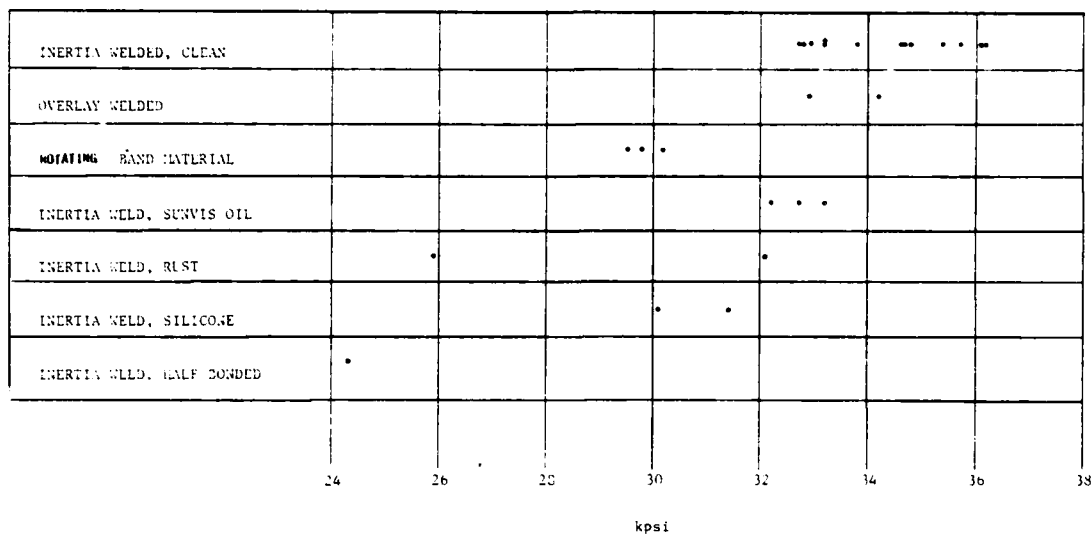


FIGURE 7. SHEAR STRENGTH FOR VARIOUS CONDITIONS

3.10 Bend Testing

Bend test samples were prepared from two projectiles with inertia welded rotating bands and from one projectile with a welded overlay rotating band. All projectiles were in the heat treated condition. The purpose of bend testing--a qualitative assessment of weld strength and ductility--was to determine whether the bond between the rotating band and the projectile body would fail under severe bending. Figure 8 illustrates the test setup for the two orientations tested--"vertical" and "horizontal;" Photograph No. 11496 shows bend test results for both sample types; and Photograph No. C3959 shows an enlarged view of a horizontal sample from an inertia welded part.

None of the samples showed any band-steel separation. The horizontal samples were bent 90 degrees; both overlay welded bands and three of four inertia welded bands had severe cracking of the steel and tearing of the band, but no separation at the weld interface. The vertical samples were

CHAMBERLAIN MANUFACTURING CORPORATION

bent up to 180 degrees with a 1/2-inch radius of curvature; there were some cracks in the steel and severe deformation of the band, but no separation at the interface.

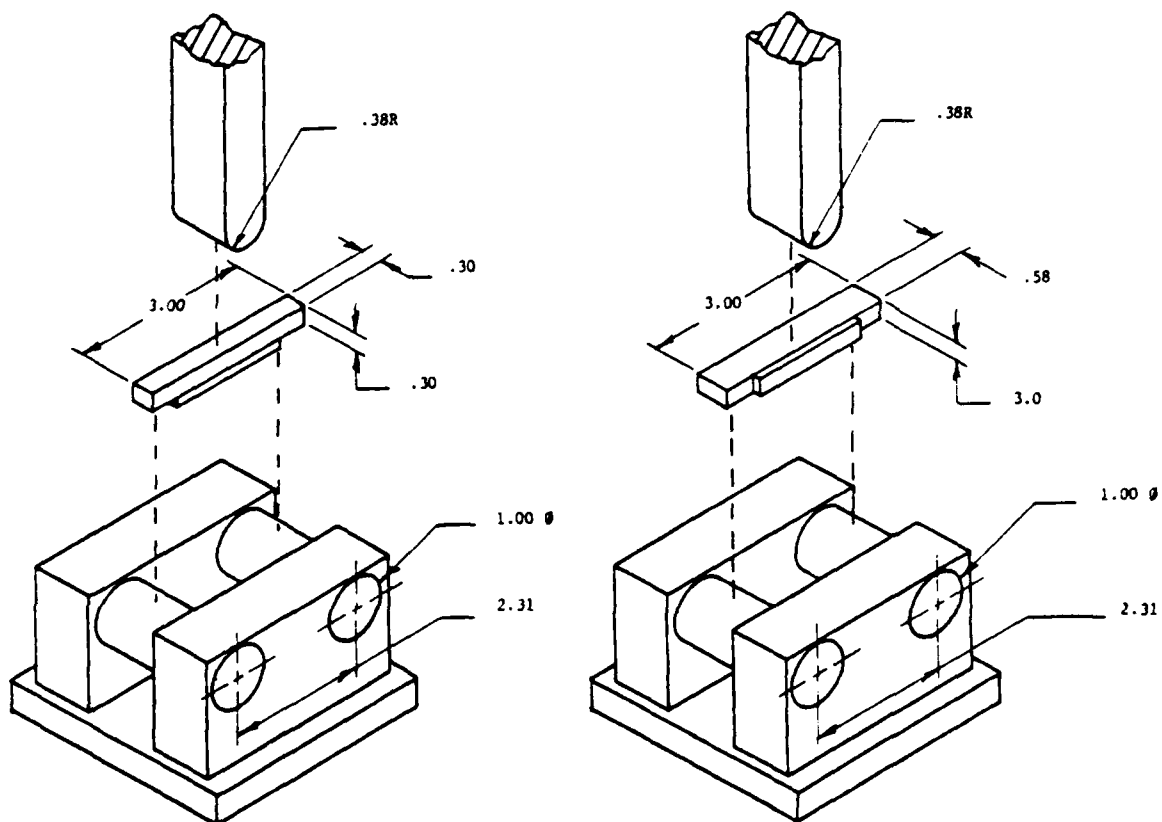


FIGURE 8. BEND TEST SETUP FOR VERTICAL (LEFT)
AND HORIZONTAL (RIGHT) SAMPLES

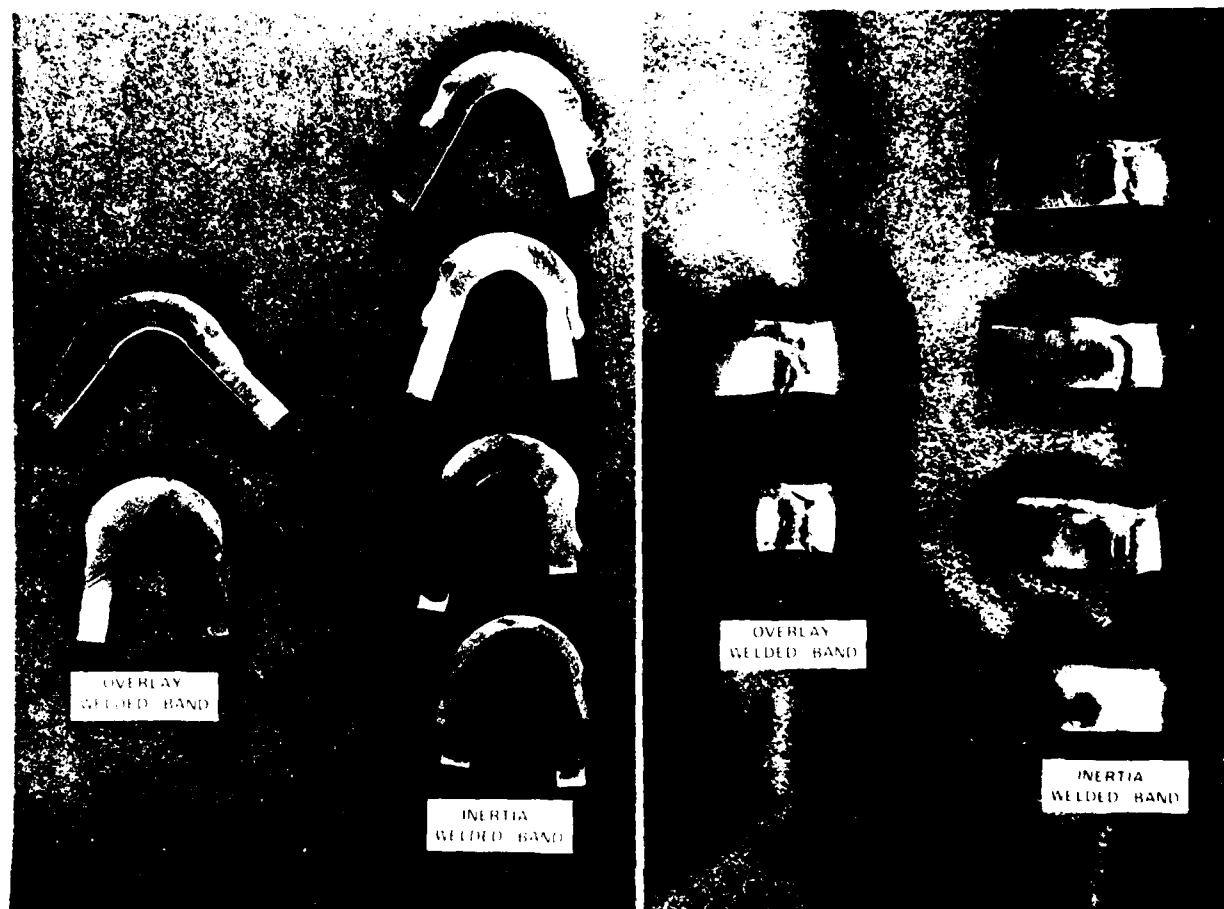


PHOTO NO. 11496

BEND TEST RESULTS FOR VERTICAL (LEFT) AND HORIZONTAL (RIGHT) SAMPLES

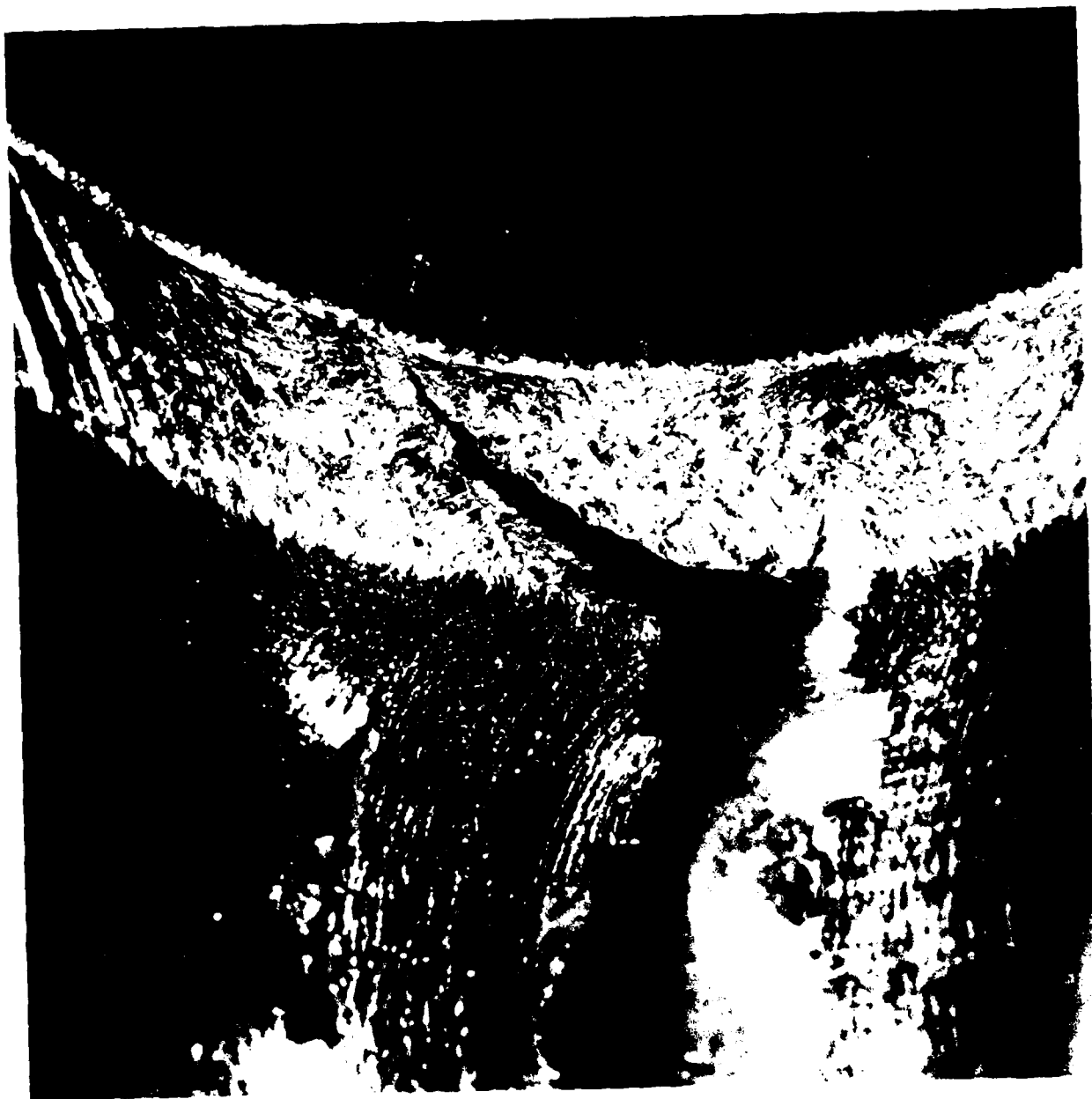


PHOTO NO C-3959
HORIZONTAL BEND TEST SAMPLE FROM INERTIA WELDED BAND

CHAMBERLAIN MANUFACTURING CORPORATION

4. HEAT TREATMENT OF PROJECTILES WITH INERTIA WELDED ROTATING BANDS

4.1 Order of Processes

When inertia welded rotating bands are to be used on projectiles requiring heat treatment, the heat treatment can be performed either before or after band welding. In either case, the inertia welding will heat a shallow region of the band seat above the critical temperature for the steel. The adjacent, ambient-temperature steel will extract the heat rapidly enough to give an effective quench and to convert the heated material to brittle martensite.

If bands are welded after the projectile bodies have been heat treated, the resulting martensite layer can be left as is, or it can be tempered by heating the steel to the temperature that had been used in tempering the projectile during heat treatment. However, as described above in Section 3, inertia welding bands prior to projectile heat treatment follows the current practice used for projectiles having overlay welded bands.

4.2 Investigation of Disbond Attributable to Heat Treatment

Work performed during previous contracts had suggested that heat treatment may be responsible for increasing areas of disbond at the inertia welded band- body interface. To investigate this, 61 each M483A1 Projectiles with rotating bands inertia welded (but not heat treated) under a previous contract (DAAA25- 76-C-0345) were selected for experimentation. Ultrasonic scans of the 61 rotating bands were taken; the projectiles were heat treated (a relatively fast oil quench, Houghton G, was used); and the bands were ultrasonically scanned a second time.

CHAMBERLAIN MANUFACTURING CORPORATION

4.2.1 Results of Initial Experimentation

All of the rounds showed some increase in disbond along the forward and aft edges of the band. Although the bands were configured to have an excess width, it appeared in some cases that areas of disbond would remain after machining to the finish width of 1.49 inches. (To ensure that this would not happen on inertia welded rounds to be test fired, the width of the bands to be welded at Chamberlain's New Bedford Division was increased by 0.2 inch.) The following results apply to a central, 1.49-inch wide region of the 61 heat treated and ultrasonically scanned bands. This region represents the material that would remain after finish machining:

Identification before Heat Treatment

Level 1, 99.99 to 100 percent bonding, 42 rounds total

Round Nos. 3-15, 17, 20, 21, 23-29, 31-33, 35, 36, 40,
41, 43, 45, 46, 49, 52-56, 58, 59, 61

Level 2, 99.90 to 99.99 percent bonding, 10 rounds total

Round Nos. 2, 16, 18, 19, 22, 30, 38, 39, 50

Level 3, 99.60 to 99.90 percent bonding, 5 rounds total

Round Nos. 37, 42, 48, 51, 57

Level 4, 98.60 to 99.60 percent bonding, 0 rounds

Total rounds: 57 (ultrasonic scans taken of four rounds--34, 44, 47 and 60--prior to heat treatment were too imperfect to read accurately)

CHAMBERLAIN MANUFACTURING CORPORATION

Identification after Heat Treatment

Level 1, 99.99 to 100 percent bonding, 35 rounds total

Round Nos. 3-5, 7, 8, 10-12, 14, 15, 17, 20, 21, 23, 24,
27-29, 31-33, 35, 36, 40, 41, 43, 46, 49, 52, 53, 55, 56,
58, 59, 61

Level 2, 99.90 to 99.99 percent bonding, 11 rounds total

Round Nos. 1, 9, 22, 25, 26, 30, 34, 39, 45, 47, 54

Level 3, 99.60 to 99.90 percent bonding, 11 rounds total

Round Nos. 2, 6, 13, 18, 37, 38, 44, 48, 51, 57, 60

Level 4, 98.60 to 99.60 percent bonding, 4 rounds total

Round Nos. 16, 19, 42, 50

Total Rounds: 61

Seventeen of the 57 rounds (or 30 percent) showed some degree of increased disbonding, as detailed in Table 5. However, the increases are considered small; none of the rounds was rated worse than the fourth designated level.

CHAMBERLAIN MANUFACTURING CORPORATION

TABLE 5. INCREASE IN DISBONDING AFTER HEAT TREATMENT

ROUND NO.	LEVEL BEFORE HEAT TREATMENT			LEVEL AFTER HEAT TREATMENT		
	1	2	3	2	3	4
2		X			X	
6	X				X	
9	X			X		
13	X				X	
16		X				X
18		X			X	
19		X				X
25	X			X		
26	X			X		
37 ¹			X		X	
38		X			X	
39 ¹		X		X		
42			X			X
45	X			X		
48 ¹			X		X	
50		X				X
54	X			X		
¹ Experienced increased disbonding but remained in designated category						

It appears that the inertia welded rounds that contain comparatively greater areas of disbond in the as-welded condition are also the rounds that later show a greater increase in disbonding after heat treatment. Data substantiating this point are presented in Table 6; plotted data appear as part of Figure 9.

There is the possibility that ultrasonic waves will be efficiently transmitted across the interface between copper and steel that are only in

CHAMBERLAIN MANUFACTURING CORPORATION

intimate contact, not actually bonded. If the transmission is comparable to that across an inertia welded interface, then the ultrasonic scan could indicate a good weld where none actually exists. If this condition does exist, the thermal strains during heat treatment could presumably cause separation of the rotating band from the body around regions of disbond. Thus, the degradation of the ultrasonic scan after heat treatment may be caused by tearing loose of the band in welded areas, separation of the band in areas which were not welded, or a combination of these effects.

Inertia welding rotating bands on previously heat-treated projectile bodies has been discussed as a possible production sequence. If intimate contact between the band and the band seat gives the same ultrasonic response as a good weld, then it is possible to get incorrect scans for inertia welded projectiles. This could be verified by destructive testing (e.g., shear testing).

4.2.2 Ultrasonic Scanning Verification

Chamberlain shipped the 61 heat treated projectile bodies to AMMRC for comparative ultrasonic scanning using a multiple-head transducer capable of inspecting the entire band in one rotation. This is a more suitable inspection system for production, since scan time is reduced from several minutes to about 10 seconds per round. Direct comparisons were made between all the corresponding ultrasonic scanning tapes; in each case, the tape from AMMRC's scanner agreed almost exactly with the tape from Chamberlain's. The multiple-head transducer, therefore, was judged to be acceptable as an inspection tool.

CHAMBERLAIN MANUFACTURING CORPORATION

TABLE 6. DISBOND INCREASES (BY LEVEL)

NO.	LEVEL OF BONDED AREA (%)	ROUNDS BEFORE HEAT TREATMENT		ROUNDS SHOWING INCREASED DISBONDING		ROUNDS AFTER HEAT TREATMENT	
		NO.	% OF 57	NO.	PERCENTAGE	NO.	% OF 61
1	99.99-100	42	74	7	17	35	57
2	99.90-99.99	10	17	7	70	11	18
3	99.60-99.90	5	9	3	60	11	18
4	98.60-99.60	0	0	--	--	4	7

4.3 "Fast" Oil Quench Tolerance

The M483Al body is made of AISI 1340 steel, which requires a quench-and-temper heat treatment to obtain the required mechanical properties. Several years ago, Chamberlain established that quenching projectiles in a relatively high-speed oil after arc welding rotating bands resulted in an unacceptable number of cracks in the steel body adjacent to the rotating band. This cracking did not occur in bodies that did not have rotating bands applied. By using a slower quench oil (a Houghton mar-tempering oil), cracking was avoided, but the mechanical properties, although acceptable, were very close to minimum requirements.

As stated in Section 4.2, the 61 projectiles used in the disbonding investigation were heat treated using the fast Houghton G oil quench. Fifty-one of these projectiles were tested for cracks by a qualified inspector using magnaflux with longitudinal and circumferential magnetization. The inspector found no cracks, and Chamberlain engineers concluded that bodies with inertia welded bands can tolerate a faster quench rate than bodies with arc welded bands.

CHAMBERLAIN MANUFACTURING CORPORATION

4.4 Use of Water Base Quench

In late 1979, Chamberlain performed tests to determine whether a water base quench could be used for M483A1 bodies with welded overlay rotating bands. (The primary reasons for exploring the possibility of switching to a water base quench would be to eliminate fire hazard and to ease the difficult and expensive waste disposal of spent quench oil.) The work done at this time showed that an unacceptably large number of projectiles showed cracks when quenched in a UCON-HT (High temperature) water-base quench medium.

However, since bodies with inertia welded bands demonstrated resistance to cracks in fast oil quenching, 13 bodies with inertia welded bands were heat treated using the UCON-HT water base quench medium at 140°F. Thorough magnaflux inspection revealed no cracks.

A more severe quench was performed on 11 each M483A1 bodies by using the UCON-HT at 120°F. Again, no cracks were detected by magnaflux inspection, and Chamberlain personnel concluded that this quench-temperature combination resulted in parts that easily met the strength requirements.

4.4.1 Results of Related Investigations

The 11 bodies heat treated using a 120°F UCON-HT quench and the 13 bodies heat treated using a 140°F UCON-HT quench were ultrasonically inspected for quality of the rotating band welds. The results are shown in Table 7; plotted data appear in Figure 9.

Heat treatment caused an increase in the amount of disbond in all 24 projectiles tested. In each case, the growth of regions that were disbanded prior to heat treatment constituted the increase. Company analysts observed this occurrence earlier, when the 61 projectiles having high-quality inertia welded bands were heat treated using a fast oil

CHAMBERLAIN MANUFACTURING CORPORATION

quench. In that group of projectiles, the increase in disbond due to heat treatment was greater for those having a significant amount of disbond before heat treatment. The level of disbond in these early tests, however, was at worst only a few percent--much less than in the tests involving a UCON-HT quench.

TABLE 7. EFFECT OF UCON-HT QUENCH (AT TWO DIFFERENT TEMPERATURES)
ON BONDING QUALITY

PERCENT OF AREA BONDED USING 140°F UCON-HT QUENCH			PERCENT OF AREA BONDED USING 120°F UCON-HT QUENCH		
ROUND NO.	BEFORE HEAT TREAT	AFTER HEAT TREAT	ROUND NO.	BEFORE HEAT TREAT	AFTER HEAT TREAT
1	99.3	64.0	1	99.0	70.7
2	98.4	86.0	2	96.6	64.0
3	97.2	77.3	3	94.6	70.7
4	96.4	73.3	4	92.7	86.7
5	95.8	78.7	5	90.6	57.3
6	95.2	77.3	6	85.0	57.7
7	93.9	62.7	7	83.3	45.3
8	93.3	76.0	8	83.0	62.7
9	92.2	76.0	9	82.5	60.0
10	92.2	89.3	10 ¹	52.0	13.9
11	87.9	77.3	11 ¹	12.7	5.3
12	86.2	78.7			
13	83.4	60.0			
¹ Round is not plotted in Figure 9.					

CHAMBERLAIN MANUFACTURING CORPORATION

The weld quality deteriorated more than was observed using a slower (Houghton G) oil quench, but the degradation was much less than that experienced with a UCON-HT quench when original weld quality was inferior (see Table 5, above). The worst of the four bodies tested showed 95.3 percent of the rotating band area to be bonded. Bodies with this amount of disbond were successfully test fired in a previous program conducted for ARRADCOM (DAAA25-76-C-0345) by Chamberlain. The data from Table 7 (plotted in Figure 9) show that rotating band bonds tended to deteriorate slightly more with a 120°F UCON-HT quench than with a 140°F quench. Data for four shells with very good bonds (Table 8) are seen in Figure 9 to suffer little or no deterioration when quenched into 120°F UCON-HT. This is also true for the 57 rounds quenched in the slower Houghton G oil.

TABLE 8. EFFECT OF HEAT TREATMENT USING UCON-HT QUENCH
ON HIGH-QUALITY INERTIA WELDED ROTATING BANDS

PERCENT OF AREA BONDED USING 120°F UCON-HT QUENCH	
BEFORE HEAT TREATMENT	AFTER HEAT TREATMENT
100	100
100	98.72
99.97	99.75
98.89	95.31

4.5 Related Stress Study

A mathematical model was developed to examine the stresses in the M483A1 Projectile during the quench phase of heat treatment. This work was done as a separate project at Chamberlain in 1981, and a report documenting the project is included in this report as Appendix A.

The stresses in the steel during rapid cooling in the quench oil were calculated using finite element analysis. Computations predicted that with no rotating band, the stress level in the steel did not reach high enough levels to be of concern. Stresses were significantly higher with a rotating band attached, but still not high enough to cause fracture of the steel unless there was a crack existing in the forward region of the band seat prior to quenching.

The magnitude of the required crack is difficult to calculate precisely, but is in the vicinity of 0.05 inch. Localized copper penetration (which would have nearly the same effect as a crack) of this magnitude occurs in some instances during overlay welding. Conversely, cracking has not been observed during inertia welding.

The mathematical analysis is supported by the following observed behavior:

1) increasing frequency of cracking with increasing quench severity for projectiles with welded overlay bands; and 2) absence of cracking with severe quenches in projectiles with inertia welded bands.

4.6 Conclusions

Heat treatments with quench severity far in excess of that required to obtain required strength properties do not generate cracks in M483A1 Projectiles having inertia welded rotating bands. Heat treatment often causes some growth of disbonded regions, but for initially high-quality welds, the increase in disbond is either nil or very slight. This is true even for the most severe quenches used.

Single-sweep ultrasonic scans performed at AMMRC with a multiple-head transducer agree with scans generated using a more conventional and much slower single-transducer method. The rapid scan would accommodate 100-percent testing in production.

CHAMBERLAIN MANUFACTURING CORPORATION

5. VARIATION OF BAND AND BAND SEAT GEOMETRY

5.1 Band Seat Parameters

In work performed under a prior ARRADCOM contract (DAAA25-76-C-0345), Chamberlain consistently achieved high-quality inertia welding of rotating bands to M483A1 Projectiles. Under Contract -0093, however, obtaining consistently good welding along the forward edge of the rotating band has been difficult.

The values: rotational speed = 2200 rpm; inertial mass (WK^2) = 425 lb-ft²; and ram pressure = 3800 psi were determined in Contract -0345 to be optimum for obtaining good welds. Chamberlain elected to use these values for all welding under the subject contract. However, Company personnel have noted that the band seat diameters and the inside and outside diameters of the rotating band are not the same in the Contract -0093 work as in the Contract -0345 work. These diameter measurements are shown in Table 9.

The overall diameter of the band/body assembly is equal to the band seat diameter plus the difference of the rotating band's outside and inside diameters (see Note 1 of Table 9) at the point when the band has just come in contact with the band seat and has not been severely compressed. The actual process may not be so neatly divisible into two stages (i.e., the rotating band's setting followed by severe compressional loading); however, the overall diameter is felt to be a useful comparative parameter.

5.2 Rotating Collet Geometry

The geometry of the rotating collet that holds the rotating band is such that when the collet pads are opened to accept the band prior to welding, the pads are not parallel (in the axial direction) to the axis of the projectile body. The collet pad diameter is less at the aft end of the rotating band than at the forward end. As the collet pads close during the

CHAMBERLAIN MANUFACTURING CORPORATION

welding operation, the angle between the pads and the projectile axis decreases, and at some specific value of the collet diameter, the pads and projectile axis are parallel. If the weld is made at the diameter where parallelism occurs, the pressure from forward to aft on the rotating band should be uniform, and a good weld should be obtained. Figure 10 depicts the collet geometry.

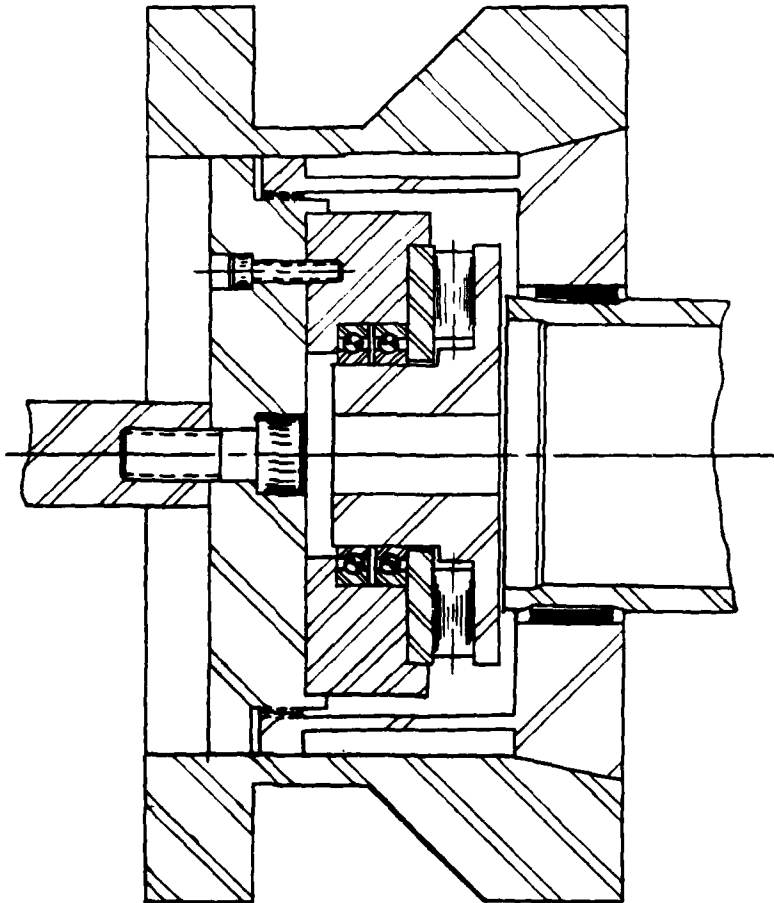


FIGURE 10. COLLET GEOMETRY OF INERTIA WELDER AT
CHAMBERLAIN R&D DIVISION

CHAMBERLAIN MANUFACTURING CORPORATION

TABLE 9. BAND SEAT AND ROTATING BAND
DIMENSIONS FOR C-0345 AND C-0093 INERTIA WELDS

CONTRACT WELDS	BAND SEAT DIAMETER (inches)	ROTATING BAND		OVERALL DIAMETER ¹ (inches)	OVERALL DIAMETER DEVIATION (inches)
		I.D. (in.)	O.D. (in.)		
-0345	6.050	6.190	6.575	6.435	0
-0093 (early)	6.050	6.200	6.617	6.467	+0.032
-0093 (early)	6.081	6.190	6.617	6.517	+0.082
-0093-1	6.040	6.220	6.617	6.437	+0.002
-0093-2	6.040	6.220	6.572	6.392	-0.043
-0093-3	6.040	6.220	6.520 to 6.600 ⁽²⁾	6.340 to 6.420	-0.015 to -0.045
-0093-4	6.050	6.220	6.440 to 6.660 ⁽²⁾	6.270 to 6.430	-0.005 to -0.165
¹ Overall diameter = band seat diameter plus (band O.D. - band I.D.) ² These rotating bands were tapered on the outside diameter, with the larger diameter forward.					

Welds made under Contract -0345 were good, so presumably the overall diameter was correct. The last column in Table 9 shows the deviation of the overall diameters from that of the -0345 welds. The overall diameters for welds made early in Contract -0093 were larger than ideal. From the above analysis, the angle of the collets relative to the projectile axis should be such that there would be less pressure, and therefore poorer bonding, at the forward edge of the band. In general, this effect is what was observed.

5.3 Band and Band Seat Dimensional Variants

Welds 0093-1, -2, -3, and -4 (see Table 9) were made with band and band seat dimensions varied to obtain different distributions of pressure along the axial direction of the band. For welds -3 and -4, tapered bands with the larger diameter forward to increase pressure along the forward edge of the band were used. These four tests were done in duplicate, with the welds labelled 1A and 1B, 2A and 2B, etc. Photograph No. 11230 (1 of 2 and 2 of 2) shows ultrasonic scans of the eight welds. The forward edge of the rotating bands is the top edge of each segment in the photographs.

1A



1B



2A



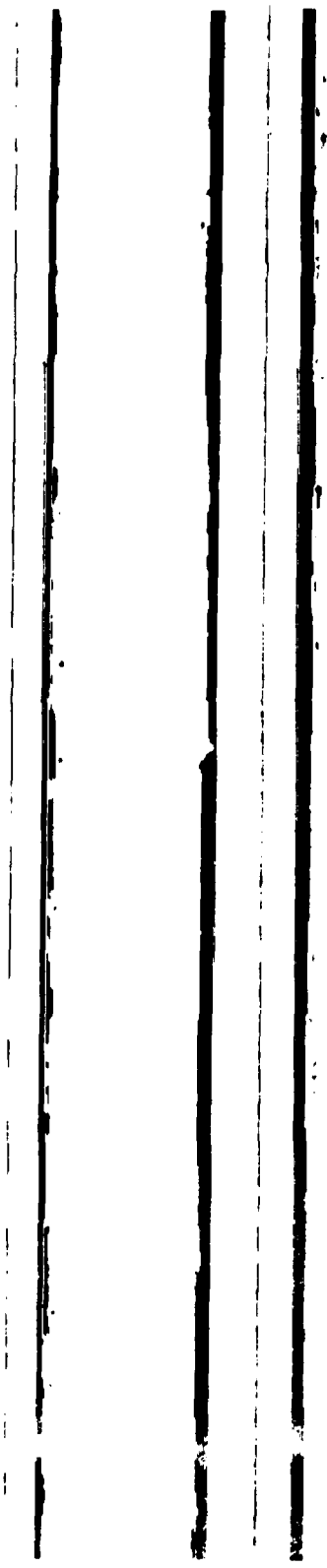
2B



PHOTO NO. 11230 (1 of 2)

ULTRASONIC SCANS OF INERTIA WELDED ROTATING BANDS ON M483 PROJECTILES.

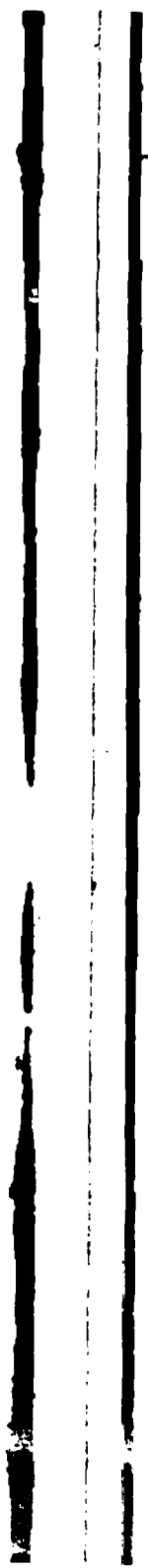
3A



3B



4A



4B



PHOTO NO. 11230 (2 of 2)
ULTRASONIC SCANS OF INERTIA WELDED, TAPERED-O.D. ROTATING BANDS
ON M483 PROJECTILES.

CHAMBERLAIN MANUFACTURING CORPORATION

Welds 1A and 1B, with overall diameters nearly equal to the -0345 welds, still show some leading edge disbond, but not as much as was observed in most of the early -0093 welds. Welds 2A and 2B, with a somewhat smaller overall diameter, are perfect as far as the edges are concerned, indicating a uniform forward-to-aft pressure. The relatively gently tapered bands used in welds 3A and 3B are quite good, but show a very slight tendency to disbond at the aft edge. Bands for welds 4A and 4B were more severely tapered; disbond at the aft edge indicates that there is insufficient pressure in that area. The measured percentages of bonded areas are given in Table 10.

TABLE 10. BONDED AREA FOR INERTIA WELDS INTRODUCED IN TABLE 9

WELD NUMBER	BONDED AREA (%)
0093-1A	99.31
0093-1B	99.93
0093-2A	99.93
0093-2B	99.95
0093-3A	100.0
0093-3B	100.0
0093-4A	98.9
0093-4B	90.7

5.3.1 Effect of Band/Band Seat Geometry Variants on Weld Quality

This test series indicates that the high incidence of leading-edge disbond for inertia welds made with the equipment at Chamberlain R&D Division was due primarily to nonuniform pressure on the rotating bands during welding. In the limited number of tests made, small dimensional changes in the parts being welded resulted in a significant increase in weld quality. These welds were the last made on the R&D equipment; all other welds made under

CHAMBERLAIN MANUFACTURING CORPORATION

the subject contract were made on the new equipment at Chamberlain's New Bedford Division. The -0345 welds appear to be on the high side of the allowable overall diameter range, with a value 0.043 inch less (as in Welds 0093-2A and -2B) also giving good welds. There appears to be no need to go to the more complicated tapered band (0093-3 and -4), even though good welds were obtained with this geometry.

The design of the collet assembly used on the New Bedford inertia welder is such that the collet pads should always be parallel to the projectile axis, so that the problem of fore-to-aft variation in pressure should not occur. The collet geometry of the New Bedford inertia welder is shown in Figure 11.

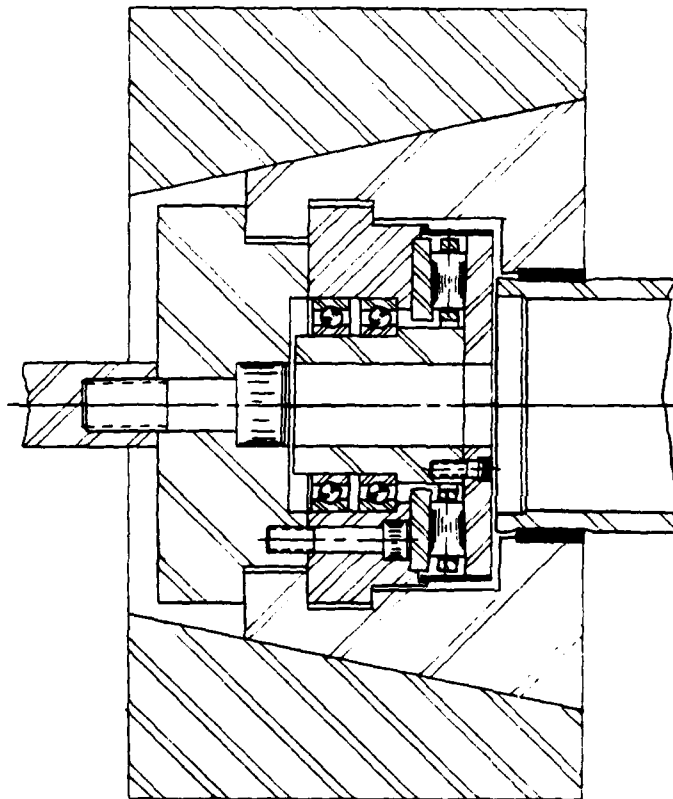


FIGURE 11. GEOMETRY OF COLLET OF INERTIA WELDER
AT CHAMBERLAIN'S NEW BEDFORD DIVISION

CHAMBERLAIN MANUFACTURING CORPORATION

6. EFFECT OF BAND SEAT COATINGS AND BAND SEAT RAMP ANGLES ON WELDS

Chamberlain has used coatings effectively in inertia welding experiments under ARRADCOM contracts DAAK10-79-C-0093 and DAAK10-78-C-0426. These experiments and some observations on the results are discussed in the following paragraphs.

6.1 Hydraulic Fluid Lubrication

Two sets of inertia welds, identified as K6-K9 and K51-K54, were made under Contract -0426. The machine parameters for both sets were identified: $WK^2 = 90 \text{ lb-ft}^2$; flywheel spin rate = 2500 rpm; and ram pressure = 1250 psi. The only significant difference between the two sets was that Welds K6-K9 were made using clean, dry bands, and Welds K51-K54 were made using bands lubricated with hydraulic fluid.

The ultrasonic scans made after heat treatment of both sets of welds, appearing as Photograph Nos. 11605 and 11606, show that Welds K51-K54 have better quality in the central regions and have smoother edges than Welds K6-K9.

Company personnel noted that dynamic data taken during these weld trials were more easily repeated with lubricated bands than with dry bands. Figure 12 and 13 are computer plots of data taken during Weld Trials K6 and K7, respectively. These plots show flywheel rpm, ram pressure, band temperature and tailstock displacement, all versus time, that occurred during the weld. The flywheel rpm curve is of particular interest. Figure 12 shows the flywheel going from maximum rpm to a stop in approximately 400 milliseconds. Figure 13 shows this same event taking place in 150 milliseconds. These two figures represent the maximum and minimum times required for welds K6-K9 as shown by the rpm curve drop--a time variation which is considered excessive.



PHOTO NO. 11606
ULTRASONIC SCANS OF WELDS K51-K54 USING HYDRAULIC FLUID AS A
LUBRICANT ON THE BAND. TOP OF SCAN IS TOP EDGE OF WELD.



PHOTO NO. 11605
ULTRASONIC SCANS OF WELDS K6-K9 USING CLEAN, DRY PARTS. TOP OF
SCAN IS TOP OF WELD.

CHAMBERLAIN MANUFACTURING CORPORATION

Figures 14 and 15, which are computer plots for Weld Trials K52 and K54, provide representative data from the K51-K54 set of welds. All data curves are similar enough, from weld to weld, to support the conclusion that the use of lubricated bands yields repeatable dynamic data.

The strength of the welds was not adversely affected by lubrication. Tensile tests showed that joint strength was approximately 40,000 psi for welds using either dry or lubricated bands.

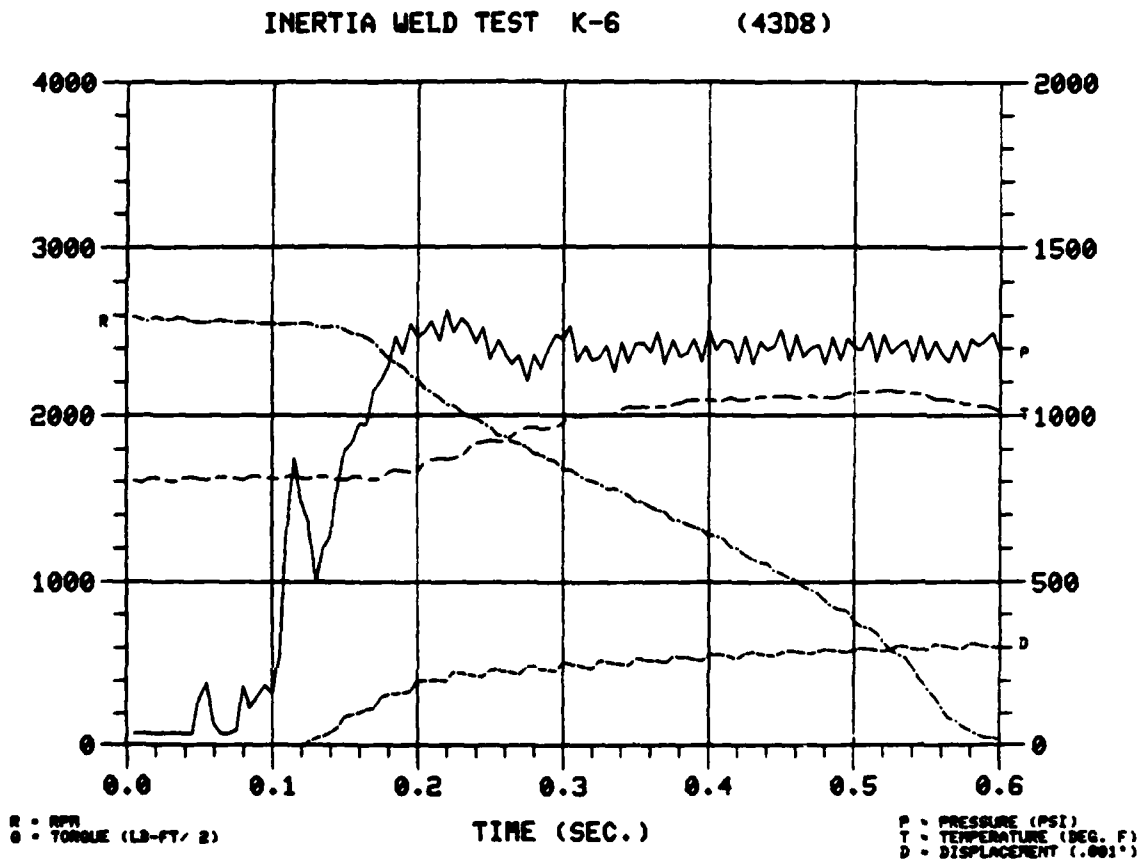


FIGURE 12. COMPUTER PLOT SHOWING 400-MILLISECOND
FLYWHEEL STOP TIME FOR WELD K6

CHAMBERLAIN MANUFACTURING CORPORATION

6.2 Resin-Based Solder Flux

A resin-based solder flux was used on rotating bands inertia welded to three M483A1 Projectiles. Dynamic data for these welds are unavailable because the inertia welder at the Company's Research and Development Division was not equipped to record such data on 155-mm, M483A1 welds.

Ultrasonic scans showed equally good results for welds using either dry or flux-lubricated bands. Scans taken after heat treatment showed that, in general, degradation was less severe on welds using lubricated bands than

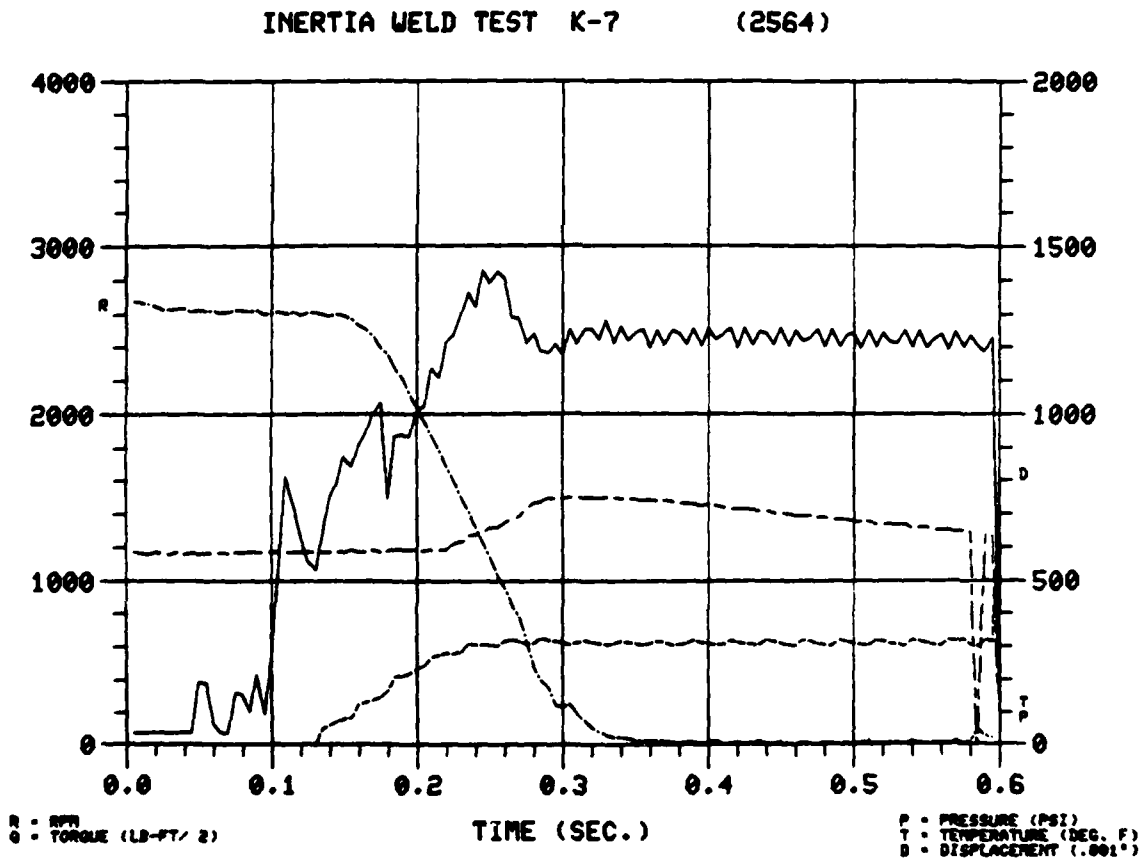


FIGURE 13. COMPUTER PLOT SHOWING 150-MILLISECOND
FLYWHEEL STOP TIME FOR WELD K7

CHAMBERLAIN MANUFACTURING CORPORATION

on welds using dry bands. The shear strength of both types of welds was comparable. Metallographic examination of the weld area of a lubricated band indicated good bonding with no flux residue.

INERTIA WELD TEST K-52 (2C80)

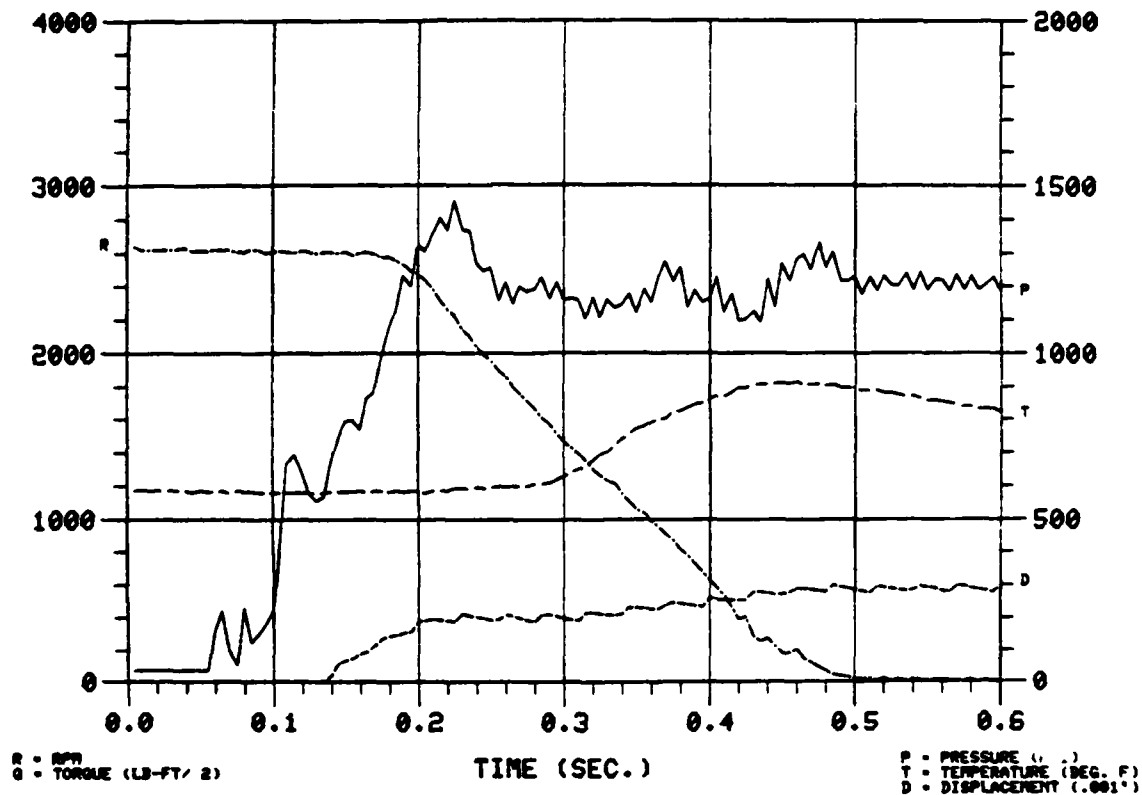


FIGURE 14. COMPUTER PLOT FOR WELD K52.

6.3 Additional Observations

Company personnel made additional observations when inertia welding lubricated bands to projectile bodies. The most noticeable effects that a lubricating film has on the welding operation are to decrease the deceleration rate and to make the operation smoother. The tooling load is

CHAMBERLAIN MANUFACTURING CORPORATION

INERTIA WELD TEST K-54 (2BD8)

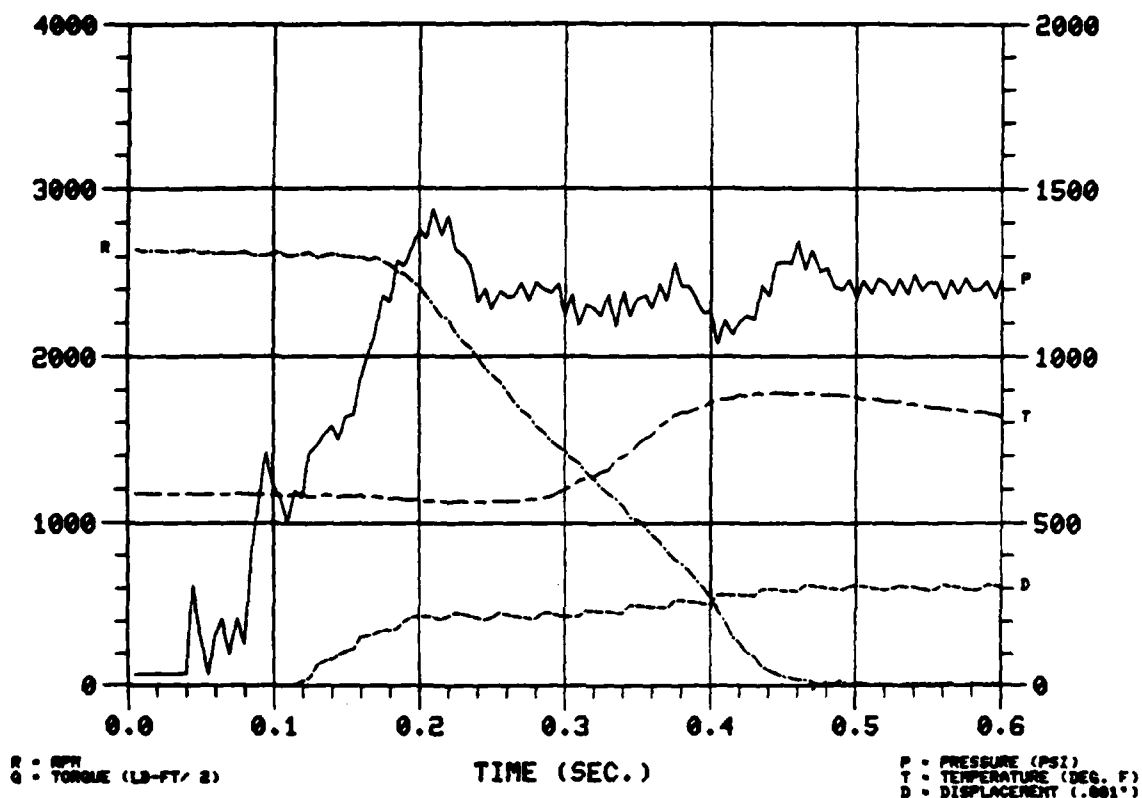


FIGURE 15. COMPUTER PLOT FOR WELD K54

not as severe, and the "chatter," or galling action, associated with dry welds is eliminated. The absence of chatter should lead to extended tooling life.

A lubricating film may reduce localized "hot spots" and uneven erosion of the band as it is swaged onto the projectile body, which could result in a more evenly distributed weld pattern. A lubricating film may tend to exclude oxygen from the weld interface, which could decrease oxidation and promote a better weld. If the proper lubricating material is used, it could promote a better welding atmosphere than if dry metals are employed.

CHAMBERLAIN MANUFACTURING CORPORATION

6.4 Investigation of Various Lubrications

6.4.1 Material Descriptions

Fourteen different lubricants, or coatings, were selected for use in welding trials conducted at Chamberlain. Each material is briefly described below.

6.4.1.1 Two hydraulic fluids from Sun Petroleum Products:

Sunvis 931®. Formulated from premium quality oils with additives to resist rust and corrosion and to supply antifoam properties.

Sunvis 831 WR(68)®. Basically a 931 oil with a zinc additive system to enhance thermal stability and wear protection; suited for higher pressures and temperatures than 931.

6.4.1.2 Six soldering and brazing fluxes from Eutectic Corporation, Flushing, New York:

Eutector Flux 157®. For use with 157 solder (tin with a small amount of silver); corrosive, but not acidic; melting temperature of approximately 425°F.

Eutecsol 682®. For soldering difficult-to-weld metals.

Eutecsol 808®. A neutral (resin base), general purpose flux.

Xuper Flo Paste®. For nickel-chromium, high-strength brazing; melting temperature of approximately 1550°F.

Xupersil Paste®. For low-melting-point silver brazing; melting temperature of approximately 1050°F.

CHAMBERLAIN MANUFACTURING CORPORATION

"T" Flux®. For extended-time welding and brazing; designed to minimize oxidation; melting temperature of 1800°F.

6.4.1.3 Four soldering fluxes from Kester Solder, Chicago, Illinois:

Formula 1544®. A liquid solution of resins in aliphatic alcohols; nonconductive and noncorrosive.

Formula 735®. A liquid solution for nonelectrical soldering; contains inorganic acids and zinc chloride, and is highly corrosive.

General purpose paste. A resin-based general purpose paste flux.

General purpose liquid. A resin-based general purpose liquid flux.

6.4.1.4 Two aerosol products from Beltraction Company, Lake Geneva, Wisconsin:

Silicone mold release.

Zinc. Finely divided powder in a liquid carrier.

6.4.2 Procedure

During the investigation, approximately every fourth weld was made with clean bands and band seats to serve as references. For all welds, the bands were first cleaned by acid etching and the band seats were cleaned with solvents. When coatings were to be used, they were applied to the inside of the bands immediately before welding.

CHAMBERLAIN MANUFACTURING CORPORATION

6.4.3 Results

Measurements of the percentage of band seat area having a good bond are presented in Table 11. These data are from ultrasonic scans taken

TABLE 11. EFFECT OF INTERFACE COATINGS ON BONDED AREA OF BAND SEAT

INTERFACE COATING	BONDED AREA OF BAND SEAT (%)		INTERFACE COATING	BONDED AREA OF BAND SEAT (%)	
	AS WELDED	AFTER HEAT TREATMENT		AS WELDED	AFTER HEAT TREATMENT
None	100	100	Eutecsol 808	100	100
	100	100		100	100
	100	100		98.8	98.4
	100	100		96.7	91.5
	99.8	99.8	Xuper Flo Paste	99.9	99.8
	99.6	99.5		90.9	59.5
	99.4	99.4		3.0	0
	100	99.3			
	99.6 *	98.7	Xupersil Paste	6.0	6.0
	100 *	94.6		2.3	2.3
	100 *	94.5		5.6	0.8
	99.7	94.5			
	99.0	85.8	"T" Flux	55.4	55.4
	94.0	25.7		25.7	25.7
Sunvis 931	100 *	100		0	0
	100	100			
	100	100	Kester 1544	99.8	99.2
	100	99.9		99.3	99.2
	100	99.4		99.8	99.1
	100 *	99.3	Kester Formula 735	98.8	98.5
	98.2	98.2		99.6	98.4
	99.8	97.6	Kester Paste	83.1	81.6
Sunvis 831	97.6	92.8		79.7	79.7
	100	100		79.7	79.7
	99.3	99.3	Kester Liquid	95.9	95.0
	98.2 *	98.0			
Eutector 157	97.3	97.0	Silicone Spray	97.0	96.2
	86.5	86.5		71.6	67.9
	78.4	78.4		56.8	56.8
Eutecsol 682	96.4	69.0	Zinc Spray	59.5	1.8
	93.4	88.8			
	93.7	82.6			
	89.5	77.6			

* Modified band seat

immediately after welding, and again after heat treatment. For each interface coating, the listing is in the order of decreasing, after-heat-treatment weld quality. Thirteen of the 14 welds made with a clean interface were 99.0 to 100 percent bonded in the as-welded condition. One of the welds showed a 6-percent disbond area concentrated entirely in the six areas corresponding to the gaps between the collet pads; this weld

CHAMBERLAIN MANUFACTURING CORPORATION

became severely disbonded after heat treatment. In the as-welded condition, this weld was 94 percent bonded, but after heat treatment, the bonded area was only 25.7 percent. There is no apparent explanation for this large degradation. Twelve of the 14 welds were 95.0 to 100 percent bonded after heat treatment. One weld, of intermediate quality, was 86 percent bonded.

Good bonds were obtained on eight welds using the Sunvis 931® hydraulic fluid, with the ninth weld being of intermediate quality. The Sunvis 831® hydraulic fluid gave good welds in all four trials. The six soldering and brazing fluxes from Eutectic Corporation gave erratic, and usually poor, results. Two of the Kester products, 1544® and 735®, gave good bonds. The other Kester products, the silicone spray, and the zinc spray were unsatisfactory.

The survey showed that four of the products tested (Sunvis 931® and 831®, and Kester 1544® and 735®) will give good bonding. Further testing using these materials would be necessary to determine whether the anticipated advantages of more consistent weld quality and less wear on the welder tooling are realized.

6.5 Modified Band Seat Configuration

For six of the tests listed in Table 11, a modified band seat configuration was used. These tests are noted in the table by an asterisk. The standard and modified band seat configurations are shown in Figure 16.

With the 15-degree ramp angle used in the standard configuration, the flat portion of the band seat is narrower than a 1.70-inch-wide band. During welding, the edges of the band will touch down on the ramps before the central portion makes contact with the band seat. This action could cause the band edges to overheat and become fluid, causing loss of pressure and contributing to intermittent welds.

CHAMBERLAIN MANUFACTURING CORPORATION

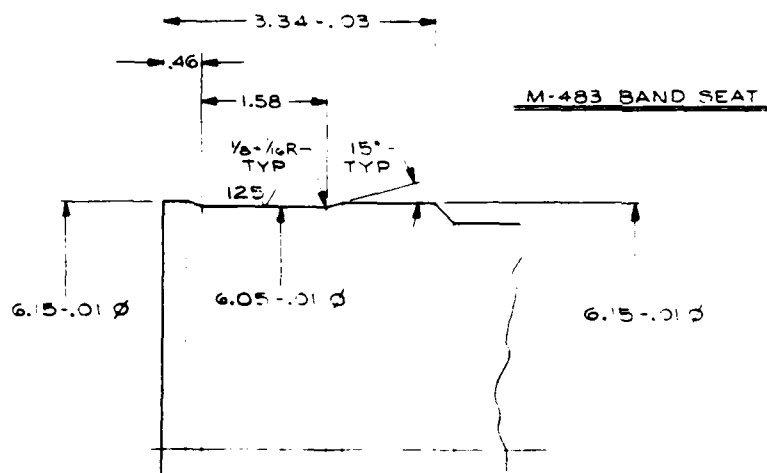
Another possible cause of poor quality bonding along band edges is that a partial seal is formed between the band and projectile body in these regions during inertia welding. The formation of this partial seal could lead to the trapping of air in the cavity between the edges of the band and the band seat. As the band is swaged onto the band seat, any trapped air is forced out past the edges of the band, which have already become heated. This action could cause rapid oxidation of the material along the band edge and contribute to poor quality welds.

A very simple method of eliminating these possible causes of poor edge welds is to change the band seat configuration. Specifically, the angle of the chamfer at the edge of the band seat should be changed from 15 degrees to 45 degrees, as shown in Figure 16. The overall width of the band seat does not change, but the width of the flat portion of the band seat increases from 1.58 inches to 1.85 inches. A 1.7-inch wide rotating band, when swaged onto the seat as shown, will fit within the flat region of the band seat without preliminary interference at the edges of the band. The welds made on projectiles with modified band seats were all acceptable but did not stand out among welds with standard band seats. Chamberlain concluded that there was no apparent advantage to the modified band seat configuration.

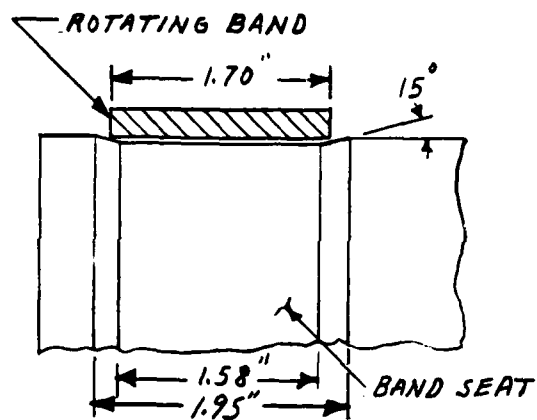
CHAMBERLAIN MANUFACTURING CORPORATION

Another possible cause of poor quality bonding along band edges is that a partial seal is formed between the band and projectile body in these regions during inertia welding. The formation of this partial seal could lead to the trapping of air in the cavity between the edges of the band and the band seat. As the band is swaged onto the band seat, any trapped air is forced out past the edges of the band, which have already become heated. This action could cause rapid oxidation of the material along the band edge and contribute to poor quality welds.

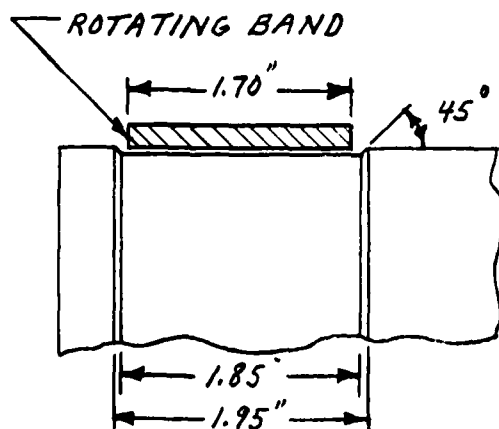
A very simple method of eliminating these possible causes of poor edge welds is to change the band seat configuration. Specifically, the angle of the chamfer at the edge of the band seat should be changed from 15 degrees to 45 degrees, as shown in Figure 16. The overall width of the band seat does not change, but the width of the flat portion of the band seat increases from 1.58 inches to 1.85 inches. A 1.7-inch wide rotating band, when swaged onto the seat as shown, will fit within the flat region of the band seat without preliminary interference at the edges of the band. The welds made on projectiles with modified band seats were all acceptable but did not stand out among welds with standard band seats. Chamberlain concluded that there was no apparent advantage to the modified band seat configuration.



STANDARD BAND SEAT
CONFIGURATION.



INTERFERENCE BETWEEN EDGES OF
ROTATING BAND AND BAND SEAT.



MODIFIED BAND SEAT
CONFIGURATION.

FIGURE 16. STANDARD AND MODIFIED BAND SEAT CONFIGURATIONS

CHAMBERLAIN MANUFACTURING CORPORATION

7. INERTIA WELDER ACCEPTANCE TEST FIRING

7.1 Test Warhead Preparation

Twenty 155-mm, M483A1 Projectiles with inertia welded rotating bands were fired on 6 and 8 May 1980 at Yuma Proving Ground (YPG). All rotating bands were inertia welded onto as-forged projectiles at Manufacturing Technology, Inc. (MTI) during acceptance testing of a new inertia welder being purchased from MTI by Chamberlain's New Bedford Division.

Rotating bands were cleaned by abrasion immediately prior to welding. The projectiles were heat treated at New Bedford after the rotating bands were inertia welded. A large number of projectiles, processed as described above, were ultrasonically scanned after heat treatment to determine the quality of the rotating band welds. Twenty projectiles, representing a wide range of weld qualities, were selected based on these scans. The weld qualities, "good," "fair" and "poor" (see Table 12) were judged by the standards used in the quasi-production run test firing, described in Section 8.

7.2 Test Results

The projectiles were arranged randomly and were fired at Zone 8, hot (145°F maximum). Visual evaluations of the rotating bands after recovery are given in Table 12. The results were encouraging; there was little band material loss even though weld quality was very poor on many of the bands. The ultrasonic scans gave reasonably good predictions of performance.

The impact area for test firing is shown in Figure 17. The test firing data are given in Table 13, and a map of the impacts in Figure 18. There is no apparent correlation between rotating band damage and deviations from the projectile's desired impact point.

CHAMBERLAIN MANUFACTURING CORPORATION

The overall results for range performance and rotating band damage are encouraging, especially when considering the generally poor weld quality of the rotating bands.

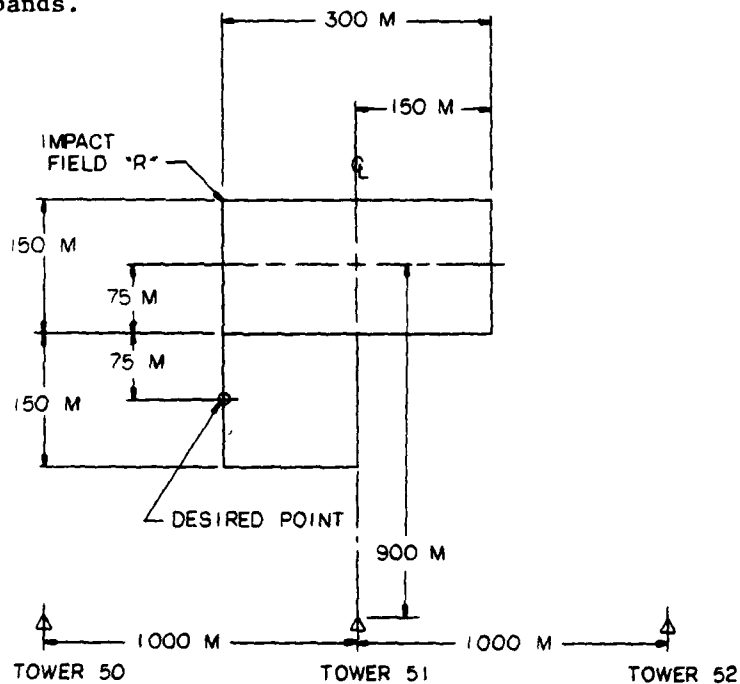


FIGURE 17. IMPACT RANGE FOR TEST FIRING

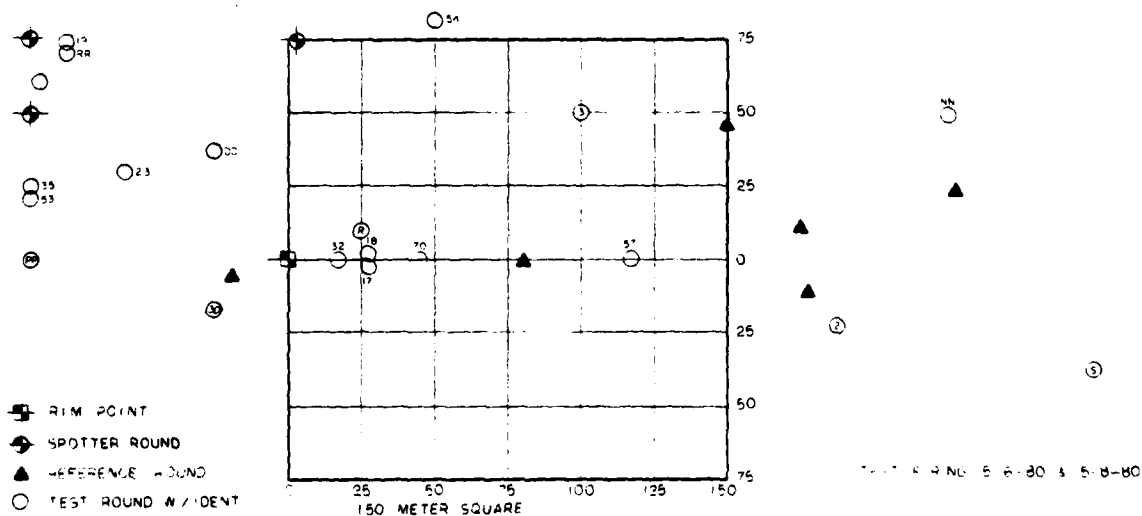


FIGURE 18. INERTIA WELD TEST FIRING DATA

CHAMBERLAIN MANUFACTURING CORPORATION

TABLE 12. ROTATING BAND WELD QUALITY AND BAND CONDITIONS AFTER TEST FIRING

Projectile Type	Ultrasonic Scan Rating			Remarks ¹
	Good	Fair	Poor	
70				Two small flakes, leading edge
32				One small flake, leading edge
18				Perfect
57				One flake, 1/4" wide x 1/8" long, trailing edge
2				Perfect
5				One flake, 1/4" wide x 1/8" long, leading edge
17				Perfect
30				One flake, 1/4" wide x 1/8" long, leading edge
PP				Two flakes, 1/4" wide x 1/8" long, leading edge
3				Perfect
54				Multiple flakes, leading edge
53				Two small flakes, leading edge
88				One flake, 5/8" wide x 1/8" long, trailing edge
100				Three chunks, 60° apart, leading edge to center
21				Perfect
35				Perfect
1				Two small flakes, 120° apart, leading edge; one V-shaped portion, leading edge to center
100				Six variable chunks, leading edge
19				Perfect
				Two flakes, 120° apart, leading edge several other small flakes

¹These remarks apply to visual examination of rotating bands after recovery.

²The worn gun tube had fired over 1700 rounds.

³"Flakes" are small areas from which the rotating band material has been removed, either by abrasion, tearing, or some other mechanism.

⁴The new gun tube was not fired before the two spotter rounds fired preliminary to the test firing.

TABLE 13. ACCEPTANCE TEST FIRING DATA

Date	Round No.	Weight (pounds)	Time to Impact (seconds)	Impact Point Relative to Target (in meters)		
				Short	Long	Left
May 6 ¹	Spotter			180		40
	S	104.3	42.39		290	40
	2	104.1	42.09		180	20
	PP	103.9	41.67	110		0
	30	104.4	40.80	20		0
	Reference	103.5	41.22		175	20
	57	104.4	41.03		115	10
	70	104.4	40.98		45	0
	32	104.4	40.89		15	0
	18	104.6	40.70		30	0
	Reference	103.5	40.80		80	0
	17	104.3	40.75		30	0
May 8 ²	R	104.5	40.80		25	5
	Reference	103.7	40.69	15		
	Spotter	103.5	40.21	148		150
	Spotter	103.6	30.98	400		140
	54	103.6	41.64		100	138
	NN	104.5	41.80			200
	19	104.4	40.23		300	150
	38	104.4	40.72		300	160
	Reference	103.6	41.26		0	180
	1	104.5	40.58		470	165
	3	104.5	40.86		50	180
	27	104.4	40.95		200	190
May 6 tests.	100	104.2	40.86		170	180
	Reference	103.7	41.38		100	210
	35	104.4	40.59		250	200
	53	104.4	40.36		350	200
	Reference	103.9	41.00		20	230

¹Fired with a worn gun tube

²Fired with a new gun tube; impact points are from center line of zone R field, not from impact point used in the May 6 tests.

CHAMBERLAIN MANUFACTURING CORPORATION

8. QUASI-PRODUCTION RUN AND TEST FIRING

8.1 Quasi-Production Run

In accordance with contractual requirements, Chamberlain's New Bedford Division conducted a quasi-production run of 260 each M483A1 Projectiles with inertia welded rotating bands. Based on work during the contract, the following machine parameters were selected:

$$WK^2 = 1477 \text{ lb-ft}^2$$

$$\text{Flywheel Spin Rate} = 1470 \text{ rpm}$$

$$\text{Ram Pressure} = 3600 \text{ psi}$$

For the entire quasi-production run, the standard band seat configuration was used and no lubricant coatings were applied. New Bedford inertia welded bands to projectile bodies, then heat treated the bodies and ultrasonically scanned the band-body interfaces. Ninety of the projectiles that were selected for firing and 17 that were not to be fired were shipped to AMMRC in Watertown, Massachusetts for ultrasonic scanning on the multiple-head transducer unit.

A total of 261 bands was inertia welded during the period 2 February through 13 March 1981. Processing information and weld quality after heat treatment are shown in Table 14. The welds, listed chronologically, were assigned CMC numbers from 1 to 261.

Of these 261 projectiles, 120 were selected for test firing according to the distribution scheme shown in Table 15. These projectiles were assigned Government numbers, also listed in Table 15.

TABLE 14. QUASI-PRODUCTION RUN OF INERT

PROJECTILE NUMBER		DATE WELDED	WELD TIME (seconds)	THRUST PRESSURE (psi)	SPINDLE RATE (rpm)	ULTRASONIC SCAN RATING			ULTRASONIC SCANS			PROJECTILE NUMBER		DATE WELDED	WELD TIME (seconds)	THRUST PRESSURE (psi)	SPINDLE RATE (rpm)	ULTRASONIC		
CNC	GOVERNMENT					GOOD	FAIR	POOR	BEFORE FIRING CNC	APRRC	AFTER FIRING CNC	CNC	GOVERNMENT					GOOD	FAIR	
1	61	2/2/81	.71	3550	1470	x			x	x		90	78		.71	3500	1470	x		
2	62		.67	3550		x			x	x		91	120		.75	3520	1470			
3	22		.66	3500		x			x	x		92	112		.73	3520	1480			
4	63		.73	3500		x			x	x		93	85		.71	3400	1470	x		
5	18		.73	3460		x			x	x		94	20		.71	3500	1480			
6	64		.68	3510		x			x	x		95	86		.64	3530	1470	x		
7			.65	3500					x	x										
8			.63	3440					x	x		96			.66	3580	1470			
9	65		.67	3500					x	x		97			.73	3570	1470			
10	8		.66	3510					x	x		98	109		.69	3580	1470	x		
11	21		.62	3500					x	x		99			.71	3540	1480			
12	108		.69	3430					x	x		100	87		.66	3520	1480	x		
13	7		.71	3480					x	x		101	88		.71	3540	1480	x		
14			.53	3440				x		x		102	45		.70	3560	1470	x		
15	14	2/5/81	.58	3510	1470	x			x	x		103			.66	3530	1470			
16			.62	3530		x			x	x		104		.72	3480	1470				
17	66		.69	3520		x			x	x		105	49	.68	3550	1470	x			
18	67		.67	3500		x			x	x		106	55	.68	3530	1470	x			
19	68		.69	3500		x			x	x		107	9	.74	3500	1480	x			
20	69		.62	3520		x			x	x		108	89	.63	3620	1480	x			
21			.62	3480		x			x	x		109	100	.64	3610	1480	x			
22	25		.71	3500		x			x	x		110		.72	3590	1480				
23	43		.68	3430		x			x	x		111	90	.67	3570	1480	x			
24	15		-	-		x			x	x		112	50	.63	3550	1480	x			
25	36		.62	3450		x			x	x		113	91	.69	3550	1480	x			
26	2		.64	3450		x			x	x		114	19	.71	3560	1480	x			
27	70		.64	3490		x			x	x		115	47	.66	3530	1470	x			
28	71		.60	3480		x			x	x		116	10	.67	3540	1470	x			
29			.66	3430		x			x	x		117	106	.64	3510	1470	x			
30	58	2/6/81	.66	3550	1470	x			x	x		118	60	.65	3500	1470				
31	3		.73	3500		x			x	x		119	35	.66	3550	1470	x			
32	17		.60	3490		x			x	x		120	92	.67	3530	1470	x			
33	107		.69	3510		x			x	x		121		.60	3520	1470	x			
34	27		.70	3500			x		x	x		122	104	.53	3520	1470	x			
35	24		.71	3530		x			x	x		123	93	.66	3410	1470	x			
36	72		.69	3520		x			x	x		124	59	.64	3510	1470				
37	52		.71	3420		x			x	x		125	33	.73	3530	1470	x			
38	39		.66	3500		x			x	x		126		.69	3520	1470				
39	102		.67	3490		x			x	x		127		.68	3490	1470				
40			.65	3490					x	x		128	105	.71	3530	1470	x			
41	30		.67	3500					x	x		129	13	.62	3470	1470	x			
42	42		.71	3450		x			x	x		130	11	.62	3510	1470	x			
43	44		.67	3490		x			x	x		131	51	.64	3530	1480	x			
44	117		.70	3440					x	x		132		.71	3530	1480				
45	74		.67	3320		x			x	x		133	101	.60	3500	1490	x			
46	75		.70	3470		1470	x			x	x		134	38	.69	3530	1480	x		
47	12		.64	3430			x			x	x		135		.71	3480	1480			
48	54		.58	3380			x			x	x		136	16	.65	3520	1480	x		
49	76		.67	3500			x			x	x		137	5	.64	3540	1480	x		
50			.73	3550						x	x		138	23	.66	3570	1480	x		
51	41		.66	3550			x			x	x		139	99	.67	3510	1470	x		
52	6		.69	3510			x			x	x		140	119	.71	3530	1480			
53			.64	3530						x	x		141	94	.68	3540	1480	x		
54			.72	3480						x	x		142	31	.67	3480	1480	x		
55	1		-	3480			x			x	x		143		.64	3500	1470	x		
56	113		.71	3500						x	x		144	95	.66	3500	1480	x		
57	37		.73	3470			x	x		x	x		145	32	.67	3490	1480	x		
58	26		-	3510				x		x	x		146		.60	3520	1480			
59			.69	3480						x	x		147	116	.62	3540	1470			
60	48		.71	3510			x			x	x		148		.68	3500	1470	x		
61	77		.70	3510			x			x	x		149	115	.66	3530	1470			
62		2/7/81	.67	3520	1480				x	x		150		.68	3540	1470				
63			.63	3530					x	x		151	114	.71	3490	1470	x			
64	110		.72	3540		x			x	x		152	96	.66	3520	1470				
65			.67	3550					x	x		153	118	.68	3510	1470	x			
66			.66	3560					x	x		154	34	.60	3510	1470	x			
67			.75	3530					x	x		155	97	.74	3500	1480	x			
68			.58	3540					x	x		156	46	.71	3480	1480	x			
69	79		.59	3500		x			x	x		157	56	.72	3480	1480				
70	80		.58	3490		x			x	x		158	98	.68	3480	1480	x			
71	83		.70	3450		x			x	x		159	53	.73	3510	1480	x			
72	81		.60	3520		x			x	x		160		.74	3520	1480				
73			.66	3530					x	x		161		.65	3510	1480	x			
74	82		.73	3510		x			x	x		162		.62	3590	1480	x			
75			.63	3510					x	x		163		.69	3570	1480	x			
76	111		.66	3520					x	x		164		.75	3550	1480				
77	84		.68	3530		x	x		x	x		165		.66	3570	1480	x			
78	29		.64	3470					x	x		166		.60	3540	1480	x			
79			.73	3540					x	x		167		.68	3520	1480	x			
80	103		.68	3540		x			x	x		168		.62	3520	1480	x			
81	28		.67	3490					x	x		169		.62	3530	1480	x			
82	57		.73	3510					x	x		170		.60	3540	1480				
83	4		.71	3490					x	x		171		.64	3550	1480	x			
84	40		.72	3580		x			x	x		172		.64	3550	1480				
85			.68	3570					x	x		173		.67	3490	1480	x			
86			.70	3500					x	x		174		.64	3520	1480				
87			.67	3550		x			x	x		175		.64	3820	1460				
88	73		.69	3530		x			x	x		176		.58	3820	1740				
89			.68	3500		x			x	x		177		.70	3770	1790	x			

OF INERTIA WELDED M483 PROJECTILES

PENCIL DATE (Yr)	ULTRASONIC SCAN RATING			ULTRASONIC SCANS			PROJECTILE NUMBER		DATE WELDED	WELD TIME (seconds)	THRUST PRESSURE (psi)	SPINDLE RATE (rpm)	ULTRASONIC SCAN RATING			ULTRASONIC SCANS						
	GOOD	FAIR	POOR	BEFORE FIRING		AFTER FIRING	CMC	GOVERNMENT					GOOD	FAIR	POOR	BEFORE FIRING CMC	AFTER FIRING AMRC	AFTER FIRING CMC				
				CMC	AMRC																	
1470	x			x	x		178		3/9/81	.62	3750	1490		x		x						
1470			x	x		x	179			.70	3770	1790	x			x						
1480		x		x			180			.62	3750	1490			x							
1470	x			x	x		181			.68	3730	1790		x		x						
1480		x		x	x		182			.68	3830	1810			x							
1470	x			x	x		183			.61	3820	1820		x		x						
							184			.68	3830	1820			x							
							185			.68	3830	1820			x							
1470			x	x			186					1820			x							
1470			x	x	x		187			.69	3850	1820			x							
1470	x			x			188		.71	3860	1820		x		x							
1480			x	x	x		189		.59	3870	1830				x							
1480	x			x	x		190		.71	3920	1830				x							
1470	x			x	x		191		.70	3850	1830				x							
1470			x	x			192		.70	3900	1830	x			x							
1470			x	x	x		193		.70	3900	1830		x		x							
1470	x			x	x		194		.80	3530	1460	x			x							
1470	x			x	x		195		.58	3490	1450	x			x							
1480	x			x	x		196		.71	3510	1450	x			x							
1480	x			x	x		197		.62	3480	1450	x			x							
1480	x			x	x		198		.71	3470	1450	x			x							
1480			x	x			199		.71	3510	1450			x								
1480	x			x	x		200		.62	3460	1450	x			x							
1480	x			x	x		201		.69	3510	1450	x			x							
1480	x			x	x		202		.68	3470	1450			x								
1480	x			x	x		203		.73	3480	1450			x								
1480	x			x	x		204		.68	3410	1450	x			x							
1470	x			x	x		205		.70	3460	1450	x			x							
1470	x			x	x		206		.67	3410	1450	x			x							
1470			x	x			207		.66	3460	1450			x								
1470	x			x	x		208		.57	3450	1450	x			x							
1470	x			x	x		209		.64	3440	1450	x			x							
1470	x			x	x		210		.69	3430	1450			x								
1470	x			x	x	x	211		.68	3450	1460	x			x							
1470	x			x	x		212		.69	3450	1450	x			x							
1470			x	x			213		3/11/81	.71	3440	1450		x		x						
1470	x			x	x		214			.68	3410	1450			x							
1470			x	x			215			.62	3440	1450			x							
1470			x	x	x	x	216			.65	3460	1450		x		x						
1470	x			x	x		217			.67	3470	1450	x			x						
1470	x			x	x		218			.71	3460	1450	x			x						
1470	x			x	x		219			.71	3440	1450	x			x						
1490	x		x	x			220			.62	3430	1450	x			x						
1480			x	x			221			.68	3430	1450	x			x						
1490	x			x			222			.69	3510	1450	x			x						
1480	x			x		x	223		.69	3510	1450	x			x							
1480				x			224		.67	3520	1450	x			x							
1480	x			x			225		.63	3480	1450	x			x							
1480	x			x			226		.65	3490	1450	x			x							
1480	x			x			227		.67	3520	1450	x			x							
1470	x			x		x	228		.65	3530	1450	x			x							
1480		x		x		x	229		.65	3490	1450	x			x							
1480	x			x			230		.68	3500	1450	x			x							
1480	x			x			231		.67	3510	1450	x			x							
1470	x			x			232		.69	3500	1450	x			x							
1480	x			x			233		.67	3480	1450	x			x							
1480	x			x			234		.56	3490	1450	x			x							
1480				x			235		.71	3460	1450	x			x							
1470		x		x			236		.69	3470	1450			x								
1470	x			x			237		.64	3500	1450	x			x							
1470				x			238		.62	3470	1450			x								
1470			x	x			239		.71	3480	1450			x								
1470	x			x		x	240		.67	3460	1450			x								
1470	x			x			241		.69	3500	1450			x								
1470				x			242		.67	3500	1450			x								
1470	x			x			243		.71	3490	1450			x								
1480	x			x			244		.71	3480	1450			x								
1480	x			x			245		.71	3490	1450			x								
1480		x		x			246		.73	3500	1450			x								
1480	x			x			247		3/12/81	.68	3560	1450			x							
1480	x			x			248			.71	3530	1450			x							
1480			x	x			249			.75	3500	1450			x							
1480	x			x			250			.66	3520	1450			x							
1480	x			x			251			.73	3490	1450			x							
1480	x			x			252			.73	3520	1450			x							
1480	x		x	x			253			.73	3490	1450			x							
1480	x			x			254			.60	3470	1450			x							
1480	x			x			255			.64	3460	1440			x							
1480	x			x			256			.75	3450	1440			x							
1480	x			x			257		.69	3490	1440	x			x							
1480	x			x			258		.62	3530	1440			x								
1480	x			x			259		.60	3510	1440			x								
1480	x			x			260		.68	3510	1440	x			x							
1480	x			x			261		.64	3520	1450	x			x							
1460				x																		
1760				x																		
1790	x			x																		

CHAMBERLAIN MANUFACTURING CORPORATION

Appendix B¹ contains scans generated by Chamberlain, before firing, for all 120 welds, and scans generated by AMMRC for 90 of the welds. Agreement is quite good in most cases. Fifteen of the projectiles recovered after firing were selected for a second scanning test. These scans, also included in Appendix B, show little or no increase in disbonding due to firing and ground impact.

8.2 Test Firing

The firing report prepared by Yuma Proving Ground (YPG) personnel is included as Appendix C. The round-by-round data for the firing of 120 projectiles with inertia welded rotating bands and 40 control projectiles with welded overlay bands show no significant difference in performance attributable to the method of band application. Included in the firing report is an evaluation by YPG personnel of the condition of the rotating bands on 31 recovered projectiles, 24 with inertia welded bands and seven with welded overlay bands. Again, no significant differences in band condition due to method of band application are apparent.

All recovered rounds, which included 110 of the 120 with inertia welded bands, were sent to ARRADCOM for further evaluation. Ten of the 110 were considered by ARRADCOM personnel to have significant loss of band material. These 10 projectiles, whose photographs appear in Appendix D, were among the 15 rounds described earlier that were scanned after firing and showed little or no increase in disbond due to firing or ground impact. Small flaws are seen along the leading edge of nine of the photographed bands. In the opinion of Chamberlain personnel experienced in ballistic testing, these flaws are very similar to flaws commonly observed on recovered rounds with welded overlay bands. The photograph of Round No. 120 shows a

¹Appendix B accompanies this report under separate cover so that 8 1/2- by 14-inch paper could be used to present clearly the ultrasonic scanning tapes.

CHAMBERLAIN MANUFACTURING CORPORATION

local deeper flaw; but the raised metal behind the flaw raises doubt that this happened in the gun tube and suggests that it probably occurred upon ground impact or recovery.

TABLE 15. DISTRIBUTION SCHEME FOR M483A1 PROJECTILES

GROUP	ZONE NO.	ZONE CONDITION	GOVERNMENT PROJECTILE NO.	ULTRASONIC SCAN RATING
A	3	Cold	1-25	Good
	3	Cold	26-27	Fair
	3	Cold	28-30	Poor
B	8	Hot	31-55	Good
	8	Hot	56-58	Fair
	8	Hot	59,60	Poor
C	8	Overcharge, Hot	61-110	Good
	8	Overcharge, Hot	111-119	Fair
	8	Overcharge,	120	Poor

Prior to the firing tests, the ultrasonic scans of 259 inertia welds (261 welds were made, but two parts were lost in machining) were visually evaluated and placed in categories of good, fair or poor. The distribution of welds after this preliminary sorting was as follows:

CHAMBERLAIN MANUFACTURING CORPORATION

GOOD WELDS : 161 (62 percent)
FAIR WELDS : 35 (14 percent)
POOR WELDS : 63 (24 percent)

As noted in Table 15, six welds rated "poor" were included in the test firing. All six performed well in flight. Five of the six were recovered; four showed no loss of band material. Of these six rounds rated "poor," Round No. 59 had the poorest weld with 84 percent of the band seat area bonded. This round was not recovered, but flight and impact data show that its performance was well within the range of the control round parameters. Comparing the scans of the 63 welds rated "poor" indicated that 32 of these welds had bonded areas of less than 84 percent.

As noted earlier in this report, disbond distribution and total disbond area are both factors in determining ballistic performance. Considering only the total disbond area, at least 31 of the 63 welds rated "poor" could be expected to show acceptable flight and impact performance.

Based on the test firing results, the distribution for the quasi-production run is:

ACCEPTABLE WELDS : 227 (88 percent)
UNTESTED WELDS : 32 (12 percent)

The firing tests have shown: 1) that statements during the contract period of a 24-percent reject rate (63 of 259 welds) were incorrect; and 2) that the performance-rated reject rate is a maximum of 12 percent. Further testing is required to show whether the value is lower.

8.3 Inertia Weld Tooling

Development problems were encountered with the tooling before and after the quasi-production run. These problems were solved or tolerated to the extent necessary to complete the 261 welds for the quasi-production run.

CHAMBERLAIN MANUFACTURING CORPORATION

The serrated inserts for the jaws that clamp the rotating rotating band to the projectile body were initially made from a low-carbon steel with the serrated edge carburized. These worked well for a small number of welds, but the temperatures reached during welding were such that the carburized surface softened. When this occurred, the serrations folded over and could no longer hold the band. This was alleviated by fabricating the inserts from A-9 tool steel. The softening temperature of this steel is high enough that the serrations did not fail. However, cracks emanating from the bolt holes developed. Four sets of inserts were required to complete approximately 300 welds.

Problems also were encountered with the rotating chuck assembly. In several instances, the slide mechanism that opens and closes the jaws would fail to open far enough to release a welded projectile; the jaws would not close enough to retain the band in its proper position. Manufacturing Technology, Inc. (MTI), Mishawaka, Indiana, was contacted to aid in solving this problem. MTI personnel believed that the surfaces were galled, a condition believed to be attributable to improper surface treatment. The chuck assembly was returned to MTI to for polishing and nitriding of the chuck surface. This was helpful, but Chamberlain personnel found that frequent lubrication of the chuck assembly was also helpful. In two instances, the chuck jaws became "frozen" and disassembly was necessary to make the chuck operational. The only readily-available explanation for the chuck's binding this tightly was that the galled surfaces may have caused the problem.

The thrust bearing was the source of most of the tooling problems. Initially, a Torrington® bearing was used but was found to be inadequate. The bearings were mounted in a cage arrangement that was spot welded together to contain the bearings. These bearings would last for only a few welds, then would break up.

The thrust bearing assembly was then modified. Although this bearing worked more successfully, it still would last for only 30 to 50 welds

CHAMBERLAIN MANUFACTURING CORPORATION

before the steel fractured between the roller bearing cavities.

Chamberlain personnel believed that a softer solid material would stand up to the forces present during welding. A thrust bearing of bronze was made and used for the remaining welds in the quasi-production run. This bearing lasted over 100 welds and was still in good condition at the conclusion of the run. Thus, the life expectancy of this bearing was not determined.

There was a problem in that, after two or three welds, the bolts holding the thrust plate would be very loose, necessitating tightening. This was attributed to the rotational forces present during flywheel acceleration and could be remedied by modifying the thrust plate to use left-handed hold-down bolts.

The experience gained during this contract indicates that, although further refinements of the current design could improve reliability in the inertia welder, a major design change is preferable. Chamberlain and the manufacturer of the inertia welder agree that a better method would be to rotate the projectile body while the band and clamping mechanism are stationary. The clamping device would be similar to a hydraulic band setter and could be as massive and powerful as necessary, since it would not be part of a rotating collet, as in the present design.

CHAMBERLAIN MANUFACTURING CORPORATION

9. CONCLUSIONS

9.1 Disbond-free welds can be obtained when the band seat and rotating band are clean. Disbond-free welds can also be achieved when certain lubricants are used.

9.1.1 The necessary degree of rotating-band cleanliness can be obtained either by machining the inside diameter of the band without using a lubricant or by acid etching the band.

9.1.2 The necessary degree of band cleanliness can be obtained by washing the projectile body with detergent and rinsing it with hot water, immersing the aft half of each body (including the band-seat area) in a commercial degreaser solution, then wiping the part dry.

9.1.3 If cleaned, bodies exposed to air for up to 69 days with no protection (and up to 79 days with a rust-preventative coating) will still yield good inertia welds if mated with freshly-machined bands.

9.1.3.1 Machined bands can be stored for at least 24 hours without being welded and not harm weld quality. Acid-etched bands must be used within 10 minutes after etching, since their more chemically-active surface will tarnish quickly and contribute to poor welds.

9.2 Ultrasonic scanning is a reliable, nondestructive means of determining the quality of inertia welded rotating bands on projectile bodies.

9.2.1 Destructive tests substantiate ultrasonic scanning's capability by providing direct, visual evidence of bonding quality that corroborates the scanning tapes' accuracy. Destructive tests that played such a role included torch heating, tear tests and shear tests.

9.2.2 Light microscopy and dye penetrant testing of inertia weld cross-sections could detect obvious areas of disbond, but were not

AD-A121 268

PROCESS PARAMETERS FOR BANDING 155-MM M483A1
PROJECTILES IN HIGH-CAPACITY..(U) CHAMBERLAIN MFG CORP
WATERLOO IA RESEARCH AND DEVELOPMENT DIV..

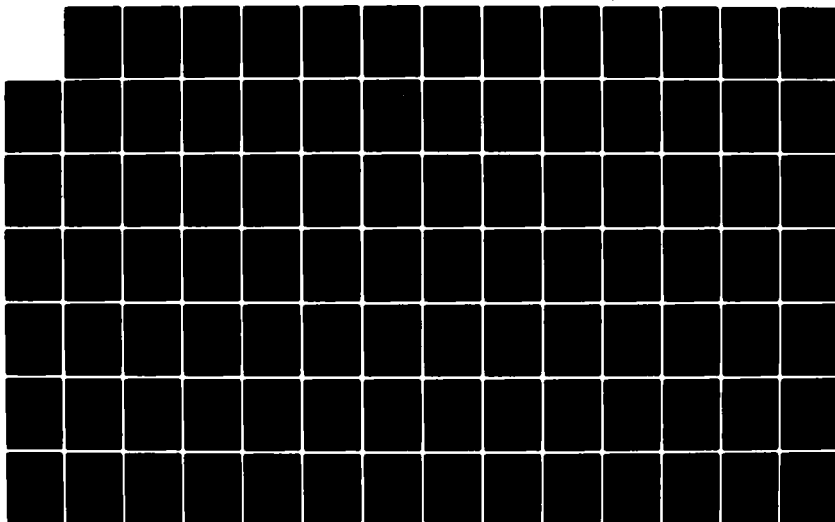
2/3

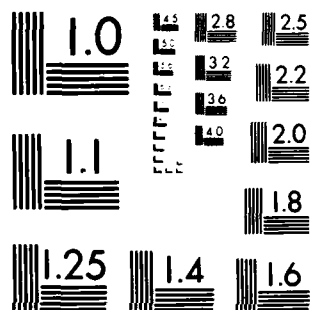
UNCLASSIFIED

J A YTTERHUS SEP 82 C8184-PR-072

F/G 19/1

NL





MICROCOPY RESOLUTION TEST CHART
NATIONAL BUREAU OF STANDARDS-1963-A

CHAMBERLAIN MANUFACTURING CORPORATION

sufficiently sensitive to distinguish disbond areas in which the band and body were in intimate contact.

9.3 Heat treatment has little or no deleterious effect on welds that have a low percentage of disbond area in the as-welded condition.

9.3.1 When inertia weld quality is poor, heat treatment will usually increase the disbonded area.

9.3.2 Heat treating projectiles with inertia welded rotating bands will often increase disbond along the forward and aft edges of the band.

9.3.3 Projectiles with inertia welded rotating bands can be quenched at higher quench rates, without cracking, than can projectiles with welded overlay bands.

9.4 High-quality inertia welds can be obtained by applying certain lubricants to the band seat prior to welding.

9.4.1 When welding with the proper lubricant, the "chatter" or galling action associated with dry welds is eliminated. This will presumably lead to extended tooling life.

9.5 Twenty projectiles with inertia welded rotating bands, representing a wide range of weld quality, were test fired. Little loss of band material occurred; in several instances, the loss could be correlated with areas ultrasonic scanning showed to be disbonded.

9.5.1 Flight characteristics of projectiles that suffered some band material loss were not adversely affected.

9.6 A total of 120 inertia welded projectiles from the 261-projectile quasi-production run were test fired. These projectiles represented a wide

CHAMBERLAIN MANUFACTURING CORPORATION

range of weld quality. Their dynamic performance was equal to that of 40 control projectiles with welded overlay bands.

9.6.1 Based on the firing performance of the projectiles with the largest areas of disbond, the reject rate for the quasi-production run was determined to be less than or equal to 12 percent.

9.6.2 Only 10 of these 120 test-fired projectiles lost band material in firing. This loss is minimal and does not affect flight performance.

9.6.3 Based on tooling problems and the resultant percentage of poor welds, additional effort is required to ready the inertia welding process for production.

10. RECOMMENDATIONS

10.1 Redesign tooling so that the projectile body is spun and the rotating band is clamped by a device similar to a conventional band setter.

10.2 Make an in-depth analysis of available data to determine whether a positive correlation exists between inertia welding machine parameters and weld quality.

10.3 If a positive correlation between machine parameters and weld quality does exist, install a minicomputer system on the inertia welder to monitor and display those parameters. This will give the inertia welding machine operator a visual display depicting weld quality.

10.4 Perform additional inertia weld testing to determine whether using the proper lubricant materials will provide extended tooling life and consistent weld quality during production operations.

10.5 Conduct additional firing tests with projectiles with intentionally poorly-welded rotating bands to determine the lower limit of weld quality that will perform successfully under dynamic conditions.

10.6 Conduct an economic analysis of the inertia welding process. This analysis should consider all the necessary procedures discussed in this report to determine the cost effectiveness of using the inertia welding process to band M483A1 Projectiles.

CHAMBERLAIN MANUFACTURING CORPORATION

DISTRIBUTION LIST

Commander
U.S. Army Armament Research and
Development Command
ATTN: DRDAR-TSS
DRDAR-QAR-Q
DRDAR-LCU-SS
DRDAR-LCU-M (10)
DRDAR-QAR-I
Dover, NJ 07801

Administrator
Defense Technical Information Center
ATTN: Accessions Division (12)
Cameron Station
Alexandria, VA 22314

Commander
U.S. Army Munitions Production Base
Modernization Agency
ATTN: SARPM-PBM-MA (2)
Dover, NJ 07801

Director
U.S. Army Materiel Systems Analysis Activity
ATTN: DRSXY-MP
Aberdeen Proving Ground, MD 21005

Commander/Director
Chemical Systems Laboratory
U.S. Army Armament Research and
Development Command
ATTN: DRDAR-CLJ-L
DRDAR-CLB-PA
APG, Edgewood Area, MD 21010

Director
Ballistics Research Laboratory
U.S. Army Armament Research and
Development Command
ATTN: DRDRAR-TSB-S
Aberdeen Proving Ground, MD 21005

CHAMBERLAIN MANUFACTURING CORPORATION

DISTRIBUTION LIST, CONTINUED

Chief

Benet Weapons Laboratory, LCWSL

U.S. Army Armament Research and
Development Command

ATTN: DRDAR-LCB-TL

Watervliet, NY 12189

Commander

U.S. Army Armament Materiel Readiness Command

ATTN: DRSAR-LEP-L

Rock Island, IL 61299

Director

Industrial Base Engineering Activity

ATTN: DRXIB-MT (2)

Rock Island, IL 61299

Director

U.S. Army TRADOC Systems Analysis Activity

ATTN: ATAA-SL

White Sands Missile Range, NM 88002

Commander

U.S. Army Materiel Development and Readiness Command

ATTN: DRCMT

5001 Eisenhower Avenue

Alexandria, VA 22333

CHAMBERLAIN MANUFACTURING CORPORATION

(This page left blank intentionally.)

APPENDIX A

AN ELASTIC FINITE ELEMENT MODEL OF THE AUSTENSITE TO MARTENSITE
QUENCH FOR AXISYMMETRIC AND TWO-DIMENSIONAL GEOMETRIES

CHAMBERLAIN DOCUMENT NO. C8099-PR-002

ROBERT B. EVANS

TABLE OF CONTENTS

	PAGE
SELECTED SYMBOLS AND UNITS	iv
INTRODUCTION	1
MODEL DESCRIPTION	3
Overview	3
Thermal Analysis	6
Stress Analysis	13
Fracture Analysis	16
Discussion	20
COMPUTER PROGRAM THEORY	22
CONVEC	22
E12202	32
SAAS III	32
BENCHMARK ANALYSES	34
Temperature Invariant Convection Coefficient	34
Infinite Cylinder Thermal Stress Analysis	37
M483 PROJECTILE ANALYSIS	45
Problem Statement	45
Thermal Analysis	48
Stress Analysis	60
Fracture Analysis	76
Discussion	77
ENDNOTES	80
BIBLIOGRAPHY	83

TABLE OF CONTENTS

	PAGE
ACKNOWLEDGMENTS	86
APPENDIX A: FORTRAN LISTING OF CONVEC	87
APPENDIX B: COMPUTER OUTPUT FOR INFINITE CYLINDER ANALYSIS	91
E12202 Output	91
SAAS III Output	96

SELECTED SYMBOLS AND UNITS

Physical quantity	Symbol	SI to English conversion
length	L	1m = 3.2808 ft
area	A	1m ² = 10.7639 ft ²
volume	v	1m ³ = 35.3134 ft ³
temperature	T	°F = 9/5 °C + 32
convection coefficient	h	1W/m ² °C = 0.1761 Btu/h ft ² °F
conductivity	k	1W/m °C = 0.5778 Btu/h ft °F
specific heat	c _p	1kJ/Kg °C = 0.23884 Btu/lb _m °F
density	ρ	1Kg/m ³ = 0.06243 lb _m /ft ³
thermal diffusivity	α	1m ² /s = 10.7639 ft ² /s
heat flow	q	1W = 3.4121 Btu/h
modulus of elasticity	E	1MPa = 1.45038x10 ² lb _f /in ²
Poisson's ratio	ν	-
coefficient of thermal expansion	Δ	1m/m °C = 1.8 in/in °F
stress	σ	1MPa = 1.45038x10 ² lb _f /in ²
stress intensity factor	K _I	1MPa√m = 0.910 ksi√in

INTRODUCTION

The most common method to harden steel by heat treatment is the austenite to martensite quench followed by a tempering operation.¹ The steel piece is brought to some temperature above the austenitizing temperature and then quenched in an agitated liquid bath. The quenchant, bath temperature, initial temperature, and agitation are chosen such that the piece cools quickly enough to transform directly to martensite. The piece is subsequently tempered to the desired hardness.

Two mechanisms account for the stresses that occur in the piece during the austenite to martensite quench.² One mechanism is the non-uniform thermal contractions of the piece due to temperature gradients. The other mechanism is the volumetric expansion due to the difference in form between the close-packed austenite crystal structure and the more open crystal structure of martensite. Since martensite is an extremely brittle microstructure, these thermal and transformation stresses can result in quench cracks.

The research reported in this thesis is directed toward developing a mathematical model of the temperatures and stresses during the austenite to martensite quench process for axisymmetric and two-dimensional geometries. Whereas the temperatures and stresses due to the austenite to martensite quench have been investigated for some geometries,³ a general-purpose axisymmetric and two-dimensional quench model is not available in the public domain. The availability in the public domain of several finite element heat transfer⁴ and stress analysis⁵ programs

greatly facilitates the development of a general-purpose axisymmetric and two-dimensional quench model.

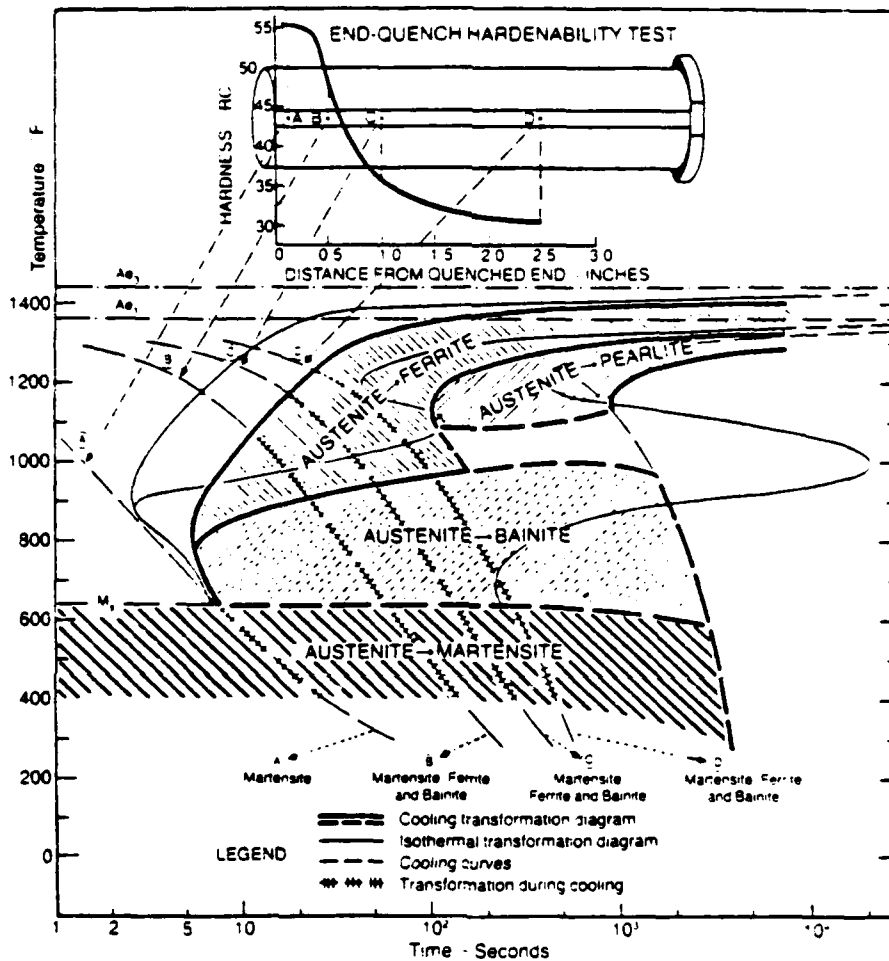
This thesis presents a description of a proposed general-purpose axisymmetric and two-dimensional model of the austenite to martensite quench operation. In addition, several analyses are presented that benchmark the model against closed-form analytical solutions. Lastly, an illustrative analysis is presented for the M483 projectile currently being produced by Chamberlain Manufacturing Corporation, New Bedford, Massachusetts.

MODEL DESCRIPTION

Overview

The scope of this quench model can best be described by use of a continuous cooling transformation diagram (C-T diagram). Figure 1 shows a typical C-T diagram for 4140 steel. A Jominy-end quench curve is also shown in Figure 1. Cooling curves for various points at different distances from the quenched end are superimposed on the C-T diagram. A pure austenite to martensite transformation is obtained for those points close enough to the quenched end such that their cooling curve misses the nose of the C-T diagram. Cooling curve A shows such an austenite to martensite transformation. For those points further from the quenched end, such as B, C, and D, microstructures other than martensite will form upon cooling. Since transformations other than austenite to martensite are isothermal with heat generation, the quench model is only valid for those cooling curves missing the nose of the C-T diagram. The quench model methodology will require that the convection coefficient curves calculated from a standardized test be scaled such that the slowest cooling spot within the piece to be analyzed misses the nose of the C-T diagram.

As can be seen in Figure 1, cooling curves for a given piece vary from point to point. At temperatures above M_s (the temperature at which the austenite begins to transform to martensite) these temperature gradients result in thermal stresses. As faster cooling areas of the problem geometry drop below the M_s temperature, they begin to expand due to the difference in volume between the austenite and martensite crystal



Source: United States Steel Company, Atlas of Isothermal Transformation Diagrams (Pittsburgh: U.S. Steel, 1951), p. 13.

Fig. 1 Continuous cooling diagram and end-quench hardenability test data curve for 4140 steel.

structure. This volumetric expansion is approximately 4.2% after the transformation is complete.⁶ The quench model assumes zero expansion at the M_s temperature with a linearly increasing expansion up to 4.2% at M_f (the temperature at which the austenite is completely transformed to martensite). The stress resulting from the transformation expansion will be referred to as a transformation stress. In the elastic analysis, superposition can be used and thus the thermal and transformation stresses can be added together to obtain the total stress at a point.⁷

The quench model can be compartmentalized into three analyses. A thermal analysis is required to determine the temperature distribution within the piece at any specified time. Next, this temperature distribution is used in a stress analysis to determine the stress distribution at any given time. Finally, areas of significant surface tensile stress are checked in a linear elastic fracture mechanics analysis to predict critical surface thumbnail crack sizes.

Two general-purpose axisymmetric and two-dimensional finite element computer codes were selected from the public domain as the nucleus of the quench model. These codes are SAAS III (stress analysis of axisymmetric solids, written under government contract by the Aerospace Corporation, San Bernadino, California) and El2202 (a steady state and transient thermal analysis program, written under government contract by the Aerojet-General Corporation, Sacramento, California). Documentation for both codes is available from the National Technical Information Service, Springfield, Virginia.^{8,9} Both codes were keypunched

from the documentation and loaded into the Chamberlain in-house minicomputer. Some modifications in program size (mainly DIMENSION and COMMON size reductions) were required to fit the programs into the minicomputer. In addition, the Calcomp plotter graphics were changed to operate on a Tektronix 4014 CRT terminal.

A third computer program CONVEC was written using a finite difference algorithm to calculate convection coefficients for boiling heat transfer in a specified quenchant. Input to this program is a temperature history obtained from a standardized quench test. This test consists of quenching a standardized specimen and recording its center-point temperature. The convection coefficient curve (convection coefficients as a function of surface temperature) obtained from the standardized test specimen is then scaled to a level necessary to insure an austenite to martensite transformation throughout the actual problem geometry. Details of the convection coefficient curve scaling methodology will be presented in the next section.

An overview of the model methodology is shown in Figure 2. The rectangular boxes indicate the basic flow of the model methodology. Circles indicate major inputs and outputs to the model. Reference to Figure 2 may prove helpful in maintaining an overall model perspective during the more detailed discussion to follow.

Thermal Analysis

The first step in the thermal analysis is to determine the quenching characteristics of the quenchant. This is accomplished through a standardized quench test and the use of CONVEC. The standard test specimen is quenched in the specified quenchant and the center point temperature

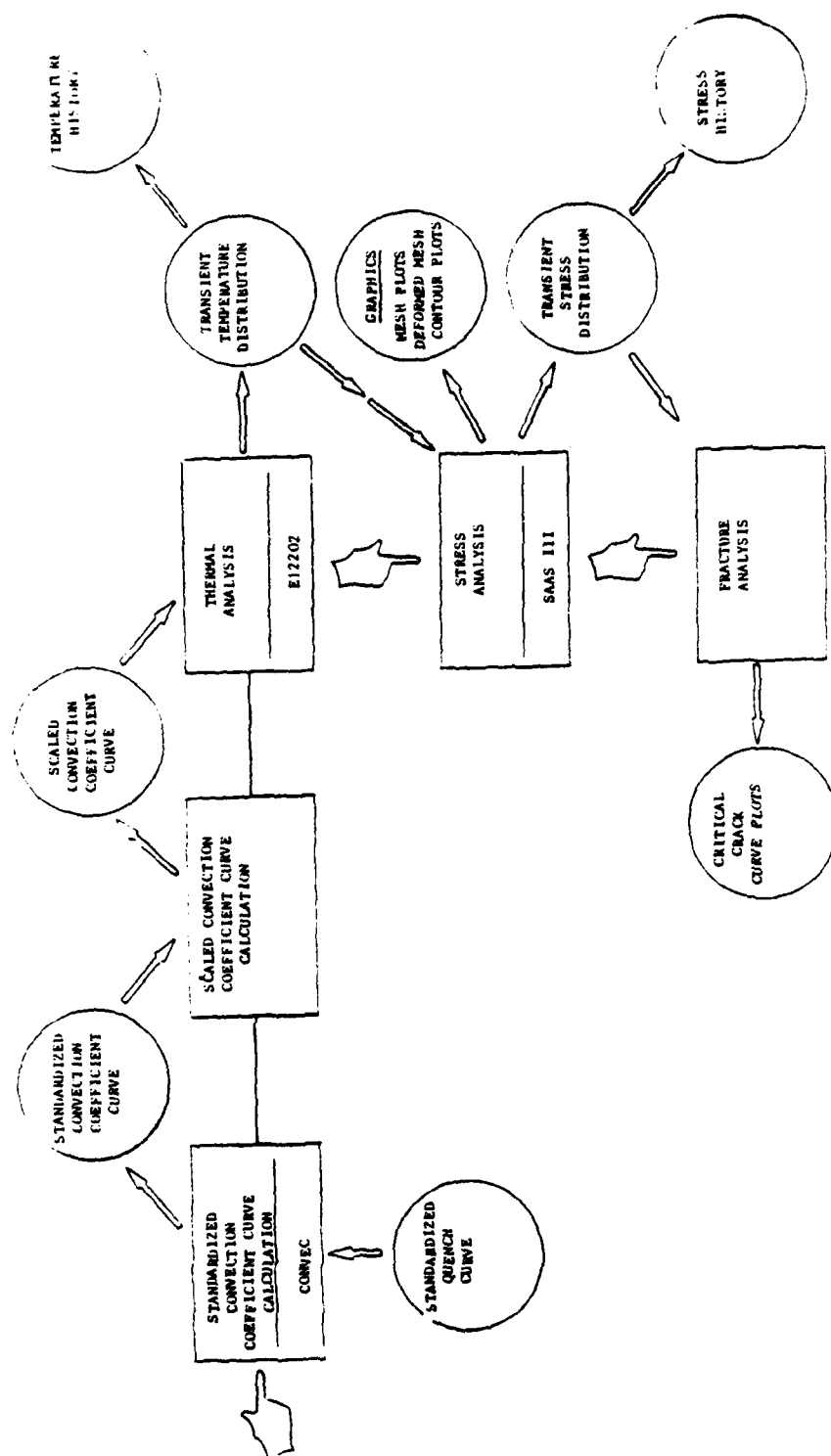


Fig. 2 Quench model overview.

is recorded by thermocouple. Typical data for various quenchants manufactured by the E. F. Houghton & Company are shown in Figure 3. Included in Figure 3 is a description of the standard test specimen. CONVEC uses the standardized cooling curve to calculate the convection coefficients as a function of surface temperature of the test specimen.

The second step of the thermal analysis is to scale the standardized convection coefficient curve such that all points within the problem geometry miss the nose of the C-T diagram. This is accomplished by running the actual problem geometry with program E12202 using the standardized convection coefficient curve. The problem is then rerun with the standardized convection coefficient curve multiplied uniformly by a scale factor. This is repeated with larger scale factors until the slowest cooling spot within the problem geometry misses the nose of the C-T diagram.

The last step of the thermal analysis is to run the problem with the final scaled convection coefficient curve and output the resultant transient temperature distribution to a diskfile for future use during the stress analysis. The temperature distribution is also output to the line-printer. Temperature histories of specified points can then be constructed from the printed output.

The thermal analysis method is based upon principles of pool boiling heat transfer. The primary heat transfer mechanism in pool boiling is vapor bubble formation and agitation. Therefore, pool boiling is not strongly geometry dependent.¹⁰ Figure 4 shows a typical cooling curve

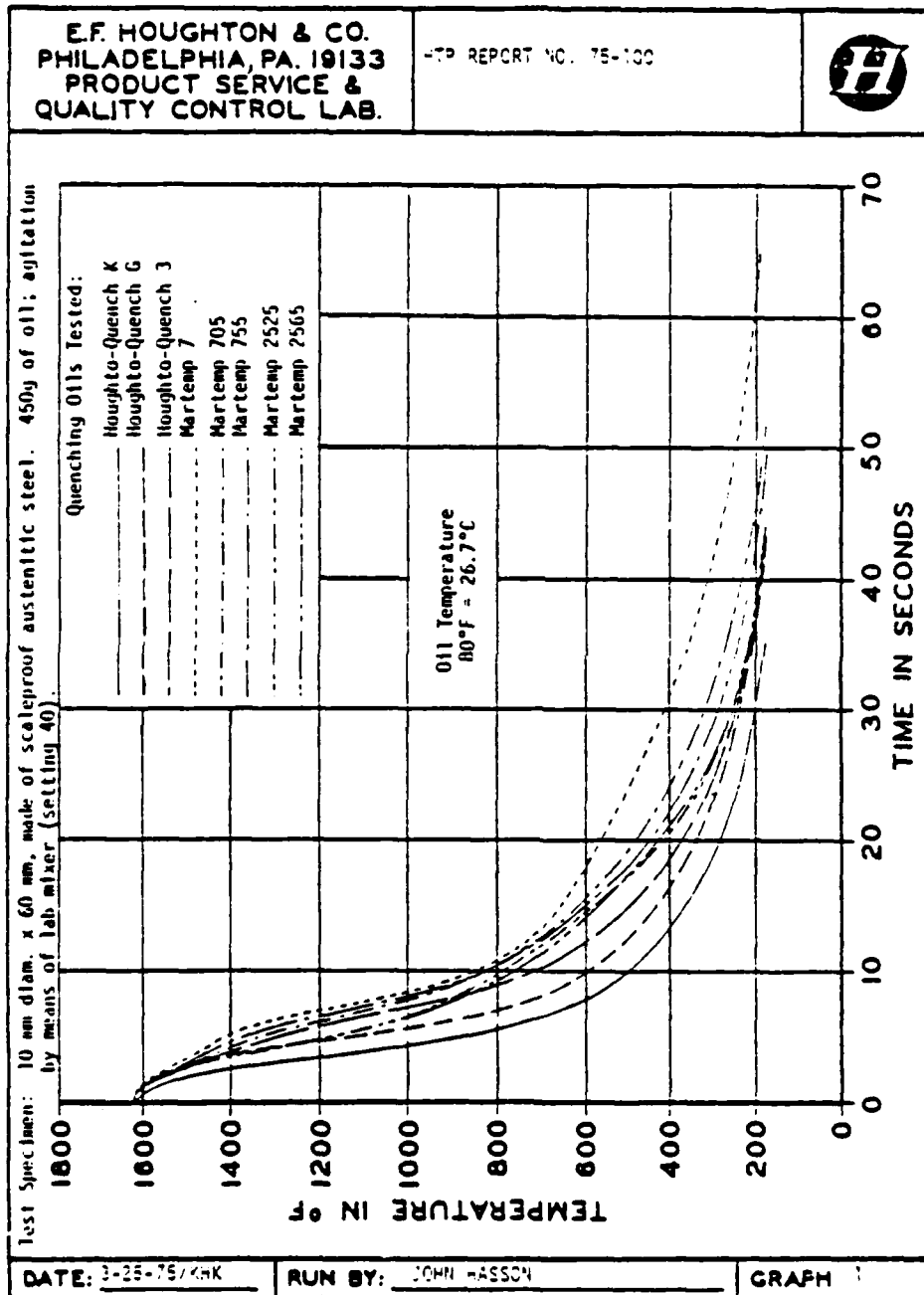


Fig. 3 Temperature curves for standardized test specimen quenched in different quenching oils.

during a quench. The slope of the cooling curve indicates three different stages of heat transfer.¹¹ The slow rate of heat transfer during the first stage is caused by a thin vapor blanket that surrounds the piece. The mechanism of heat transfer across the vapor film during the first stage is referred to as film boiling.¹² Gradually, the vapor film becomes unstable and breaks up into rapid bubble formation. This mechanism of heat transfer is referred to as nucleate boiling.¹³ The heat transfer during this second stage is much faster than the first stage. As the temperature of the piece continues to decrease, bubbles form and rise less rapidly and the cooling curve enters the slower third stage. When the temperature finally drops below the boiling point, the heat transfer mechanism changes to that of pure convection. At this point, geometry becomes an important factor as a boundary layer develops.

The convection coefficient is an indicator of the rate of heat transfer through the surface of the specimen. Figure 5 shows a plot of the convection coefficient as a function of the excess surface temperature of the specimen above the saturation temperature for a typical quench. The three stages of heat transfer are indicated. Since pool boiling heat transfer is not strongly geometry dependent, a convection coefficient curve calculated for a standardized test specimen is used in the quench model for the actual problem geometry.

The justification for uniform scaling of the standardized convection coefficient curve is based on data obtained from the E. F. Houghton & Company. Figure 6 shows thermocouple data of the rate of temperature change in a standardized test specimen for several different quenchants

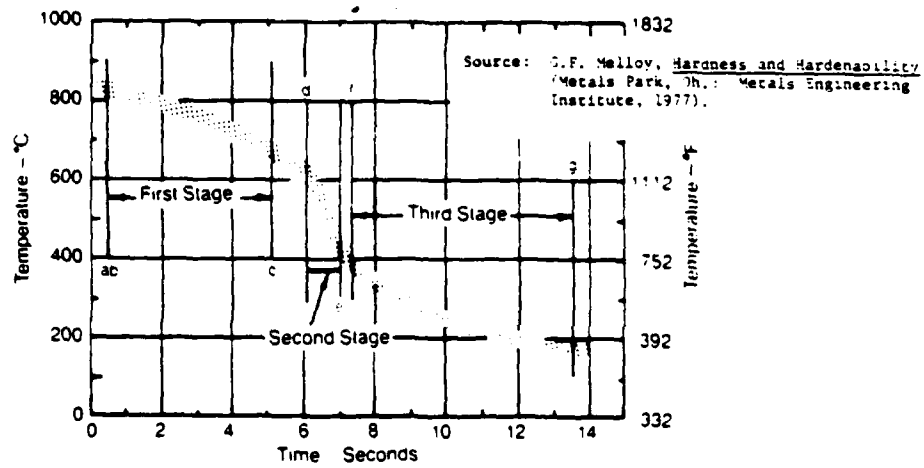


Fig. 4 Typical quench cooling curve.

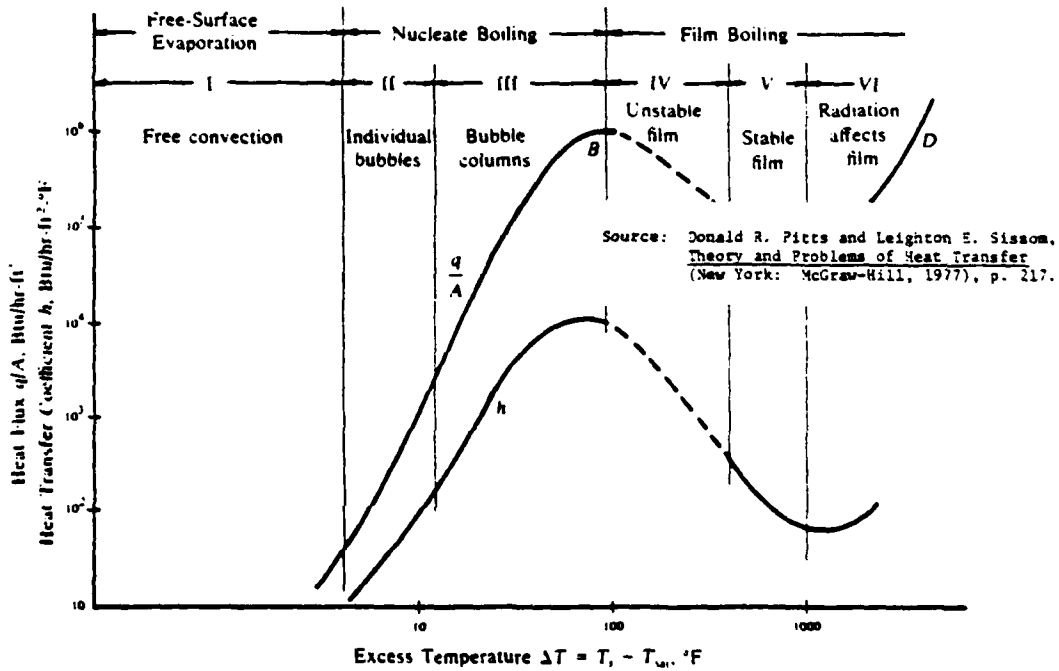


Fig. 5 Typical heat flux and convection coefficient curves for pool boiling heat transfer.

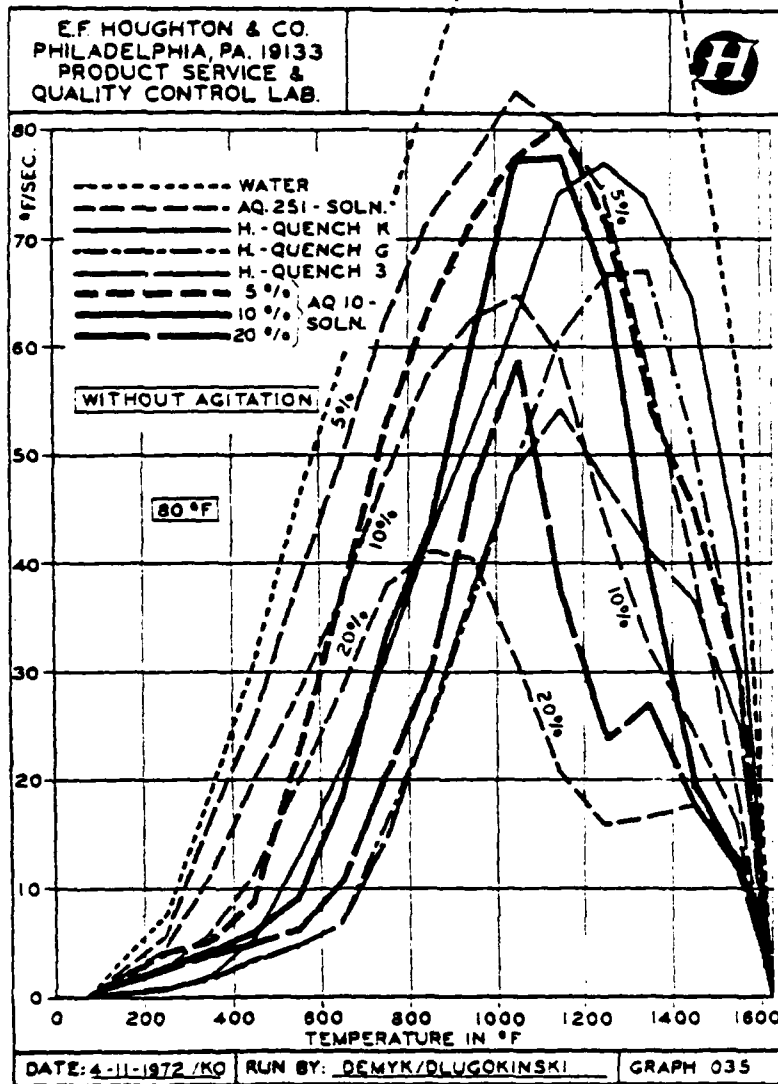


Fig. 6 Rate of temperature change for standardized test specimen quenched in different quenchants without agitation.

without quench tank agitation. Figure 7 shows the rate of temperature change for the same quenchants with agitation. Figure 8 compares the effects of agitation for Houghto-Quench G. Agitation is shown not to shift the second stage boiling. Agitation uniformly increases the rate of heat transfer. The standardized convection coefficient curve calculated by CONVEC thus provides the general shape of the actual convection coefficient curve. The scale factor accounts for agitation in the actual quench.

Stress Analysis

The stress analysis is accomplished with SAAS III. Program El2202 transfers the temperature distribution at user specified time increments to diskfile. SAAS III reads a user specified temperature distribution from diskfile and performs an elastic stress analysis. SAAS III has both a linear free strain option (used for the transformation stress calculation) and a thermal strain option (used for the thermal stress calculation). However, both options cannot be used during the same computer run. Therefore, to obtain the complete transient stress distribution, two runs must be made for each temperature distribution stored by El2202 on diskfile. After the necessary number of runs has been accomplished and output sent to the line-printer, stress histories can be constructed for any specified point in the problem geometry. Also, SAAS III provides grid mesh plots, deformed mesh plots, and contour plots.

The superposition principle is used to add the thermal stress and transformation stress to obtain the total stress distribution. Super-

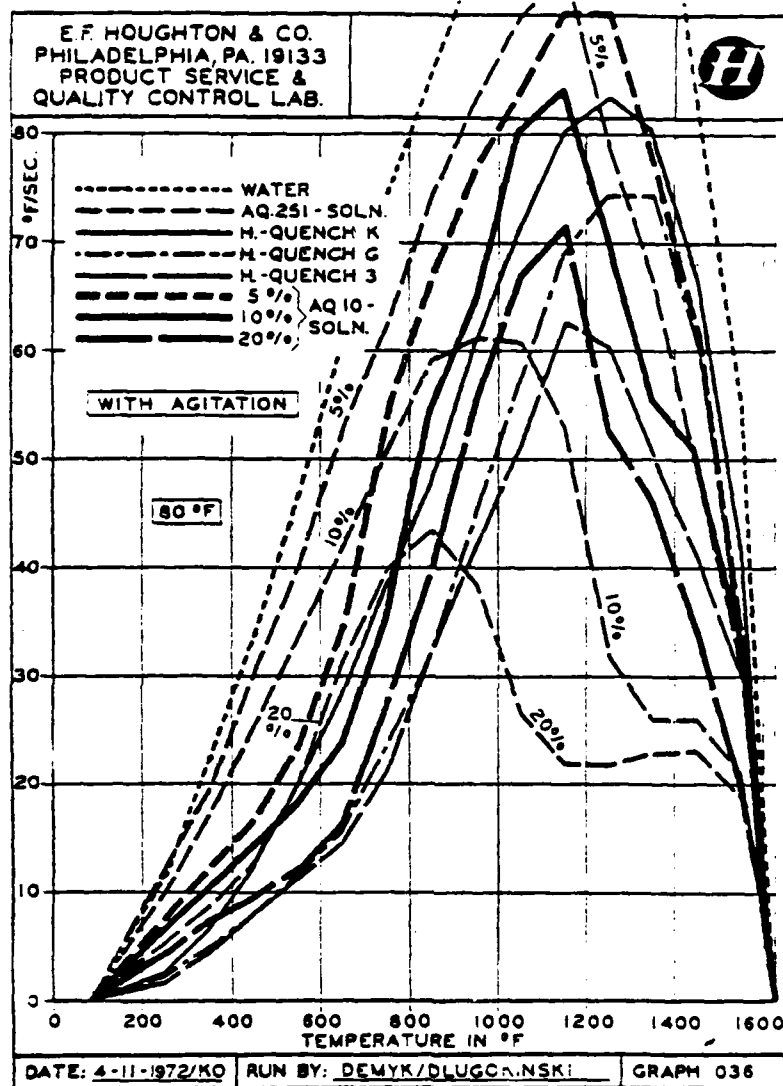


Fig. 7 Rate of temperature change for standardized test specimen quenched in different quenchants with agitation.

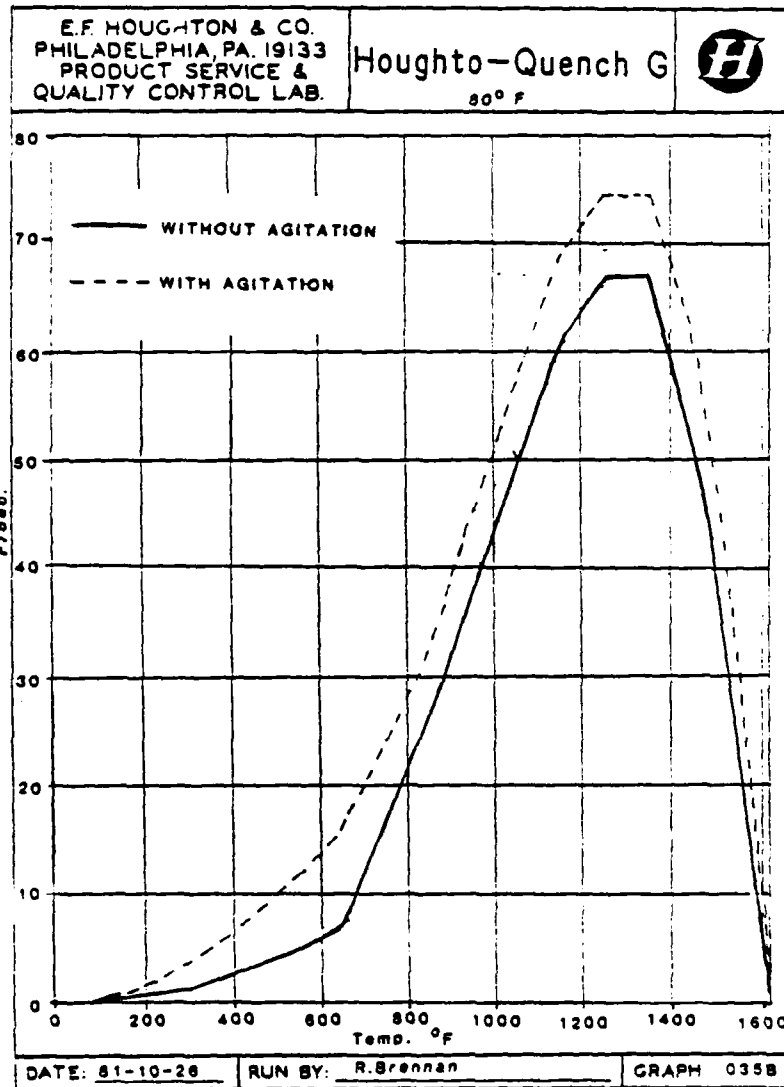


Fig. 8 Comparison of the rate of temperature change for standardized test specimen quenched in Houghto-Quench G oil with and without agitation.

position is valid only for an elastic analysis. The typically high yield strengths of untempered martensitic structures helps to ensure the validity of an elastic analysis at temperatures below M_s . High thermal stresses in the low yield strength austenitic microstructures may result in plastic deformation. However, at temperatures above M_s , Young's modulus decreases rapidly with increasing temperature. This results in lower stress levels at elevated temperatures. SAAS III shows the Von Mises stress distribution on the printed output as well as in the form of contour plots. This information is useful in checking the elastic analysis assumption for a given problem.

Fracture Analysis

The fracture analysis portion of the model is based upon principles of linear elastic fracture mechanics (LEFM). An LEFM computer program is not a part of the quench model. Rather, the quench model prescribes a methodology with which to analyze areas of surface tension for critical surface thumbnail crack size. A two-dimensional plane strain LEFM approach was used for both two-dimensional and axisymmetric applications of the model. It was assumed that the localized nature of the stress field at the tip of a crack would make a two-dimensional plane strain LEFM approach approximately valid for axisymmetric applications. The scope of the research described in this thesis, the absence in the literature of analytical solutions to the stress field at the tip of a surface thumbnail crack in an axisymmetric geometry, and the scarcity of fracture toughness values for other than the ASTM E-399-74 standard test specimen precluded a more detailed fracture analysis for axisymmetric geometries.

In addition, the scarcity of data for plane strain fracture toughness values for untempered martensitic microstructures at elevated temperatures further hampers the quantitative capabilities of the fracture analysis portion of the quench model. However, LEFM theory provides an excellent framework in which to qualitatively define and examine the pertinent mechanisms in action during the quench operation that could lead to quench cracks.

The fracture analysis presupposes an initial surface thumbnail crack as a result of some operation on the piece prior to the martensitic transformation. LEFM provides a quantitative basis to describe the way in which the nominal stress level, initial crack size, and material toughness interact to result in a brittle fracture.¹⁴

LEFM is based upon analytical solutions to the stress field at the tip of a crack. The form of the analytical solutions shows that the magnitude of the stress field in the crack opening mode is proportional to a stress intensity factor K_I .¹⁵ The stress intensity factor for a part-through thumbnail crack in a plate under uniform tensile stress is given by¹⁶

$$K_I = 1.12 \sigma \sqrt{\pi \frac{a}{Q}}$$

The shape factor Q is given in graphical form in Figure 9.

The fracture toughness for a given material under plane strain conditions is determined by experiment and denoted K_{IC} . Substituting the value for K_{IC} into the foregoing equation gives a relation between the nominal stress level, initial crack size, and material toughness.

This relationship is illustrated for a crack depth to length ratio of 0.5 and different values of K_{Ic} in Figure 10.

Figure 10 is referred to in the quench model as the critical crack curve plot. By superimposing the nominal stress level at a specified point of the problem geometry on the critical crack curve plot, the critical crack length for a given material toughness can be determined. A discussion and example of the utility of the critical crack curve plot is presented in the M483 Projectile Analysis.

The validity of using LEFM as opposed to an elastic-plastic analysis is based upon the assumption of plane strain conditions and the absence of large plastic zones.¹⁷ From an LEFM viewpoint, plane strain conditions have reference to the amount of dimpling that occurs normal to the surface at the crack tip. This dimpling effect is the result of strains in the direction normal to the crack opening mode due to Poisson's ratio. This strain is resisted at points inward from the surface and hence the term plane strain conditions. The term does not refer to the nominal stress distribution. Plane strain conditions are met when this dimpling effect is localized at the surface. Quantitative guidelines to ensure plane strain conditions have been set in ASTM standard E-399-74 for a standardized test specimen. This standard specifies specimen thickness, B , as

$$B \geq 2.5 \left(\frac{K_{Ic}}{\sigma_{ys}} \right)^2$$

and initial crack length, a , as

$$a \geq 2.5 \left(\frac{K_{Ic}}{\sigma_{ys}} \right)^2$$

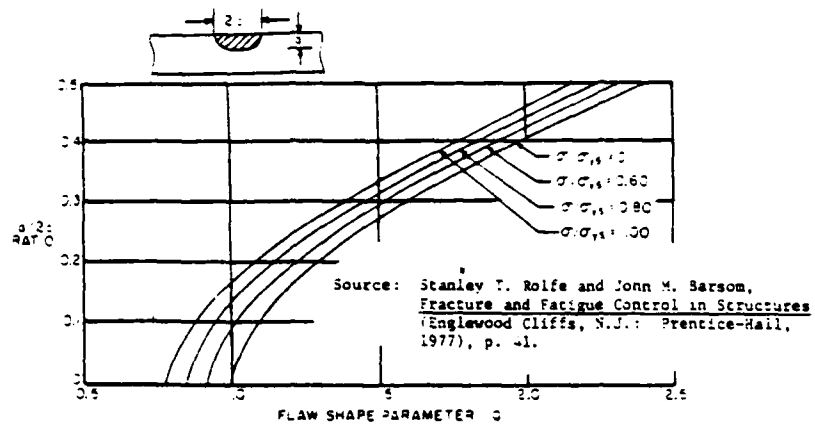


Fig. 9 Flaw shape parameter curve.

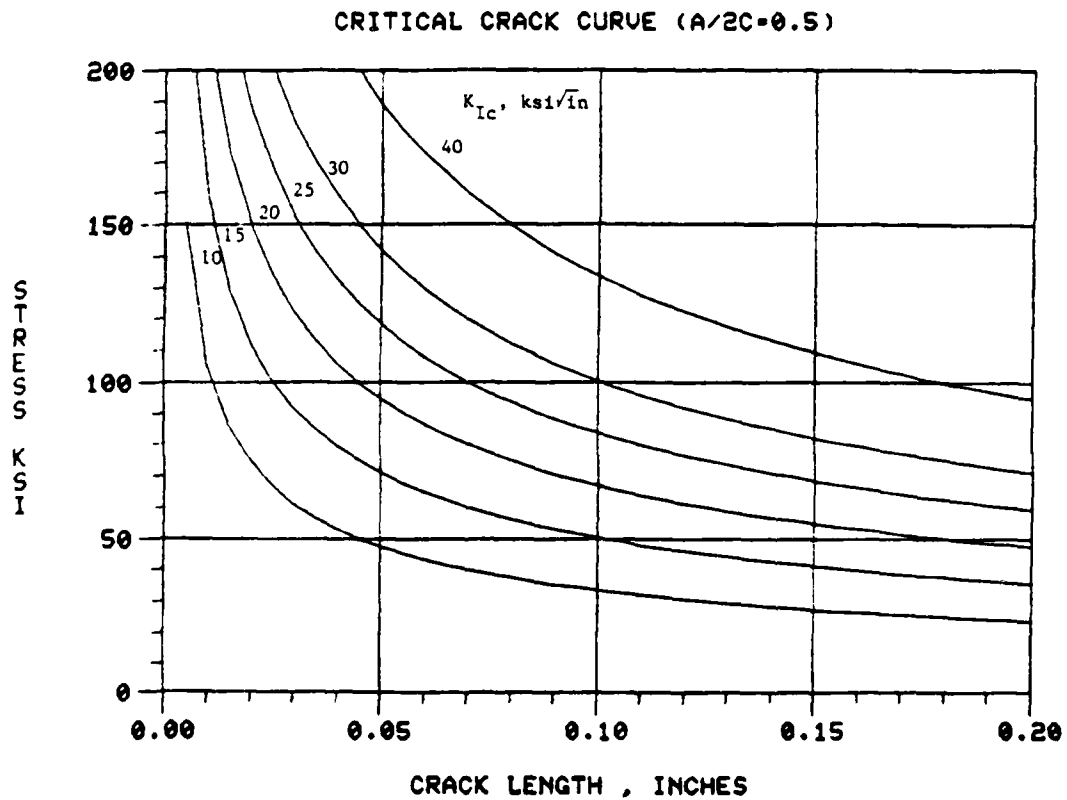


Fig. 10 Critical crack curve plots for surface thumbnail crack in an infinite plate under uniform tension.

While these conditions must be checked for each specific problem analyzed, the typically high yield strengths of untempered martensitic structures coupled with their low values of toughness make these geometric restrictions for plane strain easily met.

Discussion

The development of a general-purpose computer code generally follows a building block pattern. Few, if any, of the general-purpose finite element or finite difference codes popular in industry today entered the marketplace in their present form. There is a continuing effort to make the simplifying assumptions more general. SAAS III is a typical example. As its name implies, there were two previous releases of the code that were of a less general-purpose nature. It is to be recognized that this proposed quench model is at the first stages of its potential development.

The simplifying assumptions behind this quench model can be listed as follows:

1. Axisymmetric or two-dimensional geometries.
2. Pure austenite to martensite transformation.
3. Geometry independent pool boiling.
4. Convection coefficient curve scaling.
5. Equal convection coefficient at all points on surface of standardized test specimen.
6. Convection coefficient function of temperature only.
7. Temperature dependent properties obtained under equilibrium conditions.

8. Elastic stress distribution.
9. Linear elastic fracture mechanics.
 - a. Plane strain conditions.
 - b. No large plastic zone at tip of crack.
10. Surface thumbnail crack.
11. Extrapolation of a two-dimensional analytical solution of K_I for a surface thumbnail crack under uniform stress distribution to an axisymmetric application with non-uniform stress distribution.
12. No multiple crack affects.

Areas in which future development could greatly increase the quench model's accuracy and utility are as follows:

1. Unify the model into one self-contained design package.
2. Validate the convection coefficient curve scaling methodology with more extensive empirical data.
3. Develop a methodology by which transformations other than austenite to martensite can be incorporated into the model.
4. Investigate more appropriate stress intensity factor relationships for axisymmetric geometries.

COMPUTER PROGRAM THEORY

CONVEC

CONVEC is a FORTRAN IV computer program that calculates constant convection coefficients between specified points along the standardized cooling curve for the quenchant. Figure 11 shows a cooling curve composed of twelve specified points. This curve was constructed from the data for Houghto-Quench G oil shown in Figure 3. Starting with the initial center-point temperature T_0 of the test specimen at time $\tau = 0$, CONVEC uses an explicit finite difference formulation to calculate the constant convection coefficient h_1 necessary at the surface of the test specimen for the center-point to arrive at temperature T_1 at the end of the first interval. The initial guess h'_1 is chosen midway between a user specified upper and lower bound on the actual value for h_1 . The program then calculates a predicted temperature T'_1 using the first guess h'_1 . The program uses a numerical bisection method to iteratively guess values of h'_1 until T'_1 converges to T_1 and h'_1 converges to h_1 . The program then proceeds on to the next interval and so forth down the standardized cooling curve. From the output of CONVEC, a stepwise function of the convection coefficient versus test specimen surface temperature can be constructed as shown in Figure 12. A FORTRAN listing of CONVEC is given in Appendix A.

Finite Difference Formulation

The explicit finite difference formulation of the transient heat transfer into the standardized test specimen can be derived from a thermal

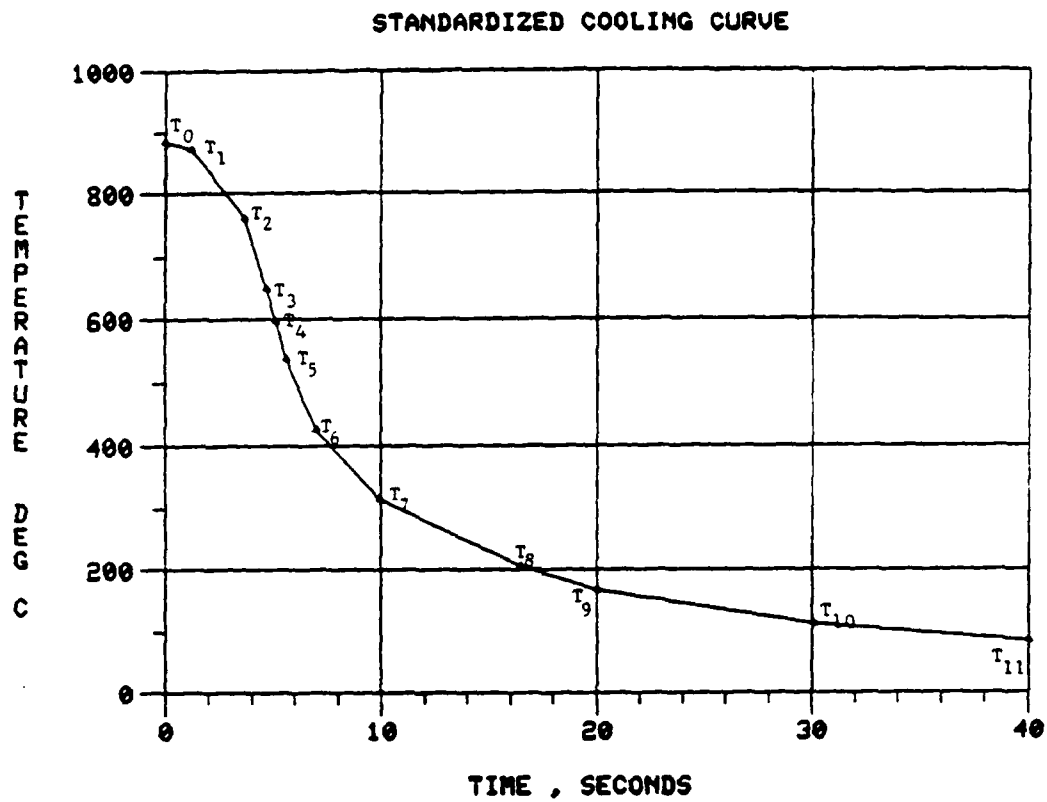


Fig. 11 Standardized cooling curve for Houghto-Quench G oil.
Temperature points taken from Fig. 3.

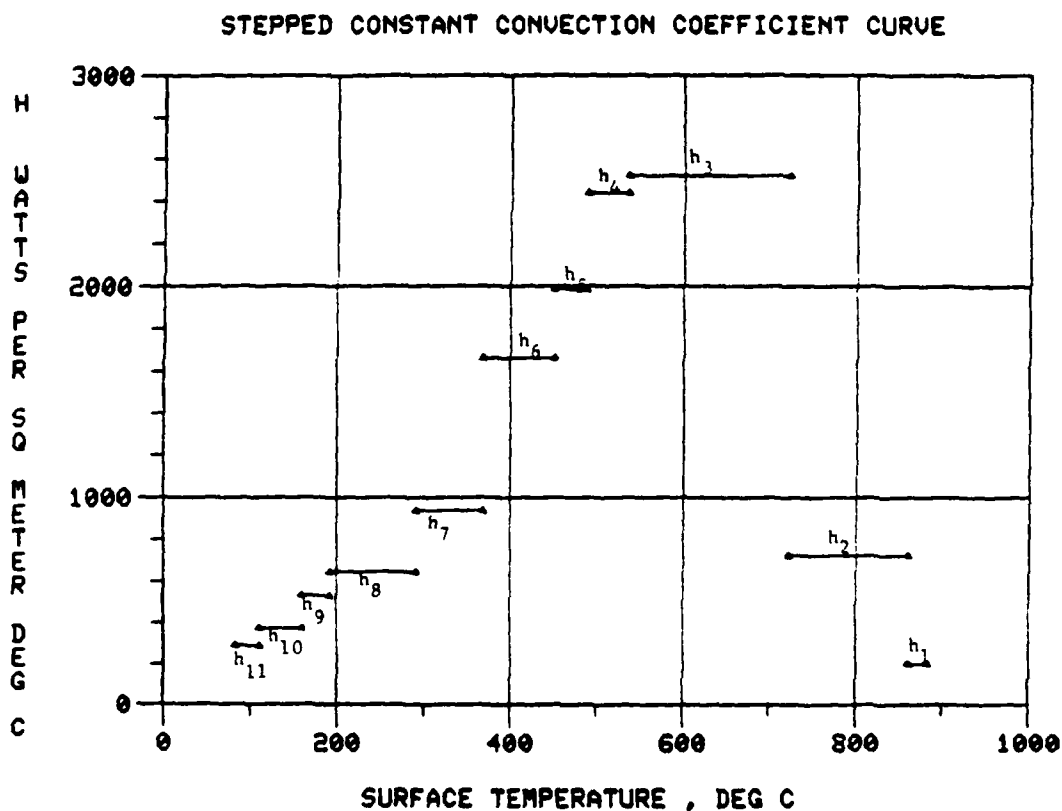


Fig. 12 Stepped constant convection coefficient curve calculated by CONVEC from temperature points of Fig. 11.

resistance and thermal capacity viewpoint. The general formulation is well documented by Holman¹⁸ and is briefly outlined in the following paragraphs in terms of the specific application at hand.

Consider the volume of the cylindrical standardized test specimen to be represented by solid rings of rectangular cross section as shown in Figure 13. The symmetry of the problem allows a consideration of just one quadrant of the geometry. Each solid ring is considered to be a volume element of uniform temperature. The rate of heat flow into a given volume element i determines its rate of temperature change:

$$q_i = c_i \rho_i v_i \frac{dT_i}{d\tau} \quad (1)$$

where q_i = rate of heat flow into the volume element i

c_i = specific heat of volume element i

ρ_i = density of volume element i

v_i = volume of volume element i

T_i = temperature of volume element i

τ = time

The thermal capacity is then defined as

$$C_i = \rho_i c_i v_i \quad (2)$$

so that Eq (1) becomes

$$q_i = C_i \frac{dT_i}{d\tau} \quad (3)$$

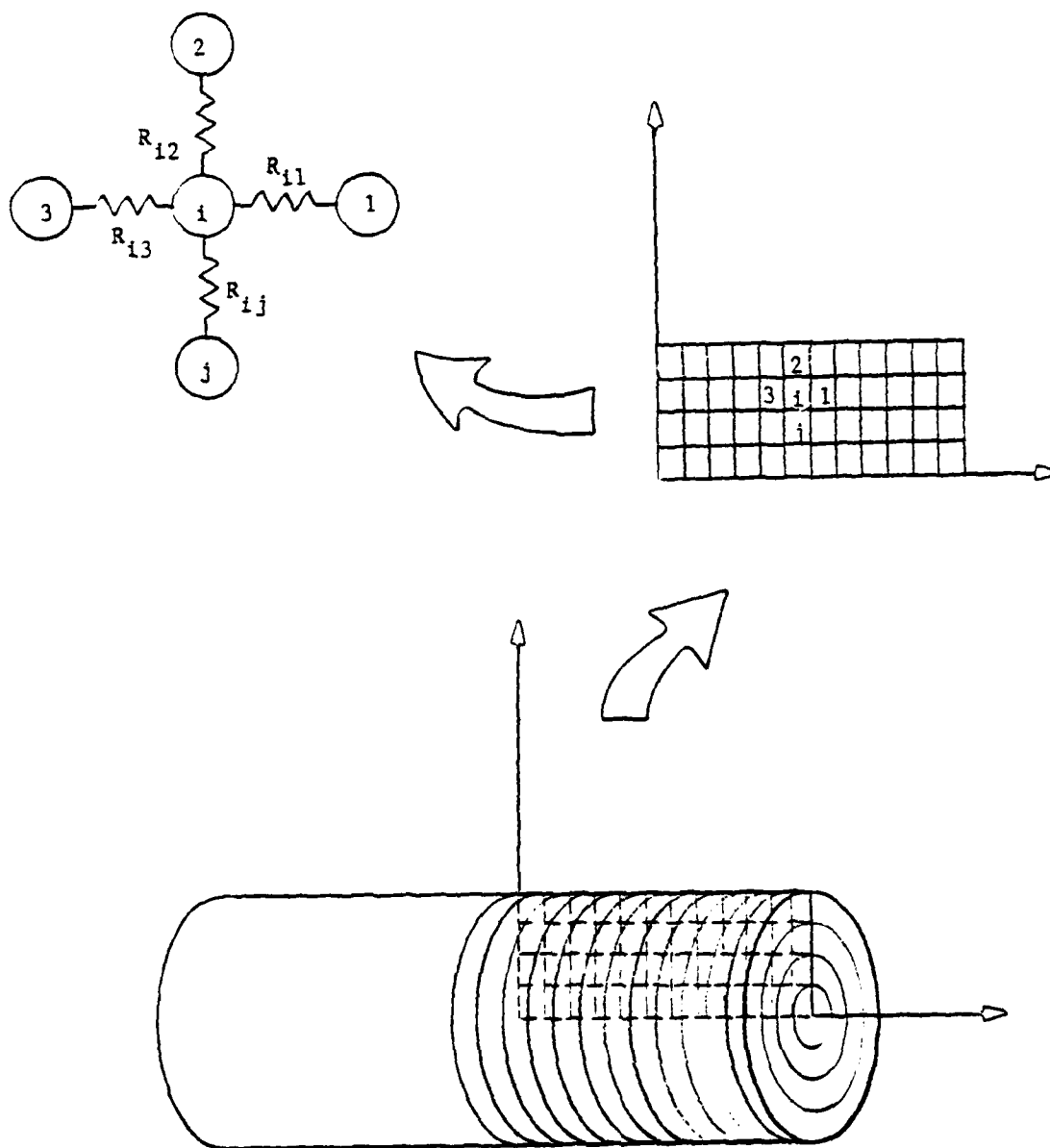


Fig. 13 Resistance-capacity finite difference thermal model of standardized test specimen.

Using the finite difference approximation

$$\frac{dT_i}{d\tau} = \frac{T_i^{p+1} - T_i^p}{\Delta\tau}$$

where T_i^{p+1} = temperature of volume element i at the end of time step $\Delta\tau$

T_i^p = temperature of volume element i at the beginning of time step $\Delta\tau$

Eq (3) becomes

$$q_i = C_i \frac{T_i^{p+1} - T_i^p}{\Delta\tau} \quad (4)$$

The heat transfer into one face of volume element i exposed to a convection environment can be derived as follows. By Fourier's law of heat conduction

$$q_{\text{conduction}} = k A_{iB} \frac{\partial T}{\partial X} \quad (5)$$

where k = thermal conductivity

A_{iB} = face area of volume element i

$\frac{\partial T}{\partial X}$ = temperature gradient normal to the face of volume element i

Using the finite difference approximation

$$\frac{\partial T}{\partial X} = \frac{T_{i+\frac{1}{2}}^p - T_i^p}{\Delta X_{iB}}$$

where $T_{i+\frac{1}{2}}^p$ = temperature at the midpoint of the face of volume element i at the beginning of $\Delta\tau$.

ΔX_{iB} = distance between center-point of volume element i and
the midpoint of its face

Eq (5) becomes

$$q_{\text{conduction}} = k A_{iB} \frac{T_B^P - T_i^P}{\Delta X_{iB}} \quad (6)$$

By Newton's law of cooling

$$q_{\text{convection}} = h A_{iB} (T_B^P - T_{i+\frac{1}{2}}^P) \quad (7)$$

where h = convection coefficient

T_B^P = the bulk temperature of the fluid

$q_{\text{conduction}}$ is equal to $q_{\text{convection}}$ at the volume element face and

Eqs (6) and (7) together become

$$q_{iB} = \frac{T_B^P - T_i^P}{\frac{\Delta X_{iB}}{kA_{iB}} + \frac{1}{hA_{iB}}} \quad (8)$$

The thermal resistance for the convection face is then defined as

$$R_{iB} = \frac{\Delta X_{iB}}{kA_{iB}} + \frac{1}{hA_{iB}} \quad (9)$$

It can be shown from an analogous procedure that the thermal resistance into a face of volume element i exposed to conduction from a neighboring node j is

$$R_{ij} = \frac{\Delta X_{ij}}{kA_{ij}} \quad (10)$$

where ΔX_{ij} = distance between the centerpoint of volume element i and j .

Eq (8) can then be generalized to any face of volume element i if it is remembered that j becomes B for a convection face.

$$q_{ij} = \frac{T_j^p - T_i^p}{R_{ij}} \quad (10)$$

The total heat transfer into volume element i can be obtained by summing Eq (10) for all faces.

$$q_i = \sum_j \frac{T_j^p - T_i^p}{R_{ij}} \quad (11)$$

Equating Eq (4) and Eq (11) and solving for T_i^{p+1} we get

$$T_i^{p+1} = \left(\sum_j \frac{T_j^p}{R_{ij}} \right) \frac{\Delta \tau}{C_i} + \left(1 - \frac{\Delta \tau}{C_i} \sum_j \frac{1}{R_{ij}} \right) T_i^p \quad (12)$$

This is an explicit expression for T_i^{p+1} in terms of current temperatures T_i^p and T_j^p . The second law of thermodynamics requires that the coefficient of T_i^p in Eq (11) be non-negative (otherwise heat would flow uphill on the temperature scale). Hence, the time step stability requirement becomes

$$\Delta\tau \leq \frac{C_i}{\sum_j \frac{1}{R_{ij}}} \quad (13)$$

CONVEC uses Eq (12) and Eq (13) along with appropriate material properties, thermal resistances, and thermal capacities to calculate the transient temperature distribution of the standardized test specimen. Whereas Eq (12) and Eq (13) were derived here with a simple axisymmetric geometry in view, their extension to three-dimensional problems is valid. In addition, all material properties can be treated as temperature dependent.

Due to the iterative nature of the search for constant convection coefficients along the standardized cooling curve, it was essential to streamline CONVEC as much as possible to conserve computer time. Accordingly, CONVEC was programmed exclusively for the geometry and boundary conditions of the standardized test specimen. It was this need for a fast and simple computational method that was the prime influencing factor in the choice of the resistance-capacity formulation over other more complex computational methods.

Bisection Method

The bisection method¹⁹ is used by CONVEC to iteratively arrive at a constant value of the convection coefficient h between two points on the standardized cooling curve. The bisection method was chosen for its simplicity and because it assures convergence.

Let the entire finite difference heat transfer algorithm be called TEMP. We can then think of TEMP as a functional relation for the center-point temperature of the test specimen.

$$T = \text{TEMP} (h, T_0, \tau, \Delta\tau, \text{mat'l properties, geometry})$$

where h = constant convection coefficient for interval $\Delta\tau$

T = center-point temperature of test specimen at time $\tau + \Delta\tau$

as shown on the standardized cooling curve

T_0 = center-point temperature of test specimen at time τ as

shown on the standardized cooling curve

All variables in the above equation are known except h . For assumed values of h' other than h , an error $E (h')$ can be represented by

$$E (h') = T - \text{TEMP} (h')$$

where all the other known parameters have been absorbed into TEMP to simplify the representation. The bisection method is used to find the root of this equation-- h . This method requires that h be bounded by two user specified values h_l and h_r such that

$$h_l \leq h \leq h_r$$

The physics of boiling heat transfer enable the user to place an upper and lower bound on h . An initial guess h' is then made halfway between h_l and h_r . By comparing the signs of $E(h_l)$ and $E(h')$, it can be seen whether the actual root h lies to the left or right of h' . h_l and h_r are then adjusted to include h' and a new guess is made half way between the new bounds. This iteration is continued for the number of bisections required to obtain the accuracy desired.

El2202

El2202 is a general-purpose finite element computer program that solves steady-state and transient heat transfer problems for two-dimensional and axisymmetric geometries. A complete development of the theory behind the computational method, description of the input and output format, benchmark example problems, and a FORTRAN listing of the program are given by Kimura et al.²⁰ Since El2202 was incorporated into the quench model without any alterations to its method of computation, it would be redundant to develop its mathematical basis in this thesis. The only significant modifications made to El2202 were (1) an option to read the geometry input from a diskfile created by stress analysis program, SAAS III, which has a more convenient mesh generation routine and (2) an option to store the resultant transient temperature distribution on diskfile in a format for SAAS III to access and read.

SAAS III

SAAS III is a general-purpose finite element computer program for stress analysis of two-dimensional and axisymmetric plane solids. This

program can handle different orthotropic, temperature dependent material properties in tension and compression. In addition, it has an isotropic bilinear plasticity option. A complete development of the theory behind the computational method, description of the input and output format, benchmark example problems, and a FORTRAN listing of the program are given by Crose and Jones.²¹ Since SAAS III was incorporated into the quench model without any alterations to its computational method, it would be redundant to develop its mathematical basis in this thesis. The only significant modifications made to SAAS III were (1) an option to output the geometry data to diskfile in a format to be accessed and read by E12202, (2) an option to read a transient temperature distribution from diskfile, (3) the addition of the Von Mises stress to the printed output, (4) conversion of the Calcomp plotter graphics to a Tektronix 4014 terminal, and (5) the deletion of the restart capabilities.

BENCHMARK ANALYSES

Kimura et al.²² and Crose and Jones²³ present several sample analyses that benchmark El2202 and SAAS III against known analytical solutions. All of these sample problems were rerun and verified after El2202 and SAAS III were loaded into the Chamberlain minicomputer. In addition, CONVEC's accuracy in calculating convection coefficients for heat transfer into a short solid cylinder was benchmarked against an analytical solution using temperature invariant material properties. Also, the method of analysis for thermal stress using El2202 and SAAS III together was benchmarked against an analytical solution to the thermal stress problem in an infinite cylinder.

Temperature Invariant Convection Coefficient

By assuming constant material properties, the heat transfer into a short solid cylinder can be analytically determined by a coupled one-dimensional analysis of an infinite slab of finite thickness and an infinite solid cylinder. The assumption of constant material properties and convection coefficient makes the problem linear and solvable by an analytical procedure.

For an infinite slab of finite thickness $2L$ in the x direction with initial temperature T_i , ambient temperature T_∞ , constant convection coefficient h , thermal diffusivity α , conductivity k , and time τ , the appropriate one-dimensional equation is

$$\frac{\partial^2 \theta}{\partial x^2} = \frac{1}{\alpha} \frac{\partial \theta}{\partial \tau}$$

where $\theta = T(x, \tau) - T_\infty$. The boundary conditions are

$$\frac{\partial \theta}{\partial x} = 0 \text{ at } x = 0$$

$$\frac{\partial \theta}{\partial x} = -\frac{h}{k} \theta \text{ at } x = L$$

The initial conditions are

$$\theta = \theta_i \text{ at } \tau = 0$$

With the use of the separation of variables technique and the theory of orthogonal functions, the solution to this boundary value problem can be expressed in non-dimensional form as²⁴

$$\left(\frac{\theta}{\theta_i} \right) = 2 \sum_{n=1}^{\infty} \exp(-\delta_n^2 F_0) \frac{\sin \delta_n}{\delta_n + \sin \delta_n \cos \delta_n} \cos\left(\frac{\delta_n x}{L}\right) \quad (14)$$

infinite
plate

where $F_0 = \frac{\alpha \tau}{L^2}$ and δ_n is the root of

$$\cot \delta_n = \delta_n \frac{hL}{k}, \quad n = 1, 2, 3, \dots \quad (15)$$

For an infinite solid cylinder of radius R in the r direction, the appropriate one-dimensional equation is

$$\frac{\partial^2 \theta}{\partial r^2} + \frac{1}{r} \frac{\partial \theta}{\partial r} = \frac{1}{\alpha} \frac{\partial \theta}{\partial \tau}$$

where $\theta = T(r, \tau) - T_\infty$. The boundary conditions are

$$\frac{\partial \theta}{\partial r} = 0 \text{ at } r = 0$$

$$\frac{\partial \theta}{\partial r} = \frac{-h\theta}{k} \text{ at } r = R$$

The initial conditions are

$$\theta = \theta_i \text{ at } \tau = 0$$

Again with the use of the separation of variables technique and the theory of orthogonal functions the solution to this boundary value problem can be expressed in non-dimensional form as²⁵

$$\left(\frac{\theta}{\theta_i} \right) = 2 \sum_{n=1}^{\infty} \frac{1}{\delta_n} \exp(-\delta_n^2 F_0) \frac{J_0\left(\frac{\delta_n r}{R}\right) J_1(\delta_n)}{J_0^2(\delta_n) + J_1^2(\delta_n)} \quad (16)$$

infinite
cylinder

where J_0 = Bessel function of the first kind of order zero

J_1 = Bessel function of the first kind of order one

$F_0 = \frac{\alpha \tau}{R^2}$ and δ_n is the root of

$$\delta_n \frac{J_1(\delta_n)}{J_0(\delta_n)} = \frac{hR}{k}, n = 1, 2, 3, \dots \quad (17)$$

The solution to the three-dimensional short cylinder can then be obtained by coupling Eq (14) and Eq (16) so that²⁶

$$\left(\frac{\theta}{\theta_i} \right)_{\text{short cylinder}} = \left(\frac{\theta}{\theta_i} \right)_{\text{infinite plate}} \times \left(\frac{\theta}{\theta_i} \right)_{\text{infinite cylinder}}$$

This analytical solution to the heat transfer in a short cylinder was programmed in FORTRAN. A polynomial approximation accurate to the sixth decimal place was used for J_0 and J_1 .²⁷ The bisection method was

used to solve for δ_n in Eq (15) and Eq (17). The bisection method was also used in a fashion similar to CONVEC to structure the program such that h would be calculated for given initial and final temperatures of a specified point.

Taking seven terms of the summation in Eq (14) and Eq (16) and parameters

$$r = 0.000625 \text{ m}$$

$$x = 0.00125 \text{ m}$$

$$R = 0.005 \text{ m}$$

$$L = 0.03 \text{ m}$$

$$T_i = 883.3 \text{ }^\circ\text{C}$$

$$T = 871.1 \text{ }^\circ\text{C}$$

$$T_\infty = 26.7 \text{ }^\circ\text{C}$$

$$\alpha = 7.7868 \times 10^{-6} \text{ m}^2/\text{s}$$

$$k = 28.0 \text{ W/m }^\circ\text{C}$$

$$\tau = 1.22 \text{ s}$$

the analytical solution for h is $155.8 \text{ W/m}^2 \text{ }^\circ\text{C}$. For this same problem using constant material properties, CONVEC calculates a constant h of $152.9 \text{ W/m}^2 \text{ }^\circ\text{C}$ with an error of only 1.9%.

Infinite Cylinder Thermal Stress Analysis

An analytical solution for the transient temperature distribution in an infinite cylinder was presented in the previous section as Eq (16) and Eq (17). The analytical solution for the axial stress in an infinite solid cylinder with zero axial strain can be derived from the theory

of elasticity to be²⁸

$$\sigma_z = \frac{\Delta E}{1-\nu} \left(\frac{2\nu}{R^2} \int_0^R T r \, dr - T \right) \quad (18)$$

where Δ = coefficient of thermal expansion

E = Youngs modulus

ν = Poisson's ratio

$T = T(r)$ temperature distribution

r = radial location

R = radius of cylinder

Eqs (16), (17), and (18) constitute a complete analytical solution to the axial thermal stresses in an infinite solid cylinder subjected to a convection environment. The following numerical values will be used to represent a typical calculation:

$$T_\infty = 21.1 \text{ }^\circ\text{C}$$

$$T_i = 871.0 \text{ }^\circ\text{C}$$

$$R = 0.05 \text{ m}$$

$$h = 1000.0 \text{ W/m}^2 \text{ }^\circ\text{C}$$

$$k = 215.0 \text{ W/m }^\circ\text{C}$$

$$\alpha = 8.4 \times 10^{-5} \text{ m}^2/\text{s}$$

$$\tau = 60 \text{ s}$$

$$\nu = 0.334$$

$$E = 71.0 \times 10^3 \text{ MPa}$$

$$\Delta = 7.39 \times 10^{-6} \text{ m/m }^\circ\text{C}$$

Putting Eq (17) into the form

$$\delta_n J_1(\delta_n) - J_0(\delta_n) \frac{hR}{k} = 0$$

and using a polynomial approximation for J_0 and J_1 , the first five zeros can be calculated numerically using the bisection method. The first five zeros are shown in Table 1.

Table 1 Zeros of transcendental equation

n	δ_n
1	0.662651
2	3.89185
3	7.04865
4	10.1963
5	13.3411

By putting δ_n and the other required parameters into Eq (16), the temperature at $\tau = 60s$ can be calculated for eleven radial positions. This temperature distribution is given in Table 2.

Table 2 Analytical temperature distribution for infinite cylinder

r m	T (r, τ) °C
0.	391.308
0.005	390.902
0.010	389.681
0.015	387.659
0.020	384.833
0.025	381.215
0.030	376.818
0.035	371.656
0.040	365.745
0.045	359.106
0.050	351.759

This temperature distribution is then curve fitted with a third degree polynomial to allow integration of Eq (18). The third degree polynomial fit has a maximum residual of 0.002%.

$$T(r) = 391.3006 + 5.363r - 16,800r^2 + 17,460r^3$$

Eq(18) can then be solved for the axial stress. The results are shown in Table 3.

Table 3 Analytical axial stress distribution for infinite cylinder

r	σ_z
m	MPa
.0025	-210.48
.0075	-209.85
.0125	-208.57
.0175	-206.65
.0225	-204.11
.0275	-200.95
.0325	-197.18
.0375	-192.83
.0425	-187.88
.0475	-182.37

The same parameters used in the analytical analysis were then used in El2202 and SAAS III. Appendix B contains a complete listing of the input and output for the analysis. Figure 14 shows the finite element model mesh. Temperature results using El2202 are given in Table 4.

SAPS III FINITE ELEMENT STRESS ANALYSIS
INFINITE CYLINDER THERMAL ANALYSIS
ELEMENT PLOT

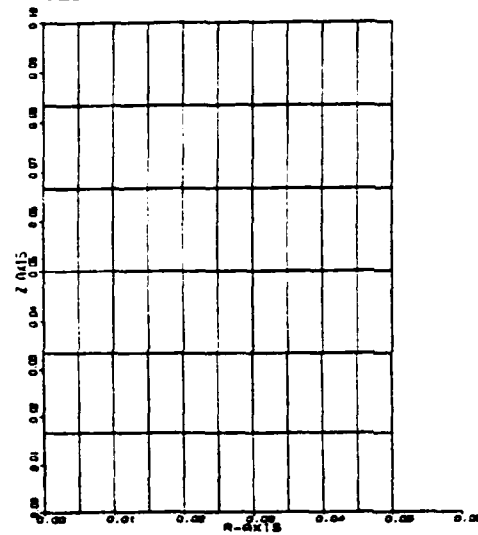


Fig. 14 Element plot for infinite cylinder analysis.

Table 4 Finite element method
temperature distribution for infinite cylinder

r m	T (r) °C
0.	392.0516
0.005	391.3694
0.010	390.0750
0.015	388.0024
0.020	385.1408
0.025	381.4940
0.030	377.0711
0.035	371.8856
0.040	365.9536
0.045	359.2940
0.050	351.9279

The maximum error compared with the analytical results was 0.19%. A comparison plot of the El2202 and analytical temperature results is shown in Figure 15.

The SAAS III axial stress results are given in Table 5.

Table 5 Finite element method
axial stress distribution for infinite cylinder

r m	σ_z MPa
0.0025	-210.84
0.0075	-210.05
0.0125	-208.72
0.0175	-206.77
0.0225	-204.21
0.0275	-201.03
0.0325	-197.24
0.0375	-192.86
0.0425	-187.90
0.0475	-182.37

The maximum error compared with the analytical results was 0.17%. A comparison plot of the SAAS III and analytical axial stress results is shown in Figure 16.

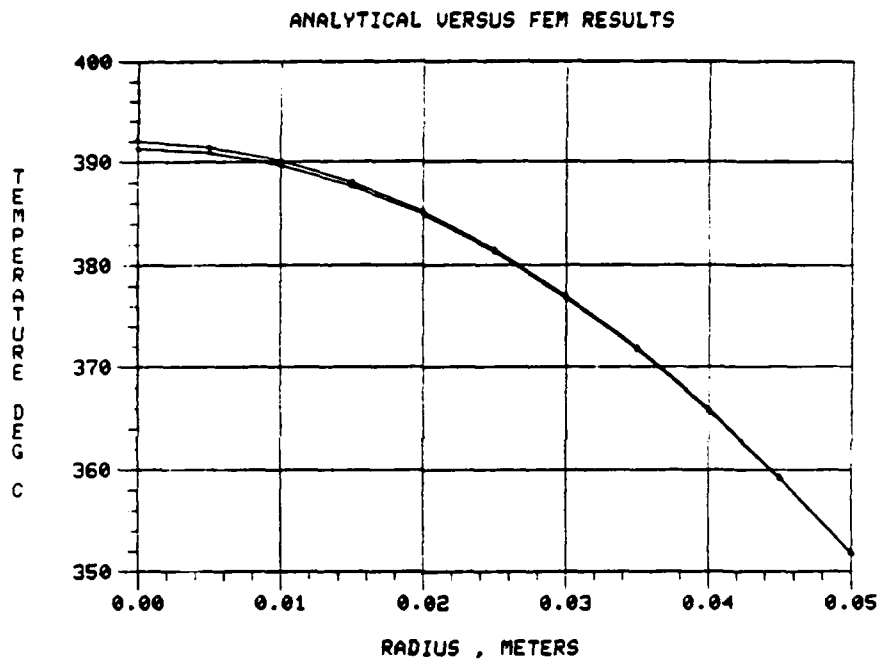


Fig. 15 Comparison of temperature results for finite element method and analytical calculation of infinite cylinder.

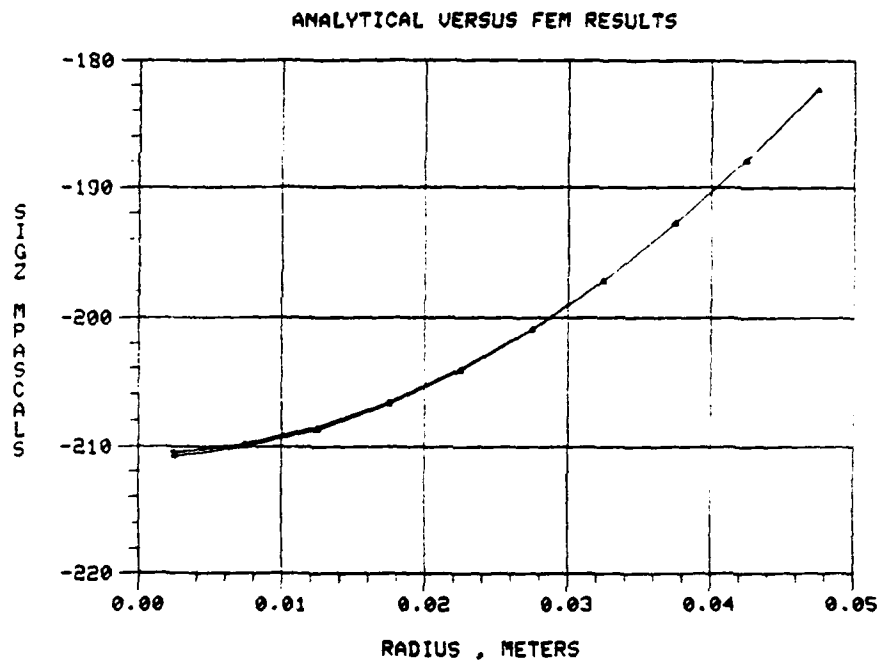


Fig. 16 Comparison of axial stress results for finite element method and analytical calculation of infinite cylinder.

M483 PROJECTILE ANALYSIS

Problem Statement

The M483 projectile is currently produced by Chamberlain Manufacturing Corporation at its New Bedford, Massachusetts, facility. Figure 17 shows the basic configuration of the projectile. In the past, there has been a periodic occurrence of cracking at the forward end of the rotating band during the quench operation. These surface cracks are circumferential in direction, typically from 1/2 in to 4 1/2 in long and 0.015 in to 0.230 in deep measured after the quench operation. The crack opening mode is in the longitudinal direction of the projectile.

The quench operation itself is conducted in batches of nine projectiles. The projectiles are heated to 871.1 °C under controlled atmosphere conditions and dropped into a bath of highly agitated Houghto-Quench G oil maintained at 51.7 °C. The controlled atmosphere conditions keep the quench scale on exposed surfaces to a minimum.

The copper rotating band is applied to the band seat area in molten form prior to the heat treatment. As the molten copper is being laid onto the band seat area, the bore of the projectile is sprayed with a water jet to draw away heat. It is assumed that this extremely harsh welding environment results in tiny cracks in the steel at the forward end of the rotating band area. The problem is to determine whether there are nominal surface tensile stresses during the quenching operation that could make these initial cracks be of critical size.

This quench cracking problem was recognized as an excellent

opportunity to illustrate the use of the proposed quench model. Accordingly, an illustrative analysis was made on the projectile. Emphasis was placed on illustrating the general procedure and capabilities of the quench model. Therefore, exhaustive efforts were not made to find the most appropriate material properties for the analysis. In fact, the projectile is manufactured by Chamberlain using AISI 1340 steel, but AISI 4140 material properties were used in the analysis because they were easier to find in the literature. The same projectile is currently manufactured by a Chamberlain competitor using AISI 4140 steel. Table 6 lists the material properties used in the analysis. The symbols and units of Table 6 are SI and given in the Symbols and Units section of this thesis. The sources cited in Table 6 can be found in the Bibliography.

Table 6 Material properties used in M483 projectile analysis

COMPONENT	MATERIAL	TEMPERATURE (°C)	PROPERTY (SI)	SOURCE
Standardized test specimen	304 SS		k	Eckert and Drake
		0.	16.3	
		100.	17.0	
		200.	17.0	
		300.	19.0	
		400.	19.0	
		600.	22.0	
		800.	26.0	
		1000.	31.0	
			$\rho \times c_p \times 10^{-6}$	Peckner and Bernstein
		-17.2	3.0392	
		101.3	3.2730	
		204.4	3.4833	
		426.7	3.8342	
		648.9	4.0914	
		883.4	4.2548	

Table 6 (Continued)

COMPONENT	MATERIAL	TEMPERATURE (°C)	PROPERTY (SI)	SOURCE
Rotating Band	90% Cu-10% Zn		k	Hoyt
		0.	202.5	
		400.	268.2	
		883.3	268.2	
		$\rho \times c_p \times 10^{-6}$		Eckert and Drake
		constant	3.380	
		$E \times 10^{-5}$		Hoyt
		constant	1.076	
		ν		Hoyt
		constant	0.355	
		$\Delta \times 10^6$		Hoyt
		constant	16.6	
Projectile body	4140 Steel		k	Department of Defense
		17.8	37.9	
		204.4	37.5	
		426.7	34.6	
		648.9	31.7	
		791.7	25.8	
		871.1	27.0	
		$\rho \times c_p \times 10^{-6}$		North American Aviation
		0.	3.736	
		176.7	3.768	
		204.4	4.034	
		426.7	4.857	
		696.7	6.298	
		760.0	12.400	
		795.6	8.201	
		855.0	4.528	
		1169.0	4.919	
		$E \times 10^{-5}$		Department of Defense
		constant	1.999	
		ν		Department of Defense
		constant	0.32	

Table 6 (Continued)

COMPONENT	MATERIAL	TEMPERATURE (°C)	PROPERTY (SI)	SOURCE
			$\Delta \times 10^6$	
		-17.8	12.0	North American Aviation
		117.2	14.7	
		426.7	17.5	
		696.7	19.3	
		756.1	13.9	
		815.6	13.6	
		871.1	14.9	

Thermal Analysis

Houghto-Quench G oil is used in the M483 quench. Figure 3 shows a standardized cooling curve for Houghto-Quench G. Choosing the twelve temperature points along the standardized cooling curve shown in Figure 11, CONVEC predicted the stepped constant convection coefficient curve shown in Figure 12.

El2202 was then used to convert the stepped constant convection coefficient curve into a continuous curve. This was accomplished by reconnecting the points of Figure 12 as shown in Figure 18. It was then assumed that a continuous curve lay between the two curves shown in Figure 18. The geometry, material properties, and boundary conditions of the standardized test specimen were input to El2202 and a calculation was made with the minimum and maximum convection coefficient curves shown in Figure 18. Figure 19 shows the predicted center-point temperature of the standardized test specimen using the minimum and maximum convection curves of Figure 18. The actual center-point cooling curve was seen to be approximately midway between the minimum and maximum cooling curves of Figure 19. Figure 20 shows a continuous convection

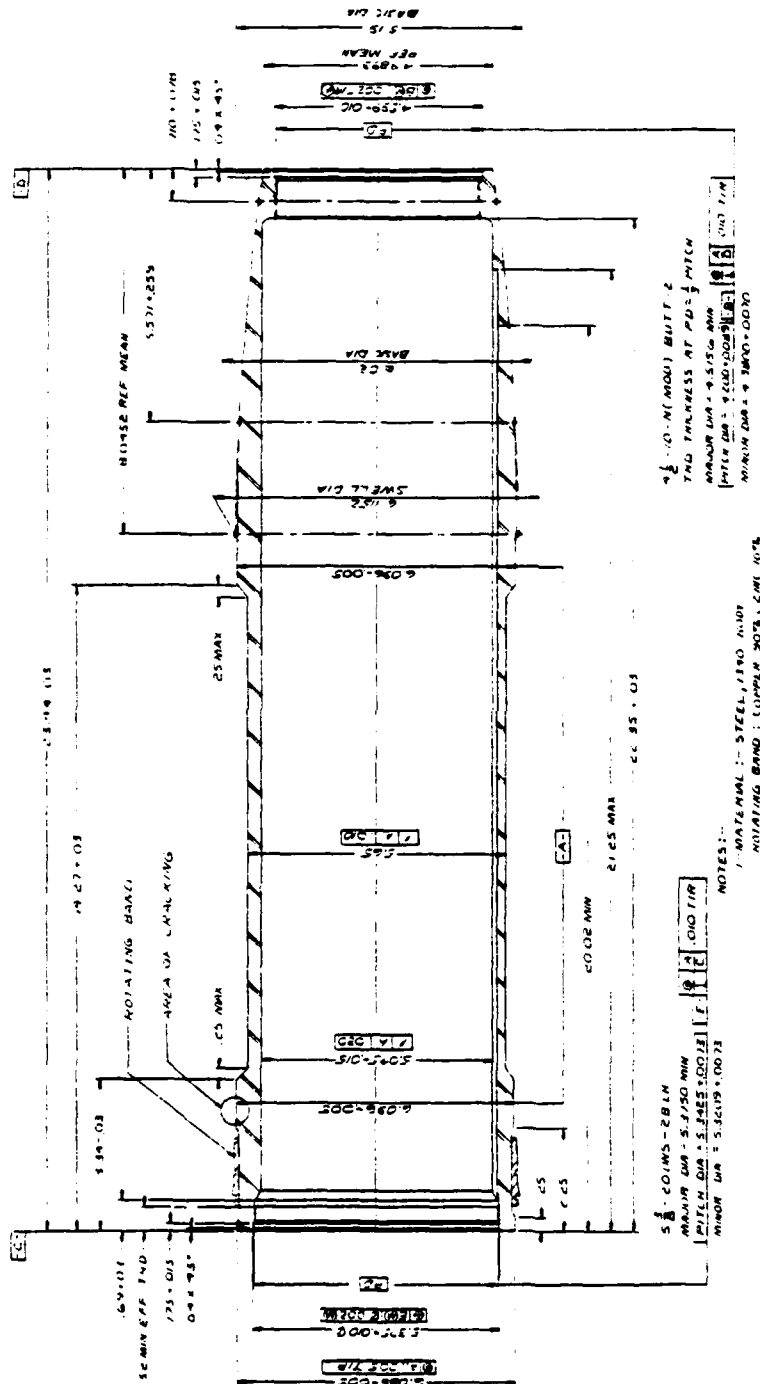


Fig. 17 Configuration of M483 projectile.

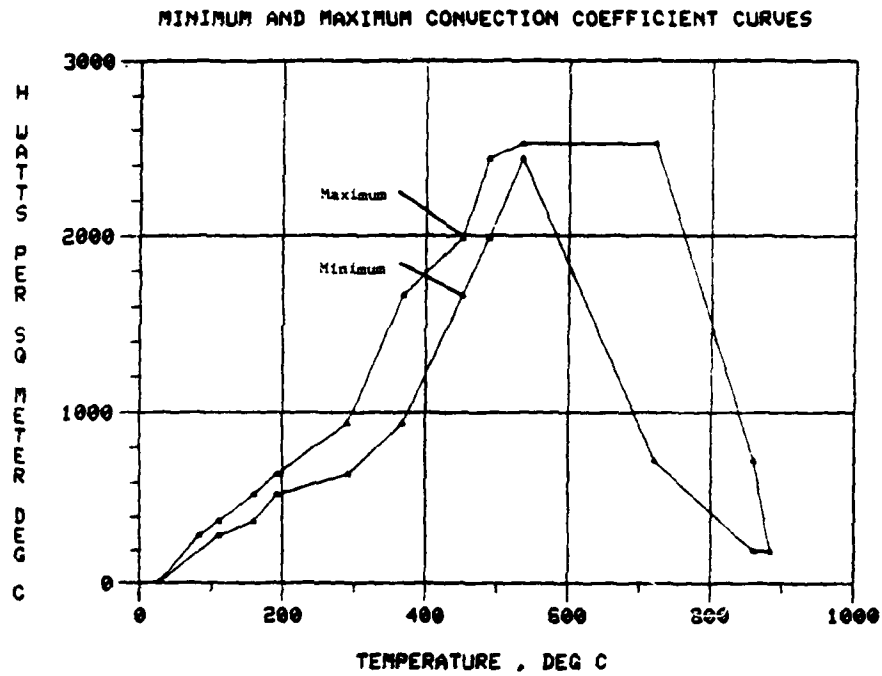


Fig. 18 Minimum and maximum convection coefficient curves taken from Figure 12.

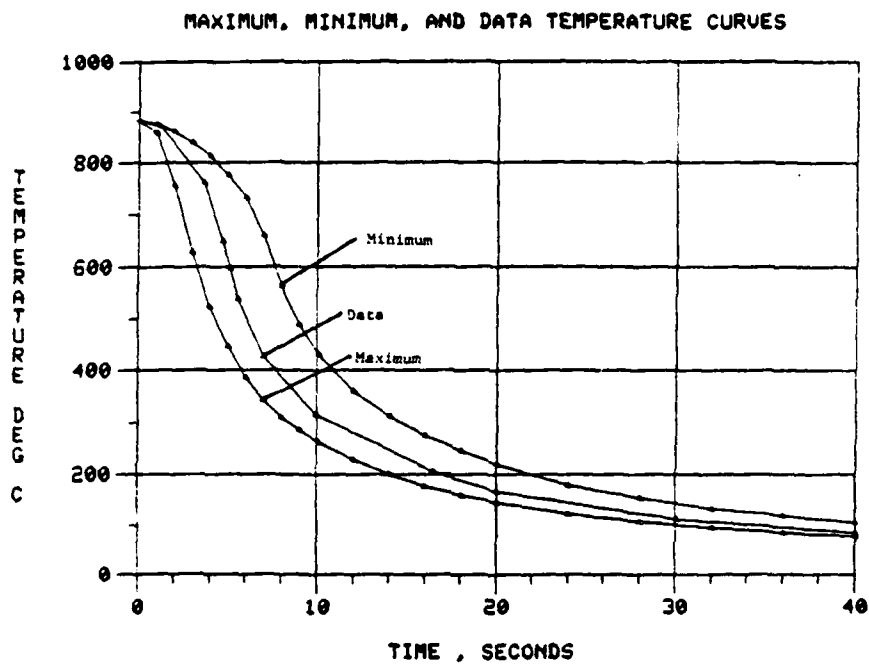


Fig. 19 El2202 prediction of standardized test specimen center-point temperature using maximum and minimum convection coefficient curves of Figure 18 compared with the actual center-point temperature curve.

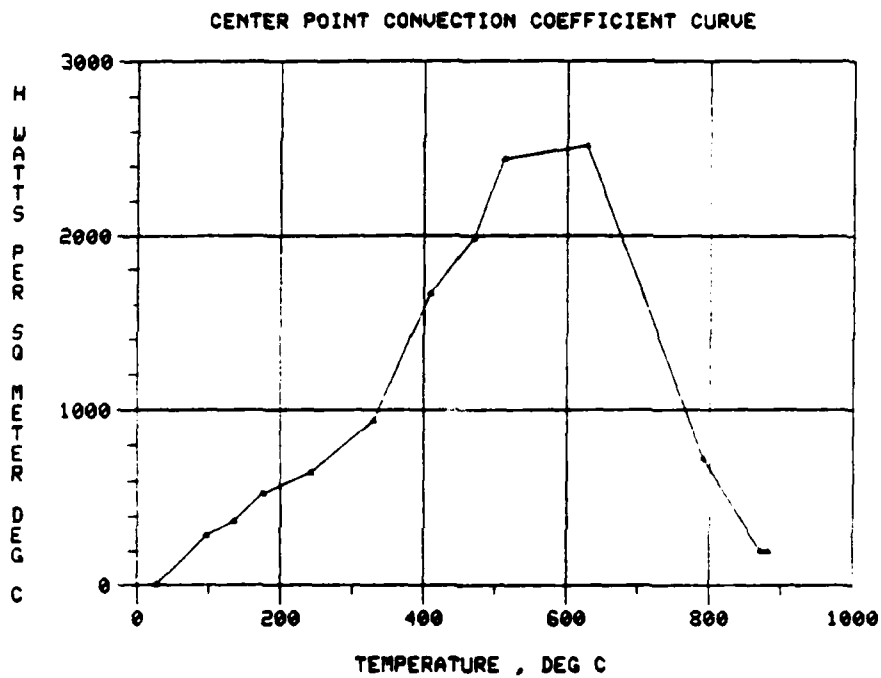


Fig. 20 Continuous convection coefficient curve taken halfway between minimum and maximum curve of Figure 18.

coefficient curve taken halfway between the minimum and maximum curves of Figure 18. Figure 21 shows a comparison of El2202's prediction of the center-point temperature using the continuous convection coefficient curve of Figure 20 with the actual cooling curve. A second continuous convection coefficient curve was chosen slightly weighted towards the maximum curve of Figure 18. Figure 22 shows this second continuous convection coefficient curve. Figure 23 shows a comparison of El2202's prediction of the center-point temperature using the continuous curve of Figure 22 with the actual cooling curve. Comparing Figures 23 and 21, it was seen that a continuous convection coefficient curve weighted 0.6 towards the maximum curve of Figure 18 gave the best prediction of the center-point temperature. Therefore, Figure 22 was used as the best approximation of the standardized convection coefficient curve.

The next step in the quench model was to scale the standardized convection coefficient curve of Figure 22 such that the slowest cooling point in the M483 geometry missed the nose of the C-T diagram. Figure 24 shows the finite element idealization of M483. Just the rear half of the projectile was considered in the analysis, the dividing line being taken at the midpoint of the thinnest section of the projectile. This boundary was considered insulated in the thermal analysis and fixed in the Z-direction in the stress analysis. Figure 25 shows the simplified C-T diagram used in the analysis. Figure 26 shows the scaled cooling curves of node 28 superimposed on the C-T diagram. It was seen that the convection coefficient curve of Figure 22 had to be scaled by a factor of five to insure that the slowest cooling spot of the

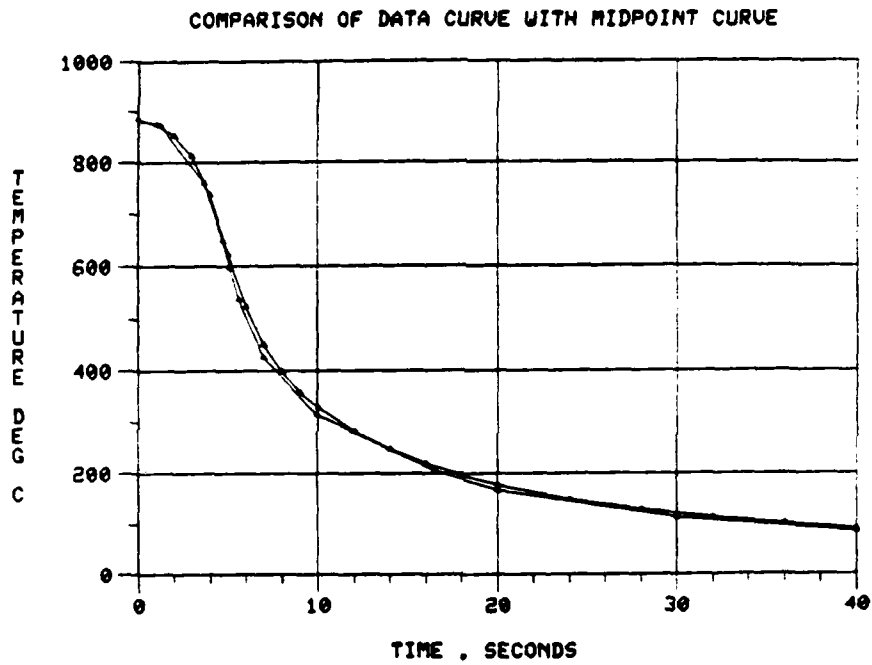


Fig. 21 E12202 prediction of the standardized test specimen center-point temperature using the continuous convection coefficient curve of Figure 20 compared with the actual center-point temperature curve.

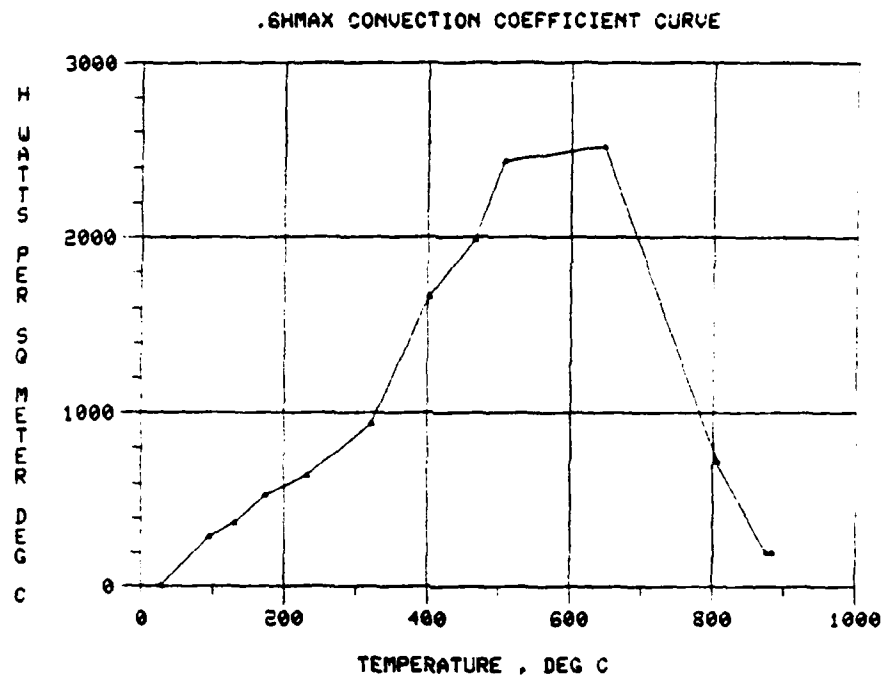


Fig. 22 Continuous convection coefficient curve weighted 0.6 towards the maximum curve of Figure 18.

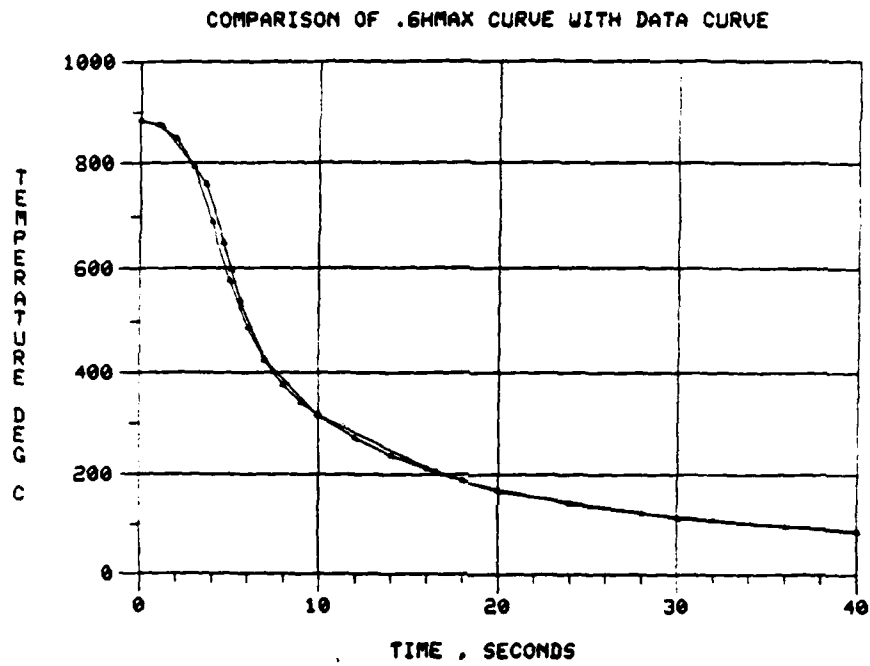


Fig. 23 E12202 prediction of the standardized test specimen center-point temperature using the continuous convection coefficient curve of Figure 22 compared with the actual center-point temperature curve.

SAAS III FINITE ELEMENT STRESS ANALYSIS
 M483 QUENCH STRESS ANALYSIS
 ELEMENT PLOT

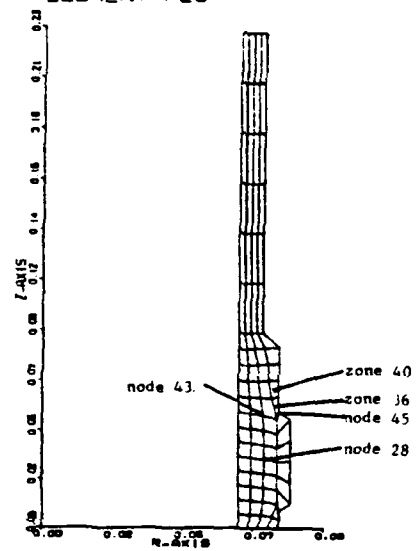


Fig. 24 Finite element idealization of the M483 projectile geometry.

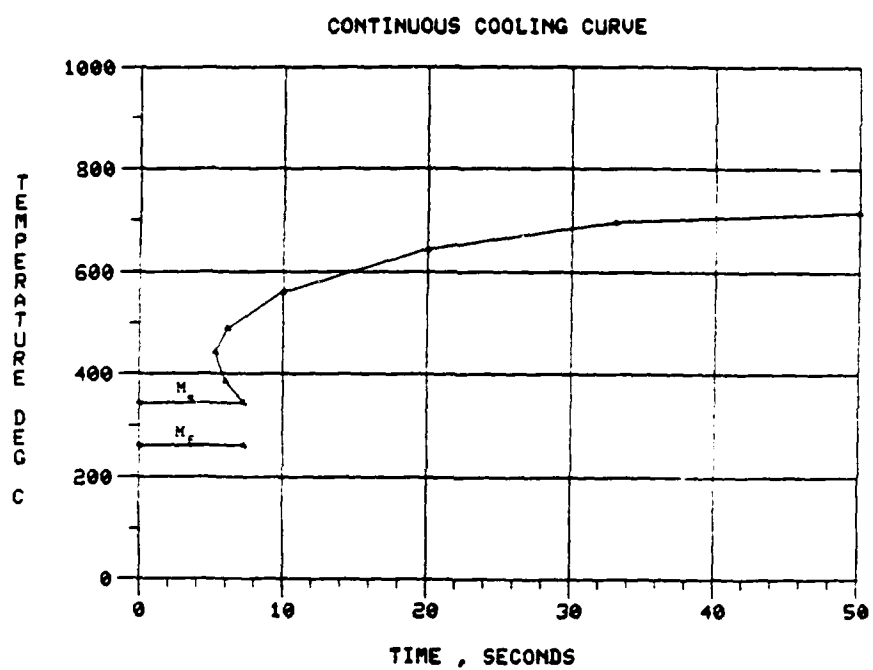


Fig. 25 Simplified C-T diagram for AISI 4140 steel taken from Figure 1.

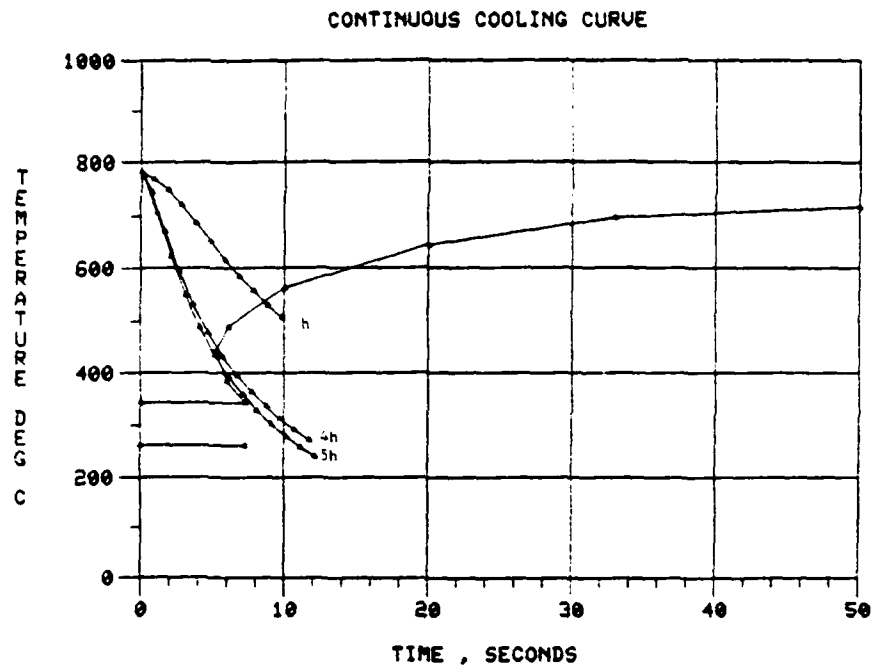


Fig. 26 Cooling curves of node 28 using the convection coefficient curve of Figure 22 scaled uniformly by a factor of 1, 4, and 5 superimposed on the C-T diagram.

problem geometry missed the nose of the C-T diagram.

A complete thermal run was made with E12202 and the scaled convection coefficient curve. The transient temperature distribution at time intervals of 0.5 seconds was stored on diskfile. Figure 27 shows the temperature history of nodes 43 and 45 of Figure 24 superimposed on the C-T diagram.

Stress Analysis

The stress analysis was accomplished with SAAS III by accessing the transient temperature distribution stored on diskfile by E12202. Since SAAS III cannot handle a coupled thermal expansion and free strain (used for the transformation expansion) analysis simultaneously, superposition was used to break the analysis up into two separate analyses. Superposition can be viewed as:

1. A thermal expansion of the steel body against the thermal fixed copper band.
2. A transformation expansion of the steel body against the thermal fixed copper band.
3. A thermal expansion of the copper band against the thermal and transformation fixed steel body.

Analyses (1) and (3) were coupled into a single thermal stress analysis. Therefore, two runs of SAAS III were required to obtain the stress distribution for a given temperature distribution.

The course mesh of Figure 24 was used in an initial stress analysis. The stress history of zone 36 is shown in Figure 28 for the longitudinal

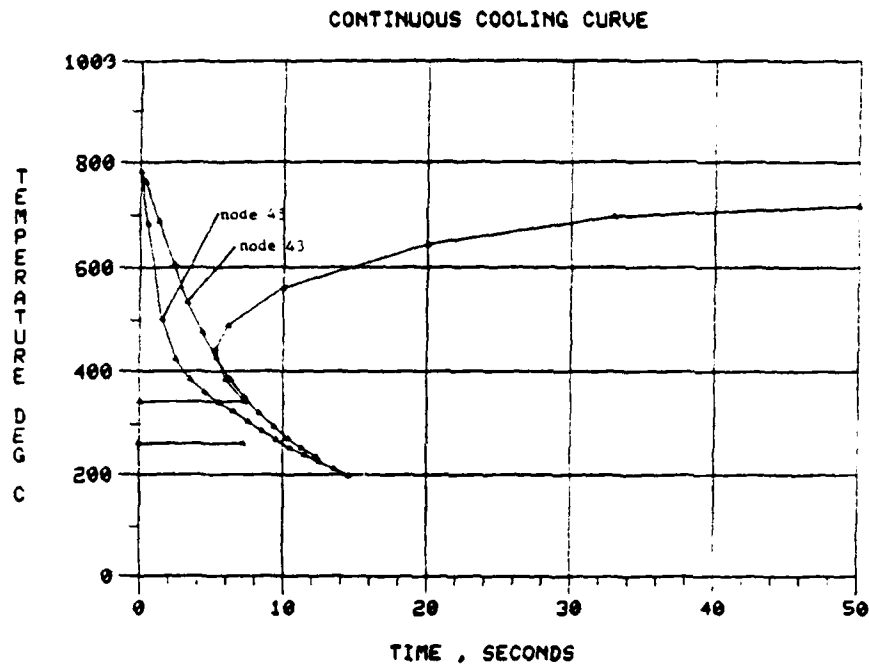


Fig. 27 Cooling curves of node 43 and 45 using the convection coefficient curve of Figure 22 scaled uniformly by a factor of 5 superimposed on the C-T diagram.

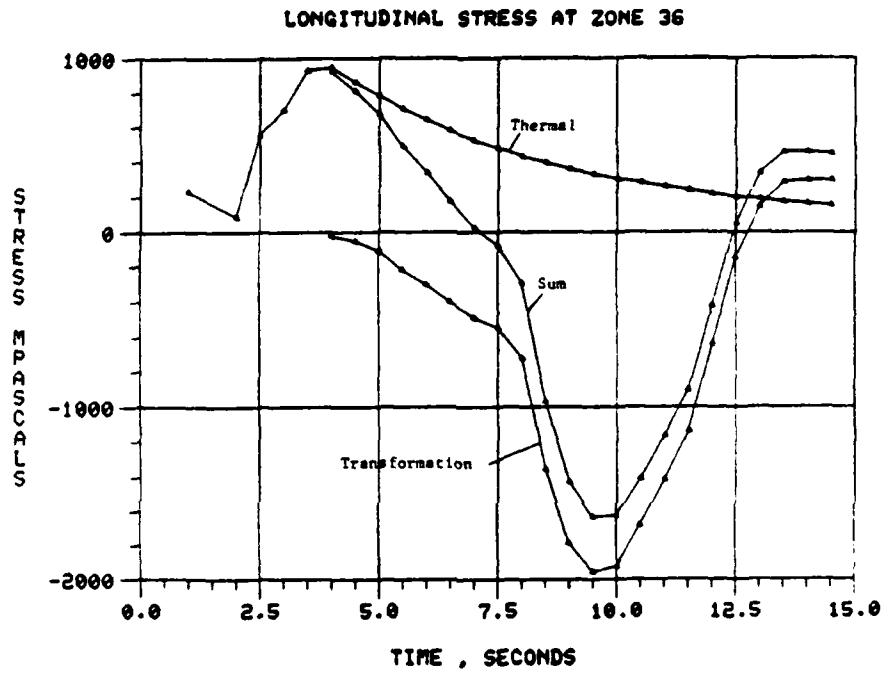


Fig. 28 Longitudinal stress history of zone 36 of Figure 24.

direction. The sum of the thermal stress and transformation stress histories for all three coordinate directions are shown in Figure 29. The times at which zone 36 reaches the M_s and M_f temperatures are also indicated in Figure 29. It can be seen from Figure 29 that the maximum stress at zone 36 after the martensite transformation is in the longitudinal direction. Figure 30 shows the stress histories for zone 40.

After the initial stress analysis with the mesh of Figure 24, the mesh was refined in the area of interest at the front of the copper band as shown in Figure 31. The thermal analysis and stress analysis were rerun with the refined mesh to obtain the maximum stresses after the martensite transformation as indicated in Figure 31. These maximum stresses were found to occur at 13.5 seconds.

An insight into the mechanism behind the maximum longitudinal stresses can be gained by an examination of the deformed element plots of Figures 32 and 33. The temperature contour plot of Figure 34 indicates that nearly all of the steel has completely transformed to martensite by 13.5 seconds. Therefore, the deformation shown in Figure 32 is due to the expansion of the martensite against the unexpanded copper band. There are longitudinal compressive stresses in the steel immediately beneath the copper band, but longitudinal tensile stresses result in the steel at the front and back of the copper band where the steel "bulges" out from underneath the band. Figure 33 shows the deformation as a result of the thermal expansion of the steel and copper. The cooler, thin portions of the geometry have contracted more than the thicker

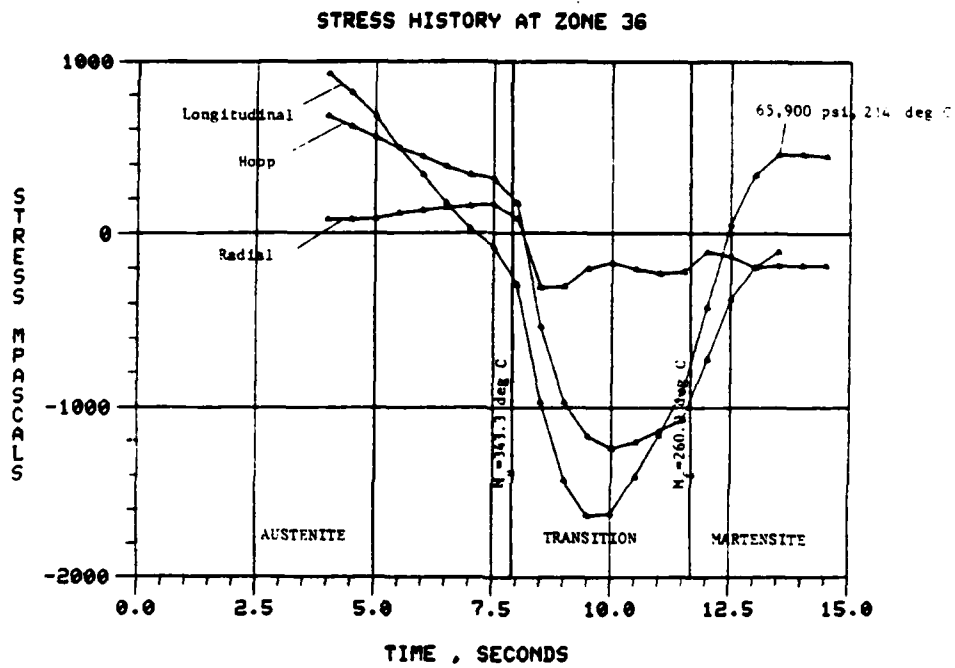


Fig. 29 Longitudinal, hoop, and radial stress history of zone 36 of Figure 24.

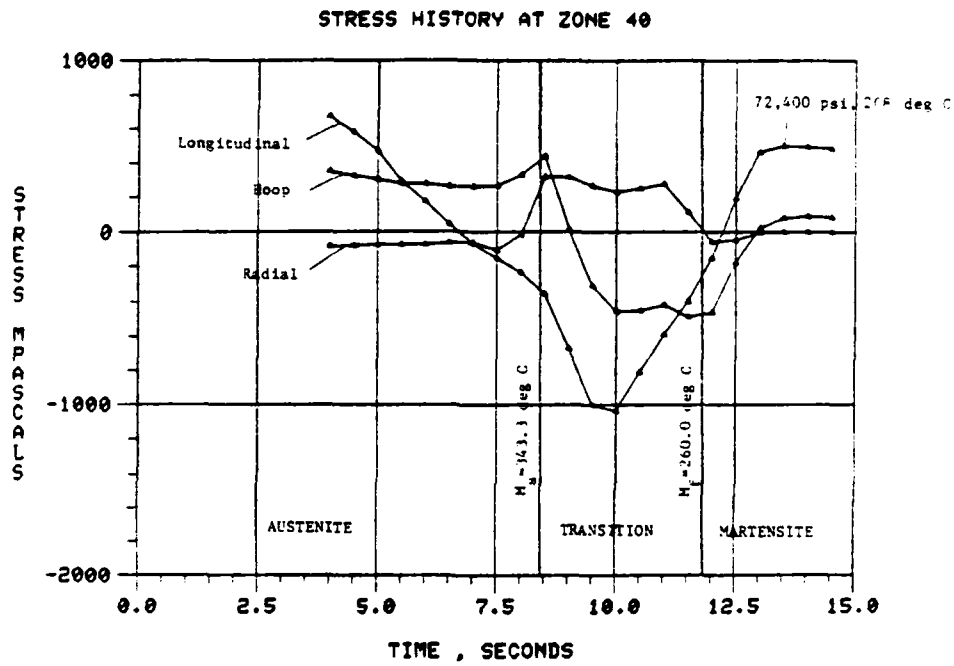


Fig. 30 Longitudinal, hoop, and radial stress history of zone 40 of Figure 24.

SAPS III FINITE ELEMENT STRESS ANALYSIS
 M483 QUENCH-THERMAL FINE MESH-13.5 SEC
 ELEMENT PLOT

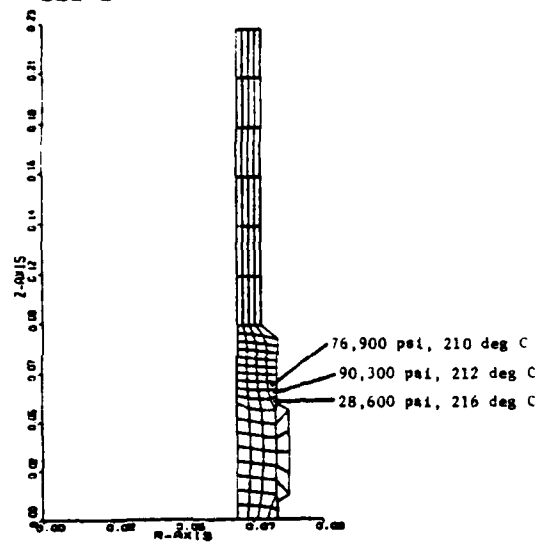


Fig. 31 Refined finite element idealization of the M483 projectile geometry indicating the maximum longitudinal stresses after the martensite transformation.

M483 QUENCH-TRANS.FINE MESH-13.5 SEC
DEFORMED ELEMENT PLOT

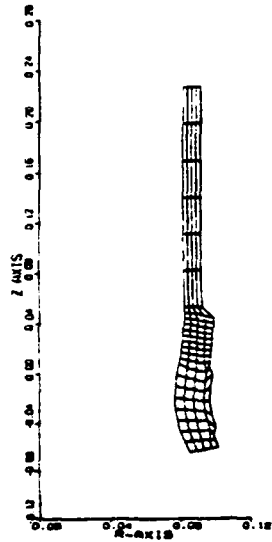


Fig. 32 Deformed element plot due to transformation expansion
at 13.5 seconds into the quench.

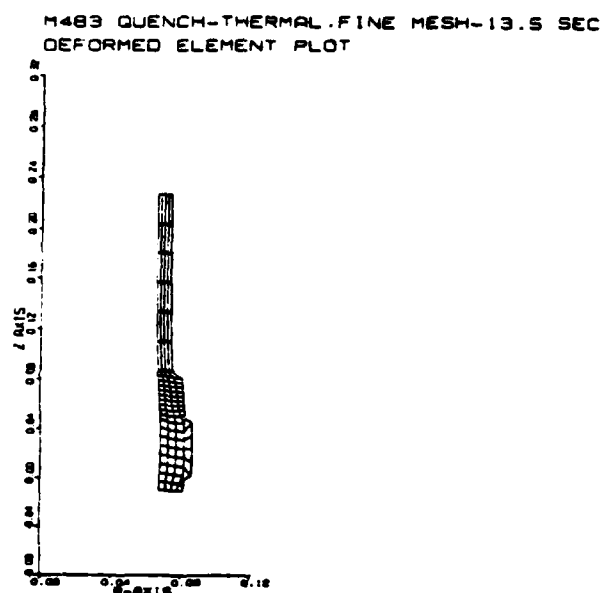
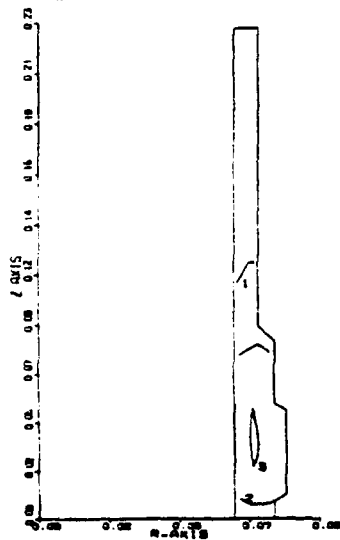


Fig. 33 Deformed element plot due to thermal expansion at 13.5 seconds into the quench.

M483 QUENCH-THERMAL FINE MESH-13.5 SEC
TEMPERATURE



CONTOURS REQUESTED

1 0.1300E+03
2 0.2000E+03
3 0.2600E+03
4 0.2700E+03

(deg C)

Fig. 34 Temperature contour plot (deg C) at 13.5 seconds into the quench.

sections--again resulting in longitudinal tensile stresses at the surface of the steel in front of the copper band. The contour plots of Figures 35 and 36 show the distribution of the longitudinal stresses throughout the geometry at 13.5 seconds.

An examination of the Von Mises stress output indicated that the steel body remained well within the elastic range. The yield strength of untempered 4140 martensite exceeds 200,000 psi even at temperatures of 260°C.²⁹ There was plastic deformation indicated in the copper band. The band yield strength is around 54,000 psi at room temperature.³⁰

The effects of the copper band on longitudinal tensile stresses in the steel at the front of the band were analyzed by first rerunning the thermal analysis and stress analysis without the copper band. Figure 37 shows the geometry without the copper band and the maximum longitudinal stress in the area of interest after the martensite transformation. Next, a bilinear stress-strain relation for the copper was used with the plastic analysis option of SAAS III. As long as stresses within the steel body do not exceed the elastic limit, superposition can still be used to add the thermal and transformation stresses in the steel. Copper yield strengths of 54,000 psi, 36,000 psi and 18,000 psi with an elastic to plastic modulus ratio of 0.2 were used in the plastic analysis. Figure 38 shows the results of the plastic analysis.

The comparative results of the several different stress analyses are summarized in Figure 39. The results confirm the expectation of large surface tensile stresses in the longitudinal direction at the front of the copper band after the martensite transformation.

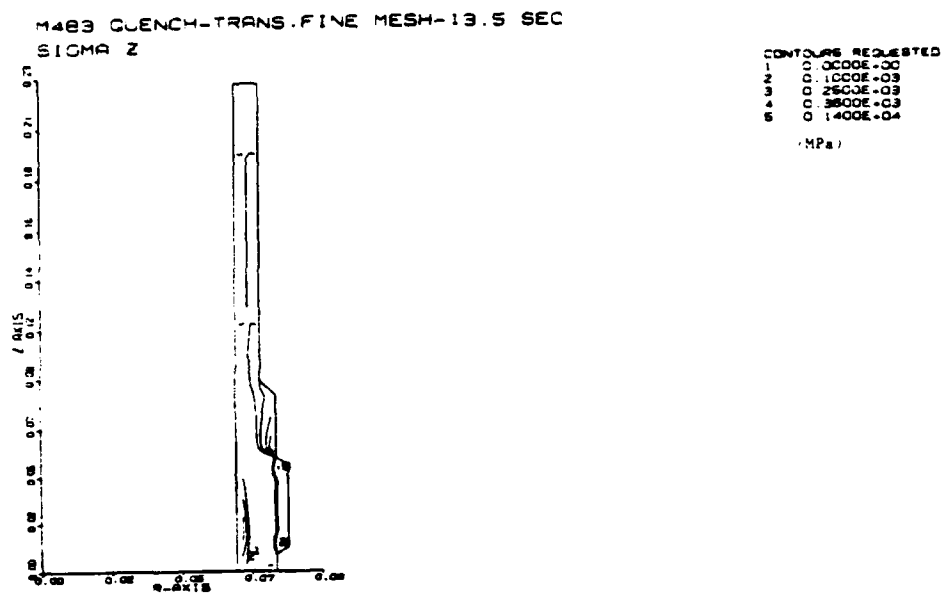


Fig. 35 Longitudinal stress contour plot (MPa) due to transformation expansion at 13.5 seconds into the quench.

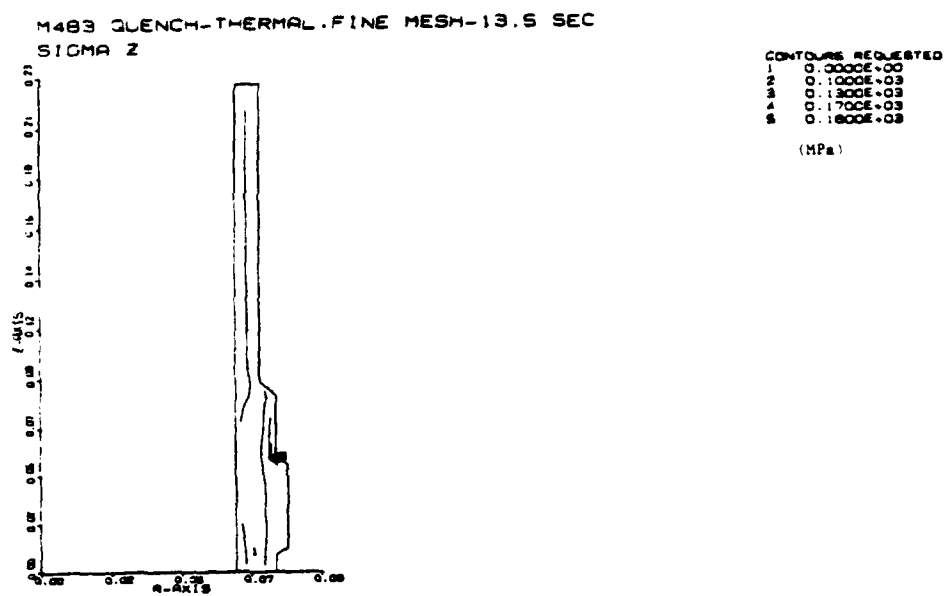


Fig. 36 Longitudinal stress contour plot (MPa) due to thermal expansion at 13.5 seconds into the quench.

SARS III FINITE ELEMENT STRESS ANALYSIS
 M483 QUENCH-NO BAND-TRANSFORM-13.0 SEC
 ELEMENT PLOT

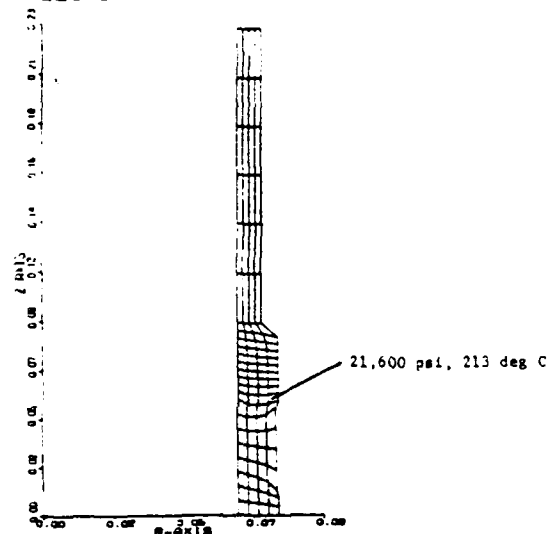


Fig. 37 Finite element idealization of the M483 projectile geometry without the rotating band and indicating the maximum longitudinal stress after the martensite transformation.

SAAS III FINITE ELEMENT STRESS ANALYSIS
 M483 QUENCH-THERMAL FINE MESH-13.6 SEC
 ELEMENT PLOT

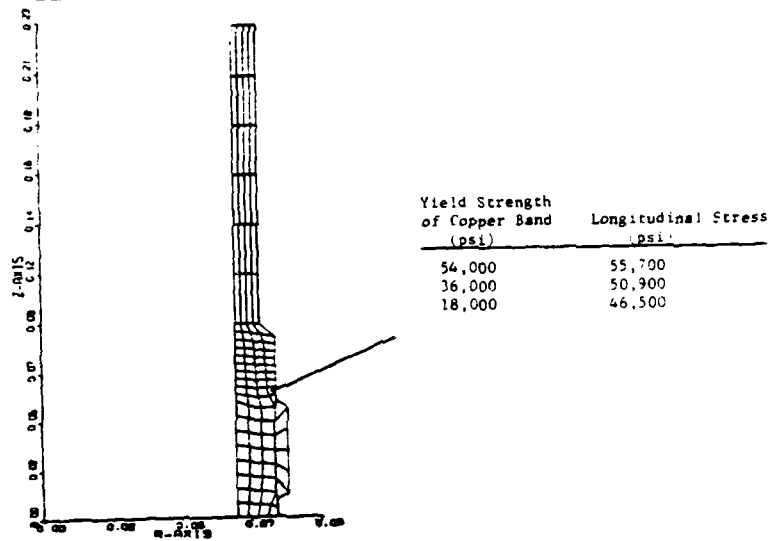


Fig. 38 Results of the plastic rotating band analyses.

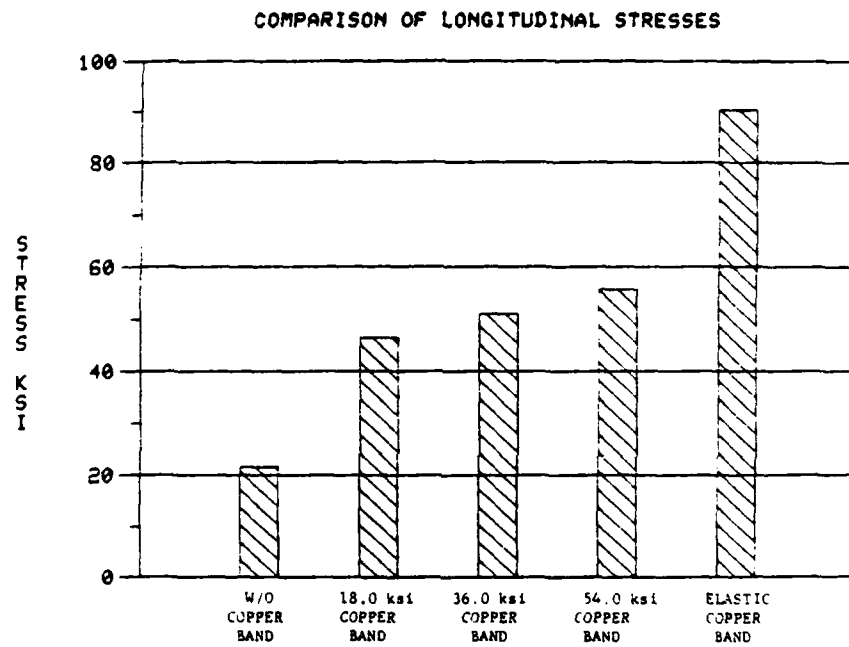


Fig. 39 Summary of the results for the M483 stress analyses.

Fracture Analysis

LEFM provides a framework in which to relate the longitudinal tensile stresses calculated in the preceding section with an initial critical crack length. The validity of LEFM in the current application must first be established. Following the guidelines of ASTM standard E-399-74 for the conditions for a valid K_{Ic} test using a standardized test specimen, the specimen thickness, B, must be

$$B \geq 2.5 \left(\frac{K_{Ic}}{\sigma_{ys}} \right)^2 \quad (1)$$

and initial crack length, a, must be

$$a \geq 2.5 \left(\frac{K_{Ic}}{\sigma_{ys}} \right)^2 \quad (2)$$

It has already been stated that untempered AISI 4140 martensite has a yield strength of over 200,000 psi at the temperature of the maximum longitudinal stress. K_{Ic} of untempered AISI 4140 martensite is less than 20 ksi/in at room temperature.³¹ While K_{Ic} data of martensite at elevated temperatures could not be found, the tendency of K_{Ic} towards a constant value at temperatures much above the transition temperature³² "inspired" a guess of K_{Ic} of around 20-30 ksi/in. Using these assumed material properties, Eq (1) and Eq (2) prescribe a minimum specimen thickness and crack length of 0.051 in. The wall thickness of M483 exceeds this requirement by a factor of ten. The implications of extrapolating ASTM E-399-74 requirements to an axisymmetric application were not investigated.

Figure 40 shows the longitudinal stresses calculated in the previous section overlaid on the critical crack curve plots of Figure 10. Figure 40 shows that for a 36,000 psi yield strength copper band and steel with a K_{Ic} of 20 ksi $\sqrt{\text{in}}$, an initial crack length of greater than 0.17 in would result in fracture.

Discussion

Confidence levels in the accuracy of the model decrease during the fracture analysis. This is due to the simplifications necessary in using LEFM. Firstly, any available K_{Ic} data are those determined from test specimens whose configurations do not represent an axisymmetric application. Even these K_{Ic} data are extremely scarce for untempered martensitic structures at elevated temperatures. Secondly, the stress intensity factor used in the model is calculated from a two-dimensional analytical analysis. This discrepancy is minimized by the small crack size and localized stress field. Thirdly, the stress intensity factor used in the model is calculated for a uniform tensile stress load. Lastly, the whole analysis is based upon a single thumbnail crack. In reality, there may be a number of cracks around the circumference at the front of the rotating band. Other studies have indicated that the interaction of multiple cracks is an important consideration in the fracture analysis.³³

Despite the above limitations on the accuracy of the fracture analysis, it was included in the model to provide a rationale for determining the effects on the susceptibility of quench cracking to changes in the material properties or quench process. If in actual

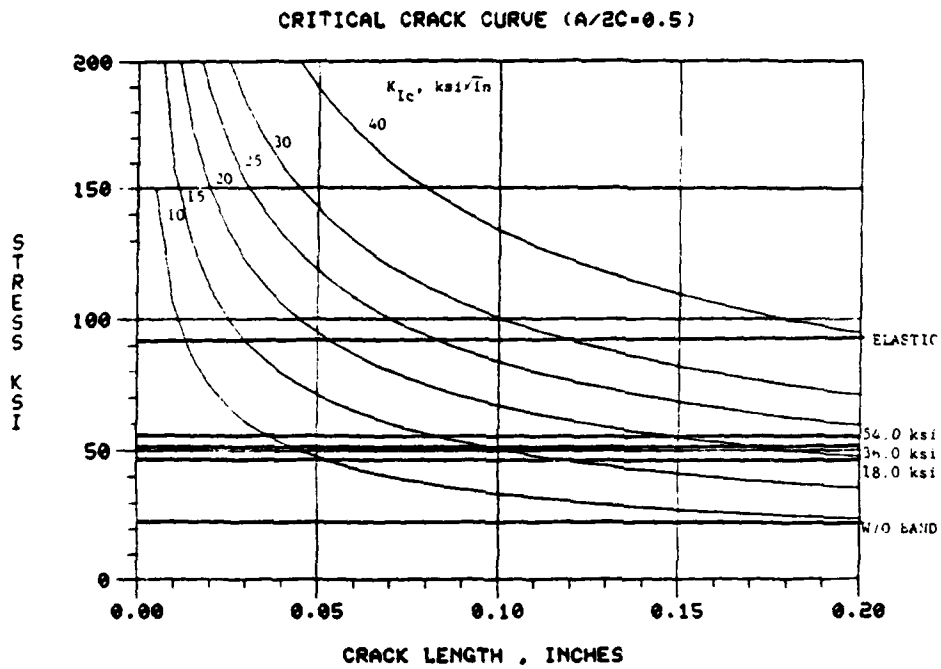


Fig. 40 Stress analysis results overlaid on the critical crack curve plot taken from Figure 10.

practice the M483 projectile was experiencing quench cracking problems with AISI 4140 steel, several possible solutions to the problem could be recommended strictly from an LEFM viewpoint.

1. Increase material toughness.
 - A. Choose a higher quality grade of AISI 4140 steel. K_{Ic} has been found to be significantly greater for steels produced in high quality processes such as the vacuum-induction melting and vacuum-arc remelting process.³⁴
 - B. Choose a different steel of altogether higher material toughness.
2. Reduce initial crack size.
 - A. Reduce the harshness of the band welding operation.
 - B. Remove surface cracks prior to heat treatment.
3. Reduce nominal stress level.
 - A. Choose a more hardenable steel not requiring as severe a quench to make the martensite transformation.
 - B. Choose a modified quench such as an interrupted process to reduce the thermal gradients between the center and surface of the piece.
 - C. Minimize the thickness of the copper band.

After a possible solution was selected, the analysis could be rerun with the quench model and the comparative effects of the change in material or process determined.

ENDNOTES

- ¹ United States Steel Company, Atlas of Isothermal Transformation Diagrams (Pittsburgh: U.S. Steel, 1951), p. 13.
- ² George Kraus, Principles of Heat Treatment of Steel (Metals Park, Oh.: American Society for Metals, 1980), p. 229.
- ³ John D. Vasilakis, Temperatures and Stresses Due to Quenching of Hollow Cylinders (Watervliet, N.Y.: Benet Weapons Laboratory, 1978) (Technical Report ARLCB-TR-78014).
- ⁴ L.A. Kimura, E.A. Thomas, and F. Yee, Engineering Operations Report: Digital Computer Programs for Steady-state or Transient Temperature Analysis of Plane and Axisymmetric Bodies by the Finite Element Method (Sacramento: Aerojet-General Corporation, 1972) (NTIS TID SNA 2007).
- ⁵ James G. Crose and Robert M. Jones, SAAS III: Finite Element Stress Analysis of Axisymmetric and Plane Solids with Different Orthotropic, Temperature-Dependent Material Properties in Tension and Compression (San Bernardino: The Aerospace Corporation, 1971) (NTIS AD-729 188).
- ⁶ Morris Cohen, "The Martensite Transformation" in Phase Transformations in Solids, ed. R. Smoluchowski, J.E. Mayer, and W.A. Weyl (New York: John Wiley & Sons, 1951), p. 609.
- ⁷ S.P. Timoshenko and J.N. Goodier, Theory of Elasticity, 3rd ed. (New York: McGraw-Hill, 1970), p. 243.
- ⁸ Kimura et al.
- ⁹ Crose and Jones.

- 10 J.P. Holman, Heat Transfer, 4th ed. (New York: McGraw-Hill, 1976), p. 371.
- 11 Kraus, p. 141.
- 12 Holman, p. 364.
- 13 Holman, p. 364.
- 14 Stanley T. Rolfe and John M. Barsom, Fracture and Fatigue Control in Structures (Englewood Cliffs, N.J.: Prentice-Hall, 1977), p. 15.
- 15 Rolfe and Barsom, p. 16.
- 16 Rolfe and Barsom, p. 39.
- 17 Rolfe and Barsom, p. 22.
- 18 Holman, pp. 129-135.
- 19 Peter A. Stark, Introduction to Numerical Methods (New York: Macmillan, 1970), pp. 95-97.
- 20 Kimura et al.
- 21 Crose and Jones.
- 22 Kimura et al.
- 23 Crose and Jones.
- 24 James R. Welty, Engineering Heat Transfer (New York: John Wiley & Sons, 1978), pp. 121-127.
- 25 Welty, p. 127.
- 26 Holman, p. 119.
- 27 National Bureau of Standards, Handbook of Mathematical Functions, 4th ed., ed. Milton Abramowitz and Irene A. Stegun (Washington, D.C.: GPO, 1965), pp. 369-370.

- ²⁸ Timoshenko and Goodier, p. 445.
- ²⁹ W.F. Simmons and H.C. Cross, "Report on Elevated-Temperature Properties of Wrought Medium Carbon Alloy Steels" in ASTM Special Technical Publication No. 199 (n.p.: ASTM, 1957).
- ³⁰ Samuel L. Hoyt, Metal Data (New York: Reinhold, 1952), n.p.
- ³¹ W.E. Wood, E.R. Parker, and V.F. Zackay, An Investigation of Metallurgical Factors Which Affect Fracture Toughness of Ultra High Strength Steels (Watertown, Mass.: Army Materials and Mechanics Research Center, 1973) (AMMRC CTR 73-24).
- ³² F.J. Witt and T.R. Mager, A Procedure for Determining Bounding Values on Fracture Toughness K_{Ic} at any Temperature (Oak Ridge, Tenn.: Oak Ridge National Laboratory, 1972) (ORNL-TM-3894).
- ³³ B.D. Goldthorpe, "Fatigue and Fracture of Thick Walled Cylinders and Gun Barrels" in Case Studies in Fracture Mechanics, ed. Thomas P. Rich and David J. Cartwright (Watertown, Mass.: Army Materials and Mechanics Research Center, 1977) (NTIS AD-A045 877).
- ³⁴ Richard W. Hertzberg, Deformation and Fracture Mechanics of Engineering Materials (New York: John Wiley & Sons, 1976), p. 336.

BIBLIOGRAPHY

- Cohen, Morris. "The Martensite Transformation." In Phase Transformations in Solids. Ed. R. Smoluchowski, J.E. Mayer, and W.A. Weyl. New York: John Wiley & Sons, 1951, pp. 588-660.
- Croze, James G., and Robert M. Jones. SAAS III: Finite Element Stress Analysis of Axisymmetric and Plane Solids with Different Orthotropic, Temperature-Dependent Material Properties in Tension and Compression. San Bernardino: The Aerospace Corporation, 1971. NTIS AD-729 188.
- Eckert, E.R.G., and R.M. Drake. Heat and Mass Transfer. 2nd ed. New York: McGraw-Hill, 1959.
- Department of Defense. Metallic Materials and Elements for Aerospace Vehicle Structures. n.p.: Department of Defense, 1971. MIL-HDBK-5B.
- Goldthorpe, B.D. "Fatigue and Fracture of Thick Walled Cylinders and Gun Barrels." In Case Studies in Fracture Mechanics. Ed. Thomas P. Rich and David J. Cartwright. Watertown, Mass.: Army Materials and Mechanics Research Center, 1977. NTIS AD-A045 877.
- Hertzberg, Richard W. Deformation and Fracture Mechanics of Engineering Materials. New York: John Wiley & Sons, 1976.
- Holman, J.P. Heat Transfer. 4th ed. New York: McGraw-Hill, 1976.
- Hoyt, Samuel L. Metal Data. New York: Reinhold, 1952.
- Kimura, L.A., E.A. Thomas, and F. Yee. Engineering Operations Report: Digital Computer Programs for Steady-state or Transient Temperature

- Analysis of Plane and Axisymmetric Bodies by the Finite Element Method. Sacramento: Aerojet-General Corporation, 1972. NTIS TID SNA 2007.
- Kraus, George. Principles of Heat Treatment of Steel. Metals Park, Oh.: American Society for Metals, 1980.
- Melloy, G.F. Hardness and Hardenability. Metals Park, Oh.: Metals Engineering Institute, 1977.
- National Bureau of Standards. Handbook of Mathematical Functions. 4th ed. Ed. Milton Abramowitz and Irene A. Stegun. Washington, D.C.: GPO, 1965.
- North American Aviation. North American Aviation Data Sheet on Alloy Steel - AISI 4130, Al-2604. n.p.: North American Aviation, n.d.
- Peckner, Donald, and I.M. Bernstein. Handbook of Stainless Steels. New York: McGraw-Hill, 1977.
- Pitts, Donald R., and Leighton E. Sissom. Theory and Problems of Heat Transfer. New York: McGraw-Hill, 1977.
- Rolfe, Stanley T., and John M. Barsom. Fracture and Fatigue Control in Structures. Englewood Cliffs, N.J.: Prentice-Hall, 1977.
- Simmons, W.F., and H.C. Cross. "Report on Elevated-Temperature Properties of Wrought Medium Carbon Alloy Steels." In ASTM Special Technical Publication No. 199. n.p.: ASTM, 1957.
- Stark, Peter A. Introduction to Numerical Methods. New York: Macmillan, 1970.
- Timoshenko, S.P., and J.N. Goodier. Theory of Elasticity. 3rd ed. New York: McGraw-Hill, 1970.

United States Steel Company. Atlas of Isothermal Transformation Diagrams. Pittsburgh: U.S. Steel, 1951.

Vasilakis, John D. Temperatures and Stresses Due to Quenching of Hollow Cylinders. Watervliet, N.Y.: Penet Weapons Laboratory, 1978. Technical Report ARLCB-TR-78014.

Welty, James R. Engineering Heat Transfer. New York: John Wiley & Sons, 1978.

Witt, F.J., and T.R. Mager. A Procedure for Determining Bounding Values on Fracture Toughness K_{Ic} at any Temperature. Oak Ridge, Tenn.: Oak Ridge National Laboratory, 1972. ORNL-TM-3894.

Wood, W.E., E.R. Parker, and V.F. Zackay. An Investigation of Metallurgical Factors Which Affect Fracture Toughness of Ultra High Strength Steels. Watertown, Mass.: Army Materials and Mechanics Research Center, 1973. AMMRC CTR 73-24.

ACKNOWLEDGMENTS

I would like to express my appreciation to Chamberlain Manufacturing Corporation for financially sponsoring this research and especially my supervisor, Paul Herman and group manager, Terry Graham for giving me free latitude to pursue what I wanted with the money I was granted. In addition, special thanks go to Art Ytterhus for his help with some of the metallurgical aspects of the research, Bob Lowe for his assistance with the computer system, and Karilyn Pryor for her excellent typing assistance.

R.B.E.

AD-A 121 268

PROCESS PARAMETERS FOR BANDING 155-MM M483A1
PROJECTILES IN HIGH-CAPACITY..(U) CHAMBERLAIN MFG CORP
WATERLOO IA RESEARCH AND DEVELOPMENT DIV..

3/3

UNCLASSIFIED

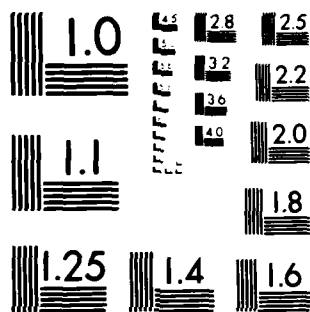
J A Ytterhus Sep 82 CB184-PR-072

F/G 19/1

NL .

END
DATE
FILMED
- 24
DTIC

END
DATE
FILMED
1 1975
DTIC



MICROCOPY RESOLUTION TEST CHART
NATIONAL BUREAU OF STANDARDS-1963-A

APPENDIX A: FORTRAN LISTING OF CONVEC

```

      SUBROUTINE RESIS(H)
C SUBROUTINE RESIS CALCULATES THE THERMAL RESISTANCES
C SURROUNDING EACH ZONE.
      COMMON RN(12,4),RE(12,4),RS(12,4),RW(12,4),R(12,4),Z(12,4)
      COMMON CUN(12,4),C(12,4),TC(20),LONT(20),TCAP(20),CAP(20)
      COMMON DT,TAU,X,Y,NT,TAMB,DEN,NCAP
      COMMON SUMR(12,4),SUMTR(12,4)
      DO 104 I=1,12
      DO 104 J=1,4
      RN(I,J)=X/(R(I,J)+X/2.)/6.283185/CON(I,J)/Y
      RE(I,J)=Y/(R(I,J)/6.283185/CON(I,J)+X)
      RS(I,J)=X/(R(I,J)+X/2.)/6.283185/CON(I,J)/Y
104  RW(I,J)=RE(I,J)
      DO 106 I=1,12
      MS(I,1)=1.E15
106  RN(I,4)=RN(I,4)/2.+1./(R(I,4)+X/2.)/H/6.283185/Y
      DO 108 J=1,4
      RW(I,J)=1.E15
108  RE(12,J)=RE(12,J)/2.+1./H/6.283185/R(12,J)/X
      RETURN
      END

      SUBROUTINE TEMP(H,T,TP)
C SUBROUTINE TEMP CALCULATES THE TEMPERATURE DISTRIBUTION
C AT THE END OF A TIME STOP FOR A GIVEN CONVECTION COEFFICIENT.
      COMMON RN(12,4),RE(12,4),RS(12,4),RW(12,4),R(12,4),Z(12,4)
      COMMON CON(12,4),C(12,4),TC(20),CONT(20),TCAP(20),CAP(20)
      COMMON DT,TAU,X,Y,NT,TAMB,DEN,NCAP
      COMMON SUMR(12,4),SUMTR(12,4)
      DIMENSION T(12,4),TP(12,4)
C INTERPOLATE THE CONDUCTIVITY
      DO 100 I=1,12
      DO 100 J=1,4
      DO 102 N=2,NT
102  IF(T(I,J).GE.TC(N))GO TO 100
100  CON(I,J)=(T(I,J)-TC(N-1))/(TC(N)-TC(N-1))*(CONT(N)-CONT(N-1))+CONT
      1(N-1)
C INTERPOLATE THE SPECIFIC HEAT
      DO 120 I=1,12
      DO 120 J=1,4
      DO 103 N=2,NCAP
103  IF(T(I,J).GE.TCAP(N))GO TO 120
120  C(I,J)=(T(I,J)-TCAP(N-1))/(TCAP(N)-TCAP(N-1))*(CAP(N)-CAP(N-1))+CA
      1P(N-1)
      DO 121 I=1,12
      DO 121 J=1,4
121  C(I,J)=DEN*C(I,J)+6.283185*R(I,J)*X*Y
C CALCULATE THE THERMAL RESISTANCES
      CALL RESIS(H)
C CALCULATE SUMR
      DO 104 I=1,12
      DO 104 J=1,4
104  SUMR(I,J)=1./RN(I,J)+1./RE(I,J)+1./RS(I,J)+1./RW(I,J)
C CALCULATE SUMTR
      DO 106 I=2,11
      DO 106 J=2,3
106  SUMTR(I,J)=T(I,J+1)/RN(I,J)+T(I+1,J)/RE(I,J)+T(I,J-1)/RS(I,J)+T(I-
      1,J)/RW(I,J)
      DO 108 I=2,11
      SUMTR(I,1)=T(I,2)/RN(I,1)+T(I+1,1)/RE(I,1)+T(I-1,1)/RW(I,1)
108  SUMTR(I,4)=TAMB/RN(I,4)+T(I+1,4)/RE(I,4)+T(I,3)/RS(I,4)+T(I-1,4)/R
      1W(I,4)
      DO 112 J=2,3
      SUMTR(1,J)=T(1,J+1)/RN(1,J)+T(2,J)/RE(1,J)+T(1,J-1)/RS(1,J)
112  SUMTR(12,J)=T(12,J+1)/RN(12,J)+T(12,J-1)/RS(12,J)+TAMB/RE(12,J)+T
      111,J)/RW(12,J)

```

```

SUMTR(1,1)=T(1,2)/RN(1,1)+T(2,1)/RE(1,1)
SUMTR(1,4)=TAMB/RN(1,4)+T(2,4)/NE(1,4)+T(1,3)/RS(1,4)
SUMTR(12,1)=T(12,2)/RN(12,1)+TAMB/RE(12,1)+T(11,1)/RW(12,1)
SUMTR(12,4)=TAMB/RN(12,4)+TAMB/NE(12,4)+T(12,3)/RS(12,4)+T(11,4)/
RW(12,4)
C CALCULATE THE NEW TEMPERATURE DISTRIBUTION
DO 110 I=1,12
DO 110 J=1,4
110 TP(I,J)=SUMTR(I,J)+DT/C(I,J)*(1.-(DT/C(I,J))*SUMR(I,J))+T(I,J)
RETURN
END

C MAINLINE
C THIS PROGRAM CALCULATES CONSTANT CONVECTION COEFFICIENTS
C BETWEEN SPECIFIED POINTS ON A STANDARDIZED COOLING
C CURVE.
C INPUTS TO THE PROGRAM ARE-
C DEN=DENSITY OF TEST SPECIMEN MATERIAL
C TI=INITIAL TEMPERATURE OF TEST SPECIMEN
C TAMB=TEMPERATURE OF BATH QUINCHMANT
C NT=NUMBER OF POINTS SPECIFIED ALONG A CONDUCTIVITY-TEMPERATURE
C CURVE FOR THE TEST SPECIMEN MATERIAL
C TC(NT)=TEMPERATURE OF POINT ON CONDUCTIVITY-TEMPERATURE CURVE
C CONT(NT)=CONDUCTIVITY OF POINT ON CONDUCTIVITY-TEMPERATURE CURVE
C NTAU=NUMBER OF POINTS SPECIFIED ALONG THE STANDARDIZED
C COOLING CURVE
C TIME(NTAU)=TIME OF POINT ON STANDARDIZED COOLING CURVE
C TF(NTAU)=TEMPERATURE OF POINT ON STANDARDIZED COOLING CURVE
C NCAP=NUMBER OF POINTS SPECIFIED ALONG A SPECIFIC HEAT-TEMPERATURE
C CURVE FOR THE TEST SPECIMEN MATERIAL
C TCAP(NCAP)=TEMPERATURE OF POINT ON SPECIFIC HEAT-TEMPERATURE CURVE
C CAP(NCAP)=SPECIFIC HEAT OF POINT ON SPECIFIC HEAT-TEMPERATURE CURVE
C TAU=TIME OF LAST POINT ON STANDARDIZED COOLING CURVE
C HMIN=LOWER BOUND ON CONVECTION COEFFICIENT, GREATER THAN ZERO
C HMAX=UPPER BOUND ON CONVECTION COEFFICIENT
C NMAX=NUMBER OF BISECTIONS
COMMON RN(12,4),RE(12,4),RS(12,4),RW(12,4),R(12,4),Z(12,4)
COMMON CON(12,4),C(12,4),TC(20),CONT(20),TCAP(20),CAP(20)
COMMON DT,TAU,X,Y,NT,TAMB,DEN,NCAP
COMMON SUMR(12,4),SUMTR(12,4)
DIMENSION TF(200),TIME(200)
DIMENSION TOL(12,4),TOM(12,4),TOLP(12,4),TOMP(12,4)
DIMENSION T(12,4)
CALL FREMAT
1000 FORMAT(V)
C CALCULATE NODAL POINT LOCATIONS
X=.00125
Y=.0025
DO 100 I=1,12
P(I,1)=6.25E-4
R(I,2)=R(I,1)+X
R(I,3)=R(I,2)+X
100 R(I,4)=R(I,3)+X
DO 101 J=1,4
101 Z(1,J)=.00125
DO 102 J=1,4
DO 102 I=2,12
102 Z(I,J)=Z(I-1,J)+.0025
C READ PROGRAM INPUTS
READ(5,1000)DEN
READ(5,1000)TI,TAMB
READ(5,1000)NT,NTAU,NCAP
DO 106 N=1,NT
106 READ(5,1000)TC(N),CONT(N)
DO 107 N=1,NTAU
107 READ(5,1000)TIME(N),TF(N)
DO 109 N=1,NCAP
109 READ(5,1000)TCAP(N),CAP(N)
READ(5,1000)TAU,HMIN,HMAX,NMAX
C INITIALIZE TEMPERATURE DISTRIBUTION
DO 114 I=1,12
DO 114 J=1,4

```

```

      T(I,J)=TI
      TOL(I,J)=TI
114  TOM(I,J)=TI
      N=1
      TAU=0.
C INITIALIZE ITERATION TO FIND CONSTANT CONVECTION COEFFICIENTS
C BETWEEN A SPECIFIED PAIR OF POINTS ON THE STANDARDIZED
C COOLING CURVE
      40  HL=HMIN
           HR=HMAX
           N=N+1
112  CHECK=TIME(N)-TAU
      DT=.1
C MAKE SURE THAT ASSUMED TIME STEP OF 0.1 SEC IS LESS THAN THE
C INTERVAL BETWEEN THE TWO POINTS ON THE STANDARDIZED COOLING
C CURVE
      DO 105 I=1,10
      IF(ABS(AINT((CHECK+.001)/DT)-DT-CHECK).LT..001)GO TO 113
105  DT=DT-.01
113  CONTINUE
C BEGIN BISECTION
      DO 84 L=1,NMAX
      HM=(HL+HR)/2.
      WRITE(6,1004)HL,HM,HR,DT
1004  FORMAT(' ',F8.2,F8.4)
      TAU1=0.
      42  TAU1=TAU1+DT
C CALCULATE TEMPERATURE OF CENTER-POINT USING LOWER BOUND ON H
      CALL TEMP(HL,TOL,TOLP)
C CALCULATE MAXIMUM STABLE TIME STEP
      DTL=C(1,1)/SUMR(1,1)
      DO 200 I=1,12
      DO 200 J=1,4
      IF(C(I,J)/SUMR(I,J).LT.DTL)DTL=C(I,J)/SUMR(I,J)
200  CONTINUE
C CALCULATE TEMPERATURE OF CENTER-POINT USING H HALFWAY BETWEEN
C UPPER AND LOWER BOUND
      CALL TEMP(HM,TOM,TOMP)
C CALCULATE MAXIMUM STABLE TIME STEP
      DTM=C(1,1)/SUMR(1,1)
      DO 202 I=1,12
      DO 202 J=1,4
      IF(C(I,J)/SUMR(I,J).LT.DTM)DTM=C(I,J)/SUMR(I,J)
202  CONTINUE
C CHECK THAT ASSUMED TIME STEP DOES NOT EXCEED MAXIMUM ALLOWABLE
C STABLE TIME STEP
      IF(DT.GT.DTL)DT=DTL
      IF(DT.GT.DTM)DT=DTM
C SET TEMPERATURE DISTRIBUTION TO NEW VALUES
      DO 204 I=1,12
      DO 204 J=1,4
      TOM(I,J)=TOMP(I,J)
204  TOL(I,J)=TOLP(I,J)
C IF TIME OF SECOND SPECIFIED POINT OF STANDARDIZED COOLING CURVE
C NOT YET REACHED, CALCULATE TEMPERATURE DISTRIBUTION
C FOR ANOTHER TIME STEP.
      IF(CHECK-TAU1.GT.DT/2.)GO TO 82
C COMPARE SIGNS OF ERROR FROM TRUE TEMPERATURE AND READJUST UPPER
C AND LOWER BOUND ON H ACCORDINGLY
      IF((TFIN)-TOM(1,1))*(TFIN)-TOL(1,1))20,30,40
20  HR=HP
   GO TO 50
30  HR=HM
   40  HL=HP
C STOP ITERATION IF H IS NOT SIGNIFICANTLY CHANGING DURING ITERATION
80  IF(ABS((HR-HL)/HL).LT..00001)GO TO 108
C CHECK TO SEE IF MAXIMUM NUMBER OF BISECTIONS ACCOMPLISHED
212  IF(L.EQ.NMAX)GO TO 84
C REINITIALIZE TEMPERATURES FOR NEXT BISECTION
      DO 210 I=1,12
      DO 210 J=1,4
      TOL(I,J)=T(I,J)
210  TOM(I,J)=T(I,J)
      44  CONTINUE
108  TAU=TAU+TAU1
C REINITIALIZE TEMPERATURES FOR NEXT TWO POINTS ON
C STANDARDIZED COOLING CURVE
      DO 206 I=1,12

```

```

      DO 206 J=1,4
      T(I,J)=TOM(I,J)
206   TOL(I,J)=TOM(I,J)
      WRITE(6,1008)OT
1008  FORMAT(' ',F8.4)
      WRITE(6,1002)TAU,TF(IN),TOM(1,1),TOM(1,4),HM
      IF(ABS(TAUM-TAU).GT.0T)GO TO 80
1002  FORMAT(' TIME=',F15.2,' TARGET=',F15.2,' CENTER=',F15.2,' SURFACE=
1',F15.2,' H=',F15.2)
      STOP
      END

```

APPENDIX B: COMPUTER OUTPUT FOR INFINITE CYLINDER ANALYSIS

E12202 Output

***** PROGRAM E12202 ***** FEM TWO-DIMENSIONAL TEMPERATURE ANALYSIS PROGRAM

ASYMMETRIC SOLID BODY

INFINITE CYLINDER THERMAL ANALYSIS

NUMBER OF NODAL POINTS-- 77
 NUMBER OF ELEMENTS-- 60
 NUMBER OF CONVECTION BC-- 6
 NUMBER OF MATERIALS-- 1
 OUTPUT INTERVAL-- 000
 TIME INTERVAL-- 0.100
 INITIAL TIME-- 0.000
 MAXIMUM TIME-- 59.900

M	TABLE-K	M	TABLE-R	RHO-CP	TABLE-Q	Q
1	0	0.215000E+03	0	0.255950E+07	0	0.000000E+00

***** PROGRAM E12202 ***** FEM TWO-DIMENSIONAL TEMPERATURE ANALYSIS PROGRAM

H.P. NO.	CODE	X	Y	T	TO	CODE TABLE
1	0	0.0000	0.0000	0.0000	0	A71.0000
2	0	0.0050	0.0000	0.0000	0	A71.0000
3	0	0.0100	0.0000	0.0000	0	A71.0000
4	0	0.0150	0.0000	0.0000	0	A71.0000
5	0	0.0200	0.0000	0.0000	0	A71.0000
6	0	0.0250	0.0000	0.0000	0	A71.0000
7	0	0.0300	0.0000	0.0000	0	A71.0000
8	0	0.0350	0.0000	0.0000	0	A71.0000
9	0	0.0400	0.0000	0.0000	0	A71.0000
10	0	0.0450	0.0000	0.0000	0	A71.0000
11	0	0.0500	0.0000	0.0000	0	A71.0000
12	0	0.0550	0.0000	0.0000	0	A71.0000
13	0	0.0600	0.0000	0.0000	0	A71.0000
14	0	0.0650	0.0000	0.0000	0	A71.0000
15	0	0.0700	0.0000	0.0000	0	A71.0000
16	0	0.0750	0.0000	0.0000	0	A71.0000
17	0	0.0800	0.0000	0.0000	0	A71.0000
18	0	0.0850	0.0000	0.0000	0	A71.0000
19	0	0.0900	0.0000	0.0000	0	A71.0000
20	0	0.0950	0.0000	0.0000	0	A71.0000
21	0	0.1000	0.0000	0.0000	0	A71.0000
22	0	0.1050	0.0000	0.0000	0	A71.0000
23	0	0.1100	0.0000	0.0000	0	A71.0000
24	0	0.1150	0.0000	0.0000	0	A71.0000
25	0	0.1200	0.0000	0.0000	0	A71.0000
26	0	0.1250	0.0000	0.0000	0	A71.0000
27	0	0.1300	0.0000	0.0000	0	A71.0000
28	0	0.1350	0.0000	0.0000	0	A71.0000
29	0	0.1400	0.0000	0.0000	0	A71.0000
30	0	0.1450	0.0000	0.0000	0	A71.0000
31	0	0.1500	0.0000	0.0000	0	A71.0000
32	0	0.1550	0.0000	0.0000	0	A71.0000

***** PROGRAM E12202 ***** FEM TWO-DIMENSIONAL TEMPERATURE ANALYSIS PROGRAM

N	I	J	K	L	MATERIAL	56	62	73	72	61	1
1	1	2	13	12	1						
2	2	3	14	13	2						
3	3	4	15	14	3						
4	4	5	16	15	4						
5	5	6	17	16	5						
6	6	7	18	17	6						
7	7	8	19	18	7						
8	8	9	20	19	8						
9	9	10	21	20	9						
10	10	11	22	21	10						
11	11	12	23	22	11						
12	12	13	24	23	12						
13	13	14	25	24	13						
14	14	15	26	25	14						
15	15	16	27	26	15						
16	16	17	28	27	16						
17	17	18	29	28	17						
18	18	19	30	29	18						
19	19	20	31	30	19						
20	20	21	32	31	20						
21	21	22	33	32	21						
22	22	23	34	33	22						
23	23	24	35	34	23						
24	24	25	36	35	24						
25	25	26	37	36	25						
26	26	27	38	37	26						
27	27	28	39	38	27						
28	28	29	40	39	28						
29	29	30	41	40	29						
30	30	31	42	41	30						
31	31	32	43	42	31						
32	32	33	44	43	32						
33	33	34	45	44	33						
34	34	35	46	45	34						
35	35	36	47	46	35						
36	36	37	48	47	36						
37	37	38	49	48	37						
38	38	39	50	49	38						
39	39	40	51	50	39						
40	40	41	52	51	40						
41	41	42	53	52	41						
42	42	43	54	53	42						
43	43	44	55	54	43						
44	44	45	56	55	44						
45	45	46	57	56	45						
46	46	47	58	57	46						
47	47	48	59	58	47						
48	48	49	60	59	48						
49	49	50	61	60	49						
50	50	51	62	61	50						
51	51	52	63	62	51						
52	52	53	64	63	52						
53	53	54	65	64	53						
54	54	55	66	65	54						
55	55	56	67	66	55						
56	56	57	68	67	56						
57	57	58	69	68	57						
58	58	59	70	69	58						
59	59	60	71	70	59						
60	60	61	72	71	60						

***** PROGRAM E12202 ***** FEM TWO-DIMENSIONAL TEMPERATURE ANALYSIS PROGRAM

I	J	TEMPERATURE	H-TAB	T-TAB	RADIATION	EPSILON	F-FACTOR	F-TABLE NO.
11	22	0.100000E+04	0	0	0	0.000000E+00	0.000000E+00	0
22	33	0.100000E+04	0.210000E+02	0	0	0.000000E+00	0.000000E+00	0
33	44	0.100000E+04	0.210000E+02	0	0	0.000000E+00	0.000000E+00	0
44	55	0.100000E+04	0.210000E+02	0	0	0.000000E+00	0.000000E+00	0
55	66	0.100000E+04	0.210000E+02	0	0	0.000000E+00	0.000000E+00	0
66	77	0.100000E+04	0.210000E+02	0	0	0.000000E+00	0.000000E+00	0
NUMBER OF CONVECTION BOUNDARY CARDS - - - 6								
TIME=	0.00000	2	3	4	5	6	7	8
1	0.00000	2	3	4	5	6	7	8
7	0.00000	8	9	10	11	12	13	14
13	0.00000	14	15	16	17	18	19	20
19	0.00000	20	21	22	23	24	25	26
25	0.00000	26	27	28	29	30	31	32
31	0.00000	32	33	34	35	36	37	38
37	0.00000	38	39	40	41	42	43	44
43	0.00000	44	45	46	47	48	49	50
49	0.00000	50	51	52	53	54	55	56
55	0.00000	56	57	58	59	60	61	62
61	0.00000	62	63	64	65	66	67	68
67	0.00000	68	69	70	71	72	73	74
73	0.00000	74	75	76	77	78	79	80
TIME=	59.99966	2	3	4	5	6	7	8
1	59.99966	2	3	4	5	6	7	8
7	59.99966	8	9	10	11	12	13	14
13	59.99966	14	15	16	17	18	19	20
19	59.99966	20	21	22	23	24	25	26
25	59.99966	26	27	28	29	30	31	32
31	59.99966	32	33	34	35	36	37	38
37	59.99966	38	39	40	41	42	43	44
43	59.99966	44	45	46	47	48	49	50
49	59.99966	50	51	52	53	54	55	56
55	59.99966	56	57	58	59	60	61	62
61	59.99966	62	63	64	65	66	67	68
67	59.99966	68	69	70	71	72	73	74
73	59.99966	74	75	76	77	78	79	80

END OF PROBLEM--INFINITE CYLINDER THERMAL ANALYSIS

SAAS III Output

MCASE = 1

10 20 30 40 50 60 70 80
 123456789012345678901234567890123456789012345678901234567890
 INFINITE CYLINDER THERMAL ANALYSIS

1 1 1 1 1 1 1 1
 11 7 4 2 1 1 1 1
 1 1 0. 0. 11 1 1 1
 11 1 0.5 0. 11 7 0.5 1
 1 1 0. 0. 1 7 0. 1
 1 7 0. 0. 11 7 0.5 1
 1 11 1 1 1 2:
 1 11 7 7 2:
 1 1 11 1 7
 1 1
 1 1 1 71.13
 2 .334

7.39E-6

END OF CASE

INFINITE CYLINDER THERMAL ANALYSIS

START PARAMETER----- 1
 STOP PARAMETER----- 0
 IF 1, PLOT DEFLECTION 0
 IF 1, SMALL PLOT, IF 2, LARGE
 PLOT, OTHERWISE NO PLOT,----- 1
 NUMBER OF APPROXIMATIONS----- 0
 IF 1, GENERATE MESH----- 1
 NUMBER OF TEMPERATURE CARDS--- -1
 NUMBER OF NODAL POINTS----- 0
 NUMBER OF ELEMENTS----- 0
 NUMBER OF INTERNAL PRESSURES-- 0
 NUMBER OF MATERIALS----- 1
 NUMBER OF EXTERNAL PRESSURES-- 0
 NUMBER OF SURFACE CARDS----- 0
 REFERENCE TEMPERATURE----- 0.0000E+00

NUMBER OF TENSION-COMPRESSION APPROXIMATIONS----- 0

MESH GENERATION INFORMATION

MAXIMUM VALUE OF I IN THE MESH----- 11

MAXIMUM VALUE OF J IN THE MESH----- 7

NUMBER OF LINE SEGMENT CARDS----- 4

NUMBER OF BOUNDARY CONDITION CARDS----- 2

NUMBER OF MATERIAL BLOCK CARDS----- 1

NUMBER OF ITERATIONS----- 0

POLAR COORDINATE PARAMETER I----- 0.0000E+00

POLAR COORDINATE PARAMETER J----- 0.0000E+00

I CURVATURE MODIFICATION----- 0

J CURVATURE MODIFICATION----- 0

INPUT I1 J1 R1 I2 J2 R2 I3 J3 R3 I4 J4 R4 I5 J5 R5 I6 J6 R6 I7 J7 R7 I8 J8 R8 I9 J9 R9 I10 J10 R10
 1 1 0.000 0.000 11 1 0.050 0.000 0 0 0.000 0.000 0 0.000 0.000 1
 DI= 10. DJ= 0. DIFF= 10. RINC= 0.005 ZINC= 0.000 ITER= 9 IINC= 1 JINC= 0 KAPPA=1

INPUT I1 J1 R1 I2 J2 R2 I3 J3 R3 I4 J4 R4 I5 J5 R5 I6 J6 R6 I7 J7 R7 I8 J8 R8 I9 J9 R9 I10 J10 R10
 1 1 0.050 0.000 11 7 0.050 0.100 0 0 0.000 0.000 1
 DI= 0. DJ= 6. DIFF= 6. RINC= 0.000 ZINC= 0.017 ITER= 5 IINC= 0 JINC= 1 KAPPA=1

INPUT I1 J1 R1 Z1 I2 J2 R2 Z2 I3 J3 R3 Z3 IPTION
 1 1 0.000 0.000 1 7 0.000 0.100 0 0 0.000 0.000 1
 OI= 0. DJ= 6. DIFF= 6. MINC= 0.000 ZINC= 0.017 ITER= 5 IINC= 0 JINC= 1 KAPPA=1

I J AR AZ
 1 2 0.000 0.017
 1 3 0.000 0.033
 1 4 0.000 0.050
 1 5 0.000 0.067
 1 6 0.000 0.083

INPUT I1 J1 R1 Z1 I2 J2 R2 Z2 I3 J3 R3 Z3 IPTION
 1 7 0.000 0.100 1 7 0.050 0.100 0 0 0.000 0.000 1
 OI= 10. DJ= 0. DIFF= 10. MINC= 0.005 ZINC= 0.000 ITER= 9 IINC= 1 JINC= 0 KAPPA=1

I J AR AZ
 1 7 0.005 0.100
 3 7 0.010 0.100
 4 7 0.015 0.100
 5 7 0.020 0.100
 6 7 0.025 0.100
 7 7 0.030 0.100
 8 7 0.035 0.100
 9 7 0.040 0.100
 10 7 0.045 0.100

COORDINATES CALCULATED AFTER 45 ITERATIONS

I	J	MP	TYPE	R-ORIGINATE	Z-ORIGINATE	R LOAD OR DISPLACEMENT	Z LOAD OR DISPLACEMENT
1	1	1	2-0	0.000	0.000	0.000000E+00	0.000000E+00
2	1	2	2-0	0.005	0.000	0.000000E+00	0.000000E+00
3	1	3	2-0	0.010	0.000	0.000000E+00	0.000000E+00
4	1	4	2-0	0.015	0.000	0.000000E+00	0.000000E+00
5	1	5	2-0	0.020	0.000	0.000000E+00	0.000000E+00
6	1	6	2-0	0.025	0.000	0.000000E+00	0.000000E+00
7	1	7	2-0	0.030	0.000	0.000000E+00	0.000000E+00
8	1	8	2-0	0.035	0.000	0.000000E+00	0.000000E+00
9	1	9	2-0	0.040	0.000	0.000000E+00	0.000000E+00
10	1	10	2-0	0.045	0.000	0.000000E+00	0.000000E+00
11	1	11	2-0	0.050	0.000	0.000000E+00	0.000000E+00
1	2	12	1-0	0.000	0.017	0.000000E+00	0.000000E+00
2	2	13	0-0	0.005	0.017	0.000000E+00	0.000000E+00
3	2	14	0-0	0.010	0.017	0.000000E+00	0.000000E+00
4	2	15	0-0	0.015	0.017	0.000000E+00	0.000000E+00
5	2	16	0-0	0.020	0.017	0.000000E+00	0.000000E+00
6	2	17	0-0	0.025	0.017	0.000000E+00	0.000000E+00
7	2	18	0-0	0.030	0.017	0.000000E+00	0.000000E+00
8	2	19	0-0	0.035	0.017	0.000000E+00	0.000000E+00
9	2	20	0-0	0.040	0.017	0.000000E+00	0.000000E+00
10	2	21	0-0	0.045	0.017	0.000000E+00	0.000000E+00
11	2	22	0-0	0.050	0.017	0.000000E+00	0.000000E+00

1	3	23	1.0	0.000	0.033	0.0000000E+00	0.0000000E+00
2	3	24	0.0	0.005	0.033	0.0000000E+00	0.0000000E+00
3	3	25	0.0	0.010	0.033	0.0000000E+00	0.0000000E+00
4	3	26	0.0	0.015	0.033	0.0000000E+00	0.0000000E+00
5	3	27	0.0	0.020	0.033	0.0000000E+00	0.0000000E+00
6	3	28	0.0	0.025	0.033	0.0000000E+00	0.0000000E+00
7	3	29	0.0	0.030	0.033	0.0000000E+00	0.0000000E+00
8	3	30	0.0	0.035	0.033	0.0000000E+00	0.0000000E+00
9	3	31	0.0	0.040	0.033	0.0000000E+00	0.0000000E+00
10	3	32	0.0	0.045	0.033	0.0000000E+00	0.0000000E+00
11	3	33	0.0	0.050	0.033	0.0000000E+00	0.0000000E+00
1	4	34	1.0	0.000	0.050	0.0000000E+00	0.0000000E+00
2	4	35	0.0	0.005	0.050	0.0000000E+00	0.0000000E+00
3	4	36	0.0	0.010	0.050	0.0000000E+00	0.0000000E+00
4	4	37	0.0	0.015	0.050	0.0000000E+00	0.0000000E+00
5	4	38	0.0	0.020	0.050	0.0000000E+00	0.0000000E+00
6	4	39	0.0	0.025	0.050	0.0000000E+00	0.0000000E+00
7	4	40	0.0	0.030	0.050	0.0000000E+00	0.0000000E+00
8	4	41	0.0	0.035	0.050	0.0000000E+00	0.0000000E+00
9	4	42	0.0	0.040	0.050	0.0000000E+00	0.0000000E+00
10	4	43	0.0	0.045	0.050	0.0000000E+00	0.0000000E+00
11	4	44	0.0	0.050	0.050	0.0000000E+00	0.0000000E+00
1	5	45	1.0	0.000	0.067	0.0000000E+00	0.0000000E+00
2	5	46	0.0	0.005	0.067	0.0000000E+00	0.0000000E+00
3	5	47	0.0	0.010	0.067	0.0000000E+00	0.0000000E+00
4	5	48	0.0	0.015	0.067	0.0000000E+00	0.0000000E+00
5	5	49	0.0	0.020	0.067	0.0000000E+00	0.0000000E+00
6	5	50	0.0	0.025	0.067	0.0000000E+00	0.0000000E+00
7	5	51	0.0	0.030	0.067	0.0000000E+00	0.0000000E+00
8	5	52	0.0	0.035	0.067	0.0000000E+00	0.0000000E+00
9	5	53	0.0	0.040	0.067	0.0000000E+00	0.0000000E+00
10	5	54	0.0	0.045	0.067	0.0000000E+00	0.0000000E+00
11	5	55	0.0	0.050	0.067	0.0000000E+00	0.0000000E+00
1	6	56	1.0	0.000	0.083	0.0000000E+00	0.0000000E+00
2	6	57	0.0	0.005	0.083	0.0000000E+00	0.0000000E+00
3	6	58	0.0	0.010	0.083	0.0000000E+00	0.0000000E+00
4	6	59	0.0	0.015	0.083	0.0000000E+00	0.0000000E+00
5	6	60	0.0	0.020	0.083	0.0000000E+00	0.0000000E+00
6	6	61	0.0	0.025	0.083	0.0000000E+00	0.0000000E+00
7	6	62	0.0	0.030	0.083	0.0000000E+00	0.0000000E+00
8	6	63	0.0	0.035	0.083	0.0000000E+00	0.0000000E+00
9	6	64	0.0	0.040	0.083	0.0000000E+00	0.0000000E+00
10	6	65	0.0	0.045	0.083	0.0000000E+00	0.0000000E+00
11	6	66	0.0	0.050	0.083	0.0000000E+00	0.0000000E+00
1	7	67	2.0	0.000	0.100	0.0000000E+00	0.0000000E+00
2	7	68	2.0	0.005	0.100	0.0000000E+00	0.0000000E+00
3	7	69	2.0	0.010	0.100	0.0000000E+00	0.0000000E+00
4	7	70	2.0	0.015	0.100	0.0000000E+00	0.0000000E+00
5	7	71	2.0	0.020	0.100	0.0000000E+00	0.0000000E+00
6	7	72	2.0	0.025	0.100	0.0000000E+00	0.0000000E+00
7	7	73	2.0	0.030	0.100	0.0000000E+00	0.0000000E+00
8	7	74	2.0	0.035	0.100	0.0000000E+00	0.0000000E+00
9	7	75	2.0	0.040	0.100	0.0000000E+00	0.0000000E+00
10	7	76	2.0	0.045	0.100	0.0000000E+00	0.0000000E+00
11	7	77	2.0	0.050	0.100	0.0000000E+00	0.0000000E+00

NUMBER OF TEMPERATURE POINTS= 77 CASE 1

R	Z	Y	R	Z	Y
0.000	0.000	392.032	0.035	0.050	371.884
0.005	0.000	391.369	0.040	0.050	365.953
0.010	0.000	390.075	0.045	0.050	359.292
0.015	0.000	388.002	0.050	0.050	351.926
0.020	0.000	385.141	0.000	0.067	392.049
0.025	0.000	381.494	0.005	0.067	391.367
0.030	0.000	377.071	0.010	0.067	390.073
0.035	0.000	371.884	0.015	0.067	388.000
0.040	0.000	365.954	0.020	0.067	385.138
0.045	0.000	359.294	0.025	0.067	381.493
0.050	0.000	351.928	0.030	0.067	377.069
0.000	0.017	392.051	0.035	0.067	371.884
0.005	0.017	391.369	0.040	0.067	365.953
0.010	0.017	390.075	0.045	0.067	359.292
0.015	0.017	388.002	0.050	0.067	351.926
0.020	0.017	385.140	0.000	0.083	392.049
0.025	0.017	381.493	0.005	0.083	391.367
0.030	0.017	377.071	0.010	0.083	390.073
0.035	0.017	371.885	0.015	0.083	388.000
0.040	0.017	365.956	0.020	0.083	385.139
0.045	0.017	359.293	0.025	0.083	381.492
0.050	0.017	351.928	0.030	0.083	377.069
0.000	0.033	392.050	0.035	0.083	371.884
0.005	0.033	391.368	0.040	0.083	365.952
0.010	0.033	390.074	0.045	0.083	359.291
0.015	0.033	388.001	0.050	0.083	351.923
0.020	0.033	385.139	0.000	0.100	392.049
0.025	0.033	381.492	0.005	0.100	391.367
0.030	0.033	377.069	0.010	0.100	390.072
0.035	0.033	371.887	0.015	0.100	388.000
0.040	0.033	365.954	0.020	0.100	385.138
0.045	0.033	359.293	0.025	0.100	381.492
0.050	0.033	351.928	0.030	0.100	377.069
0.000	0.050	392.050	0.035	0.100	371.884
0.005	0.050	391.368	0.040	0.100	365.952
0.010	0.050	390.073	0.045	0.100	359.292
0.015	0.050	388.000			351.926
0.020	0.050	385.139			
0.025	0.050	381.492			
0.030	0.050	377.071			

N	R	Z	T
41	0.0350	0.0500	372.
42	0.0400	0.0500	366.
43	0.0450	0.0500	359.
44	0.0500	0.0500	352.
45	0.0000	0.0667	392.
46	0.0050	0.0667	391.
47	0.0100	0.0667	390.
48	0.0150	0.0667	388.
49	0.0200	0.0667	385.
50	0.0250	0.0667	381.
51	0.0300	0.0667	377.
52	0.0350	0.0667	372.
53	0.0400	0.0667	366.
54	0.0450	0.0667	359.
55	0.0500	0.0667	352.
56	0.0000	0.0833	392.
57	0.0050	0.0833	391.
58	0.0100	0.0833	390.
59	0.0150	0.0833	388.
60	0.0200	0.0833	385.
61	0.0250	0.0833	381.
62	0.0300	0.0833	377.
63	0.0350	0.0833	372.
64	0.0400	0.0833	366.
65	0.0450	0.0833	359.
66	0.0500	0.0833	352.
67	0.0000	0.1000	392.
68	0.0050	0.1000	391.
69	0.0100	0.1000	390.
70	0.0150	0.1000	388.
71	0.0200	0.1000	385.
72	0.0250	0.1000	381.
73	0.0300	0.1000	377.
74	0.0350	0.1000	372.
75	0.0400	0.1000	366.
76	0.0450	0.1000	359.
77	0.0500	0.1000	352.

N	1	2	3	4	5	6	7	8	9	10	11	12	13	14	15	16	17	18	19	20	21	22	23	24	25	26	27	28	29	30	31	32	33	34	35	36	37	38	39	40
R	0.0000	0.0050	0.0100	0.0150	0.0200	0.0250	0.0300	0.0350	0.0400	0.0450	0.0500	0.0000	0.0050	0.0100	0.0150	0.0200	0.0250	0.0300	0.0350	0.0400	0.0450	0.0500	0.0000	0.0050	0.0100	0.0150	0.0200	0.0250	0.0300	0.0350	0.0400	0.0450	0.0500	0.0000	0.0050	0.0100	0.0150	0.0200	0.0250	0.0300
Z	0.0000	0.0000	0.0000	0.0000	0.0100	0.0000	0.0000	0.0000	0.0167	0.0167	0.0167	0.0167	0.0167	0.0167	0.0167	0.0167	0.0167	0.0167	0.0167	0.0167	0.0167	0.0167	0.0333	0.0333	0.0333	0.0333	0.0333	0.0333	0.0333	0.0333	0.0333	0.0333	0.0333	0.0500	0.0500	0.0500	0.0500	0.0500	0.0500	0.0500
T	392.	391.	390.	388.	385.	381.	377.	372.	366.	359.	352.	392.	391.	390.	388.	385.	381.	377.	372.	366.	359.	352.	392.	391.	390.	388.	385.	381.	377.	372.	366.	359.	352.	392.	391.	390.	388.	385.	381.	377.

EL	I	J	K	L	MATERIAL	ANGLE	TEMPERATURE	PRESSURE
1	1	2	13	12	1	0.0	391.710	0.000
2	2	3	14	13	1	0.0	390.722	0.000
3	3	4	15	14	1	0.0	389.039	0.000
4	4	5	16	15	1	0.0	386.571	0.000
5	5	6	17	16	1	0.0	383.317	0.000
6	6	7	18	17	1	0.0	379.282	0.000
7	7	8	19	18	1	0.0	374.978	0.000
8	8	9	20	19	1	0.0	368.920	0.000
9	9	10	21	20	1	0.0	362.624	0.000
10	10	11	22	21	1	0.0	355.610	0.000
11	11	12	23	22	1	0.0	351.709	0.000
12	12	13	24	23	1	0.0	350.721	0.000
13	13	14	25	24	1	0.0	349.037	0.000
14	14	15	26	25	1	0.0	346.570	0.000
15	15	16	27	26	1	0.0	343.315	0.000
16	16	17	28	27	1	0.0	339.281	0.000
17	17	18	29	28	1	0.0	334.978	0.000
18	18	19	30	29	1	0.0	328.920	0.000
19	19	20	31	30	1	0.0	322.624	0.000
20	20	21	32	31	1	0.0	315.610	0.000
21	21	22	33	32	1	0.0	311.709	0.000
22	22	23	34	33	1	0.0	309.721	0.000
23	23	24	35	34	1	0.0	308.037	0.000
24	24	25	36	35	1	0.0	306.569	0.000
25	25	26	37	36	1	0.0	303.315	0.000
26	26	27	38	37	1	0.0	300.720	0.000
27	27	28	39	38	1	0.0	300.720	0.000
28	28	29	40	39	1	0.0	300.720	0.000
29	29	30	41	40	1	0.0	300.720	0.000
30	30	31	42	41	1	0.0	300.720	0.000
31	31	32	43	42	1	0.0	300.720	0.000
32	32	33	44	43	1	0.0	300.720	0.000
33	33	34	45	44	1	0.0	300.720	0.000
34	34	35	46	45	1	0.0	300.720	0.000
35	35	36	47	46	1	0.0	300.720	0.000
36	36	37	48	47	1	0.0	300.720	0.000
37	37	38	49	48	1	0.0	300.720	0.000
38	38	39	50	49	1	0.0	300.720	0.000
39	39	40	51	50	1	0.0	300.720	0.000
40	40	41	52	51	1	0.0	300.720	0.000
41	41	42	53	52	1	0.0	300.720	0.000
42	42	43	54	53	1	0.0	300.720	0.000
43	43	44	55	54	1	0.0	300.720	0.000
44	44	45	56	55	1	0.0	300.720	0.000
45	45	46	57	56	1	0.0	300.720	0.000
46	46	47	58	57	1	0.0	300.720	0.000
47	47	48	59	58	1	0.0	300.720	0.000
48	48	49	60	59	1	0.0	300.720	0.000
49	49	50	61	60	1	0.0	300.720	0.000
50	50	51	62	61	1	0.0	300.720	0.000
51	51	52	63	62	1	0.0	300.720	0.000
52	52	53	64	63	1	0.0	300.720	0.000
53	53	54	65	64	1	0.0	300.720	0.000
54	54	55	66	65	1	0.0	300.720	0.000
55	55	56	67	66	1	0.0	300.720	0.000
56	56	57	68	67	1	0.0	300.720	0.000
57	57	58	69	68	1	0.0	300.720	0.000
58	58	59	70	69	1	0.0	300.720	0.000
59	59	60	71	70	1	0.0	300.720	0.000
60	60	61	72	71	1	0.0	300.720	0.000
61	61	62	73	72	1	0.0	300.720	0.000

VEL	FPSM	FPSZ	FPS1	FPSN7	FPSNAX	FPSMIN	ANGLE	FRPM	EPSPM	TEMPERATURE
1	0.032	-0.269	0.092	-0.000	0.092	-0.249	0.00	0.092	-0.149	592
2	0.031	-0.269	0.092	-0.000	0.091	-0.249	0.00	0.091	-0.000	591
3	0.031	-0.267	0.093	-0.000	0.091	-0.247	0.00	0.091	-0.000	589
4	0.030	-0.266	0.094	-0.000	0.090	-0.246	0.00	0.090	-0.000	587
5	0.029	-0.263	0.095	-0.000	0.089	-0.243	0.00	0.089	-0.000	583
6	0.007	-0.260	0.096	-0.000	0.087	-0.240	0.00	0.087	-0.000	579
7	0.005	-0.277	0.094	-0.000	0.085	-0.277	0.00	0.085	-0.277	574
8	0.003	-0.273	0.100	0.000	0.083	-0.273	0.00	0.083	-0.273	569
9	0.001	-0.268	0.102	-0.000	0.081	-0.268	0.00	0.081	-0.268	563
10	0.079	-0.263	0.105	0.000	0.079	-0.263	0.00	0.079	-0.263	556
11	0.079	-0.263	0.105	0.000	0.079	-0.263	0.00	0.079	-0.263	552
12	0.052	-0.269	0.092	-0.000	0.091	-0.249	0.00	0.091	-0.249	549
13	0.031	-0.267	0.093	-0.000	0.091	-0.247	0.00	0.091	-0.247	549
14	0.030	-0.266	0.094	-0.000	0.090	-0.246	0.00	0.090	-0.246	547
15	0.029	-0.263	0.095	-0.000	0.089	-0.243	0.00	0.089	-0.243	543
16	0.007	-0.260	0.096	-0.000	0.087	-0.240	0.00	0.087	-0.240	539
17	0.005	-0.277	0.094	-0.000	0.085	-0.277	0.00	0.085	-0.277	534
18	0.003	-0.273	0.100	-0.000	0.083	-0.273	0.00	0.083	-0.273	529
19	0.001	-0.268	0.102	-0.000	0.081	-0.268	0.00	0.081	-0.268	524
20	0.079	-0.263	0.105	-0.000	0.079	-0.263	0.00	0.079	-0.263	519
21	0.052	-0.269	0.092	-0.000	0.092	-0.249	0.00	0.092	-0.249	512
22	0.031	-0.267	0.093	-0.000	0.091	-0.249	0.00	0.091	-0.249	511
23	0.030	-0.266	0.094	-0.000	0.090	-0.247	0.00	0.090	-0.247	509
24	0.029	-0.263	0.095	-0.000	0.089	-0.243	0.00	0.089	-0.243	507
25	0.007	-0.260	0.096	-0.000	0.087	-0.240	0.00	0.087	-0.240	503
26	0.005	-0.277	0.094	-0.000	0.085	-0.277	0.00	0.085	-0.277	500
27	0.003	-0.273	0.100	-0.000	0.083	-0.273	0.00	0.083	-0.273	499
28	0.001	-0.268	0.102	-0.000	0.081	-0.268	0.00	0.081	-0.268	497
29	0.079	-0.263	0.105	-0.000	0.079	-0.263	0.00	0.079	-0.263	493
30	0.052	-0.269	0.092	-0.000	0.092	-0.249	0.00	0.092	-0.249	492
31	0.031	-0.267	0.093	-0.000	0.091	-0.247	0.00	0.091	-0.247	489
32	0.030	-0.266	0.094	-0.000	0.090	-0.246	0.00	0.090	-0.246	489
33	0.029	-0.263	0.095	-0.000	0.089	-0.243	0.00	0.089	-0.243	487
34	0.007	-0.260	0.096	-0.000	0.087	-0.240	0.00	0.087	-0.240	483
35	0.005	-0.277	0.094	-0.000	0.085	-0.277	0.00	0.085	-0.277	479
36	0.003	-0.273	0.100	-0.000	0.083	-0.273	0.00	0.083	-0.273	474
37	0.001	-0.268	0.102	-0.000	0.081	-0.268	0.00	0.081	-0.268	469
38	0.079	-0.263	0.105	-0.000	0.079	-0.263	0.00	0.079	-0.263	465
39	0.052	-0.269	0.092	-0.000	0.092	-0.249	0.00	0.092	-0.249	462
40	0.031	-0.267	0.093	-0.000	0.091	-0.247	0.00	0.091	-0.247	459
41	0.030	-0.266	0.094	-0.000	0.090	-0.246	0.00	0.090	-0.246	457
42	0.029	-0.263	0.095	-0.000	0.089	-0.243	0.00	0.089	-0.243	453
43	0.007	-0.260	0.096	-0.000	0.087	-0.240	0.00	0.087	-0.240	449
44	0.005	-0.277	0.094	-0.000	0.085	-0.277	0.00	0.085	-0.277	445
45	0.003	-0.273	0.100	-0.000	0.083	-0.273	0.00	0.083	-0.273	441
46	0.001	-0.268	0.102	-0.000	0.081	-0.268	0.00	0.081	-0.268	437
47	0.079	-0.263	0.105	-0.000	0.079	-0.263	0.00	0.079	-0.263	433
48	0.052	-0.269	0.092	-0.000	0.092	-0.249	0.00	0.092	-0.249	429
49	0.031	-0.267	0.093	-0.000	0.091	-0.249	0.00	0.091	-0.249	425
50	0.030	-0.266	0.094	-0.000	0.090	-0.247	0.00	0.090	-0.247	421
51	0.029	-0.263	0.095	-0.000	0.089	-0.243	0.00	0.089	-0.243	417
52	0.007	-0.260	0.096	-0.000	0.087	-0.240	0.00	0.087	-0.240	413
53	0.005	-0.277	0.094	-0.000	0.085	-0.277	0.00	0.085	-0.277	409
54	0.003	-0.273	0.100	-0.000	0.083	-0.273	0.00	0.083	-0.273	405
55	0.001	-0.268	0.102	-0.000	0.081	-0.268	0.00	0.081	-0.268	401
56	0.079	-0.263	0.105	-0.000	0.079	-0.263	0.00	0.079	-0.263	397
57	0.052	-0.269	0.092	-0.000	0.092	-0.249	0.00	0.092	-0.249	392
58	0.031	-0.267	0.093	-0.000	0.091	-0.249	0.00	0.091	-0.249	389
59	0.030	-0.266	0.094	-0.000	0.090	-0.247	0.00	0.090	-0.247	385
60	0.029	-0.263	0.095	-0.000	0.089	-0.243	0.00	0.089	-0.243	381
61	0.007	-0.260	0.096	-0.000	0.087	-0.240	0.00	0.087	-0.240	377
62	0.005	-0.277	0.094	-0.000	0.085	-0.277	0.00	0.085	-0.277	373
63	0.003	-0.273	0.100	-0.000	0.083	-0.273	0.00	0.083	-0.273	369
64	0.001	-0.268	0.102	-0.000	0.081	-0.268	0.00	0.081	-0.268	363
65	0.079	-0.263	0.105	-0.000	0.079	-0.263	0.00	0.079	-0.263	356
66	0.052	-0.269	0.092	-0.000	0.092	-0.249	0.00	0.092	-0.249	352
67	0.031	-0.267	0.093	-0.000	0.091	-0.249	0.00	0.091	-0.249	349
68	0.030	-0.266	0.094	-0.000	0.090	-0.247	0.00	0.090	-0.247	345
69	0.029	-0.263	0.095	-0.000	0.089	-0.243	0.00	0.089	-0.243	341
70	0.007	-0.260	0.096	-0.000	0.087	-0.240	0.00	0.087	-0.240	337

57	0.085	-0.277	0.094	0.000	0.084	-0.277	0.00	0.085	-0.277	0.000	374.
58	0.083	-0.273	0.100	0.000	0.083	-0.273	0.00	0.083	-0.273	0.000	369.
59	0.081	-0.268	0.102	0.000	0.081	-0.268	0.00	0.081	-0.268	0.000	363.
60	0.079	-0.263	0.105	0.000	0.079	-0.263	0.00	0.079	-0.263	0.000	346.

APPENDIX B

This appendix appears under separate cover as Chamberlain Document No. C8184-PR-072(A), entitled "Ultrasonic Scanning Tapes Generated by Chamberlain and AMMRC in Connection with Quasi-Production Run of Inertia Welded Rotating Bands onto M483A1 Projectiles."

APPENDIX C

YUMA PROVING GROUND FIRING REPORT NO. 81-PI-0138-L5

1
1
1
1

ORDAR-LCU-DS

29 JUN 1981

DEPARTMENT OF THE ARMY
U.S. Army Yuma Proving Ground
Yuma, Arizona 85364

FIRING REPORT NO. 81-PI-0138-L5

Projectile, 155-mm, M483A1

Dates of Firing: 31 March and 2, 6,
7, 8 April 1981

Product Improvement Test

Authority: Letter, TECOM, ORDAR-LCU-M
dated 28 January 1980

Test Program Request: LCU-M 2495,
Amendment 1

TECOM Project No. 2-MU-003-483-073
CS

1. ITEM UNDER TEST

Projectile, 155-mm, M483A1, lot No. LS81B001S799

2. SUPPORTING MATERIEL AND EQUIPMENT

2.1 WEAPON

Howitzer, 155-mm, M198, consisting of:

Gun, 155-mm, XM199E9, serial No. 26

Cannon, 155-mm, XM199E9, serial No. 27484

Carriage, 155-mm, XM198, serial No. 6

Recoil, 155-mm, XM45, serial No. 8

2.2 AMMUNITION

Projectile, 155-mm, M483A1, inert, lot No. LS79B001S308

Projectile, 155-mm, M107, inert, lot No. YPG-80MQ01S079

Charge, Propelling, 155-mm, M3A1, lot No. RAD67238

Charge, Propelling, 155-mm, M203, lot No. IND79K069960

Charge, Propelling, 155-mm, M203, lot No. IND78J069806

Charge, Propelling, 155-mm, M203, lot No. IND78K001S037

Fuze, MTSQ, M577, lot No. HAT-1-3

Fuze, Dummy, M73

Primer, Percussion, M82, lot No. LS-130-93

Primer, Electric, M52A3B1, lot No. LC-21-97

2.3 EQUIPMENT

Gage, Pressure, Copper Crusher, T-17 and M11, Metal of 1975, Annealed 1975, lot No. APG 2-75.

Transit, survey
Observation instruments
Field plotting board
Stopwatches
Polaroid camera for fuze settings
Communication equipment
Smear cameras
Spin cameras
Velocity coils
Recovery vehicles

3. OBJECTIVE

To provide performance data on rotating bands applied by the combination of gas metal overlay and inertia welding processes.

4. PROCEDURE

The test was conducted as outlined in Amendment 1, TPR 2475 (Incl 3).

The first two days of firing were conducted with the M203 propelling charge and projectiles (No. 61 through 120) conditioned at 145°F.

The third and fourth days of firing were conducted with the M203 propelling charge conditioned at 70°F and the projectiles (No. 31 through 60) at -60°F.

The fifth and sixth days of firing were conducted with the M3A1 propelling charge and the projectiles (No. 1 through 30) conditioned at -60°F.

5. RESULTS

The round-by-round data, including spin rates and pitch angle, are contained in Inclosure 1.

Thirty-one projectiles were inspected and showed normal rotating band wear (Incl 2). One hundred and fifty projectiles were returned to Large Caliber Laboratories, U.S. Army Armament Research and Development Command (ARRADCOM), for a detailed rotating band inspection.

The projectiles fired with excess propellant conditioned at 145°F averaged 62,000 psi pressure and an average velocity of 850 meters per second. The projectiles fired at ambient charge (70°F) averaged 47,000 psi pressure and an average instrument velocity of 805 meters per second.

6. OBSERVERS

Mr. William Sharpe, ARRADCOM, Dover, NJ 07801
Ms. Judith Wood, ARRADCOM, Dover, NJ 07801
Mr. David G. Hughes, Chamberlain Mfg, Boston, Mass.
Dr. J. A. Ytterhus, Chamberlain Mfg, RD DIV, Waterloo, Iowa

SUBMITTED:



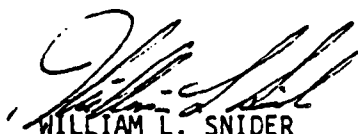
ANTHONY BEREZNUK
Project Engineer

REVIEWED:



JAMES A. GILLASPIE
Acting Chief, Munitions and Weapons
Engineering Branch

APPROVED:



WILLIAM L. SNIDER
Chief, Test Engineering Division

4 Incls

1. Round-by-Round data
2. Projectile Evaluation
3. Copy, Amendment 1, TPR 2475
4. Distribution List

ROUND-BY-ROUND DATA

Gun Positions: 4 to Tower 22																Trunnion Elevation: 134 meters															
Tubt Rd No.	Time Fired (MST)	Azimuth (line of fire)	Projectile		Chamb Press. (ksi)	Fuze Set (sec)	Propellant		Proj Temp (of)	Inst Vel. (M/S)	Projectile Impact		Spin Rate	Pitch Angle	Recovered Projectile																
			Model	Sam. Wt (lb)			Model	Zone			Excess oz.	Range Horiz (m)				Defl (m)															
Date: 31 March 1981																															
520	0947	86°00'	M483A1	W	103.4	48.4	Δ98	8	0	145	NA	NA	NA	ND	ND																
521	0955			S	103.7	58.1			+8		NA	NA	NA	ND	ND																
522	1053			C	103.8	60.3			+12		853.1	19196	226	280	-0.1																
523	1115			61	103.3	61.6			+14		851.9	19210	226	272	-0.5	X															
524	1127			62	103.4	61.2					852.8	19310	220	273	-0.7	X															
525	1134			63	103.3	61.6					852.8	19373	225	275	-0.2	X															
526	1220			C	103.5	62.7					852.7	19360	238	276	-0.1	X															
527	1232			64	103.3	62.9					854.8	19408	197	274	-1.5	X															
528	1237			65	103.4	61.6					854.0	19323	207	277	-0.3	X															
529	1242			66	103.3	63.4					854.1	19308	197	241	-4.3	X															
530	1247			C	104.0	62.1					854.8	19519	210	276	+0.6	X															
531	1254			67	103.4	63.0					850.4	18954	139	285	-11.9																
532	1259			68	103.3	62.4					855.8	19316	217	284	+1.4	X															
533	1305			69	103.4	61.6					854.2	19361	221	277	-0.9	X															
534	1311			C	104.0	62.2					853.5	19442	220	283	-1.1																
535	1316			70	103.3	62.7					854.8	19463	221	277	+1.5	X															
536	1321			71	103.4	61.7					856.1	19435	223	280	-0.6	X															
537	1326			72	103.3	61.2					851.9	18709	195	277	-5.7																
538	1332		C	103.9	63.5					855.6	19423	226	277	-1.2																	
539	1337		73	103.4	61.2					854.9	19411	228	278	-0.2	X																
540	1342		74	103.3	63.3					855.6	19401	242	266	+0.8	X																
541	1347		75	103.4	62.3					854.3	19127	242	277	+7.5	X																
542	1352		C	103.7	62.4					854.8	19387	203	276	ND	X																
543	1357		76	103.4	60.4					852.1	19237	228	278	ND	X																
544	1402		77	103.3	62.8					854.9	19429	228	262	ND	X																
545	1407	86°00'	M483A1	78	103.3	62.1	Δ98 +	8 +14	145	145	851.3	19227	235	275	ND	X															

ROUND-BY-ROUND DATA (Continued)

Tube No.	Time fired (M:SS)	Azimuth (line of fire)	Projectile		Fuze Set (sec)	Cham Press. (ksi)	Propellant		Proj Temp (°F)	Inst Vel. (M/S)	Impact		Spin Rate	Pitch Angle	Recovered Projectile		
			Model	Wt No. (lb)			Zone	Excess oz.			Range (m)	Defl (m)					
Date: 2 April 1981																	
546	0826	85°00'	M483A1	W	103.5	46.8	M203	8	0	145	NA	NA	NA	ND	X		
547	0835			S	104.1	62.5					NA	19558	53	ND		ND	
548	0910			C	103.6	61.2					850.6	19504	57	268		+1.7	X
549	0918			79	103.4	61.4					853.4	19528	61	276		-0.8	X
550	0923			80	103.4	61.1					850.7	19346	67	282		+0.2	X
551	0929			81	103.3	60.5					853.2	19403	43	277		+1.4	X
552	0934			C	103.9	61.6					857.8	19656	58	281		+0.8	X
553	0939			82	103.3	62.0					857.1	19556	58	260		+0.2	X
554	0943			83	103.4	62.1					855.1	19521	57	278		+1.4	X
555	0949			84	103.3	61.4					855.3	19479	69	285		+0.9	X
556	0953			C	104.0	61.9					856.3	19610	49	274		-0.2	X
557	0958			85	103.3	62.0					857.7	19586	52	284		+0.6	X
558	1004			86	103.3	62.8					856.2	19458	61	284		+1.4	X
559	1009			87	103.4	63.7					859.3	19689	67	277		+0.4	X
560	1014			C	104.0	62.5					856.1	19357	88	281		+6.0	X
561	1020			88	103.3	63.4					858.3	19583	57	277		-0.7	X
562	1024			89	103.3	62.5					857.8	19569	64	273		-0.2	X
563	1030	90	103.4	61.6	857.8	19515	66	278	-0.3	X							
564	1035	C	103.8	62.3	860.8	19715	43	277	-0.2	X							
565	1040	91	103.3	62.7	857.0	19555	42	279	+0.6	X							
566	1045	92	103.4	63.2	853.5	19035	14	277	-8.5	X							
567	1050	93	103.4	62.5	857.8	19603	37	279	-1.0	X							
568	1054	C	104.0	62.4	859.5	19749	36	276	-0.6	X							
569	1100	94	103.3	63.4	856.7	19568	46	283	-0.8	X							
570	1104	95	103.4	63.0	860.6	19662	47	286	-0.9	X							
571	1109	96	103.3	62.4	856.7	NA	NA	278	-ND	X							
572	1114	C	103.9	62.8	858.3	19631	69	283	+0.4	X							
573	1119	97	103.4	62.8	859.5	19537	75	280	+0.4	X							
574	1123	85°00'	M483A1	98	103.4	62.3	M203	8	+18	145	859.0	19662	47	280	-1.5	X	

ROUND-BY-ROUND DATA (Continued)

Tube No.	Time Fired (MST)	Alt (ft)	Azimuth (line of fire)	Projectile		Cham Press. (ksi)	Fuze Set (sec)	Propellant		Proj Temp (of)	Inst Vel. (M/S)	Projectile Impact		Spin Rate	Pitch Angle	Recovered Projectile	
				Model	Sam. No.			Wt (lb)	Model			Zone	Excess oz.				Temp (of)
575	1128	400	85000'	M483A1	99	103.3	62.9	M203	8	+18	145	858.9	19617	80	279	+1.0	X
576	1219			C	103.7	62.5						860.3	19356	116	279	+1.1	X
577	1223			100	103.3	62.0						856.4	19543	122	276	+1.1	X
578	1228			101	103.4	62.8						856.1	19510	145	279	+0.2	X
579	1233			102	103.4	62.4						854.5	19440	53	281	+6.8	X
580	1243			C	103.8	62.4						855.3	19623	162	276	ND	X
581	1248			103	103.3	62.0						855.2	19572	184	280	+1.0	X
582	1253			104	103.4	61.7						856.1	19613	183	281	-0.5	X
583	1300			105	103.4	62.0						854.9	19595	216	274	+0.6	X
584	1305			C	103.5	61.1						852.9	19572	234	277	+0.6	X
585	1310			106	103.4	62.0						852.4	19453	226	284	-0.5	X
586	1315			107	ND	62.2						854.5	19572	234	278	-0.3	X
587	1320			108	ND	61.6						855.2	19500	235	279	+0.4	X
588	1325			C	ND	62.1						855.3	19687	251	276	+0.6	X
589	1330			109	ND	62.2						855.3	19556	265	280	+0.2	X
590	1336			110	ND	60.9						854.4	19477	278	276	+0.3	X
591	1341			111	ND	62.4						854.2	19545	273	275	+0.6	X
592	1351			C	ND	60.9						852.7	19556	265	276	-0.3	X
593	1355			112	ND	60.5						852.0	19437	266	273	+0.1	X
594	1400		113	ND	56.3						852.9	19565	256	ND	-0.4	X	
595	1404		114	ND	54.7						843.0	19249	271	279	+0.6	X	
596	1407		C	ND	54.6						837.6	19191	255	278	-0.3	X	
597	1413		115	ND	54.5						837.7	19024	255	269	-0.5	X	
598	1418		116	ND	55.9						837.6	NA	NA	275	-6.4	X	
599	1422		117	ND	54.8						846.7	19357	265	278	+0.4	X	
600	1427		C	ND	53.3						839.5	19094	261	280	-0.3	X	
601	1431		118	ND	54.1						845.0	19346	259	278	0.0	X	
602	1436		119	ND	54.3						837.3	19148	263	272	+1.0	X	
603	1444	400	85000'	M483A1	120	ND	NA	M203	8	+18	145	837.3	19149	281	273	+1.2	X

NOTE: Projectiles No. 594 through 603 were fired with a modified charge designated for another test.

ROUND-BY-ROUND DATA (Continued)

Table No.	Time Fired (M:SS)	Azimuth (line of fire)	Projectile		Cham Press. (ksi)	Fuze Set (sec)	Propellant		Proj Temp (°F)	Inst Vel. (M/S)	Impact		Spin Rate	Pitch Angle	Recovered Projectile		
			Model	Sam. No.			Model	Zone			Range Horiz (m)	Height (m)					
Date: 6 April 1981																	
604	0926	400	86000'	M483A1	W	103.7	43.3	A98	8	0	70	NA	17824	206	ND	ND	X
605	0922	400	86000'		S	103.9	46.2					NA	18204	180	ND	ND	X
606	0952	365	88000'		S	103.3	43.7				70	NA	17126	165	ND	ND	X
607	0957	380			S	103.7	46.6				-60	NA	17828	196	ND	ND	X
608	1038				C	103.5	47.0					803.3	17733	178	263	-0.8	X
609	1045				31	103.3	46.7					802.6	17665	191	267	+2.1	X
610	1050				32	103.3	46.7					802.0	17649	175	268	-1.1	X
611	1054				33	103.4	46.7					801.6	17627	174	266	-1.3	X
612	1103				C	103.7	47.9					804.4	17728	185	263	-0.3	X
613	1113				34	103.4	47.3					808.2	17845	173	265	-0.9	X
614	1117				35	103.3	46.6					0	17716	188	267	-1.7	X
615	1122				36	103.4	47.0					803.0	17684	171	263	-1.2	X
616	1217				C	103.0	48.2					805.5	17785	140	262	-2.4	X
617	1221				37	103.4	47.1					803.5	17739	149	271	-0.4	X
618	1224				38	103.2	47.1					803.8	17670	146	263	-0.8	X
619	1228				39	103.3	45.2					801.5	17626	155	263	+0.3	X
620	1231				C	103.6	47.2					803.4	17734	136	266	-1.1	X
621	1236				40	103.4	47.3					802.2	17585	142	265	-0.9	X
622	1238				41	103.4	46.0					802.9	17652	139	266	+0.6	X
623	1241				42	103.3	48.6					807.3	17836	134	264	-0.7	X
624	1244				C	103.8	47.6					0	17735	152	270	-0.7	X
625	1247				43	103.4	47.6					805.6	17752	145	262	+0.3	X
626	1253				44	103.4	45.8					800.4	17601	156	266	+0.1	X
627	1256	380			45	103.4	47.4					804.2	17674	149	265	-0.5	X
628	1337	370			C	103.7	47.9					802.4	17586	147	272	-0.6	X
629	1341				46	103.4	46.9					802.9	17456	162	267	-0.6	X
630	1344				47	103.3	48.0					802.2	17431	127	261	-0.8	X
631	1347				48	103.3	48.6					804.4	17499	133	260	-1.8	X
632	1351				C	103.8	47.5					797.5	17402	142	257	-2.7	X
633	1354				49	103.4	47.6					803.3	17515	142	257	-1.4	X
634	1357				50	103.3	47.3					801.2	17507	147	260	+0.3	X
635	1401	370	88000'	M483A1	51	103.4	46.1	A98	8	0	70	799.8	17371	143	259	-1.3	X

ROUND-BY-ROUND DATA (Continued)

Tube No.	Time fired (M:SS)	QZ (°)	Azimuth (line of fire)	Projectile		Chamb. Press. (ksi)	Fuze Set (sec)	Propellant		Proj Temp (°F)	Inst Vel. (M/S)	Projectile Impact		Spin Rate	Pitch Angle	Recovered Projectile
				Model	Sam. No.	Wt (lb)		Model	Zone			Range (m)	Defl (m)			
636	1404	370	88°00'	M483A1	C	103.4	46.8	M203	8	70	805.6	17630	180	264	+0.4	X
637	1407				52	103.4	47.9				803.1	17427	154	267	-0.8	X
638	1411				53	103.4	47.1				830.5	17435	139	261	+0.6	X
639	1415	370	88°00'	M483A1	54	103.4	46.5	M203	8	70	800.4	17387	142	264	-1.3	X
Date: 7 April 1981																
640	0853	370	88°00'	M483A1	W	103.7	42.0	M203	8	70	0	17183	161	ND	ND	
641	085				S	103.4	42.9				784.9	17115	162	ND	-0.2	
642	0904				C	103.5	45.8			-60	798.9	17427	167	261	+0.3	X
643	0910				55	103.3	45.7				799.8	17365	178	256	-1.4	X
644	0914				56	103.5	46.4				802.4	17363	175	269	-0.3	X
645	0918				57	103.4	46.1				800.1	17386	180	270	+1.0	X
646	0921				C	103.1	45.2				802.1	17509	188	266	+0.2	X
647	0924				58	103.4	45.2				800.3	17399	178	266	-0.1	X
648	0928				59	103.3	46.3				801.9	17442	177	263	-0.2	X
649	0931		88°00'		60	103.4	44.6	M203	8	70	798.5	17329	165	255	ND	
650	1045		87°00'		W	103.5	7.5	M3A1	3	-60	251.0	3808	22	ND	ND	
651	1049				S	103.3	6.7				248.8	3765	19	ND	ND	
652	1052				S	103.3	7.1				248.8	3748	25	ND	ND	
653	1058				C	103.8	7.1			-60	249.1	3753	23	78	-1.1	X
654	1102				1	103.4	7.2				247.6	3690	19	81	-2.9	X
655	1105				2	103.3	7.1				247.0	3679	17	78	-2.7	X
656	1109				3	103.4	7.2				248.3	3709	22	82	-3.9	X
657	1222				C	103.6	7.4				249.8	3772	22	81	+2.6	X
658	1227				4	103.4	7.4				248.1	3710	37	79	-4.8	X
659	1231				5	103.3	7.2				248.1	3700	11	ND	ND	
660	1235				6	103.3	7.2				246.6	3676	21	78	-2.9	X
661	1238				C	103.4	7.3				248.5	3728	11	81	+1.3	X
662	1242				7	103.4	7.2				247.3	3694	16	78	-0.7	X
663	1246				8	103.4	6.9				246.3	3684	17	79	-1.3	X
664	1249				9	103.4	7.1				248.0	3716	11	79	-3.7	X
665	1253	370	87°00'	M483A1	C	103.6	7.3	M3A1	3	-60	249.0	3748	15	81	-0.7	X

ROUND-BY-ROUND DATA (Concluded)

Tube Rd No.	Time Fired (MST)	QC (°)	Azimuth (line of fire)	Projectile		Cham Press. (ksi)	Fuze Set (sec)	Propellant			Proj Temp (°F)	Inst Vel. (M/S)	Impact		Spin Rate	Pitch Angle	Recovered Projectile
				Model	No.	Wt (lb)		Model	Zone	Excess oz.			Range Horiz (m)	Defl (m)			
666	1256	370	87°00'	M483A1	10	103.4	7.3	Δ98	3	0	-60	247.6	3689	14	80	-4.1	X
667	1300				11	103.4	7.2					248.3	3735	14	80	-3.2	X
668	1304				12	103.4	7.3					248.8	3733	16	80	-2.7	X
669	1308				C	103.9	7.3					249.4	3762	17	81	-0.6	X
670	1311				13	103.3	7.3					248.7	3732	21	81	-1.2	X
671	1315				14	103.4	7.1					247.9	3718	16	79	-1.1	X
672	1318				15	103.4	7.4					249.8	3763	12	81	-3.8	X
673	1322				C	103.5	7.2					249.6	3684	17	82	-3.6	X
674	1325				16	103.4	7.5					249.2	3750	17	80	-2.0	X
675	1329				17	103.4	7.0					246.5	3681	24	80	-2.4	X
676	1332				18	103.4	7.2					248.3	3737	13	83	-3.2	X
677	1336				C	103.7	7.6					250.6	3792	14	82	-1.1	X
678	1339				19	103.4	7.5					248.9	3731	20	80	-2.1	X
679	1343				20	103.4	7.4					249.6	3778	17	82	-0.6	X
680	1346	370	87°00'	M483A1	21	NA	7.4	Δ98	3	0	-60	250.5	3790	18	81	+0.1	X
Date: 8 April 1981																	
681	0916	370	90°00'	M107	W	95.0	6.8	Δ98	3	0	-60	265.2	4270	38	ND	ND	
682	0919			M107	W	95.0	7.2					266.9	4331	46	ND	ND	
683	0921			M107	W	95.0	6.5					264.1	4206	47	ND	ND	
684	0924			M483A1	S	103.8	7.2					245.6	3675	34	ND	ND	X
685	0932				C	104.1	7.2					247.2	3706	37	82	+0.4	X
686	0935				22	103.3	7.2					245.5	3633	36	81	-1.9	X
687	0938				23	103.4	7.0					246.7	3681	33	80	-3.4	X
688	0941				24	103.4	7.2					246.9	3677	32	82	-2.2	X
689	0944				C	103.6	7.4					246.6	3749	33	81	-2.6	X
690	0946				25	103.4	7.4					247.8	3694	36	80	-4.6	X
691	0949				26	103.5	7.2					248.6	3722	34	80	-3.3	X
692	0952				27	103.4	7.3					248.6	3714	31	78	ND	
693	0955				C	103.6	7.2					249.4	3758	35	ND	-0.7	X
694	1004				28	103.3	7.4					249.5	3743	34	79	-4.0	X
695	1007				29	103.6	7.5					249.7	3728	31	82	-5.4	X
696	1011	370	90°00'	M483A1	30	103.4	8.3	Δ98	3	0	-60	252.4	3050	38	83	+0.2	X

LEGEND: C- Control Rounds MA- Not Applicable ND- No Data S- Spotter Rounds W- Warmer Rounds

PROJECTILE EVALUATION

<u>Tube No.</u>	<u>Projectile No.</u>	<u>Remarks</u>
None	Spotter	Slight wear on front end of rotating band
524	62	No wear showing, good condition
525	63	No wear showing, good condition
526	Control	1/8" wear on front end rotating band in spots, good condition
527	64	Very slight wear, good condition
528	65	1/16" wear on front end of rotating band, good condition
530	Control	1/8" wear on front end of rotating band in spots, good condition
532	68	Good condition
533	69	Good condition
535	70	Slight wear at front end of rotating band, good condition
536	71	1/8" wear spots on front end of rotating band, good condition
539	73	Good condition
540	74	Slight wear at front end of rotating band, good condition
542	Control	1/8" wear spots around 2/3 of rotating band, good condition
544	77	Good condition
558	Control	Good condition
553	Control	Brass showing all the way around, fair condition
554	1	Slight wear, good condition
555	4	Slight wear, good condition
559	5	Slight wear, good condition

Incl 2, Page 1 of 2

PROJECTILE EVALUATION (Concluded)

<u>Tube No.</u>	<u>Project No.</u>	<u>Remarks</u>
662	7	Slight wear, good condition
666	10	Slight wear, good condition
667	11	Slight wear, good condition
668	12	Good condition
670	13	Slight wear, good condition
672	15	Slight wear, good condition
675	17	Slight wear, good condition
677	Control	Brass showing front edge, good condition
678	19	Slight wear, good condition
679	20	Slight wear, good condition
680	21	Slight wear, good condition

NOTE. Remarks stating brass showing, 1/8" or 1/16" wear spots, refer to the front portion of the rotating band wearing away flush with the diameter of the rear bourrelet.

The remaining recovered rounds were not checked prior to shipping to ARRADCOM.

COPY AMENDED

Amendment 1, TPR 2475

8 January, 1981

R 002000Z JAN 81
FM CDARRCOM DOVER NJ //DRDAR-LCU-M//
TO RULNAPU/CDRTECOM APG MD //DRSTE-CM-F/DRSTE-TO-O/DRDAR-TSE-OC//
INFO RUMHNDAXCDRYPG YUMA AZ //STEYP-MTW/DRDAR-TSE-OB//
RUCIAFB/CDARRCOM ROCK ISL IL //DRSAR-LEM/DRSAR-PDM-M//

BT

UNCLAS

FOR STULLENBARGER FOSTER NEALLY KICHLIN RANDOL PARK

SUBJ: TPR 2475 AMEND 1

A. 2-MN 003-483-073

1. IN ACCORDANCE WITH SUBJECT TPR REQUEST THE FOLLOWING TEST
MATRIX BE CONDUCTED AT YPG:

ROUND IDENT	NO. RDS	TEST
WARMER (M107)	4	PROPELLANT CHARGE M3A1 M73 DUMMY FUZE
TEST 1-30	30	CONDITION AT MINUS 60 DEGREES
CONTROL	11	F: FIRE ZONE 3; PROPELLANT
	(SAME WEIGHT ZONE AS TEST RD)	CHARGE M3A1 AT MINUS -60 DEGREES F.
TEST 31-60	30	CONDITION AT MINUS 60
CONTROL	11	DEGREES F; FIRE ZONE
	(SAME WEIGHT ZONE AS TEST RDS)	8; PROPELLANT CHARGE M3A1 AT 70 DEGREES F,
TEST 61-120	60	CONDITION AT PLUS 145
CONTROL	21	DEGREES F: FIRE WITH M3A1 CHARGE ADJUSTED BY TEMPERATURE TO 62,500 PSI PLUS OR MINUS 2500 PSI

ROUND IDENTIFY CAN BE FOUND ON REAR BOURRELET OF PROJECTILE
2. BALLISTIC TESTING ON EACH DAY OF TESTING SHALL BE PRECEDED
BY A MINIMUM OF 2 SPOTTER ROUNDS. FIRST ROUND OF EACH PHASE AND
EVERY 4TH ROUND SHALL BE A CONTROL ROUND. ZONE 3 PHASE SHALL BE
PRECEDED BY FIRING OF 4 EA M107 PROJECTILES TO WARM TUBE.

3. ALL TESTING SHALL BE DONE WITH A M199 CANNON WITH MINIMUM
90 PERCENT REMAINING LIFE.

4. TEST AND CONTROL ROUNDS SHALL HAVE BEEN INERT LOADED AND
SHALL BE FIRED FOR RECOVERY WITH M577 DUMMY FUZES AND INERT
EXPULSION CHARGES.

5. SPIN PATTERNS SHALL BE PAINTED ON ALL TEST ROUNDS.

6. THE FOLLOWING DATA SHALL BE RECORDED

A. RANGE DEFLECTION AZIMUTH

B. QE

C. MUZZLE VELOCITY (GE RADAR, GE211 PREFERRED)

D. AS FIRED WEIGHT

E. SNEAR CAMERA AT 60 FEET

F. TWO SPIN CAMERAS

ENC 3, Page 1 of 2

COPI AMENDED

Amendment 1, TPR 2475 (Concluded)

7. INITIAL FUNDING FOR THIS AMENDMENT ARRIVED AT YPG IN AUGUST 1980. REQUEST FOR FUNDING IN EXCESS OF THAT AVAILABLE SHOULD BE MADE TO W. SHARPE, ARRADCOM, DARDAR-LCU-M. TEST HARDWARE IS EXPECTED TO ARRIVE AT YPG BY 28 FEBRUARY 1981.

8. YPG SHALL BE REQUIRED TO PROVIDE

A. 4 EA 155MM M107 PROJECTILES

B. 43 EA STANDARD INERT M483 A1 PROJECTILES

C. 41 EA CHARGE M3A1

D. 126 EA CHARGE M3A1

E. 1 EA M199 CANNON, 90 PERCENT LIFE REMAINING

BT

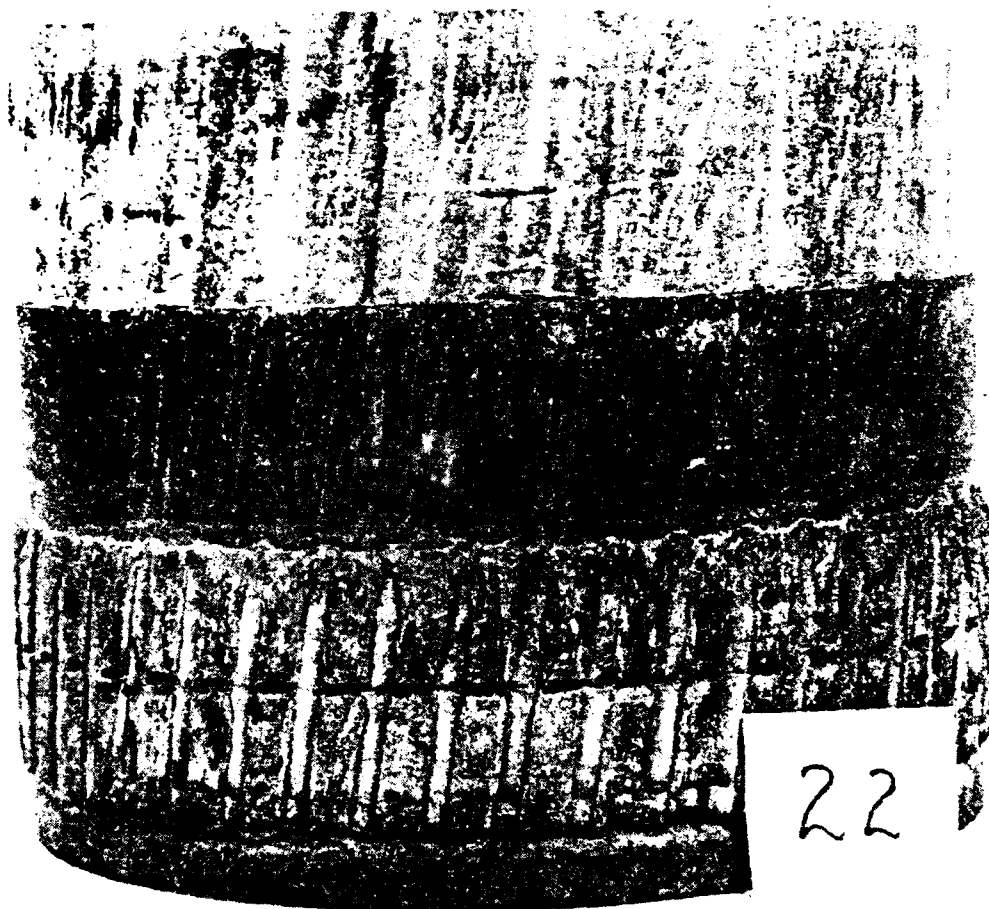
DISTRIBUTION LIST

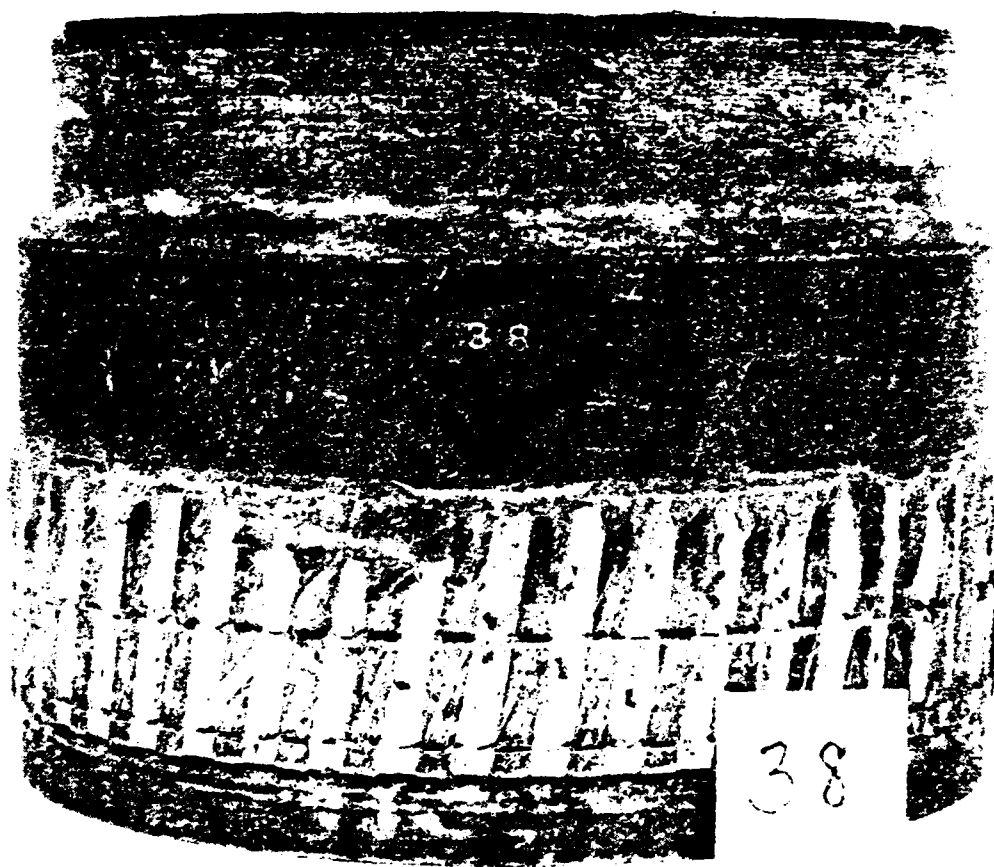
<u>ADDRESSES</u>	<u>NO. OF COPIES</u>
Commander US Army Ammunition Research and Development Command ATTN: DRDAR-LCU-DS	1
DRDAR-TSE-O	1
DRDAR-TSS	1
DRDAR-QAR	1
DRDAR-FFT	1
Dover, NJ 07801	
Project Manager for Selected Ammunition ATTN: DARCOM-FM/SA, Mr. L. McClellan	1
Dover, NJ 07801	
Project Manager for Cannon Artillery Weapons Systems ATTN: DRCPM-CAWS-TE	2
Dover, NJ 07801	
Project Manager for Munitions Production Base Modernization and Expansion ATTN: DRCPM-PBM-MA, Mr. Y. Wong	1
Dover, NJ 07801	
Commander US Army Test and Evaluation Command ATTN: DRSTE-CM-F, Mr. W. Vomocil	1
Aberdeen Proving Ground, MD 21005	
Director US Army Ballistic Research Laboratories ATTN: DRDAR-TSB-S	2
Aberdeen Proving Ground, MD 21005	
Commander US Army Yuma Proving Ground ATTN: STEYP-FIO-TL	1
STEYP-MTW	3
Yuma, AZ 85364	

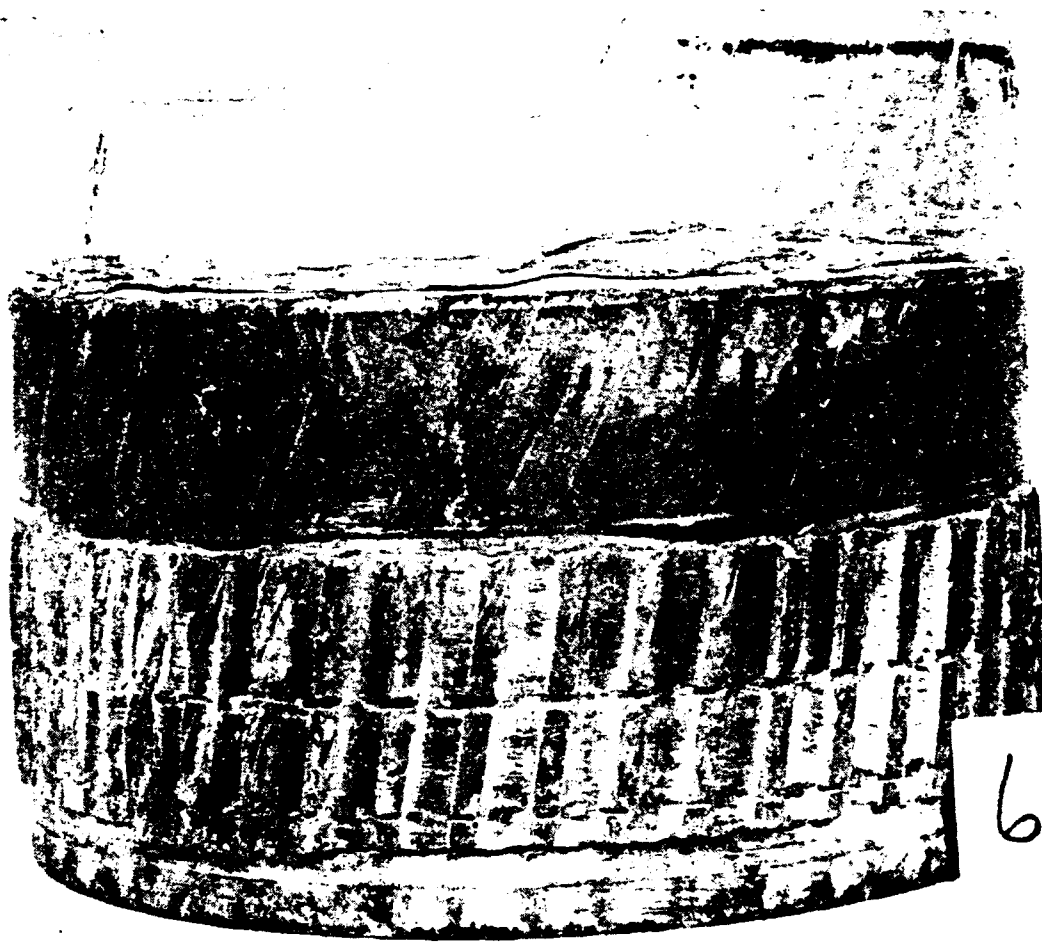
APPENDIX D

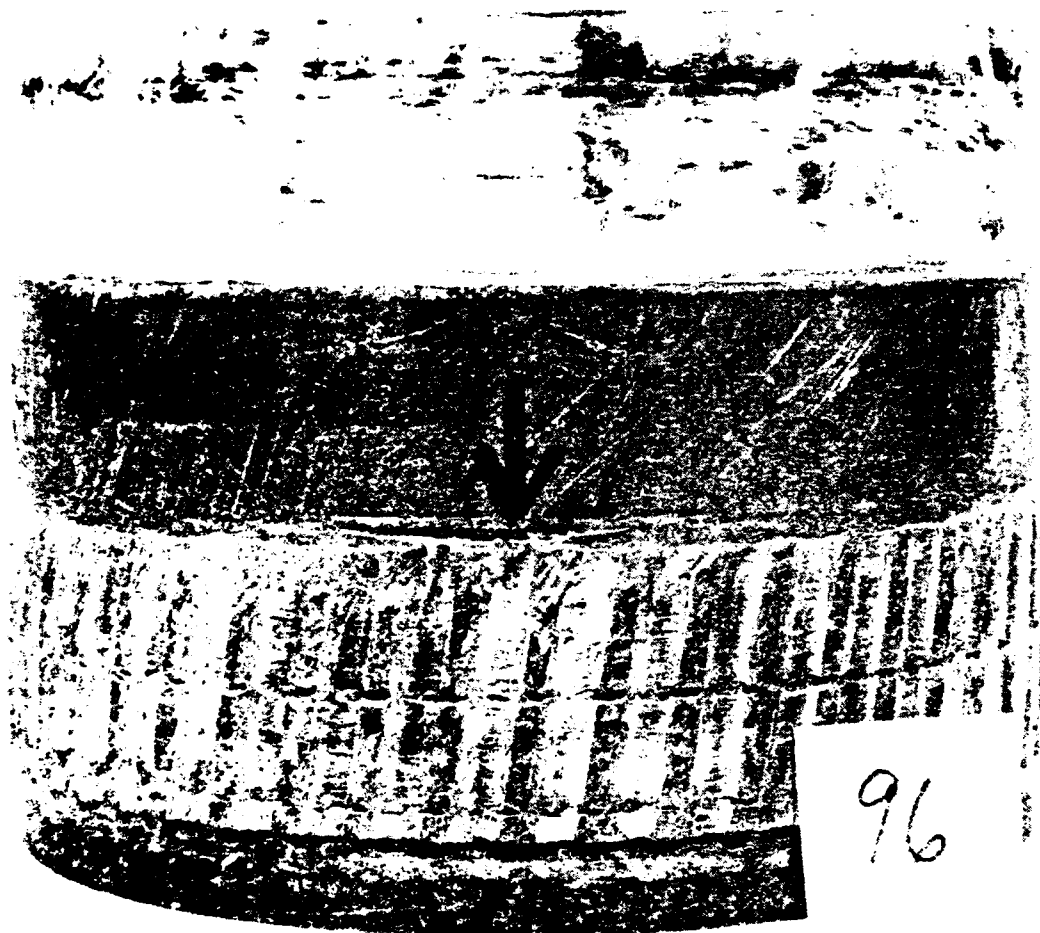
YUMA PROVING GROUND PHOTOGRAPHS OF RECOVERED M483A1
PROJECTILES HAVING INERTIA WELDED ROTATING BANDS

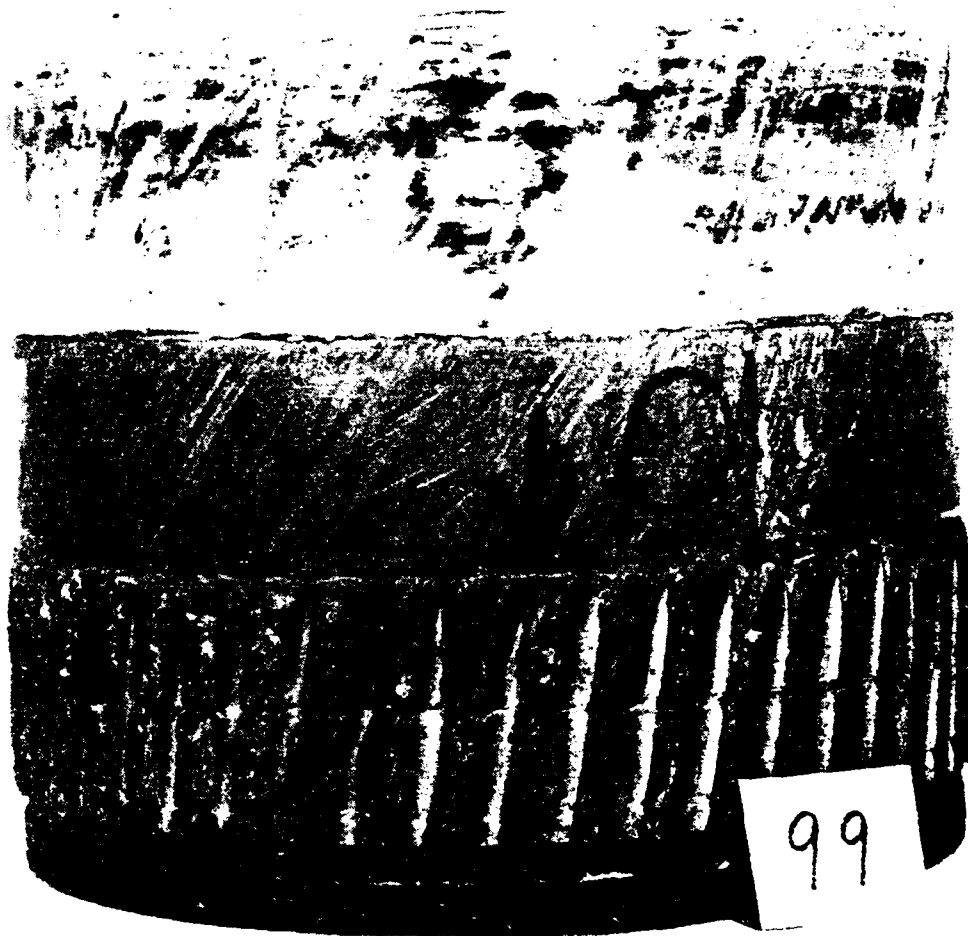
These photographs, taken by YPG personnel, represent the 10
projectiles (out of 120 fired and 110 recovered) that were
judged by YPG to have significant loss of band material.
All 10 photographs are referenced by CMC Photograph No. 11607.

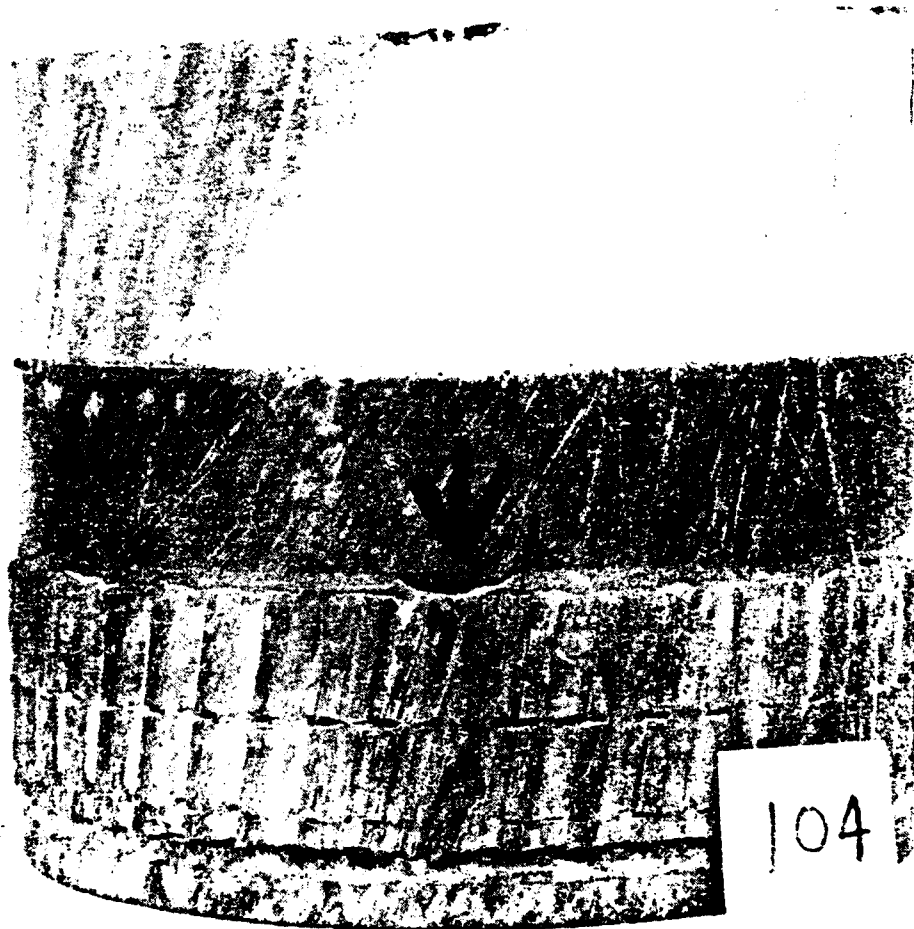




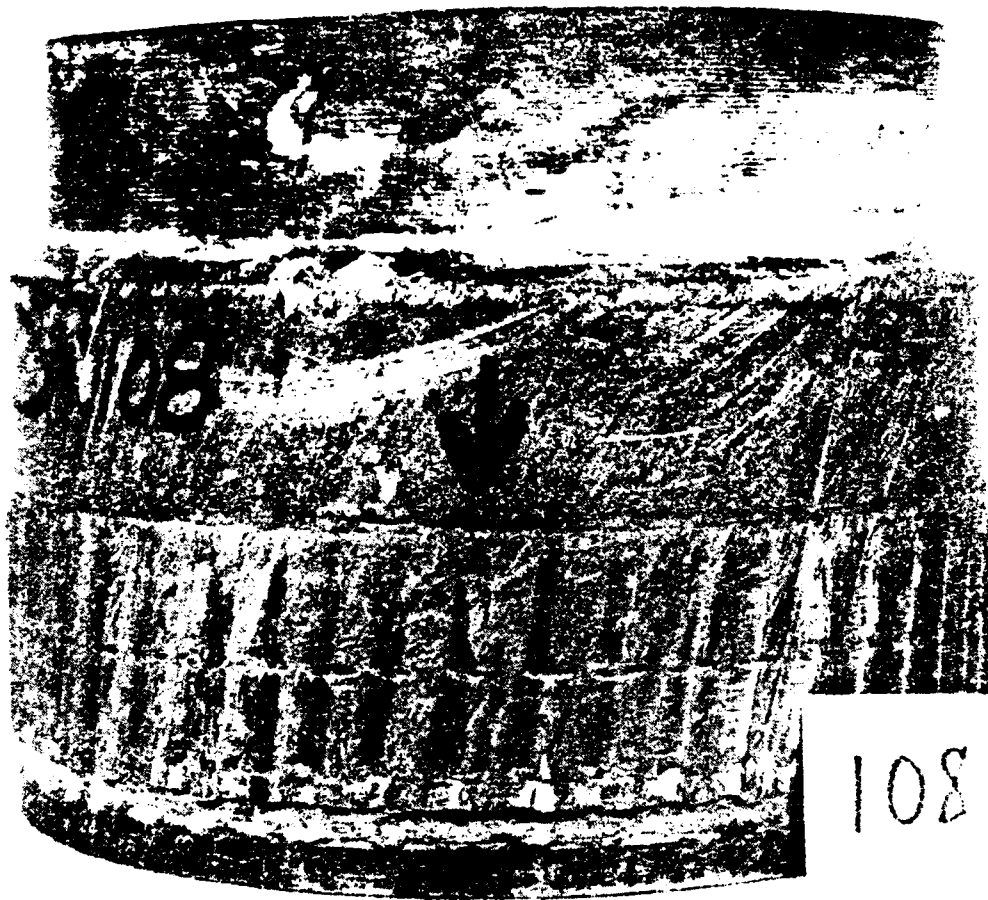




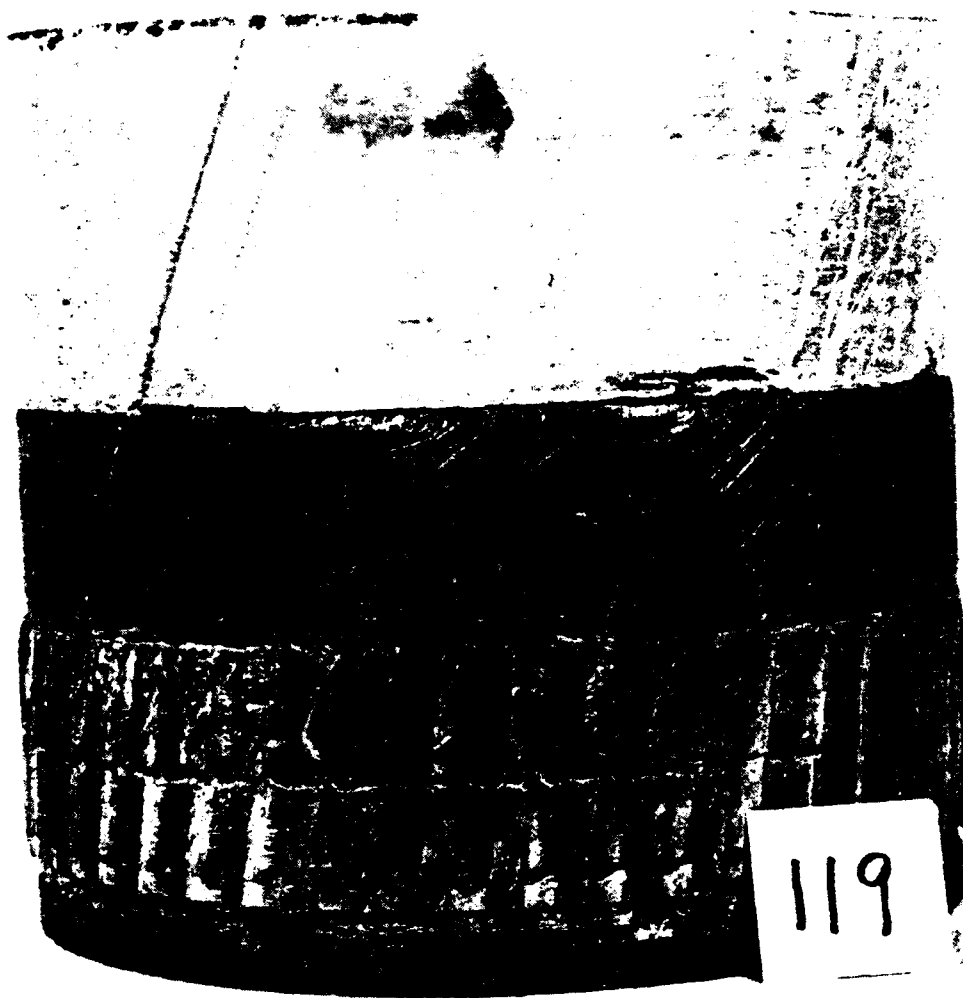


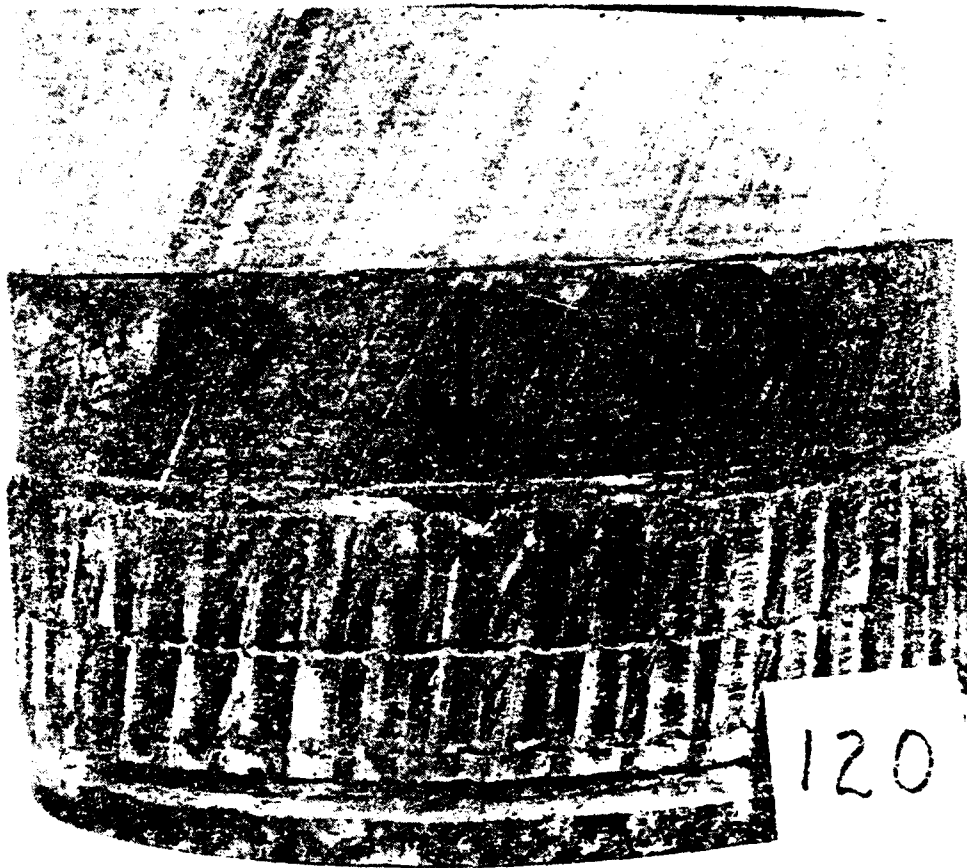






108





END

DATE
FILMED

1-83

DTIC